Characterisation of the role of mitochondrial translocator protein 18kDa (TSPO) in the regulation of energy homeostasis

Submitted by Nicole Anne Morrissey, to the University of Exeter as a thesis for the degree of Doctor of Philosophy by Research in Medical Studies, August 2020.

Acknowledgements

I have been joking that my acknowledgement section of my thesis is going to be a thesis in itself. It is no exaggeration that people by my side in my PhD journey are responsible for me achieving completion of my journey. I hope that I can do them proud.

First and foremost, I would like to thank my primary supervisor Prof. Kate Ellacott for all her help and support in undertaking this project and for providing me with this opportunity to do so. As well as her wisdom, knowledge, experience in the field of neuroendocrinology, her kindness, listening, unending support and encouragement was crucial to this project. Time spent undertaking a PhD is a challenge to personal development as well as training and education, and I owe Prof. Ellacott much gratitude for her role in all of these aspects. I would like to thank my second supervisor, Dr. Craig Beall, for his insight, advice and perspective that I would not have otherwise thought up. I want to thank him also for his economical advice, which I refer to as “Beall’s Bottle Rule!” I wish to thank the University of Exeter and the College of Medicine and Health, for firstly the funding to undertake this project but also the support from the postgraduate research office. I am appreciative for the hard work by the staff team in the Biological Services Units at the University. I am also grateful to Prof. Simon Luckman and his team for hosting me as a visiting scientist during my PhD, and for their training and support since my MRes studies.

The ‘Beallacott’ team has been a fantastic group of colleagues and support during my PhD. I have loved every day working with you all. I especially want to thank Dr. Josie Robb for your continued support and advice in both work and life, Dr. Alastair MacDonald for being my team-mate from Day 1, and Katherine Pye for your help and advice with genotyping and more. Dr. Ana Cruz, Dr. Paul Weightman Potter, Dr. Ben Hall and Julia Vlachaki Walker also deserve special shout-outs for the laughs and entertainment both in and outside of the lab. The RILD Level 4 group is a great environment to work in, and so I would like to thank every colleague there for making it so.

It is important to have a work-life balance, and so I would like to thank the people who have helped make Exeter an enjoyable place to live during my PhD. To

Sensei/Dr. Rich Catterick and Sensei/Dr. Helen Catterick for making Exeter Martial Arts a wonderful environment to work off steam and to meet new people, as well as their support. To the instructors and students at Spin City Exeter for providing another welcoming environment to pursue my hobbies and meet new people. I have been so lucky to have lived in house shares with groups of amazing people. I could not believe my luck to move into a house with such fun, friendly and hilarious housemates as Tobias, Connor, Ben and Julia. Connor and I lived in that house for the majority of our respective PhD projects, and I am grateful for his company and understanding throughout. I also had the privilege of living with some truly wonderful ladies for the last 6-9 months of my time in Exeter. I am so grateful to Beth, Delane and Polly for building a comfortable, supportive and beautiful environment to live in during the last stages of my PhD.

I wish to express my gratitude to the partners who have stood by my side during the PhD process. To Danny for his unwavering support before and after my move to Exeter, to Eder for his insight as a researcher and also his cooking, and finally to Gavin for being a rock during the writing-up process amongst a global pandemic. Gavin: thank you for shopping, cooking, cleaning for/with me while I was writing, for providing me with chocolate and encouraging me to maintain a good work-life balance but also pushing me to do more when I could.

I want to thank my family for their unconditional support before and during the PhD, for providing me with food and shelter, for financial support, and for always finding the funny side of my research. I want to also acknowledge the support of my friends – from Wakefield and from Manchester – for keeping my spirits up when things were tough, for forgiving my lack of response at tough times, and for visiting me if and when they could.

I also wish to dedicate this thesis (corrected version) to both my grandmothers who unfortunately both passed away before I had my *viva voce* examination. I'm sure they would be asking me "Why I am not finished yet" and "Why don't I study Parkinson's disease instead", much to my entertainment.

Abstract

Obesity is a chronic condition where the body's ability to regulate energy balance is compromised. Prolonged consumption of saturated fatty acids triggers inflammation throughout the body, including the brain. Within the brain, astrocytes and microglia respond to nutrients and inflammatory signals with reactive gliosis. The mitochondrial translocator protein of 18 kDa (TSPO) is used to mark reactive glia. However, the function of TSPO – or its relevance to gliosis - is not well-understood. *In vitro* studies suggest involvement in mitochondrial metabolism, including altering substrate use. *In vivo* work suggests a role for TSPO modulating systemic glucose homeostasis. The hypothesis underlying my project was: TSPO is involved in metabolic flexibility and is regulated in states of energy imbalance, and manipulation of TSPO expression will alter energy homeostasis.

I validated a common TSPO antibody, which proved it to be unreliable for immunohistochemical characterisation of TSPO in the mouse brain. Comparison between brain tissue taken from TSPO knock-out (-/-) and wild-type mice indicated a low level of immunoreactivity throughout the mouse brain that was specific. This included immunoreactivity around the ventricles of the brain that was attributed to tanycytes. However, the majority of the immunoreactivity was not specific to TSPO and confounds results that use this antibody.

I characterised the metabolic phenotype of the germline global TSPO -/- mice. These mice did not exhibit differences in body weight or food intake in response to an overnight fast compared to littermate controls. Male TSPO -/- mice consumed less high-fat diet than controls in the first week of exposure, but there were no long-term differences. Basal blood glucose levels or glucose clearance in the glucose tolerance test were also unaffected by genotype, though female TSPO -/- mice may have enhanced protection against diet-induced loss of glucose tolerance compared to wild-type. These data were consistent with experiments using PK11195, a TSPO ligand. These findings are important for comparisons across the literature that involve different knock-out mouse models.

In conclusion, global modulation of TSPO does not impact energy homeostasis on the organismal level and its functions are likely cell-type specific. Therefore,

systemic modulation of TSPO signalling it is unlikely to offer translational potential in treating obesity.

List of Contents

List of Tables

List of Figures

Figure 6.4.1 Visual summary of conclusions arising from this study.

Appendix 1 Full representative immunoblots that were processed with anti-TSPO and anti-GFAP for semi-quantification of diet-induced regulation.

Author's declaration

All work was conducted by the author, with support from research and technical staff, at the University of Exeter College of Medicine and Health laboratories.

Diagrams of organs and cells were downloaded from the SciDraw resource hub and edited for use in Chapter 1 (Fig 1.2.1; Fig 1.2.2; Fig 1.4.1) and Chapter 6 (Fig 6.4.1).

Brain tissue was gifted for processing from Prof. Simon Luckman at The University of Manchester for use in Chapter 3 (Fig 3.2.2.11-20), which is specified and detailed in Chapter 2.5.

In Chapter 3, Dr. Josie Robb contributed the immunocytochemical staining of TSPO in primary cultured astrocytes (Fig 3.2.3.1).

In Chapter 4, Dr. Josie Robb cultured and lysed the mouse primary cortical astrocyte that I used as a positive control in my Western Blot analysis (Fig 4.2.1.2-3).

In Chapter 5, Katherine Pye performed the confirmation of genotype of the TSPO wild-type (+/+) and knock-out (-/-) mouse cohort and provided the gel images (Fig 5.2.1.1).

List of Abbreviations

3V	Third ventricle
+/+	Wild-type
-/-	Knock-out
ACBP	Acyl-CoA-binding protein
acc	Anterior commissure
ACTH	Adrenocorticotropic hormone
AD	Alzheimer's disease
AgRP	Agouti-related peptide
ANOVA	Analysis of variance
ANT1	Adenine nucleotide transporter 1
AP	Area postrema
APS	Ammonium persulfate
Arc	Arcuate nucleus of the hypothalamus
ATP	Adenosine triphosphate
AUC	Area Under Curve
BAT	Brown adipose tissue
BBB	Blood-brain barrier
BNST	Bed nucleus of the stria terminalis
BNSTl	Bed nucleus of the stria terminalis, lateral division
BNSTv	Bed nucleus of the stria terminalis, ventral division
BSA	Bovine serum albumin
BSU	Biological services unit
C1/A1	Noradrenaline/adrenaline cell group
CC	Central canal
cc	Corpus Callosum
CNS	Central nervous system
Cpt1a	Carnitine palmitoyltransferase-1 subunit-a
CRAC	Cholesterol-binding amino acid consensus
CRH	Corticotropin releasing hormone
CSF	Cerebrospinal fluid
DAPI	4',6-diamidino-2-phenylindole, dihydrochloride
DIO	Diet-induced obese

DMH	Dorsomedial nucleus of the hypothalamus
DMSO	Dimethyl sulfoxide
DMV	Dorsal motor nucleus of the vagus nerve
DOB	Date of birth
EDTA	Ethylenediaminetetraacetic acid disodium salt
EGTA	Ethylene glycol-bis(β-aminoethyl ether)-N,N,N′,N′-tetraacetic acid
EYFP	Enhanced yellow fluorescent protein
F	Female
F4/80	EGF-like module-containing mucin-like hormone receptor-like 1
FA	Fatty acid
FAO	Fatty acid oxidation
FDG	Fluorodeoxyglucose
FFA	Free fatty acid
Fig	Figure
G6PC	Glucose-6-phosphatase (catalytic subunit)
GABA	γ-aminobutyric acid
GAD	Glutamate decarboxylase
GFP	Green fluorescent protein
GFAP	Glial fibrillary acidic protein
GI	Gastrointestinal
GLP-1	Glucagon-like peptide-1
GLUT	Glucose transporter
GmbH	German Research Center for Environmental Health
GTT	Glucose tolerance test
H&E	Hematoxylin and eosin
HCl	Hydrochloric acid
HFD	High-fat diet
HPA	Hypothalamic-pituitary-adrenal
IBA1	Ionised calcium-binding adaptor molecule 1
ICD-11	International Classification of Diseases
IGF-1	Insulin-like growth factor 1
IgG	Immunoglobulin-G

IL	Interleukin
IMPC	International Mouse Phenotyping Consortium
LCFA	Long-chain fatty acid
LH	Lateral hypothalamic nucleus
LPS	Lipopolysaccharide
LSN	Lateral septal nucleus
LV	Lateral ventricle
M	Male
MBH	Mediobasal hypothalamus
MC4R	Melanocortin-4 receptors
MCH	Melanin-concentrating hormone
ME	Median eminence
mRNA	Messenger ribonucleic acid
MSH	Melanocyte-stimulating hormone
NAcc	Nucleus accumbens
NaCl	Sodium chloride
NaF	Sodium fluoride
NaPPi	Sodium pyrophosphate tetrabasic decahydrate
NaOH	Sodium hydroxide
NaVO4	Sodium orthovanodate
Neo	Neomycin
NDS	Normal donkey serum
NF-κB	Nuclear factor kappa-light-chain-enhancer of activated B cells
NNT	Nicotinamide nucleotide transhydrogenase
NPY	Neuropeptide Y
NTS	Nucleus of the Solitary Tract
ODN	Octadecaneuropeptide
Opt	Optic tract
PAGE	Poly-acrylamide gel electrophoresis
PBR	Peripheral benzodiazepine receptor
PBS	Phosphate buffered saline
PBS-T	Phosphate buffered saline with Triton-X
Pck1	Phosphoenolpyruvate carboxykinase 1

PCR	Polymerase chain reaction
Pe	Periventricular hypothalamic nucleus
PET	Positron emission tomography
PFA	Paraformaldehyde
PMSF	Phenylmethanesulfonyl fluoride
POMC	Pro-opiomelanocortin
PVH	Paraventricular nucleus of the hypothalamus
qPCR	Quantitative PCR
ROI	Region of interest
SD	Standard chow diet
SDS	Sodium dodecyl sulphate
SF-1	Steroidogenic factor 1
SFA	Saturated fatty acid
SFO	Subfornical organ
SIRT1	Sirtuin 1
StAR	Steroidogenic acute regulatory protein
TBS-T	Tris-buffered saline with Tween
TEMED	N,N,N′,N′-Tetramethylethylenediamine
Tm1b	Targeted mutation
TNFα	Tumour necrosis factor α
TRH	Thyrotropin releasing hormone
TSPO	Mitochondrial translocator protein 18 kDa
TTN	Triakontatetraneuropeptide
VDAC	Voltage-dependent anion channel
VMH	Ventromedial hypothalamic nucleus
VOLT	Vascular organ of the lamina terminalis
WAT	White adipose tissue
WHO	World Health Organisation

Preface

The order in which the work is presented in this thesis is in three thematic chapters. However, this does not reflect the order in which the studies were conducted. It is essential to note that the acquisition of the TSPO global knock-out mouse line, the data in which contributed to chapter five, meant that in-house validation could be performed on the antibody which produced the data used in chapters three and four. Unfortunately, this internal validation did not confirm the expected specificity of the antibody used. This altered the conclusions of the results described in chapters three and four. Therefore, the chapters in this thesis are described with as they were conducted – prior to the knowledge of the lack of specificity in the antibody. The chapter conclusions then consider this particular finding and its contribution to the interpretation of my data but also the conclusions of data produced by other research groups.

Chapter 1: General Introduction

1.1 Obesity is a progressive disease with few therapeutic interventions

Obesity is a physiological state that is typically a result of excess calorie intake not offset by a sufficient increase in energy expenditure. This leads to an increase in weight gain, attributed primarily to fat mass. The World Health Organisation (WHO) defines obesity as an accumulation of excessive fat that might impair health, and a body-mass index of over 30 (1,2). Increased fat storage occurs primarily within the adipose tissue, but also in the other metabolic organs of the body such as the liver (3,4). In addition to the excess weight that the body is bearing, increased fat stores predispose individuals to other health complications (5). Furthermore, individuals find it difficult to lose the excess weight and maintain the weight loss regardless of dietary or physical interventions (6). As well as a predisposing factor for other diseases, obesity is becoming acknowledged as a pathology in its own right and the international classification of diseases (ICD-11) considers obesity to be under the heading of endocrine, nutrient or metabolic diseases (7). The World Obesity Federation has proposed that obesity is a chronic relapsing and progressive disease (8). The idea that obesity is progressive is consistent with the knowledge of the metabolic changes underlying obesity, which is discussed in detail below.

The mechanisms underlying obesity have gained a lot of research interest, due to it being a predisposing factor for other serious illnesses: cardiovascular illnesses (heart disease, stroke), metabolic diseases (type 2 diabetes mellitus), and musculoskeletal disorders (arthritis, osteoporosis) (5). Non-communicable diseases such as these, are estimated to be the cause of 70% of early deaths world-wide (9) and obesity is also associated with premature death and disability (10–13). Obesity is hugely prevalent throughout the world; although it is at greater incidence in countries of high-income and income-disparity (13,14). As well as socio-economic status, genetics and heritability contribute to obesity. Due to its high incidence and comorbidities, obesity places a considerable burden on public

health and the economy. While reduction of obesity would not eliminate other diseases, it has potential to alleviate them and their cost.

Current strategies to conquer the obesity epidemic primarily involve educational approaches and changes in government policy (1,2,13,15,16). Dietary limitations are the most accessible and easy to implement, but are difficult to maintain long-term compliance and benefits (6). These measures have been reinforced by societal changes in advertisement and taxes on foods deemed unhealthy. The hope is that these measures would facilitate an individual-based response that results in behavioural changes and reduction in consumption of high-sugar/high-fat foods. However, to date no nation has been successful in reducing the prevalence of obesity (17). While the blame could be attributed to the individual, obesity is a multi-factorial challenge and such factors likely limit an individuals' effort regardless of reinforcements provided by governmental policy. Even with societal support, responsibility cannot be placed solely upon on the individual to reduce the incidence of obesity as many causative factors lay outside of one's control. Further investigation into these factors is required.

Clinical interventions in individuals with obesity presenting with comorbidities has gained some success. Gastric bypass surgery remains the most effective, improving blood glucose control in patients with type-2 diabetes almost immediately (18). Pharmaceutical approaches have had varying successes but tend to only produce relatively small weight loss (19). Some drugs developed to treat type-2 diabetes, such as liraglutide (20), have been repurposed following promise in weight-loss. These drugs target one of many possible mechanisms underlying obesity-associated pathology and provide some insight to the pathophysiology.

1.2 Cross-organ communication regulates energy balance

The goal of energy homeostasis mechanisms is to maintain a steady state of energy reserves respective of energy intake and expenditure. These processes occur throughout the organism (Fig 1.2.1). Communications from tissues regarding energy and nutrient availability converge in the homeostatic hub of the

brain: the hypothalamus (21) (Fig 1.2.2). This information must be integrated to consequently inform the body of how to proceed: to initiate or cease food intake or regulate expenditure of energy. While the entire body is involved, I will focus on key hypothalamic and non-hypothalamic brain regions and the contribution from the gut, adipose tissue, and the liver.

1.2.1 Peripheral signals contributing to the regulation of energy balance

One of the initial sensors of energy intake is within the gastrointestinal (GI) tract. The gut contains the enteric nervous system, which consists of multiple cell types with different morphological, electrophysical and chemical properties (22–24). Cells of the GI lining respond depending on the nutrients absorbed and in turn secrete associated hormones. These hormones not only act locally to induce digestion, but also act in an endocrine manner across the body including the brain. One example, cholecystokinin, is secreted from the duodenum in response to fat and protein intake (25–27). It acts locally to inhibit gastric emptying, stimulates the pancreas to release digestive enzymes, and also acts in the brain to inhibit appetite. In acute absence of sufficient nutrition, the GI system secretes ghrelin to stimulate appetitive behaviour via the brain (28–31). As well as blood-borne signals, the gut is capable of signalling directly to the brain by means of the vagus nerve (32–40). This nerve conveys signals between the medulla oblongata and organs within the abdomen. The vagal afferents are sensitive to mechanosensors in the gut, which sense gastric stretch due to food consumption, and are responsive to nutrients (36,37). Gut-released peptides can also enhance vagal transmission in relation to nutritional status (25). These two means of gut-brain communication provide temporally dynamic information regarding food intake.

The vagus nerve also innervates the liver, another important metabolic organ. The liver is crucial for the regulation of whole-body glucose levels and lipid metabolism (41). It receives information regarding nutrient intake from the gut directly, via circulating hormones and nutrient transport, and indirectly through the central nervous system (CNS) (41,42). It is also sensitive to the homeostatic output of the brain and regulates glucose levels accordingly. In the post-prandial state, hepatocytes condense glucose into glycogen for storage. In response to low energy availability/glucose deprivation, the liver is the primary site of glucose

production through glycogenolysis and gluconeogenesis. In addition to glucose metabolism, hepatocytes also provide a storage site for fatty acids (FAs). Excess FAs lead to lipid accumulation and liver damage in the form of hepatic steatosis (43). This also impairs the livers' ability to maintain glucose homeostasis and so contributes to the pathology associated with obesity (44). Consequently, liver dysfunction is a key player in the progression of obesity.

Adipose tissue is the primary designated fat storage organ of the organism. Since the discovery of the hormone leptin, an adipokine that conveys information on levels of fat storage, adipose tissue has been considered a crucial organ in energy homeostasis (45,46). In turn, adipose tissue receives innervation from the sympathetic nervous system which influence fat storage and lipolysis (47,48). There are two main types of adipose depot: energy-storing white adipose tissue (WAT), which is the most abundant within an organism, and energy-expending thermogenic brown adipose tissue (BAT) (49–51). White adipocytes take up un-catabolized glucose and FAs in the circulation to store within the tissue as triglycerides (46). In states of negative energy balance these are catabolised into free FAs (FFAs) and released into the circulation to provide a source of energy (52).

In obesity, white adipocytes try to compensate for the increased FFAs in the circulation through an increase in cell size (53–55). This increase in adipocyte mass leads to competition for oxygen, resulting in hypoxia across the tissue (56,57). During hypoxia, the adipocytes shift their metabolism and nutrient up-take to focus on glycolysis (58,59). Considering the metabolic shift to glycolysis in WAT, as well as the increased calorie intake, FFAs in the circulation become elevated (54). This is a key driver for obesity-induced inflammation in adipose tissue. As well as being an important endocrine organ, adipose tissue is a host to many resident immune cells; such as macrophages, mast cells, and natural killer cells (60,61). Cellular debris from the dying adipocytes attracts additional macrophages and other immune cells to infiltrate the WAT and produce pro-inflammatory cytokines (62–64). WAT infiltrating immune cells are associated with early-stage onset of insulin resistance, which is a metabolic complication of obesity (65). Adipocyte expansion and apoptosis is alleviated in absence of pro-inflammatory signalling in adipose tissue (66). This indicates that impaired function of adipose tissue, as observed in nutrient excess, is exacerbated by its

own pro-inflammatory response to this, underlying the progressive nature of obesity.

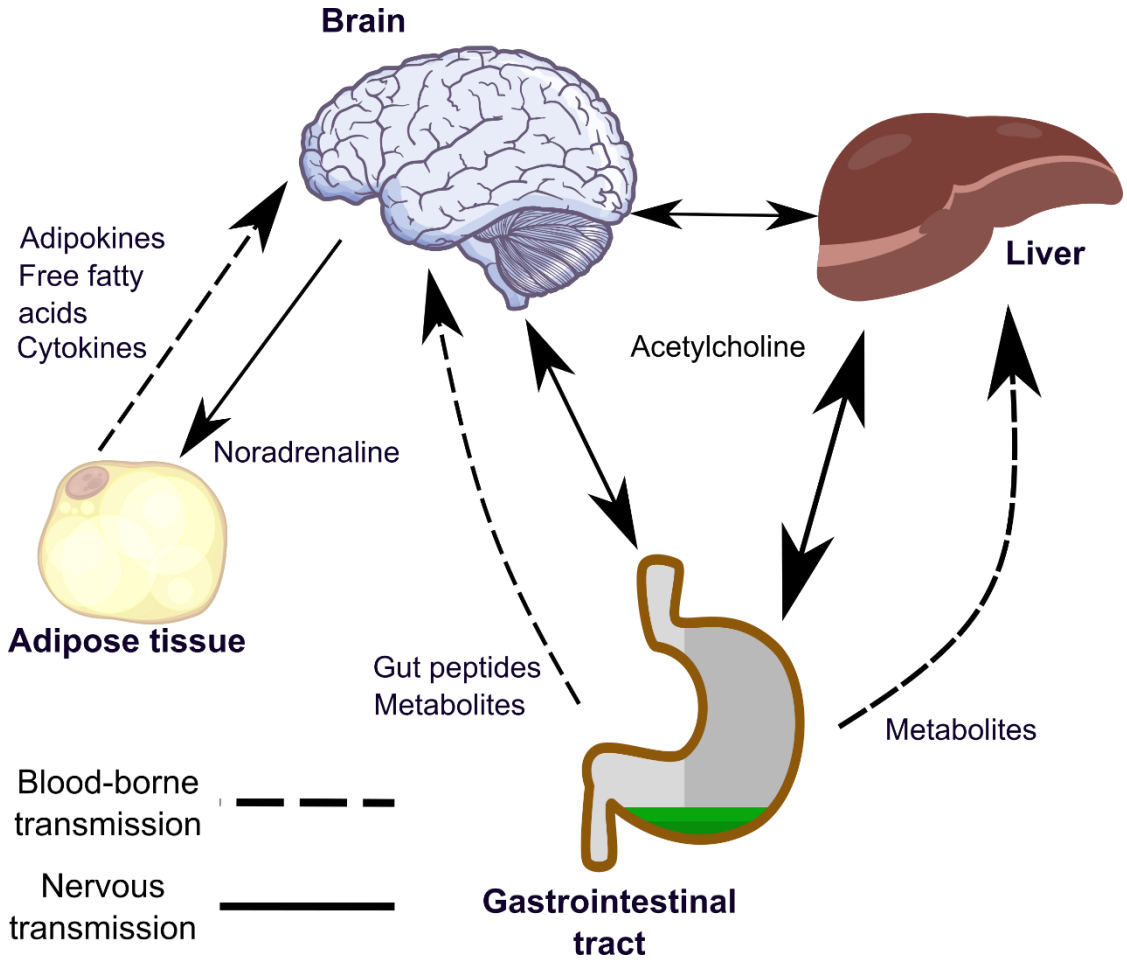

Figure 1.2.1 A snapshot of the communication pathways between the brain, digestive organs, and adipose tissue relevant in the regulation of energy homeostasis.

The brain receives signals from adipose tissue through chemical signals such as adipokines, including leptin, and cytokines. Free fatty acids released from adipose tissue also act as messenger signals to the brain. Adipose tissue is innervated by noradrenergic nervous transmission. Communication between the brain, liver and gastrointestinal tract is mediated by cholinergic transmission at the vagus nerve. The gastrointestinal system also secretes hormones that are received by the brain, such as ghrelin and cholecystokinin. Images adapted from Sci-Draw (67).

1.2.2 Hypothalamic regulation of energy balance

As mentioned above, energy homeostasis incorporates communication of information on energy intake and storage across multiple organs. Pathways sensing and responding to nutritional state and energy expenditure require organisation and integration of the information to produce an appropriate output. The hub for integration relies on the brain, primarily the hypothalamic nuclei.

The hypothalamus is an incredibly diverse and heterogeneous region of the forebrain. It supervises the regulation of multiple systems, including energy homeostasis, and its outputs are widespread throughout the CNS and the periphery. Energy homeostasis is primarily regulated by the nuclei immediately surrounding the third ventricle (3V) due to the ability of appetitive information relayed by nutrients and hormones to readily access this area (68). Below the 3V is the median eminence (ME), a circumventricular organ and an area in which the blood-brain barrier (BBB) has relatively increased permeability and so chemical signals and nutrients are able to more readily penetrate to the brain regions that lie in immediate proximity (69–73). Hypothalamic nuclei are perfectly situated to receive signals regarding the energetic state of the body. The nuclei of focus in this project were the arcuate hypothalamic nucleus (Arc), ME, the paraventricular hypothalamic nucleus (PVH), and the dorsomedial hypothalamic nucleus (DMH). Other hypothalamic nuclei involved in energy homeostasis - that will not be covered in as much detail here - are the lateral hypothalamic nucleus (LH) and the ventromedial hypothalamic nucleus (VMH).

Response to appetitive information is primarily controlled within the arcuate nucleus of the hypothalamus (Arc). There are six categorised neuronal types within the mouse Arc, from which further subtypes have been delineated (74). Appetitive behaviour is controlled by two major well-characterised neuronal populations: neurons that co-express both neuropeptide-Y (NPY) and agouti-related peptide (AgRP), and those producing pro-opiomelanocortin (POMC). These neurons are differentially-activated in response to negative or positive energy states respectively, and promote feeding or meal termination (75). NPY is an appetite-stimulating peptide, and AgRP is an inverse agonist at appetite-inhibiting melanocortin-4 receptors (MC4R) (76,77). Together, neurons that express these peptides are orexigenic. NPY/AgRP-expressing neurons also express the neurotransmitter GABA, and in turn directly inhibit the activity of

anorexigenic POMC-expressing neurons (78). POMC is post-translationally cleaved to form adrenocorticotropic hormone (ACTH) and melanocyte-stimulating hormones (MSH) which are agonists at the MC4R (79–81). Axons of both Arc AgRP/NPY and POMC neurons project to multiple hypothalamic and non-hypothalamic regions of the brain to evoke their effects (82). These neurons also receive efferent signals from across the brain.

The paraventricular nucleus of the hypothalamus (PVH) is one of the direct targets of Arc neuronal projections, as well as conveying signals down to the Arc itself. The PVH is an important nucleus in the regulation of energy intake through termination of feeding (83–86). As with the Arc, the PVH consists of a heterogeneous mix of peptidergic and non-peptidergic neurons. This enables it to regulate multiple different homeostatic mechanisms, including stress as well as energy balance (87). Neurosecretory neuronal projections from the PVH to the ME and on to the pituitary gland are critical regulators of endocrine function. It is a key projection target for melanocortin neurons from the Arc, and MC4R is highly expressed in the PVH (88). As well as appetite, the PVH is sensitive to information regarding adiposity through leptin-sensitive connections from the Arc (89,90) and leptin receptors expressed on PVH neurons (91–93). The PVH is an important hub of hypothalamic homeostatic control, crucial for mediating feeding termination as well as potentially energy balance.

The dorsomedial hypothalamic nucleus (DMH) is an intermediate point in the hypothalamus, in which inputs from other regions in the brain are integrated and their afferents sent to the corresponding brain nuclei. Lesion studies have implicated the DMH in promoting appetite and energy expenditure, indicative of a role in energy homeostasis. The DMH is sensitive to ghrelin signalling (94), from which it regulates meal size, energy expenditure, and food anticipatory activity (95,96). It also mediates the thermogenic effect of leptin signalling, as a mode of energy expenditure (97). The DMH is also reported to be involved in the adaptive physiological response to food restriction (98). It is home to several groups of peptidergic neurons, some of which are also found in the Arc and other hypothalamic and non-hypothalamic regions. However, within the DMH these peptides have different functions. For example, a key set of neuropeptide-expressing neurons in the DMH is that of NPY. Unlike NPY neurons of the Arc, DMH NPY cells are not sensitive to leptin and NPY in the DMH is expressed at

low levels under basal conditions but upregulated in energy imbalance (99,100). The output of DMH NPY neurons is important in communicating orexigenic signals that influence meal-size (100,101). DMH signalling is crucial in regulation of body weight, likely through balancing food intake and energy expenditure.

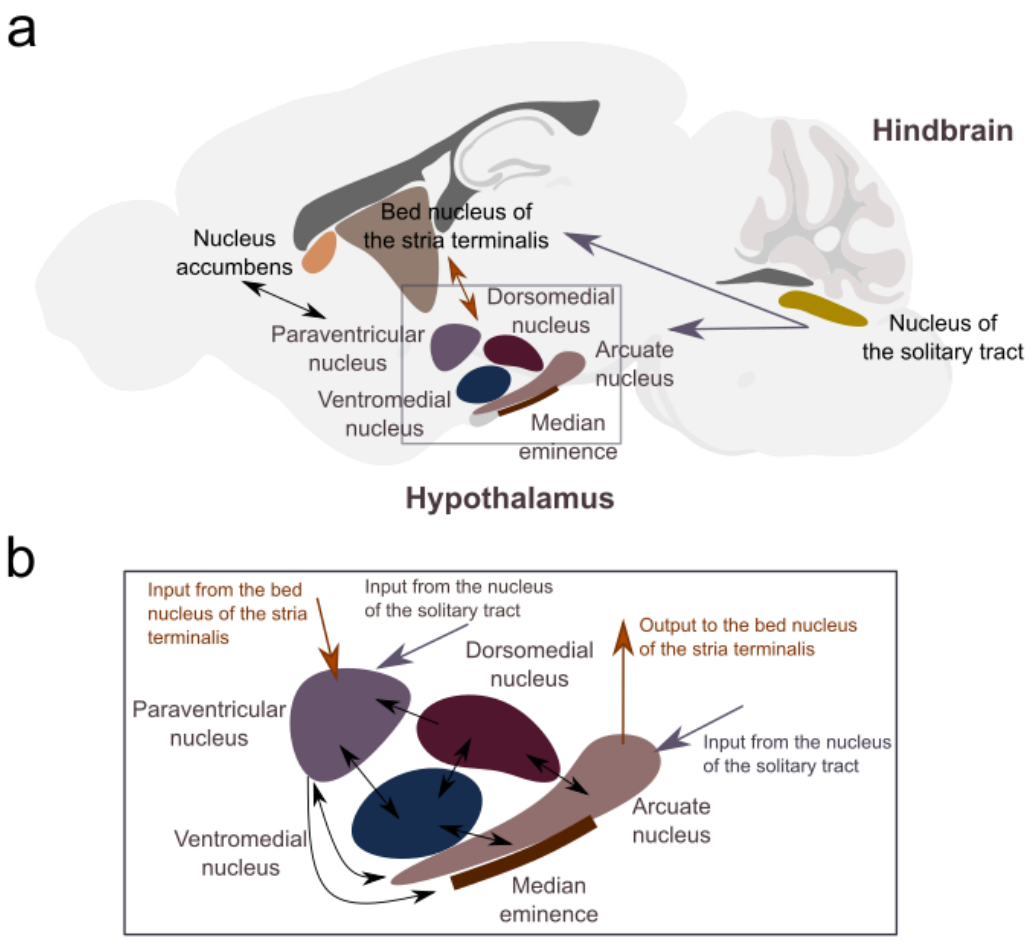

Figure 1.2.2 Hypothalamic and other brain regions that are involved in energy homeostasis.

Mouse brain figure adapted from Sci-Draw (67), depicting a sagittal view of the mouse brain and the key nuclei involved in energy homeostasis that are relevant to this study (a). Hypothalamic nuclei communicate amongst each other, as well as with other brain regions, to regulate energy balance (b).

1.2.3 Extra-hypothalamic regions that influence energy balance

Hypothalamic communication spans throughout the brain, including to the periphery, and so extra-hypothalamic regions are also capable of influencing homeostatic output. The network of brain nuclei that communicate with the

hypothalamus is extensive, but for the purpose of this project the focus here will be on a select few regions.

As aforementioned, the vagus nerve rapidly relays information from the gut to the brain via the nucleus of the solitary tract (NTS). The NTS is a small nucleus in the medulla oblongata that consists of multiple heterogeneous neuronal groups, which respond to different signals (38,102–104). The NTS is directly sensitive to signals relating to food consumption from the gut via the vagus nerve (105,106). The NTS can also directly detect blood-borne signals such as nutrients, as it lies beneath the area postrema (AP) – a circumventricular organ (107–109). In turn, the NTS relays information from the gut to higher brain regions – such as the hypothalamus and the parabrachial nucleus – usually to terminate feeding (110).

The bed nucleus of the stria terminalis (BNST), nucleus accumbens (NAcc) and the lateral septal nuclei (LSN) are forebrain targets of hypothalamic signalling that have been implicated in energy homeostasis. The BNST receives input from the Arc and also innervates the LH, and is thought to play a role in the emotional modulation of appetite control (111). Identification of BNST inputs and outputs has suggested a potential role in coordination of autonomic, somatic, and behavioural networks with endocrine regulation of energy homeostasis (112). The NAcc receives input from the Arc, and is thought to be involved in the rewarding aspects of feeding motivation (113). The LSN can inhibit food intake via the LH, which has led to the proposal that it is also involved in the emotional aspect of food intake (114). Consequently, multiple brain regions are involved in regulating different aspects of energy homeostasis– including that of emotion and reward.

The regulation of energy homeostasis is appropriately controlled by the balance of different systems, communicating through both blood-borne and neuronal messages. While it may be surprising that its efforts are overcome in the case of chronic energy excess, a preference for high-fat and high-sugar foods carries an evolutionary advantage (115). As observed in peripheral metabolic organs, the brain’s compensatory mechanisms in excessive energy intake can inflict damage to the homeostatic machinery when overcome by chronic energy excess.

1.2.4 Energy state affects cell function in the regulation of energy homeostasis

Prolonged high-fat intake leads to reduced capacity to store or metabolise FAs in adipose and hepatic tissue, increasing the levels of FAs in the circulation. FAs are able to access the brain via the circulatory system and cerebrospinal fluid (116–119), and this forms one route by which the brain can sense nutrient intake (120). During chronic high-fat feeding, lipid droplets accumulate in the brain tissue and this can impair its function (121). This is dependent on FA type: FAs are a diverse group of molecules and exert different effects, exemplified by differential distribution and uptake by different cell types, in mouse hypothalamic *ex vivo* slices (121). Furthermore, injection of saturated FAs (SFAs) into the 3V induces upregulation of hypothalamic pro-inflammatory cytokines – such as tumour necrosis factor-α (TNF-α) and interleukin-1β (IL-1β) – while unsaturated FAs do not (122). While the brain senses energy intake through the level of circulating FAs, excessive SFAs can induce pro-inflammatory signalling pathways which may be detrimental to the brain tissue if prolonged.

As described previously, lipid accumulation in peripheral tissues due to high-fat diet leads to damage: macrophage infiltration and production of pro-inflammatory cytokines. In diet-induced obesity, pro-inflammatory immune cells are able to cross the BBB and permeate the CNS (123). This includes infiltrating macrophages, which enhance secretion of pro-inflammatory mediators and also augment BBB permeability (124). Upregulation of pro-inflammatory cytokine mRNA - including *Tnfα* and *Il-1b* - is observed in hypothalamic tissue of obese mice fed high-fat chow (125). Diet-induced upregulation of nuclear factor kappa-light-chain-enhancer of activated B cells (NF-κB), toll-like receptor 4, TNF-α and IL-1β signalling has also been observed in other brain regions including the hindbrain (126–131). Genetic and pharmacological manipulation of inflammatory signalling mediators, such as NF-κB and toll-like receptor 4, influence animal food intake and weight gain (122,132,133). The inflammatory response to excess nutrient intake is an innate mechanism by which the brain can regulate energy homeostasis, which is also influenced by peripheral metabolic tissues.

There are sex-specific differences in FA metabolism and the neuroinflammatory response. Whole-brain tissue of high-fat fed female mice contains less SFA than the males of the cohort (134,135). Furthermore, exposure to high-fat diet

significantly increases uptake of SFA in brain tissue of male mice, while there is no difference in female mice (134). The sex-specific FA uptake is only observed in the brain tissue, and no differences between sexes are observed in plasma triglyceride levels between sexes. Furthermore, high-fat fed female mice have lower levels of *Tnfα* and *Il-6* mRNA in hypothalamic tissue than their male counterparts (135). This indicates that female mice have an attenuated hypothalamic pro-inflammatory response to dietary FA consumption compared to male mice, in part, due to sex-specific differences in neural FA uptake. This sexual dimorphism is abolished through knock-out of the oestrogen α-receptor (135). This difference may contribute to the observation that female mice are less susceptible to diet-induced obesity than males. If this assumption is true, then the neural pro-inflammatory pathways triggered in response to SFAs are involved in the progression of obesity.

The above studies suggest that the brain elicits complex regulation of energy status by communication between multiple peripheral organs and between brain regions. The brain decodes energetic status through a variety of means: hormones secreted by peripheral organs, neuronal communication via the vagus nerve, and pro-inflammatory responses to SFAs. In chronic high-calorie exposure the levels of circulating FAs are higher and may overwhelm the counter-regulatory response to high-fat intake which then may lead to dysregulation and hypothalamic damage.

1.3 A role for glia in regulating energy homeostasis in the hypothalamus

Glia is the term for a group of specialised cells of the nervous system, which in the CNS collectively refers to astrocytes, microglia, oligodendrocytes, and tanycytes. The name ‘glia’ is derived from the Greek word for ‘glue’, originating from their roles in CNS structure and neuronal support. However, it has become clear that glial cells play a more active role in the brain and can even influence neuronal activity. Those of focus in the energy homeostasis field, so far, have been astrocytes, microglia, and tanycytes.

1.3.1 Overview of glial cell types

While macrophages can infiltrate the brain in some states (123), the brain is generally immune-privileged. The blood-brain barrier separates the brain from the peripheral immune system, so the brain forms its own defence against injury and disease (136). Microglia are the “macrophage-like” cells of the CNS. They are mobile, phagocytic and found throughout the brain; they are specially designed for detection and removal of pathogens, debris and apoptotic neurons (137,138). In experimental paradigms using the rodent brain, ‘at rest’ microglial cell bodies remain relatively static but their processes are ever extending and retracting – surveying the brain parenchyma (139). Microglia are a self-renewing population, coupling proliferation with apoptosis so that the overall cell density remains relatively stable (140,141). As well as housekeeping, microglia are important in neurogenesis and early brain development (137,142).

Astrocytes are one of the larger forms of glial cell. Named after their star-like cytoskeletal structure, many astrocytes contain glial fibrillary acidic protein (GFAP) which is commonly used as an astrocyte cell marker. Astrocytes form the tripartite synapse with pre- and post-synaptic neurons (143). Here, they modulate neuronal communication and assist with neurotransmitter uptake from the synapse. Astrocytes also provide nearby neurons with nutrients, such as lactate and glutamate (144–147). Like microglia, astrocytes are plastic and dynamic (148–151). They are also motile, can proliferate and alter their morphology by increasing the number of processes and branching.

Tanycytes are specialised ependymal cells that are interspersed within the walls of the ventricles, most notably the 3V. Here, the cell bodies align with the ventricle while the processes reach out into the hypothalamic nuclei. There are two sub-types of tanycyte with different functions: α- and β-type. Tanycytes are involved in the interface between the BBB and the blood-cerebrospinal fluid (CSF) barrier (152–154). Consequently they are well placed to mediate the communication of nutrients and signals from the CSF of the 3V to the hypothalamus (121,155–163). They also contribute to generation of new neural cells and hormone release (164,165). A role for tanycytes in neuroinflammation has been postulated but not well-characterised (166,167). Nonetheless, tanycytes are key neural cells for nutrient sensing and hypothalamic function.

1.3.2 Glia and reactive gliosis

Upon detection of brain injury or insult, microglia and astrocytes undergo structural and functional changes to minimise the damage. This process is referred to as reactive gliosis (Fig 1.3.1). It is characterised by increased complexity (termed ramification) of processes in astrocytes (168), and retraction of processes in microglia (169,170). In both glial types, proliferation and migration to the site of damage is common, alongside secretion of chemokines (171). Evidence suggests that microglia are the first responders to the insult and subsequently trigger activation of astrogliosis (172,173).

Consumption of a high-fat diet (HFD) is a trigger for reactive gliosis. The microglial marker *Cd68* (mRNA) has been demonstrated to be upregulated in the hypothalamus following one day of high-fat feeding in rats (125). An increase in number and size of microglia was observed after three days of HFD exposure and persists for up to two weeks. Increases in *Gfap* mRNA was also observed from day one of feeding a HFD, and GFAP protein expression in the Arc peaked after 7 days before reducing to baseline at week three. Moreover, GFAP upregulation was observed again at eight months exposure to a HFD: examined as increased densitometry, associated with increased number and size of the astrocyte cytoskeleton. Microglial markers were measured until 28 days of high-fat feeding in this study (125), but also at 4 weeks (174,175), 8 weeks (176,177), 10 weeks (178), and 8 months (179) by other groups. The study by Thaler *et al* (125) was the first indication that reactive gliosis (micro- and astrogliosis) in response to high-fat diet occurs in two waves, at acute and then at chronic dietary exposure. It has since been observed in different mouse strains (175,180,181) and in humans (125), but also contradicted by others (182,183). Increases in glial expression associated with diet-induced obesity are most prominent in hypothalamic regions such as the MBH, DMH and PVH – but have also been observed in other brain regions (178,180,184). High-fat feeding increases glial markers that are indicative of proliferation and morphological changes, the hallmarks of reactive gliosis (185).

As covered previously, there are several means by which hypothalamic inflammation can be induced by diet. One route is by SFAs entering the brain through the circulation, another by peripheral immune cells and signals infiltrating the CNS, and also by cell stress and death of appetite-regulating neurons (125).

These paths are reflected in research uncovering the cellular mechanisms underlying diet-induced gliosis. Treatment of cultured primary astrocytes and primary microglia with SFAs induces secretion of pro-inflammatory cytokines (186–188). Diet-induced increases in GFAP expression are associated with the vasculature of the brain (178,180,184). Microglia of the Arc, taken from wild-type mice fed high-fat diet for 16 weeks, showed a marked accumulation in immunoglobulin-G (IgG) (189). This was not observed in leptin-deficient *ob/ob* mice, indicating that a high-fat diet and not elevated body weight alone mediates the increase in microglial inflammatory signalling. These observations both imply regulation at the BBB, suggesting increased permeability and an influx of pro-inflammatory signals. In addition, it has been suggested that circulating myeloid cells infiltrate the hypothalamus of diet-induced obese mice which may differentiate into microglia (123,174). Nonetheless, reactive gliosis in response to high-fat diet may occur through different means.

Negative energy balance can also induce reactive gliosis. In a mouse model of pancreatic-ductal adenocarcinoma with cachexia, both reactive microglia and astrocytes were identified in the MBH and hippocampus (190). Pharmacological depletion of microglia is associated with accelerated cachexia physiology, indicating that increased microglial number and reactivity may be functionally protective against weight-loss in this model. Astrocyte activation, but not microglia, was observed in the MBH of mice that underwent weight-loss following diet-induced obesity (182). These studies provide further indication that there is a range of stimuli which may elicit the reactive gliosis response within the cells. This must be considered when manipulating function of these glial cells.

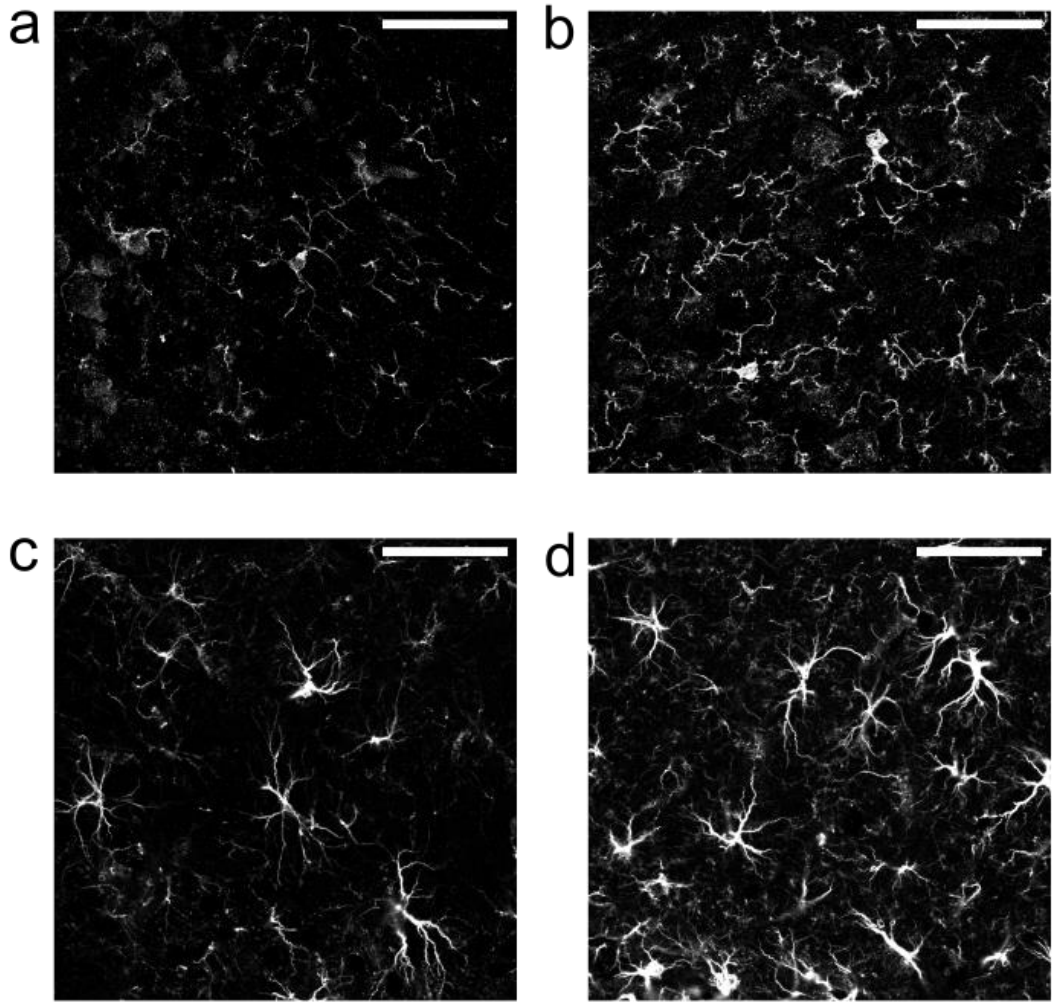

Figure 1.3.1 Example images of reactive gliosis, in microglia and astrocytes, in the mouse brain.

Ionised calcium-binding adaptor molecule 1 (IBA1) immuno-labelled microglia at resting state (a) and activated (b) in the mouse hippocampus. Increases in number and changes in cell morphology are apparent. GFAP-immunoreactive astrocytes at rest (c) and activated (d) in the mouse hippocampus show increases in number of processes. Images taken at 63x magnification and scale bars represent 50 μm.

1.3.3 Glial contribution to nutrient sensing

As described in brief above, tanycytes are important cells for nutrient sensing at the 3V and median eminence. Tanycytes take up lipid droplets from the circulation for metabolism (163). Manipulation of this process influences weight gain in mouse models (156,163,191). It is possible that one of the mechanisms that influences weight gain is via the neurogenic tanycytes by the ME, which produce appetite-regulating neurons at the Arc (156). As well as lipids, tanycytes are capable of glucose sensing and amino acid detection (160,161).

Microglia are also responsive to FAs and glucose as sources of energy. They present lipid-associated receptors, express genes involved in lipid metabolism (192), and possess the enzymes required to process energy through glycolytic and oxidative means (193). This suggests that microglia have metabolic flexibility, a finding which has been recapitulated *in vitro* (194). Common with neurons, microglia predominantly express the glucose transporter 3 (GLUT3) isoform as well as being unique in their presentation of GLUT5 (195,196). The ability of microglia to use a wide range of substrates suggests that they are highly resilient in different energy states.

Astrocytes are involved in nutrient sensing, working collectively to support neuronal function. They take up glucose in response to activation of receptors by insulin and insulin-like growth factor 1 (IGF-1) (197,198), and are considered to be crucial in mediating glucose transport across the BBB (198). Astrocytes can communicate amongst each other via gap junctions. Exposure to hyper- and hypoglycaemia in rats alters the level of proteins that form gap junctions – connexions-30 and -43 – which are enriched within the rat hypothalamus compared to other brain regions (199). Hereby, hypothalamic astrocyte crosstalk is responsive to whole-body glucose levels. Astrocytes are also responsive to lipid levels that reach the brain. Within the hippocampus, proteins responsible for lipid metabolism were identified in astrocytes but not in neurons (200). Astrocytes are also able to endocytose fatty acid products that are secreted from neurons (201). Consequently, astrocytes work with other astrocytes and also neurons to support nutrient sensing and uptake.

1.3.4 Glial regulation of energy homeostasis

As well as mediating the responses to nutrients, astrocytes can respond to feeding-associated hormones. Ablation of the insulin receptor in astrocytes impacts whole-body glucose homeostasis (198), which indicates a crucial role for astrocytes in conveying glucose levels as well as glucose sensing. This likely occurs through astrocyte-neuronal communication, as activation of astrocytic insulin receptors induces POMC neuron activity (198). Astrocytes express receptors for leptin and ghrelin; hormones which both downregulate expression of glucose transporters in the astrocytes (202,203). NTS astrocytes are responsive to glucagon-like peptide-1 (GLP-1) receptor agonists (204). In the

CNS, GLP-1 is a NTS neuropeptide involved in feeding termination, for which agonists have been developed as pharmaceutical interventions for weight-loss (205,206). Pharmacological inactivation of NTS astrocytes attenuates the feeding-suppressive effects that are mediated by synthetic GLP-1 agonists. In a separate study, chemogenetic activation of NTS astrocytes considerably reduced food intake in mice (207). These studies show that astrocytes are crucial in mediating whole-body effects of hormones and other peripheral factors.

Glia are capable of communicating signals locally across the brain parenchyma through gliotransmission. Microglia, as the immune cells of the brain, typically convey messages through release of cytokines and inflammatory mediators. For instance, preventing microglial NF-κB signalling attenuated diet-induced food intake and weight gain in mice (174). It is likely that microglia can modulate neuronal function in other ways, such as through transient contact by processes (208), though little has been reported in relation to energy homeostasis. Meanwhile, astrocytes are known to use a range of transmitters to modulate neuronal function. For example, action at astrocyte insulin receptors causes release of adenosine-triphosphate (ATP) (209). Astrocytes express acyl-CoA-binding protein (ACBP), a peptide that can bind to long-chain FAs (LCFAs) and the deletion of which induces food intake and obesity in mice (210,211). This is proposed to be mediated by melanocortin-expressing neurons (211). Other examples of astrocyte-neuronal communication are through calcium signalling, and release of D-serine and lactate (212–215). Astrocyte inflammatory signalling, such as IKKβ/NFκB pathways, is also crucial in mediating diet-induced gliosis and weight gain (216). Although the notion of gliotransmission has been disputed (217), many studies have demonstrated that glia communicate with neurons via a multitude of pathways to convey an effect such as regulating food intake.

Glial protein expression and metabolism impacts the whole organism. Disruption of astrocytic lipid uptake, through knock-out of lipoprotein lipase in GFAP-positive cells, increases body weight gain (as fat mass) and food intake in high-fat fed mice (218). Increases in expression of ionised calcium-binding adaptor molecule 1 (IBA1; a microglial cell marker) and AgRP are also observed in the MBH of the knock-out mice. These mice are less glucose-tolerant than the controls, indicating enhancement of adverse diet-induced obesity mediated effects. On the other hand, inactivation of Arc AgRP neurons was achieved by specific chemogenetic

activation of Arc astrocytes which also attenuated ghrelin-induced feeding (219). In microglia, selective deletion of uncoupling-protein 1 conveys resistance against diet-induced obesity (177). This is attributed to activation of Arc POMC neurons, which are anorexigenic. These studies suggest that glia of the Arc can modulate neuronal function to affect food intake, which may have other metabolic effects such as on glucose clearance. Other studies that support this notion include astrocytic over-expression of IL-6, which provides protection against diet-induced obesity in mice (220). Overexpression of sirtuin-1, a cellular energy sensor, specifically in astrocytes results in hyperphagia and weight gain, while downregulation causes the inverse effect (221).

The maladaptive comorbid effects of obesity are also potentially mediated by glia. A mouse model of Alzheimer's disease, fed a chronic high-fat 'Western' diet, demonstrates plaque accumulation alongside increases in the number of IBA1-positive microglia (181). Diet-induced microgliosis in rats is demonstrated to affect rhythmicity of circadian clock genes in the microglia and disrupt the expression profile of immune-related genes (222). Microglial dysfunction and inflammation through high-fat feeding is also proposed to be associated with age-related neurodegeneration (223). Chronic, but not acute, high-fat exposure is linked to hippocampal microgliosis and impaired performance in object-location tasks in rats (178). Pharmacological inactivation of microglia with minocycline rescues hippocampal-associated cognitive impairment. No significant changes in GFAP-positive cell number or size were detected within the hippocampus in this experiment, and so the cognitive decline associated with high-fat intake was proposed to be a consequence of microglial activation. However, another research group has identified increased expression of GFAP in the hippocampus of mice fed high-fat diet for 12 weeks compared to mice maintained on standard chow (224). This group also observed reduced expression of connexin-43, with no impact on memory tasks but an increase in experimental measures of anxiety. Chronic high-fat diet consumption has been shown to reduce performance of rats in object-location tasks, which is rescued by pharmacological inactivation of hippocampal microglia (178). Although the neuro-circuitry linking hypothalamic inflammation to loss of cognitive performance is not yet identified, it is clear that inflammatory signalling mediated by both astrocytes and microglia throughout the brain is crucial.

Hypothalamic glia are responsive to a wide range of stimuli that infer energy levels. Manipulation of expression for a variety of glial proteins in the mouse brain can elicit changes in food intake and weight gain, even when the animals are exposed to an obesogenic diet (174,177,218,220,221). This indicates that glial function is crucial in the regulation of energy status. This is supported by selective activation of hypothalamic astrocytes reducing food intake, including when orexigenic stimuli are present (207,219). Together, these studies suggest that homeostatic regulation is facilitated by glial-invoked action on neurons. This may be achieved by morphological changes that are observed in reactive gliosis (125,180,182), such as increased glial process connections with neurons (198,225), and also glial-mediated signalling including cytokines and gliotransmitters (174,204,216,218,220,221,226). Therefore, glia are clearly heavily involved in the regulation of energy balance and are also implemented in the comorbid consequences of obesity. Nonetheless, the underlying mechanisms within and between the cells is yet to be fully understood.

1.4 Overview of TSPO pharmacology

The mitochondrial translocator protein of 18 kDa (henceforth referred to as TSPO) is a common cell marker used to identify reactive astrocytes and microglia. It is expressed at low levels in the healthy brain, but upregulated in glia during neuroinflammation (172,227,228). Presence of neuroinflammation is a crucial indicator for status and progression of brain disease or injury, as well as a target for treatment (229). Consequently, the ability to visualise the extent of neuroinflammation *in vivo* is a useful tool both for research and in clinical practice.

Many synthetic ligands have been developed, bound to radioactive tracers, to identify sites of high TSPO expression in imaging with positron electron tomography (PET). These ligands have also been applied to study the elusive function of TSPO as well as treatment in neuropathology (230–234). They have also been used in pre-clinical studies examining TSPO function and identifying the structure of the TSPO protein. In addition, there are many endogenous small

molecules that are proposed to bind to TSPO (Fig 1.4.1) (235–237). Studying the function of these could help allude to the function of TSPO across tissues.

TSPO is a channel protein formed of five transmembrane helices alongside cytosolic loops (Fig 1.4.1) (238). It demonstrates dynamic structural changes; its tertiary structure only stabilises following ligand binding and its able to transition from monomer to polymer in the mitochondrial outer membrane (238,239). Binding of the synthetic TSPO ligand, PK11195, has been associated with the monomeric form of TSPO (240) and its aromatic residues of the cytosolic loops (241). TSPO contains a cholesterol-binding amino acid consensus (CRAC) motif, which is associated with its primary structure (237) and at which binding is preferential when the protein is in its polymeric form (239,242). A polymorphism in TSPO has been identified, although its influence on ligand binding capabilities is debated (243,244). TSPO forms a complex with many other mitochondrial proteins - such as voltage-dependent anion channel (VDAC) (245), adenine nucleotide transporter 1 (ANT1) (Fig 1.4.1) (245), and steroidogenic acute regulatory protein (StAR) – which is likely to influence the protein structure and ligand binding capability. These studies suggest that TSPO is highly dynamic in its structure and ability to bind to ligands.

1.4.1 Endogenous TSPO ligands

The most studied endogenous ligand in relation to TSPO binding is cholesterol. Cholesterol is a type of lipid and contributes to the structure of the cell membrane, as well as being an essential molecule for synthesis of steroid hormones (246). A CRAC motif was identified in the structure of TSPO, and so it was considered that TSPO was involved in cholesterol transport to the inner mitochondrial membrane (236,237). Import of cholesterol to the mitochondria is the rate-limiting step of steroidogenesis. It was thought that the channel, formed by the transmembrane helices, enabled transport of cholesterol (247). Interestingly, the human rs6971 polymorphism is associated with alterations in cholesterol binding – which results in increased plasma cholesterol levels in humans (243,248). It is apparent that TSPO can bind to cholesterol, but the downstream outcome is not clear.

An additional endogenous ligand that was proposed to bind to TSPO, and since criticized, is haem. The porphyrin ring of haem was initially found to compete for binding with benzodiazepines (244,249–252), which was associated with a role for inducing haemoglobin synthesis (253,254). Interestingly, the authors here commented on a structure-activity relationship in this function for TSPO (253). However, in an additional study, TSPO -/- mice did not show any changes in haemoglobin levels or number of erythrocytes resulting from their genotype (255). This suggests that there may be a high level of compensation in TSPO deficiency, or another scenario in which TSPO binding and function is misunderstood.

Originally identified as a benzodiazepine-like receptor, ligands of the benzodiazepine family are capable of binding to TSPO. Compounds that are synthesised *in vivo* and have benzodiazepine-like effects are typically referred to as 'endozepines' (235). These ligands are thought to be capable of anxiolytic features, are neuroprotective and can regulate metabolism (211,256–258). However, whether they require TSPO to elicit their effects is unknown. Acyl-CoA binding protein (ACBP), also known as diazepam-binding inhibitor, is an endozepine peptide that has been reported to bind to TSPO (235,259). ACBP is also crucial in fatty acid metabolism, as it can bind to esterified long-chain fatty acids (LCFAs) within the cell (256,260). It is strongly expressed in tissues with high lipid metabolism, and also in hypothalamic glia - including the tanycyte/ependymal cell layer of the 3V (261,262). ACBP activity in hypothalamic glia is proposed to be a route by which astrocytes can sense FAs and modulate appetite (210,211,262). However, there is contention as to whether ACBP elicits these functions via TSPO.

ACBP is processed within the cell to form smaller ligands: octadecaneuropeptide (ODN) and triakontatetraneuropeptide (TTN). ODN is thought to be the subunit responsible for the appetite regulatory effects within the hypothalamus (263). Competition pharmacological assays with exogenous ligands detailed that ODN acts though a metabotropic receptor on astrocytes and co-administration with a TSPO inhibitor did not inhibit its effects, suggesting that ODN does not bind to TSPO to mediate its effects (258). Consequently, appetite modulation by ACBP is unlikely to act via TSPO either. TTN, on the other hand, can stimulate aggressive behaviour in rats and steroid synthesis *in vitro* – both of which were alleviated by treatment with synthetic TSPO ligands PK11195 and Ro5-4864

(264–266). This suggests that TTN, PK11195 and Ro5-4864 bind to the same site on the TSPO structure. TTN can also enhance the LPS-induced secretion of pro-inflammatory cytokines (267–269). A selective metabotropic endozepine receptor antagonist is able to compete with ODN, indicating specificity for such receptors. In conclusion, the appetite modulating effects of ACBP are unlikely to be mediated by TSPO. However, ACBP can influence TSPO signalling via its cleavage product TTN – which has consequences on steroidogenesis and inflammation.

1.4.2 Synthetic TSPO ligands

Ligands for TSPO have been tested for capabilities in treating neuroinflammatory disorders, such as Alzheimer's disease (AD) as well as psychiatric illness (270–278). Etifoxine, an anxiolytic drug that binds to TSPO, provides protective benefits in a model of neurodegeneration in Sprague-Dawley rats (279). Both PK11195 and Ro5-4864 have therapeutic potential in a mouse model of AD and of diabetic neuropathy (230,233,280). With PK11195, the most notable changes in AD pathology are in tests of memory and less so in amyloid-β load (233) – contrary to the Ro5-4864 study (230). This suggest different pathways in which these TSPO ligands exert their effects, which may also not be mediated by TSPO. In an additional study where C57BL/6 mice were treated with LPS after PK11195 administration, cognitive function is protected in the drug-treated mice, but in the absence of any attenuation in pro-inflammatory cytokine levels (281). Studies that have investigated therapeutic potential of TSPO provide some insight as to the function of TSPO. Further information is required on the binding and specificity of TSPO ligands prior to concluding functions from such studies.

The specificity of TSPO ligands have been under scrutiny, considering their contradictory effects in downstream functions. For example, there are dose-dependent changes in effects of PK11195 and Ro5-4864 which can cause both opposite and similar physiological changes (240). Importantly, the two drugs have different binding sites on the TSPO protein (282). Treatment with PK11195 in the steroidogenic MA-10 Leydig cells increased progesterone production, which was not attenuated following TSPO knock-down in the cells (283). Although compensatory effects could be present, this indicates that PK11195 can elicit effects outside of TSPO expression which clouds the inferences regarding TSPO

function. The contradictions in TSPO ligand effects amongst the literature not only indicate a lack of specificity, but also suggest dynamics in the structure of TSPO. This may also be influenced by complexes with other mitochondrial proteins and competitive-binding with endogenous ligands.

The actions of both exogenous and endogenous ligands at TSPO indicate multiple functions for TSPO, but interpretation clouded by off-target effects of these ligands. Furthermore, it would appear that the structure of TSPO is dynamic – altering the exposure and ligand-affinity at its binding sites. The role of TSPO may be influenced by the extra- and intra-cellular environment at that time (Fig 1.6.1). Furthermore, investigations of ligand binding have been performed through competitive-binding studies with other TSPO ligands – some of which have since been reported to have off-target effects. Consequently, there is much progress to be made in understanding TSPO and its pharmacology.

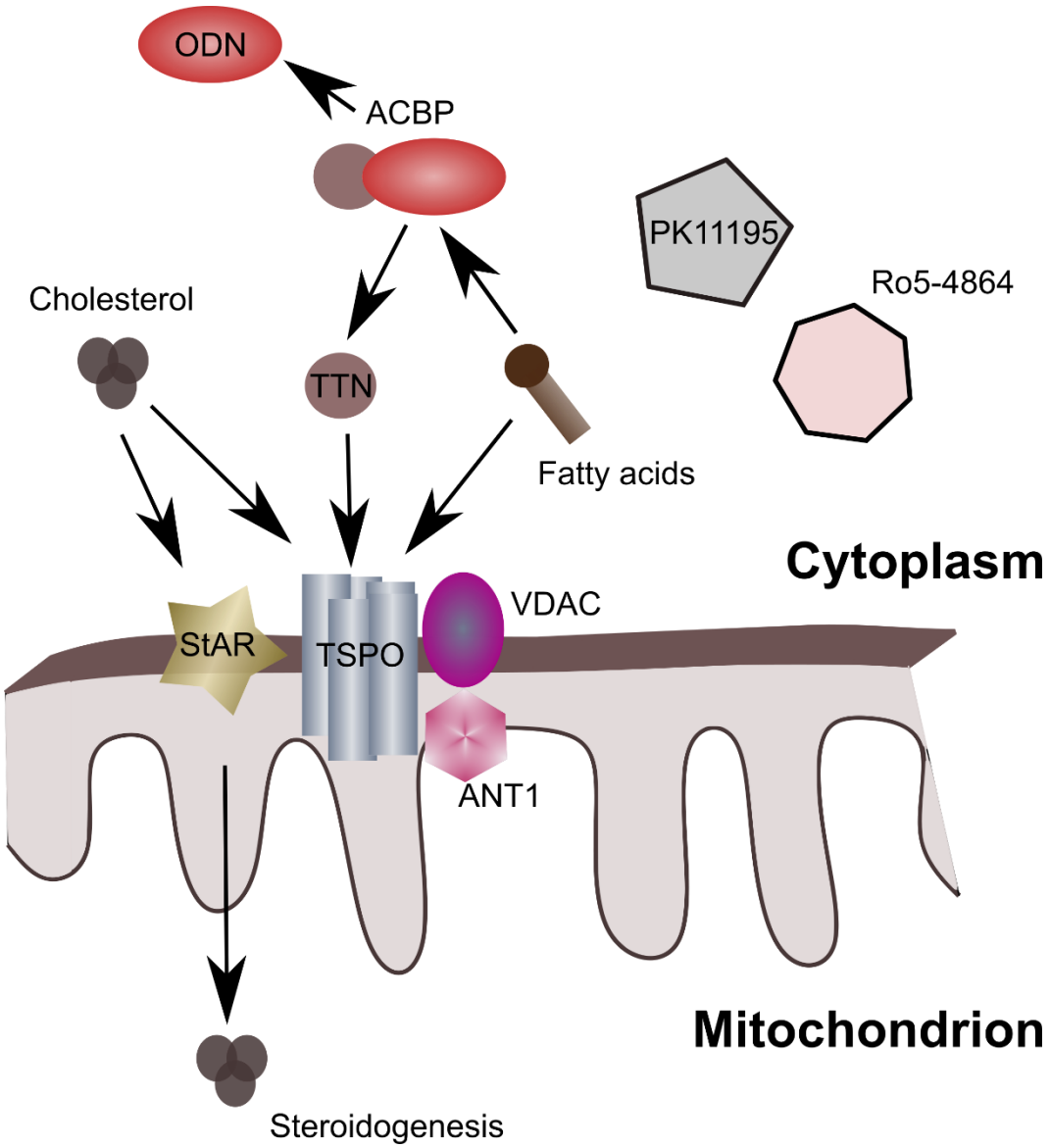

Figure 1.4.1 TSPO is identified to form complexes with multiple other mitochondrial proteins, as well as potentially bind to a wide range of ligands.
Key: Acyl-CoA binding protein (ACBP); adenosine transporter protein 1 (ANT1); octadecaneuropeptide (ODN); steroidogenic acute regulatory protein (StAR); mitochondrial translocator protein 18 kDa (TSPO); triakontatetraneuropeptide (TTN); voltage-dependent anion channel (VDAC).

1.5 TSPO expression in the brain

While TSPO expression in states of neuroinflammation is an important focus, there have been published attempts to identify expression and function of TSPO in neural cells. TSPO has been identified in regions of the mouse brain in absence of neuroinflammation: the olfactory bulb, choroid plexus, dentate gyrus, ependymal layers and in the cerebellum (284). TSPO immunoreactivity has also been identified in the endothelial cells surrounding the vasculature throughout the brain (284). TSPO expression across a range of neural cells may be a reflection of its involvement in different cellular processes.

1.5.1 TSPO expression in microglia

As previously discussed, microglia are the resident immune cells of the CNS. TSPO upregulation as a biomarker for neuroinflammation is commonly attributed to activated microglia (228,285–287). While microglia express TSPO, up-regulation in microgliosis can occur in a heterogeneous and dynamic manner. In rats with dopaminergic neuronal degeneration to model Parkinson's disease, radiolabelled ligand binding to TSPO increases alongside disease progression (288). This correlates with increased IBA1-positive immunoreactivity in *ex vivo* analysis. Interestingly, increases in TSPO radiolabelling occur in the rat striatum in the same study but in the absence of any changes in IBA1- or GFAP-immunoreactive cells. This suggests that TSPO expression can be upregulated without changes in microglia number corresponding to gliosis, possibly reflecting changes in glial function instead. In age-associated neuroinflammation, with which microgliosis can be observed, TSPO expression is not upregulated in the cortex and hippocampus of aged mice compared to young (289). Nonetheless, TSPO still co-localises with IBA1. Co-localisation also occurs with the mitochondrial marker, ATP synthase, within and outside of microglia, implicating TSPO expression in other cells. In mice with neuroinflammation induced by trimethyltin, TSPO expression coincided with microglia that were deemed to be reactive (172). This expression of TSPO appears temporally dynamic, alongside reactivity of the microglia, as expression is not identifiable until 14 days post-treatment. TSPO immunoreactivity also subsides by 6 weeks post-treatment, as does the reactive status of the microglia. These findings indicate that stimulus

and context are crucial for TSPO upregulation, and that upregulation in microglia can be dynamic.

Less is known about TSPO expression in resting microglia of healthy brains, as its expression is much lower. A study looking in the brains of healthy C57BL/6 mice did not identify any co-localisation between TSPO and the microglial markers, IBA1 and CD11b+ (284). However, this study only considered limited regions of the mouse brain and the published images taken at higher magnification appeared to focus on TSPO expression around blood vessels in the brain. This contrasts with a previous study in which TSPO was co-localised with CD11b in brain tissue from the study control group (227). It may be that expression of TSPO is not necessarily a marker of activated microglia, and could reflect other functions dependent on region and experimental model.

Manipulation of TSPO expression or function can influence microglial activity. Such manipulation can be performed by altering TSPO gene expression or through application of TSPO ligands. In microglial BV-2 cell culture, knock-down or over-expression of TSPO promotes and suppresses an inflammatory phenotype, respectively (286). Treatment of cells with TSPO ligands can also attenuate cytokine release stimulated by lipopolysaccharide (LPS), a component of bacterial endotoxins (290,291). Meanwhile, in a rodent model of neurodegeneration caused by injection of quinolinic acid into the striatum, TSPO ligands reduce neuronal cell death caused by the toxin as well as enhance the expression of the activated microglial marker OX-42 (285,292). The TSPO ligand, PK11195, also reduces the up-regulation of pro-inflammatory cytokine mRNA following quinolinic acid-induced damage (292). Modulation of either TSPO expression or activity can in turn influence the inflammatory phenotype of microglia. This occurs in both isolated cells and in vivo rodent models.

1.5.2 TSPO expression in astrocytes

TSPO expression in the brain is also attributed to astrocytes, where it is upregulated during neuroinflammation. Astrocytes contribute to multiple functions in the healthy brain, and cooperate with microglia during neuroinflammation. Induction of astrogliosis is associated with increases in TSPO expression levels. In the trimethyltin-induced neurodegenerative rat model previously discussed

(172), TSPO immunoreactivity was seen to coincide within the main cell bodies of the GFAP-positive astrocytes but not in the projections. Furthermore, the study also commented on the timeline of astrocytic reactivity in response to the toxin: Astrogliosis was observed later and over a longer period than microgliosis, and astrocytes expressed TSPO at all stages of activation unlike microglia (172). Other studies have alluded to a difference in glial dynamics regarding TSPO expression. In a model of neuroinflammation where rats received an injection of ciliary neurotrophic factor into the striatum, GFAP and TSPO expression were both upregulated and also colocalised (227). There were no changes in the level of microglial TSPO expression in these rats, indicating that upregulation of TSPO was specific to astrocytes in this experimental setting. In a mouse model of multiple sclerosis, TSPO and GFAP dual-immunohistochemical labelling showed minimal co-localisation in the corpus callosum and cortex of the mice and TSPO expression was absent in the control 'healthy' mice (293). When the researchers used a GFAP-eGFP reporter mouse line, which also received cuprizone treatment to model multiple sclerosis, the TSPO signal within the astrocytes was much clearer. In this experimental scenario the TSPO staining was localised to the astrocytic cell body as well as processes. This study emphasises that choice of cell markers and visualisation processes are very important to consider when studying co-immunoreactivity with proteins. Furthermore, the above studies collectively show that TSPO expression within astrocytes is upregulated in experimental settings of neuroinflammation. This can occur in absence of microglial expression of TSPO.

While TSPO expression is prominent in reactive astrocytes from animal models of neuroinflammation, this does not reflect expression levels in the healthy brain. In the healthy C57BL/6 mouse brain, TSPO immunoreactivity was not observed to co-localise with that of GFAP (284). As previously discussed with regards to microglia, this study appeared to focus on the vasculature of the brain and so glial expression elsewhere may have been overlooked. Meanwhile, in human brain tissue, coincidence of TSPO and GFAP immunoreactivity has been observed in post-mortem samples from both healthy individuals and patients with a range of brain diseases and injuries (294). With regards to brain disease, the level of TSPO expression in human astrocytoma has been associated with the grade of the tumour (295). These studies show that TSPO expression is present in

activated astrocytes, more so than astrocytes at rest, in the rodent and human brain.

TSPO ligands influence astrocyte function. As many synthetic TSPO ligands can pass the BBB, this provides potential for treatment of neuroinflammation. In C57BL/6 mouse primary astrocytes cultured with pro-inflammatory toll-like receptor ligands, pre-treatment with TSPO ligands reduces the secretion of pro-inflammatory cytokines (296). This reduction in the astrocyte cultures was modest compared to that in the cultured microglia from the same animals. In astrocytic T98G cells with glucose deprivation, pre-treatment with the TSPO ligand Ro5-8464 reduces cell death compared to no ligand treatment (297). Ro5-8464 pre-treatment also has protective effects on the astrocyte mitochondria, as production of reactive oxygen species were also reduced. With regard to *in vivo* markers of astrogliosis, co-injection of quinolinic acid with TSPO ligands to rats slightly reduces GFAP immunoreactivity compared to the quinolinic acid-only injected controls (285,292). PK11195, but not Ro5-4864, reduces vimentin immunoreactivity as a marker for reactive astrocytes in the rat hippocampus when co-injected into the cerebral ventricles with the bacterial endotoxin LPS (298). Furthermore, in a rat model of surgical-induced brain damage, intraperitoneal injection of Ro5-4864 had no effect on GFAP expression within the cortical injury compared to non-injected rats (299). Considering the above studies, the translational ability of targeting TSPO in reactive astrocytes appears to reflect the varied pharmacology of TSPO ligands.

1.5.3 TSPO expression in other neural cell types

TSPO expression in the brain has been reported in other neural cells, but there have been limited studies that provide insight into its function in these cells. Such cells include neurons, neural endothelial cells and tanycytes (294,300,301). It may be that there is minimal or no TSPO expression within these cells, or that the topic needs further investigation. A point to consider is what would be the function of TSPO in these cells. The possible role of TSPO in inflammation does not relate to the known roles of neurons, ependymal cells, nor tanycytes. Consequently, there may be processes involving TSPO in the brain that are outside of inflammation.

There have been minimal reports of TSPO expression in neurons. Co-immunoreactivity of TSPO with NeuN is observed in both C57BL/6 mouse and in human hippocampal brain tissue (300,302). TSPO immunoreactivity is also identified in healthy human cortical brain tissue, and less so in brain tissue taken from patients with HIV (294). However, the authors commented that this was only observed with the polyclonal antibody they used, and not the monoclonal, though specificity of both antibodies had been previously confirmed. The authors proposed that neurons may contain a different isoform of TSPO, or a structurally related protein. Subsequently, there is currently not enough evidence to confirm nor reject the notion of TSPO expression in neurons.

Although there has not been much focus on the role of TSPO in neural endothelial and ependymal cells, there is published qualitative research on expression around the ventricles and vasculature of the brain. Multiple studies that have investigated TSPO expression in glia have also identified TSPO co-immunoreactivity with endothelial cell markers (294,300) or immunoreactivity in a pattern akin to the brain vasculature (284). In the choroidal endothelial cell line RF/6A, TSPO was co-localised to the mitochondria and application of TSPO ligands altered cholesterol efflux, lipid accumulation and reduced secretion of pro-inflammatory cytokines (303). TSPO immunoreactivity has been identified to coincide with markers of tanycytes and endothelial cells which layer the 3V, which runs through the hypothalamus (301). Here, TSPO was suggested to be involved in metabolism of lipids circulating in the cerebrospinal fluid. The proposed role of TSPO in these cells of the brain appear to pertain to the roles of the cells, implicating cell-dependent function of TSPO.

TSPO imaging is a widespread application applied to many disease and injury states that involve inflammation, but cannot unpick the role of TSPO regulation in these disease states (300). Discrepancies between studies, in cases of TSPO regulation or disease paradigms, may be useful to resolve TSPO function and henceforth therapeutic translational potential. TSPO expression in the brain is attributed to multiple cell types, not all of which contribute to neuroinflammatory processes. Furthermore, the function of TSPO in these cells is not well understood. It is important to consider heterogeneity in TSPO expression, and that it may have functions in the brain outside of neuroinflammation.

Neuroinflammation puts a large metabolic demand on the tissue, and a positive correlation exists between neural uptake of fluorodeoxyglucose (FDG) and TSPO-ligand binding in mice (304). This suggests that areas of high glucose uptake in the murine brain are associated with relatively increased TSPO expression. The up-regulation of TSPO coinciding with high-glucose uptake may be involved at the interface of metabolism and neuroinflammation.

1.6 TSPO in peripheral metabolic tissue

As well as in the brain, TSPO is expressed to varying extents throughout the body (305). TSPO was first identified in the kidney, and named the peripheral benzodiazepine receptor (PBR) due to its ability to bind ligands of the benzodiazepine-like family. It is also strongly expressed in steroidogenic tissues, which implicated a role for TSPO in steroidogenesis (306,307). This is supported by its ability to bind cholesterol via a CRAC motif (236,237). In rodents, TSPO expression has been studied in white and brown adipose (308–312), cardiac (313–316), liver (317), macrophages (310,318,319), smooth muscle (320), and pancreatic tissue (321). TSPO is implicated in multiple different functions, and while the extent of TSPO function across tissues is not yet fully understood it is important to consider the overall functions of the cells and tissues in which it is expressed. Here, I will focus on TSPO expression and function in select metabolic organs.

1.6.1 TSPO in mitochondrial metabolism

One of the key roles for mitochondria is the regulation of energy production for cellular processes. Accordingly, they are responsible for a number of metabolic pathways. Important examples include oxidative phosphorylation - an aerobic process in which ATP is generated - and beta-oxidation of FAs to acetyl-CoA, which is then used to fuel the Krebs cycle and generate ATP. To complement these functions, mitochondria are highly dynamic and can undergo fission/fusion in response to energy demands. TSPO is implicated in mitochondrial processes relating to respiration and ATP production. This has been identified in a range of cell types (255,322–328). For example, knock-down of TSPO in mouse microglial

BV-2 cells impairs mitochondrial respiration and reduces ATP production (329). On the other hand, contradictory effects from *Tspo* manipulation have been measured in hepatocytes cultured from TSPO null mice (323) and in TSPO deficient MA-10 Leydig cells (330). In both studies, there was no alteration in mitochondrial respiration or ATP production resulting from absence of TSPO. This collection of studies suggest that presence of TSPO has an influence on ATP production and mitochondrial metabolism, although this effect appears to be cell and/or tissue dependent.

FAs, circulating in the blood stream or stored as lipid droplets, are also a key source of fuel for metabolism and are of particular relevance to deviations in energy state. FAs are the primary energy substrate in absence of glucose. Deletion of TSPO in mouse Leydig MA-10 cells resulted in a shift of fuel preference from glucose to FAs (330). In the hypothalamic neural cell line, A2/29, knock-down of *Tspo* enhanced FFA generation through lipophagy to produce ATP (301). As well as mitochondrial respiration, experiments in cell lines have alluded to an influence of TSPO on use of glucose as a fuel substrate. In a mouse adipocyte cell line, 3T3-L1, treatment with PK11195 increased glucose uptake following stimulation with insulin (311). TSPO expression can also be modulated by glucose treatment. In smooth muscle A10 cells, expression of TSPO increases in a dose-dependent manner with respect to glucose concentration (331). In addition, knock-out of TSPO expression in a human retinal pigment epithelial cell line resulted in an increase in glycolytic metabolites compared to wild-type cells (332). Cells, genetically manipulated to have reduced TSPO expression, exhibit increased glycolysis alongside reduced mitochondrial respiration as previously described (326,330). Some cell culture studies using immortalized cell lines may not fully represent of nutrient use in normal cells, for reasons involving altered metabolism in transformed cells and requirement for high glucose conditions in culture. If replicable *in vivo,* this could be indicative of a role for TSPO modulating glucose levels and metabolism in cells across different tissue types.

1.6.2 Adipose tissue

Adipose tissue is crucial for healthy storage of lipid reserves. It is also an important endocrine organ; it secretes adipokines – such as leptin – to convey the metabolic and health state of the tissue. Adipose tissue is an important site

of study for how metabolic disease can occur and progress. For instance, excess energy intake leads to adipose dysfunction which results in impaired fatty acid storage and leptin-mediated signalling. Furthermore, there are different forms of adipose tissue – white (WAT) and brown (BAT) – which have different contributions to energy regulation. TSPO expression has been identified in both of these forms (310,312,333). Imaging of TSPO has been applied to adipose tissue, in rodent and human studies. In female Balb/c mice that were treated with a β3 adrenergic agonist to induce browning of inguinal WAT, increased TSPO ligand binding in the browned WAT was observed while no change was measured in the interscapular BAT (312). TSPO-targeted imaging of BAT has also been used in healthy human participants (333).

TSPO expression is regulated in rodent adipose tissue in response to energetic demands. In a study in Sprague-Dawley rats, chronic administration of the antipsychotic drug olanzapine resulted in increased inflammatory markers in WAT but no changes to TSPO expression (334). This reinforces that there is a role for TSPO expression regulation outside of inflammatory processes. A model of stress in Sprague-Dawley rats, which involved a 24-hour fast, significantly increased TSPO expression in the epididymal WAT from a below-detection baseline (335). Accordingly, it has been observed that TSPO expression in epididymal WAT and interscapular BAT reduces in diet-induced obese C57BL/6J mice (310). This has been replicated in the MC4R -/- obese mice. These studies suggest that TSPO expression in adipose tissue is dynamic and reflects the metabolic status of the tissue.

1.6.3 Liver

The liver is an important metabolic organ involved in glucose homeostasis, glycogen storage, and bile production for fat metabolism amongst other roles (41,336). It is a site of metabolism for a variety of nutrients. It assists in glucose homeostasis by converting glucose into glycogen, or vice-versa, according to blood glucose levels. The liver is also important for breakdown of hormones, such as insulin, and is a source of cholesterol production (52,337–340). TSPO is strongly expressed in the rodent and human liver, and upregulation has been associated with both disease and alterations in metabolism (341,342).

TSPO can be used as a biomarker for imaging liver damage. For instance, upregulation of TSPO has been associated with liver disease progression from steatosis to non-alcoholic steatohepatitis (343). In a model of liver cirrhosis in Sprague-Dawley rats, TSPO expression correlated with disease progression (344). Immunohistochemical analysis identified expression to be localised to macrophages and hepatic stellate cells. In relation to liver damage arising from high-fat intake, exposure to a high-fat and high-cholesterol diet markedly reduced TSPO expression in the liver of Wistar rats (345). It is possible that TSPO-mediated signalling is involved in hepatic inflammation, depending on the stimulus, and may be a potential treatment target.

In addition to serving as a biomarker, manipulation of TSPO has been investigated as a potential mechanism to treat liver injury or disease. Etifoxine, a TSPO ligand used clinically for treatment of anxiety disorders (346), has been shown to increase TSPO expression in a liver cell line inoculated with hepatitis-C virus (342). The virus lowered mitochondrial membrane potential as well as liver lipid accumulation, both of which were recovered by etifoxine treatment. On the contrary, etifoxine enhanced the viral-induced insulin resistance measured in the cells. This may be situation dependent in the case of obesity versus injury/toxin induced hepatic inflammation. There may again be organism-dependent differences in TSPO regulation in the liver. The TSPO ligand PK11195 may be therapeutic in treating hepatic steatosis occurring from diet-induced obesity. Lipid accumulation in the liver was lower in high-fat fed obese mice that received chronic treatment of PK11195 (347). In addition to the reduced hepatic steatosis, chronic PK11195 treatment also improved glucose tolerance and reduced mRNA expression of pro-inflammatory markers, TNFα and Il-6, in the livers of the mice. This indicates that TSPO targeting has potential to improve liver disease state and glucose metabolism.

Whole-organism screening in zebrafish identified a novel role for TSPO in gluconeogenesis, which translated to mouse models (347). In food deprived C57BL/6 mice, administration of PK11195 enhanced fast-induced up-regulation of liver mRNA for genes involved in metabolism. These included carnitine palmitoyltransferase-1 subunit-a (Cpt1a), an important enzyme for fatty acid oxidation, phosphoenolpyruvate carboxykinase 1 (Pck1), and the catalytic subunit for glucose-6-phosphatase (G6PC) – which are involved in glucose

production (347). This effect was not seen in satiated mice. PK11195 was also able to decrease baseline glucose levels for up to 4 hours post-injection in fasted mice, suggesting that targeting of TSPO reduces hepatic glucose production despite up-regulation of gluconeogenic enzymes. These experiments indicate a translational opportunity for targeting TSPO to modulate glucose levels, which could prove to be protective in obesity.

1.6.4 Macrophages

As discussed previously, TSPO is connected to inflammatory processes in multiple tissue types. It is therefore not surprising that its expression has been detected in peripheral immune cells, such as macrophages (310,318,348–350). Macrophages are a mobile, phagocytic class of immune cell that are a crucial first-line of defence against invading pathogens (351). They are capable of infiltrating and residing in a variety of tissue types, in which they can be differentiated into sub-classifications.

Microglia, the resident macrophage-like cells of the CNS, have been demonstrated to upregulate TSPO expression in response to inflammatory stimuli (228,285–287,298,352). Subsequently, it is anticipated that macrophage expression of TSPO will also be pro-inflammatory. Radio-ligand PET imaging of TSPO has been shown to correlate with macrophage accumulation in patients of rheumatoid synovitis (353). However, in a study that used the cultured human monocytic THP-1 cell line as well as primary macrophage cultures from healthy people and patients with rheumatoid arthritis, TSPO expression was downregulated in the pro-inflammatory ‘M1’ macrophage state and unchanged in the anti-inflammatory ‘M2’ phenotype (318). This observation was repeated by another study comparing both rodent- and human-derived primary macrophage culture (350). Human-derived macrophage cells cultured into a pro-inflammatory state decreased their expression of TSPO, while rodent-derived macrophages increased their expression following pro-inflammatory stimulation. The controversy in these results suggest that there may be a species-dependent difference in macrophage TSPO regulation; Although, it could also depend on experimental setting – such as *in vivo* versus *in vitro*. Both studies used LPS as the primary pro-inflammatory stimulus, while TSPO regulation in human-derived macrophages could be more sensitive to pro-inflammatory cytokines. Meanwhile

an additional study demonstrated that the benzodiazepine, midazolam, exerted its anti-inflammatory effects in THP-1 cells through TSPO (354). The authors proposed that midazolam targeted TSPO, which in turn suppressed pro-inflammatory signalling such as NF-κB.

TSPO and high-fat diet intake is associated with inflammation throughout the organism. Macrophages have been seen to increase in number in metabolic organs such as WAT. Infiltrating macrophages in WAT of obese mice have been associated with increased TSPO expression (310). Although currently not investigated, inhibition of TSPO in models of obesity may reduce the pro-inflammatory state of macrophages. This in turn may be protective against the comorbid effects of obesity.

A breakdown of cholesterol homeostasis in macrophages can lead to lipid accumulation and the transition to a macrophage foam cell state (355–357). Macrophage foam cells are associated with cardiovascular disease, primarily atherosclerosis. Up- and down-regulation of TSPO in a human macrophage cell line increases and decreases cholesterol efflux, respectively (348). The reduction in intra-cellular cholesterol as caused by TSPO over-expression also resulted in a decrease in lipid accumulation within the macrophage cells. Consequently, it appears that TSPO expression in macrophages may be protective against cholesterol and lipid accumulation and reduce the negative impacts on atherosclerotic plaque formation in humans. Furthermore, there has been evidence to suggest that TSPO is a useful potential pharmacological target for atherosclerosis (358).

1.6.5 Steroidogenic organs

Steroidogenesis is a mitochondrial process that occurs in specific cell-types that contain the appropriate machinery. Steroidogenic cells produce steroids from cholesterol, obtained from either *de novo* synthesis or by intracellular transport of cholesterol bound to lipoproteins. Import of cholesterol into the cell is facilitated by low- or high-density lipoproteins. Once within the cell, cholesterol is either stored within lipid droplets or transported into the mitochondria. P450scc, located at the inner mitochondrial membrane, is the cholesterol side chain cleavage enzyme that metabolises cholesterol into pregnenolone. StAR is involved in

mitochondrial cholesterol import although some cases of steroidogenesis are StAR-independent, with TSPO implicated instead. Deletion of TSPO in Leydig MA-10 cells results in increased expression of StAR (359). This points to potential compensatory mechanisms for absence of TSPO that can be initiated through StAR expression. Adrenergic and gonadal cells are highly steroidogenic, as are neural cells. Steroids are an important class of signalling molecules, as well as crucial components of cell membranes.

The first attempts to generate TSPO mutant knock-out mice resulted in embryonic lethality (247). This led to the hypothesis that TSPO is essential for transportation of intra-cellular cholesterol across the mitochondrial membrane - the rate-limiting step for steroidogenesis. However, upon the subsequent successful generation of viable TSPO-deficient mouse models, the importance of its role in steroidogenesis caused much controversy within the field (322,325,360). Global TSPO deficient mice have been used by several researchers to study the impact of loss of TSPO signalling on steroidogenesis. In one such study, TSPO knock-out mice exhibited no difference in serum pregnenolone levels (325). Yet, in a different study, the TSPO null mice had significantly reduced production of steroids – particularly corticosterone (361). This study also emphasised a role for TSPO in maintaining androgen levels during aging. The TSPO knock-out mice were generated using the same method in both studies, but hormone collection and measurements differ. Methods of transgenic mouse generation and hormone measures may contribute to conflicting results between studies.

In addition to global knock-outs, tissue-specific deletion of TSPO in steroidogenic cells has also alluded to an impairment in circulating steroid levels. Steroidogenic factor 1 (SF-1) driven conditional TSPO knock-out in male mice led to impaired stimulated corticosterone secretion, but no effects on basal corticosterone levels (362). TSPO deletion in these mice occurred primarily in the adrenal cortex, which resulted in a compensatory increase of TSPO in the adrenal medulla. Expression was also reduced by half in the gonads. Plasma adrenaline levels were also greater in the knock-out mice (363). The authors concluded that the higher circulating adrenaline levels resulted in a pre-diabetic phenotype in the male mice, as exhibited by hyperglycaemia and lower c-peptide levels than controls. It is apparent that selective reduction of TSPO in steroidogenic organs impairs ability to produce adrenaline, which may have a wider impact on the organism,

including potentially glucose homeostasis. In a separate study, conditional knock-out of TSPO in the testicular Leydig cells of male mice did not alter plasma testosterone levels when compared to control mice with TSPO floxed alleles (360). Expression of StAR in the testes was also unchanged. Consequently, experimental methods applied to manipulate gene expression can have varying results – likely due to compensatory or tissue-specific mechanisms.

While conflicting findings on a role for TSPO in steroidogenesis points to species-, tissue- and method-dependant effects, it is also possible that TSPO is indirectly involved in steroid production. Application of PK11195 to astrocytic (steroidogenic) and fibroblast (non-steroidogenic) cell lines was able to modulate cholesterol import (364). Increased accumulation of cholesterol droplets and cholesterol efflux were observed, alongside reduced cholesterol esterification. Furthermore, the consideration that the structure of TSPO contains a CRAC motif (236,237) alludes to a role that involves cholesterol binding even if not transport.

Sex-dependent effects have been found in mice with reduced TSPO expression in steroidogenic organs. Gonadectomy in Sprague-Dawley rats resulted in increased *Tspo* RNA within the cerebral cortex of female, and increased *Tspo* RNA in the cerebellum of male, rats (365). In the female SF-1 driven knock-out mice, both basal and stimulated corticosterone levels were significantly lower compared to control. This effect was not observed in the male cohort (362). While the male knock-out mice exhibited increased blood cholesterol and glucose levels, as described above, no such differences were observed in the female mice (363). Sex-specific effects following manipulation of steroid synthesis are expected but consideration must be made when exploring other potential roles of TSPO.

The current literature regarding TSPO expression in tissues suggests a role in metabolism. This could be direct, such as in liver regulation of gluconeogenic enzymes, or indirect such as adrenal secretion of hormones that influence whole-body glucose levels. Pharmacological manipulation of TSPO in studies of metabolism have also contributed conflicting data, which may be due to off-target effects. Genetic manipulation of TSPO in cells provides a good basis for understanding; however, contradictions in such experimental findings point to

tissue/cell specific functions. Consequently, manipulation of TSPO expression at the tissue or system level may provide further insight to its function.

1.7 Summary of introduction

Obesity is a complex and progressive disease that affects multiple organs (7). It impairs ability to effectively sense nutrients and energy availability via the homeostatic hub of the brain, the hypothalamus(366). This region integrates signals from across the brain and throughout the body to then respond accordingly to the energetic state of the organism. Obesity causes systemic low-grade inflammation (123,125,367). This is observed in peripheral organs such as the adipose tissue and the liver, and also in the brain, where it is largely mediated by glial cells (125). Glia, primarily astrocytes and microglia, are dynamic cells that respond to brain injury or disease through structural and functional changes in order to mitigate the damage and maintain brain homeostasis. This process is termed reactive gliosis (368). Furthermore, these cells respond to saturated fatty acids (SFAs) with gliosis (175,187). This is accompanied with changes in mitochondrial metabolism of astrocytes and microglia. Prolonged exposure to the insult may lead the neuroinflammatory response to become maladaptive, which would explain energy balance dysregulation following excessive fat consumption. Reactive gliosis and the accompanying alterations in metabolism could provide insight into how homeostatic control of energy balance breaks down in obesity.

The mitochondrial translocator protein of 18 kDa (TSPO) is expressed across the organism in a heterogeneous fashion, including glial cells in the brain (298,304,319,369,370). Neural expression of TSPO is upregulated in reactive gliosis (172,227,228). This is taken advantage of in the clinic as a proxy biomarker for imaging neuroinflammation with PET imaging (230–234). TSPO is also present in metabolic organs such as adipose tissue, liver, and steroidogenic tissues (306–312,343,344). TSPO has been implicated in various functions, including mitochondrial metabolism, though the TSPO literature is clouded by seemingly conflicting data. *In vitro* studies have demonstrated that TSPO up-regulation alters the preferential route for cellular metabolism to glycolysis (326,330,332). *In vivo*, targeting TSPO expression has shown alterations in

glucose homeostasis and alterations in the susceptibility to metabolic consequences of obesity. Considering the roles of TSPO in neuroinflammation and metabolism, TSPO could be a fruitful link to study the mechanisms underlying the breakdown of energy homeostasis.

1.8 Hypothesis and aims

The overarching hypothesis of this research project is as follows: TSPO is involved in mitochondrial metabolic fuel preference and metabolic flexibility. TSPO is up- or downregulated in response to metabolic demand, which facilitates the tissue response to nutrient availability or pro-inflammatory stimuli. This hypothesis is tested using the following three research aims, which are investigated in the next three chapters.

1. To characterise the distribution of TSPO in brain regions involved in energy homeostasis
2. To examine the regulation of TSPO expression during energy imbalance
3. To investigate whether modulation of TSPO will influence regulation of energy homeostasis

Chapter 2: Materials and Methods

2.1 Chemicals

Chemical	Supplier	Catalogue number
Acrylamide 30%	Scientific-laboratory supplies	NAT1260
Agarose	Fisher	10688973
Ammonium persulfate (APS)	Sigma-Aldrich	A3678
Benzamidine	Sigma-Aldrich	1207
Bovine serum albumin	Sigma-Aldrich	A2153
Bromophenol blue sodium salt	Sigma-Aldrich	B5525
4',6-diamidino-2-phenylindole,dihydrochloride (DAPI)	Fisher	D1306
Dimethyl sulfoxide (DMSO)	Sigma-Aldrich	D2650-5X5ML
DPX Mounting Medium	Sigma-Aldrich	06522-500ML
DreamTaq HS Green Master Mix	Fisher	15689374
Eosin-Y	Sigma-Aldrich	1.02439
Ethanol	Thermo Fisher	E/0650DF/17
Ethylenediaminetetraacetic acid disodium salt (EDTA)	Sigma-Aldrich	E1644
Ethylene glycol-bis(β-aminoethyl ether)-N,N,N′,N′-tetraacetic acid (EGTA)	Melford	E1102
Fluoroshield Mounting Medium	Abcam	Ab104135
Fluoroshield Mounting Medium, with DAPI	Abcam	AB104139
GelRed nucleic acid gel stain	Cambridge Bioscience	BT41003
Generuler 1kb Plus	Fisher	10101240
Glucose	Sigma-Aldrich	G7021
Glycerol	Sigma-Aldrich	49767
Glycine	Melford	G0709

Chemical	Supplier	Catalogue number
Hematoxylin solution, Gill No. 2	Sigma-Aldrich	GHS316
Hydrochloric acid (HCl)	Fisher	258148-500ML-D
Methanol	Sigma-Aldrich	34860-2.5L-R
N,N,N′,N′-Tetramethylethylenediamine (TEMED)	Sigma-Aldrich	T7024
Normal donkey serum	Sigma-Aldrich	D9663
Paraformaldehyde	Fisher	P/0840/53
Phenol:Chloroform:Isoamyl alcohol	Fisher	10308293
Phenylmethanesulfonyl fluoride (PMSF)	Sigma-Aldrich	P7626
PK11195	Tocris	0670
Precision Plus Protein Dual Color Standards	BioRad	1610374
Primers (TSPO)	IDT	
Protein Assay Dye Reagent	BioRad	500-0006
Proteinase K (recombinant), PCR grade	Fisher	10308293
REVERT™ Total Protein stain	LI-COR	926-11021
REVERT™ Wash Solution	LI-COR	926-11012
Skimmed milk powder	Sigma-Aldrich	70166-500G
Sodium azide	Fisher	10592211
Sodium Chloride (NaCl)	Sigma-Aldrich	S7653-5KG
Sodium dodecyl sulphate (SDS)	Melford	B2008
Sodium fluoride (NaF)	Sigma-Aldrich	S7920
Sodium hydroxide (NaOH)	Fisher	10396240
Sodium orthovanodate (NaVO4)	Sigma-Aldrich	S6508
Sodium phosphate dibasic anhydrous	Sigma-Aldrich	RES20908-A702X
Sodium phosphate monobasic anhydrous	Sigma-Aldrich	RDD007-1KG

Chemical	Supplier	Catalogue number
Sodium pyrophosphate tetrabasic decahydrate (NaPPi)	Sigma-Aldrich	S6422
Sucrose	Melford	S0809
Tris	Melford	B2005
Tris-acetate-EDTA	Fisher	10041223
Triton X-100	Fisher	BP151-00
Tween-20	Sigma-Aldrich	P2287
Xylenes	Sigma-Aldrich	534056
β-mercaptoethanol	Sigma-Aldrich	M3148

Table 2.1 List of chemicals used in this research project, along with suppliers.

2.2 Equipment

Equipment	Supplier
Adult mouse, brain matrix coronal slices stainless steel	World Precision Instruments
Bioruptor Plus	Diagenode
Codefree™ Blood Glucose Monitor	SD Biosensor
Codefree™ Blood Glucose Test Strip	SD Biosensor
DM4000 B LED Fluorescent microscope	Leica
DMi8 TCS SP8 confocal microscope	Leica
PHERAstar® *FS* microplate reader	BMG Labtech
GelMax Imager	UVP
DFC340 FX Light microscope	Leica
8000 Retracting Sledge Microtome	Bright Instruments
Mini-PROTEAN tetra vertical hand-cast protein electrophoresis systems	BioRad
HistoCore BIOCUT Manual Rotary Microtome	Leica
Odyssey Clx imaging system	LI-COR
NanoDrop™ 8000 Spectrophotometer	Thermo Scientific
Sample Corer 17 Gauge	InterFocus
SimpliAmp Thermocycler	Applied Biosystems
Wide mini-sub cell GT cell nucleic acid electrophoresis system	BioRad

Table 2.2 List of equipment used in this research project.

2.3 Software

Software	Supplier
Excel 2013	Microsoft
FIJI ImageJ 1.52i	National Institutes of Health
Prism 8 & 9	GraphPad
Image Studio Lite 5.2	LI-COR
Leica Application Suite X	Leica

Table 2.3 List of software used in this research project.

2.4 Ethics statement

All procedures involving animals were carried out in accordance with the UK Animal (Scientific Procedures) Act 1986, and were approved by the University of Exeter Animal Welfare and Ethical Review Body. All steps were taken to minimise potential pain and suffering in the animals, as well as to follow the 3Rs as described by the National Centre for the Replacement, Refinement and Reduction of Animals in Research.

2.5 Animals

All animals were housed on a 12:12 light/dark cycle, with environmental conditions at 22 (± 2) °C and 55% (± 2%) humidity. Animals had *ad libitum* access to standard laboratory chow (LabDiet, EURodent diet [5LF2]) – unless specified otherwise by the experiment – and water. Housing and experiments took place in either the Hatherly (low barrier) or the Living Systems Institute Biological Services Units (BSU; intermediate barrier), both based at the University of Exeter. Regular welfare checks were made on the experimental animals by the personal licence holder and the unit staff.

The following transgenic and non-transgenic animals were used in the studies described in this work.

2.5.1 C57BL/6J mice

These mice were bred in-house, except for two cohorts acquired from Charles River, UK (Table 2.2.1). The genome of C57BL/6J mice contains mutations in the gene that codes for nicotinamide nucleotide transhydrogenase (*Nnt*) (371–373). NNT is a mitochondrial protein involved in nicotinamide reduction which in turn contributes to ATP synthesis. These mice exhibit altered redox homeostasis, but their overall health is unaffected, with the exception of moderate impairment in glucose clearance in the glucose tolerance test (371,372). Accordingly, this strain is a common “wild-type” model for obesogenic and diabetes studies. These mice are prone to pronounced weight-gain, hyperinsulinemia and hyperglycaemia when fed high-fat diet (374).

2.5.2 Tg(Trh-EGFP)FZ169Gsat/Mmucd mice

Brain tissue from Tg(Trh-EGFP)FZ169Gsat/Mmucd (TRH-eGFP) mice was gifted by Prof Simon Luckman of the University of Manchester, and used to study distribution of TSPO around thyrotropin-releasing hormone (TRH) neurons. This strain enables visualisaton of TRH-positive cells using immunohistochemistry. The mice were bred on a mixed Swiss Webster and FVB/N mouse background. The mouse strain Tg(Trh-EGFP)FZ169Gsat/Mmucd, identification number 030178-UCD, was originally obtained from the Mutant Mouse Regional Resource Center, a NCRR-NIH funded strain repository, and was donated to the MMRRC by Nathaniel Heintz at the Rockefeller University and the NINDS funded GENSAT BAC transgenic project (375).

2.5.3 Crhtm1(cre)Zjh/J X Gt(ROSA)26Sor$^{tm1(EYFP)Cos}$/J mice

Brain tissue from these mice was gifted by Prof Simon Luckman of the University of Manchester for immunohistochemical processing. These mice were used to study the distribution of TSPO in corticotropin-releasing hormone (CRH) neurons. The strain was formed from a cross of two different strains: *Gt(ROSA)26Sor$^{tm1(EYFP)Cos}$/J,* originally sourced from Jackson Labs, with originator Frank Costantini, Columbia University Medical Center, and *Crhtm1(cre)Zjh*/J – sourced from Jackson Labs, with originator Z. Josh Huang,

Cold Spring Harbour Laboratory (376). The offspring of this cross were then bred on a C57BL/6J background to generate Crhtm1(cre)Zjh/J X Gt(ROSA)26Sortm1(EYFP)Cos/J (CRH-eYFP) mice.

2.5.4 *Gad65*-GFP mice

Brain tissue from these mice was gifted by Prof Simon Luckman of from the University of Manchester for immunohistochemical processing. This mouse strain expresses GFP under the GAD65 promoter, and so allows the identification of GABA-expressing neurons. This mouse was originally produced by Szabo Gabor at the Department of Functional Neuroanatomy at the Institute of Experimental Medicine in Budapest, Hungary (377). These mice were bred on a C57BL/6J background.

2.5.5 C57BL/6N-Tspo$^{tm1b(EUCOMM)Wtsi}$/leg mice

The allele construct to knock-out TSPO was generated at the German Research Center for Environmental Health (GmbH) as part of the International Mouse Phenotyping Consortium (IMPC) (Fig 2.5.2a) (378). The protocol applied in this scenario is known as the “LacZ tagged null allele”. Here, exons 2 and 3 of the *Tspo* gene are labelled by a LacZ and a neomycin cassette. LoxP sites are spliced to either side. Following a cross with alleles expressing cre-recombinase, a knock-out of the neomycin cassette and exons 2 and 3 is made. This results in an allele that cannot produce a *Tspo* gene product, as the remaining exons (1 and 4) do not contain a start codon (325). This knock-out affects all organs that would ordinarily express TSPO. This method is similar to the generation of a different global TSPO-KO mouse line, namely C57BL/6-Tspo$^{tm1GuMu(GuwiyangWurra)}$. In this case, exons 2 and 3 were also removed and the authors indicated that the remaining exons may possibly produce an unrelated protein with no sequence similarity to that of TSPO (325). An additional global TSPO-KO mouse line has been generated from a conditional anti-Müllerian hormone type 2 receptor cre-mediated TSPO-KO line (379).

Following the creation of founder breeders by *in vitro* fertilization, transgenic mice were bred at MRC Harwell to a C57BL6/N mouse background to produce heterozygote offspring. These offspring were bred together in order to produce

the homozygous knock-out (TSPO -/-) and wild-type mice (TSPO +/+) used in this study. These – along with an additional cohort were then used for in-house breeding – arrived at the University of Exeter at ages 6-9 weeks old. The genotypes of all the mice used in the following experiments were confirmed using PCR from liver tissue collected following euthanisation (Fig 2.5.2b). The absence of protein expression in TSPO in the TSPO -/- mice was confirmed using Western blots of liver tissue from the experimental animals (Fig 2.5.2c). The experimental animal cohort were allowed to acclimatise to their surroundings for two weeks, and then individually-housed for monitoring of body weight and food intake. Individual housing was performed by the NACWO of the animal unit, to ensure that the investigators were blinded to the genotype of the animals during the study.

2.5.6 Tg(Npy-hrGFP)1Lowl mice

The wild-type offspring from heterozygous Tg(Npy-hrGFP)1Lowl (NPY-hrGFP) mice bred in-house were used in the diet-induced obese study of Chapter 4. Using wild-type offspring that were otherwise due to be destroyed reduces unnecessary breeding. This strain was originally generated on a FVB mouse background but cross-bred to be established as a C57BL/6J line (380).

Chapter	Experiment	Strain	Sex	Age (weeks)	Experiment location
3	3.2.1 Distribution	C57BL/6J	F	14	Hatherly, University of Exeter
			M	14	
	3.2.2 Co-localisation	C57BL/6J	M	18	
			F	8	
		Tg(Trh-EGFP)FZ169Gsat/Mmucd	M		University of Manchester
		Crhtm1(cre)Zjh/J X *Gt(ROSA)26Sor*$^{tm1(EYFP)Cos}$*/J*	M		
		Gad65-GFP	M		
	3.2.3 Antibody validation	C57BL/6N-Tspo$^{tm1b(EUCOMM)Wtsi}$/leg	M	21	LSI, University of Exeter
			M	8	
4	4.2.2-3 Acute high-fat diet/ Acute fast	C57BL/6J	M	18	Hatherly, University of Exeter
			M	24	
			M	20	
	4.2.4 Chronic high-fat diet	C57BL/6J	M	15 – 28	
			M	12 - 24	
			M	9 – 22	
	4.2.1 Western blot	C57BL/6J	M	13	
			M	13	
			M	11	
			M	10	
			M	9	
5	5.2.1 Characterisation of TSPO -/- mice	C57BL/6N-Tspo$^{tm1b(EUCOMM)Wtsi}$/leg	M	9 – 26	LSI, University of Exeter
			M	8 – 26	
			M	6 – 24	
			F	9 - 26	
			F	8 – 26	
	5.2.2 PK11195 feeding studies	C57BL/6J	F	13 – 15	Hatherly, University of Exeter
			M	11 – 12	
			M	6 – 8	

Chapter	Experiment	Strain	Sex	Age (weeks)	Experiment location
			M	7 – 11	
			F	10 – 14	
			F	9 - 12	
			F	7 – 10	
			F	16 – 19	
			F	13 - 16	
			F	14 – 17	
			M	20 – 21	
			M	17 – 18	
			M	9 – 11	
			M	8 – 9	
			M	14 – 15	
			M	13 – 14	
	5.2.2 PK11195 glucose tolerance test	C57BL/6J	F	8	LSI, University of Exeter
			M	11	

Table 2.5.1 List of animals used in this project.

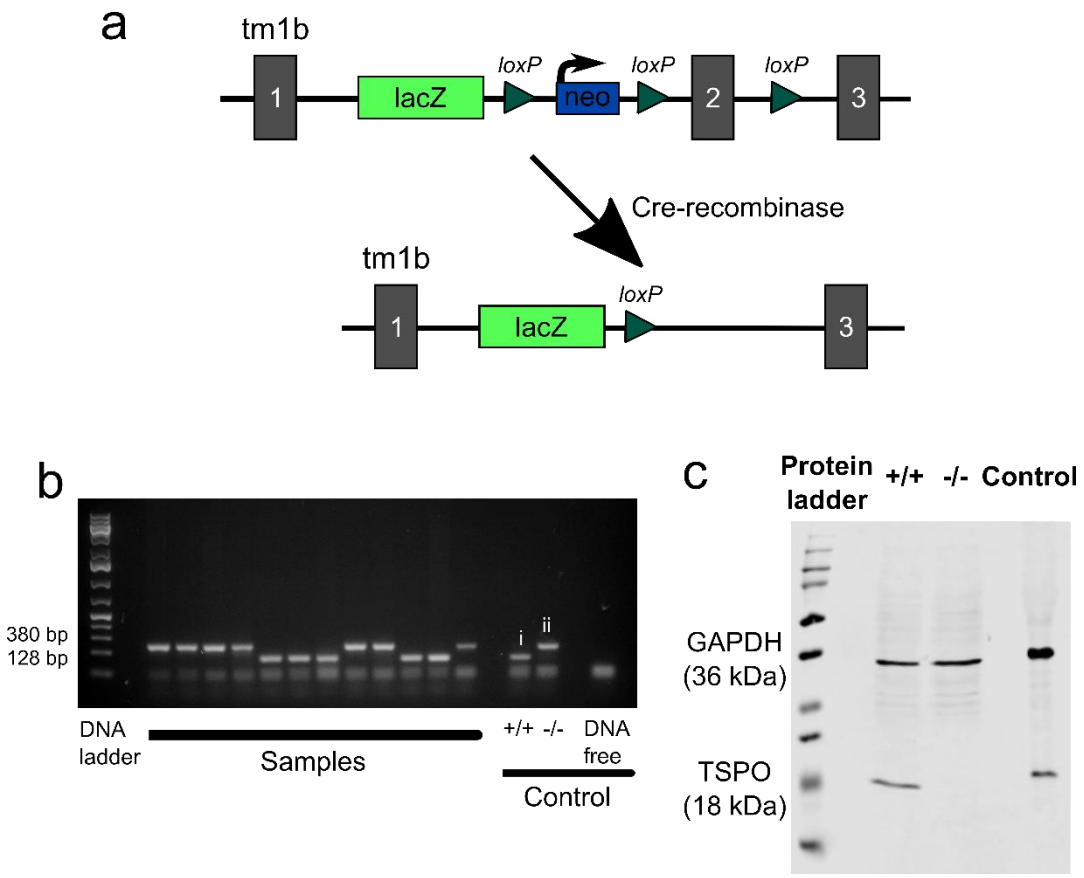

Figure 2.5.1 Generation and validation of the TSPO -/- mice.

A schematic diagram demonstrating the genetic manipulation that led to the generation of the TSPO -/- mutant allele (a). The targeted mutation (tm1b) is identifiable by splicing the cDNA to a LacZ and a neomycin (neo) cassette, and targeted by splicing to LoxP sites. Crossing the mutated allele with alleles expressing cre-recombinase resulted in knock-out of the neomycin cassette and exon 2, resulting in a null allele. PCR of liver samples taken from the experimental cohort of mice was used to confirm the presence of the wild-type (i; 128 bp) and knock-out (ii; 380 bp) alleles of the mice used in the study (b). Western blot was performed in brain tissue of animals bred in-house to confirm absence of TSPO protein (c). Protein lysate from primary cultured mouse cortical astrocytes was used as the control.

2.6 *In vivo* experimental procedures

2.6.1 Acute high-fat diet exposure

These experiments were performed in the Hatherly BSU (low barrier facility). Male C57BL/6J mice were maintained in their holding room and post-weening cages with *ad libitum* access to water. Within 30 minutes of lights-out (1900 hours), the mice were weighed and either provided with high-fat chow (TestDiet DIO 58Y1, 60% energy from fat) or maintained on their original standard chow used in-house (Table 2.6.1). After 12h, from lights-on (0700 hours), the mice were moved individually to the procedural room where they were injected via the intra-peritoneal route with 100 µL of pentobarbitone sodium (1.6 g/kg) and food intake and body weights were measured. The mice then underwent either decapitation under anaesthesia or transcardial perfusion, depending on requirement for tissue analysis.

	Nutritional profile (% from ingredients)	
Nutrient	**EURodent 5LF2 (Standard chow)**	**TestDiet DIO 58Y1 (High-fat diet)**
Protein	14.3	23.1 (casein)
Fat	5.8 (soybean oil)	34.9 (lard, soybean oil)
Cholesterol (ppm)	n/a	301 ppm
Total saturated	0.52	13.68
Total monounsaturated	0.53	14.00
Total polyunsaturated	n/a	5.15
Fibre	3.7	6.5
Carbohydrate	65.2 (starch, glucose, fructose, sucrose)	25.9 (maltodextrin, sucrose, powdered cellulose)

Table 2.6.1 The nutritional profile of the standard chow diet (EURodent 5LF2) and high-fat diet (TestDiet DIO 58Y1) used in this project.

2.6.2 Acute food deprivation

These experiments were performed in the Hatherly BSU (low barrier facility). Male C57BL/6J mice were maintained in their holding room and post-weening cages with *ad libitum* access to water. Within 30 minutes prior to lights-out, the

mice were weighed and randomly assigned to either the fasted or fed groups. The mice in the fast group had their food removed, and the empty tray returned, while the food for the mice in the fed condition went untouched. After 12 hours, from lights-on (0700 hours), the mice were moved individually to the procedural room where they were injected with 100 µL of pentobarbitone sodium (1.6 g/kg) into the peritoneum and body weights were measured. The mice then underwent either decapitation under anaesthesia or transcardial perfusion, depending on requirement for tissue analysis.

2.6.3 Chronic high-fat diet exposure

The mice used to analyse changes in TSPO and GFAP expression were male C57BL/6J. This study was undertaken in the Hatherly BSU (low barrier facility) with the mice kept in their original holding cages: group-housed at 2-3 animals per cage bar one cage in which a mouse was single-housed. The cages were randomly assigned to high-fat or standard chow. The cages allocated to the high-fat group were provided with high-fat chow (TestDiet DIO 58Y1, 60% energy from fat; Table 2.6.1), and the control cages were maintained on the facility standard chow. For 12 weeks, body weights of the mice were measured weekly and high-fat chow replaced twice a week. After the experimental period, mice were transported one at a time to the procedure room. Here, the animals were injected with 100 µL of pentobarbitone sodium (1.6 g/kg) to the peritoneum in preparation for transcardial perfusion.

In the high-fat diet exposure of TSPO wild-type (+/+) and knock-out (-/-) mice, facility standard chow was replaced with high-fat diet (TestDiet, DIO 58Y1, 60% energy from fat; Table 2.6.1). Measurements of body weight and food intake were made on days 1, 2, 3 and 7 following diet change, and then weekly until experiment endpoint. Availability of high-fat chow within the cages was assessed every couple of days and animals were provided with more if current levels were insufficient. At week 6 the mice were weighed to complete measurements of body weight, then euthanised by overdose of pentobarbitone sodium (intra-peritoneal; 1.6 g/kg; 100 µL) followed by decapitation.

2.6.4 Glucose tolerance test

Different cohorts of mice underwent this experiment in separate studies, all performed in the Living Systems Institute BSU (intermediate barrier). In all cases, the mice were acclimatised to tail handling for at least a week before the experiment. At lights-on (0700 hours), the mice were moved to a procedure room and their food removed. After 6 hours, the mice received a topical anaesthetic (EMLA cream; 2.5% lidocaine, 2.5% prilocaine; AstraZeneca) to their tail and a small cut was made at the tip – from which blood glucose was measured by a handheld blood glucose monitor and testing strips (Table 2.2). The mice then received an intra-peritoneal injection of 2 g/kg glucose (Table 2.1) dissolved in 100 µL saline (0.9% sodium chloride) and filter-sterilised. In the pharmacological experiments, mice were co-injected with sterile 5 mg/kg PK11195 or vehicle (DMSO; 3%) in sterile saline (Table 2.1). Blood glucose was measured from the tail tip cut at 15, 60, 90 and 120 minutes following glucose administration.

2.6.5 Monitoring of nocturnal food intake

The mice used in this study were also used in the fast-induced refeeding experiment, in agreement with PPL guidelines. This experiment occurred in the Hatherly BSU (low barrier). C57BL/6J mice were single-housed and handled daily for at least a week before the study, for acclimatisation, and randomly assigned to drug or control groups. Within 30 minutes prior to lights-out in the facility (1900 hours), the mice assigned to the drug group were administrated with an intra-peritoneal dose of sterile 1 mg/kg PK11195 or vehicle (DMSO; 3%) in 100 µL saline (0.9% sodium chloride dissolved in sterile water). The weight of the standard chow in each cage was recorded at the time of injection and also at 1, 2, 3, 4, 12 and 24 hours post-injection.

2.6.6 Monitoring of satiated food intake

The mice used in this study were also used in the fast-induced refeeding experiment, in agreement with PPL guidelines. This experiment occurred in the Hatherly Biological Services Unit (low barrier). C57BL/6J mice were single-housed and handled on a daily basis for at least a week before the study, for acclimatisation, and randomly assigned to drug or control groups. At lights-on

(0700 hours), the mice were injected with 1 mg/kg PK11195 or vehicle (DMSO; 3%) in 100 µL saline (0.9% sodium chloride in sterile water) via the intra-peritoneal route. The weight of standard chow was recorded at the time of injection and again at 90 minutes following injection, when the mice were then euthanised for tissue analysis.

2.6.7 Fast-induced refeeding

This procedure was performed on C57BL/6J, TSPO +/+ and TSPO -/- mice. Mice were single-housed for at least a week prior to the experimental day. Within 30 minutes before lights-out (1900 hours), standard chow was removed from the cages and the body weight of each animal recorded. After 12 hours, from lights-on (0700 hours), standard chow was weighed and returned to the respective cages. In the case of the pharmacological study on the C57BL/6J mice, the mice were randomly allocated to receive an intra-peritoneal injection of 1 or 5 mg/kg PK11195 or vehicle (DMSO; 3%) in 100 µL saline (0.9% sodium chloride in sterile water) alongside return of the standard chow. In all scenarios, the standard chow was weighed again at 1, 2, 3, 4, 12 and 24 hours post-injection/return of food.

2.7 *Ex vivo* analysis

2.7.1 Immunohistochemistry

To collect brain tissue for immunohistochemical analysis, animals were perfused transcardially with 0.01M phosphate buffered saline (PBS; made from sodium phosphate; Table 2.1) containing heparin (0.01%) followed by 4% paraformaldehyde (PFA; Table 2.1) dissolved in 0.01M PBS. Brains were dissected and post-fixed in PFA for up to 18 hours – depending on quality of the perfusion. The brains were then placed in 30% sucrose (Table 2.1) dissolved in PBS, for 18 hours and stored at -80 °C until use. The brains were re-labelled accordingly by an independent observer, for blinding, before being sectioned in the coronal plane with a freezing-stage sledge microtome (Table 2.2) at 30 µm thickness. Free-floating sections were stored in 0.01% sodium azide in PBS until immunohistochemical processing.

For immunohistochemistry, sections were washed three times for 10 minutes in PBS, then incubated in a block of 5% normal donkey serum (NDS; Table 2.1) made in PBS plus 0.3% Triton X-100 (PBS-T; Table 2.1) for 1 hour at room temperature on an orbital shaker. Primary antibodies were diluted in 1% NDS, made in PBS-T, and free-floating sections were incubated for the duration and at the dilution previously optimised (Table 2.7.1.1).

Sections were washed in three changes of PBS for 10 minutes each, before incubation with secondary antibody for 1 hour at room temperature (Table 2.7.1.2). Secondary antibodies were made to 1:500 dilution in PBS-T. The sections were washed in an additional three changes of PBS for 10 minutes. In single immunohistochemical processing, the sections were then mounted. In dual immunohistochemistry, the incubations in primary and secondary antibodies were repeated accordingly.

The sections were mounted onto glass slides from distilled water and allowed to air-dry overnight for 18 hours. Glass coverslips were then applied with fluorescent mounting medium (Table 2.1). Sections were examined and imaged using the fluorescent microscopes (Table 2.2) for analysis and figures.

In immunohistochemical processing of white adipose tissue (WAT) the tissue was washed in PBS, weighed and then stored in 3% PFA at 4 °C until use. Tissue was cut into small sections of equal size using a scalpel, and were then washed in three changes of PBS for 10 minutes each. These were blocked in 20% NDS, diluted in PBS-T, for 1 hour at room temperature on an orbital shaker. This was followed by incubation in rat anti-F4/80 - diluted 1:250 in PBS-T with 20% NDS– overnight at 4 °C on an orbital shaker. The following morning, tissue sections were washed for 5 minutes in PBS for three changes and then incubated in donkey anti-rat$^{alexa\text{-}594}$ – diluted 1:1000 in PBS-T containing 20% NDS - for 1 hour at room temperature. The tissue was washed in PBS for 10 minutes before incubation in rabbit anti-TSPO, 1:250 in PBS-T with 20% NDS, for 1 hour at room temperature. This was followed by three washes in PBS for 5 minutes each, and an incubation in donkey anti-rabbit$^{alexa\text{-}488}$ – diluted 1:1000 in PBS-T with 20% NDS a– for 1 hour at room temperature. The tissue was washed for a further 10 minutes in PBS before incubation in 1:1000 DAPI (Table 2.1) diluted in PBS.

Tissue was mounted onto glass slides, excess liquid dried by wicking away with tissue, and coverslips applied with fluorescent mounting medium. The sections were imaged using confocal microscopy (Table 2.2).

Antigen target	Host species	Dilution	Incubation	Supplier	Catalogue number
F4/80	Rat	1:500	Overnight, 4 °C	Abcam	ab6640
GFAP	Rabbit	1:1000	Overnight, 4 °C	Abcam	ab7260
GFAP	Mouse	1:5000	Overnight, 4 °C	Millipore	mab360
GFP	Chicken	1:1000	Overnight, 4 °C	Abcam	ab13970
IBA1	Goat	1:500	Overnight, 4 °C	Abcam	ab5076
TSPO	Rabbit	1:1000	1 hour, room temperature	Abcam	ab109497
Vimentin	Chicken	1:500	Overnight, 4 °C	Millipore	ab5733

Table 2.7.1.1 Primary antibodies, and their suppliers, used in this research project.

Antigen target	Fluoro-phore	Host species	Dilution	Incubation	Supplier	Catalogue number
Chicken	Alexa 594	Goat	1:500	1 hour, room temp.	Invitrogen	A-11042
Goat	Alexa 594	Donkey	1:500	1 hour, room temp.	Invitrogen	A-11058
Mouse	Alexa 568	Donkey	1:500	1 hour, room temp.	Invitrogen	A10037
Mouse	Alexa 680	Goat	1:10,000	1 hour, room temp.	Invitrogen	A21057
Rabbit	Alexa 488	Donkey	1:500	1 hour, room temp.	Invitrogen	R37118
Rabbit	800	Goat	1:10,000	1 hour, room temp.	VWR	ROCK611-132-122
Rat	Alexa 594	Donkey	1:1000	1 hour, room temp.	Invitrogen	A-21209

Table 2.7.1.2 Secondary antibodies, and their suppliers, used in this research project.

2.7.2 Hematoxylin and eosin histological staining

Liver tissue dissected from the TSPO +/+ and -/- mice was washed in 0.01M PBS, weighed and fixed in 4% PFA dissolved in PBS. Samples of equal sizes were paraffin embedded, by the Histopathology lab at the Royal Devon & Exeter Hospital. The paraffin embedded blocks were sliced using a rotary microtome (Table 2.2) into sections of 5 µm width and floated from a heat bath to Superfrost™ charged glass microscope slides.

The slides were left overnight to air-dry, then deparaffinised in two changes of 10 minutes incubation in xylene (Table 2.1). This was followed by re-hydration in two changes of 100% ethanol (Table 2.1) for 5 minutes each, then in 95% ethanol for 2 minutes and 70% ethanol for 2 minutes. After a brief wash in distilled water,

slides were incubated in hematoxylin solution (Table 2.1) for 90 seconds. The solution was washed off in warm running water for 10 minutes, followed by a rinse in distilled water. The slides were briefly dipped into 95% ethanol 10 times, and then counter-stained in eosin-y solution (Table 2.1) for 30 seconds. Slides were dehydrated through 5 minutes incubation in fresh 95% ethanol, followed by 2 changes in 100% ethanol. The slides were cleared in 2 changes of xylene for 5 minutes each, and then coverslips applied with DPX mounting medium (Table 2.1).

The mounting media was left to dry and the slides were then imaged using light microscopy (Table 2.2).

2.7.3 Quantification of protein expression

Western blot analysis was performed on brain tissue from C57BL/6J mice that were exposed to high-fat diet, food deprivation or maintained on standard chow overnight (Chapter 2.6.1-2). Mice received an overdose by intra-peritoneal administration of pentobarbitone sodium (1.6 g/kg) and then were decapitated for dissection. Brains were removed and placed into the brain matrix (Table 2.2) from which micropunches containing the dorsomedial and arcuate hypothalamic nuclei were taken at approximately -1.70 mm from bregma (381). These were stored at -80 °C until use.

20 µL of lysis buffer (Table 2.7.3.1) was added to the brain tissue micropunches, while on ice, and vortexed twice for 5 seconds. The Eppendorf tubes of brain tissue and lysis buffer were then lysed by sonication (Bioruptor Plus; Table 2.2): 5 cycles of 30 seconds pulsing at high frequency, maintained at 4 °C. Tubes were vortexed again twice for 5 seconds each and then left for 2 hours at 4 °C on a rotary turner. Lysates were then centrifuged at 12,000 RPM for 20 minutes while maintained at 4 °C, and the supernatant containing the protein was transferred to a fresh pre-cooled Eppendorf tube.

Liver tissue from TSPO +/+ and -/- mice was used for Western blot validation of TSPO genotype. Following tissue collection, samples were stored at -80 °C. 200 µL of lysis buffer (Table 2.7.3.1) was added to the liver tissue. These were centrifuged at 12,000 RPM for 20 minutes at 4 °C and the supernatant transferred

to fresh pre-cooled Eppendorf tubes. This was repeated an additional 2 times to ensure removal of lipids from the lysates.

Reagent	Concentration (mM)
Tris-HCl (pH 7.4)	25
NaF	50
NaCl	0.1
EDTA (pH 8.0)	1
EGTA (pH 8.0)	5
Triton X-100	1%
NaPPi	10
Sucrose	269
β-Mercaptoethanol	0.1%
Sodium orthovanadate	1
Benzamidine	1
Phenylmethylsulfonyl fluoride	0.1

Table 2.7.3.1 Components, and concentration, of modified RIPA lysis buffer.

Total protein quantification for all samples was conducted using the Bradford assay protocol (382). Protein assay dye reagent (Table 2.1) was diluted according to manufacturer's instructions. Samples were incubated with 200 µL of reagent for 5 minutes on a plate shaker, and absorbance at 595 nm was measured using the PHERAstar microplate reader (Table 2.2). Total protein concentration was calculated by comparison to a standard curve plotted with known concentrations of bovine serum albumin (BSA; Table 2.1).

For protein separation by SDS-PAGE, hand-cast gels were made with 15% acrylamide and a stacking section of 4% acrylamide (Table 2.7.3.2). Samples of equal protein concentration were prepared by dilution with sample buffer (Table 2.7.3.3) and lysis buffer (Table 2.7.3.1) and heated to 90 °C for 5 minutes. 10 µL of sample, as well as Precision Plus protein ladder (Table 2.1), were loaded into the hand-cast gels in tanks containing running buffer (Table 2.7.3.3). 10 µg, in 10

µL, of cortical primary astrocyte cultured from neo-natal mouse brain was added as a positive control. Running conditions were set at 90 V for 15 minutes, then 150 V for 90 minutes.

Reagent	Upper (4% acrylamide)	Lower (15% acrylamide)
ddH20	2.8 mL	2.3 mL
0.5 M Tris (pH 6.8)	1.25 mL	
1.5 M Tris (pH 8.8)		3.15 mL
30% acrylamide	850 µL	5.6 mL
10% SDS	50 µL	110 µL
20% APS	50 µL	55.4 µL
TEMED	5.35 µL	11 µL

Table 2.7.3.2 Components and concentrations to make 2x hand-cast gels for electrophoresis.

The proteins, separated on the gel, were transferred onto a nitrocellulose membrane using the sandwich method. This was placed into a tank containing transfer buffer (Table 2.7.3.3) and a current of 100 V was applied for 70 minutes. For quantification of total protein transferred, the membrane was washed in water and then incubated in total protein stain (Table 2.1) for 5 minutes. The membrane was washed twice for 30 seconds in 5 mL Wash Solution (Table 2.1) and then imaged by the LI-COR Odyssey imaging system at 700 nm (Table 2.2). Total protein stain was removed by incubation in Reversal Solution (Table 2.1) for 10 minutes, which was rinsed off in water.

Buffer	Components
Sample	125 mM Tris-HCl (pH 6.8), 20% (v/v) glycerol, 4% (w/v) SDS, bromophenol blue, 0.1% β-mercaptoethanol
Running	25 mM Tris, 192 mM glycine, 0.1% SDS
Transfer	20% (v/v) methanol, 48 mM Tris, 39 mM glycine, pH 8.3

Table 2.7.3.3 Buffers, and their components, used in gel electrophoresis.

The membranes were then blocked in 5% milk, dissolved in Tris-buffered saline with 0.1% Tween (TBS-T; Table 2.1). This was followed by three changes of 15 mL TBS-T for 5 minutes each. The membranes were incubated in primary antibody; rabbit anti-TSPO (Table 2.7.3.4) diluted in TBS-T containing 2% BSA (Table 2.1), overnight at 4 °C. The membranes were washed again in three changes of 15 mL TBS-T for 5 minutes each, before incubation for 1 hour at room temperature in secondary antibody; goat anti-rabbit^{800} (Table 2.7.3.5) diluted in TBS-T. The membranes were washed in three changes of TBS-T, for 10 minutes each, and then imaged with the LI-COR Odyssey system.

Where required, the membranes underwent further probing for GFAP quantification. After imaging, the membranes were incubated in mouse anti-GFAP (Table 2.7.3.4) - diluted in 2% BSA in TBS-T - overnight at 4 °C. Membranes were washed three times in TBS-T for 5 minutes, then incubated in Goat anti-Mouse^{680} (Table 2.7.3.5) for 1 hour at room temperature. The membranes were washed in three changes of TBS-T for 10 minutes each, then imaged with the LI-COR Odyssey system. In the case of the liver samples to confirm TSPO expression and absence in TSPO +/+ and -/- mice, the membranes were incubated in mouse anti-GAPDH primary antibody (Table 2.7.3.4) for 1 hour at room temperature instead.

Antigen target	Host species	Dilution	Incubation	Supplier	Catalogue number
GFAP	Mouse	1:5000	Overnight, 4 °C	Millipore	mab360
GAPDH	Rabbit	1:10,000	1 hour, room temperature	Sigma-Aldrich	G9545
TSPO	Rabbit	1:1000	1 hour, room temperature	Abcam	ab109497

Table 2.7.3.4 Primary antibodies, and their suppliers, used in Western blot analysis.

Antigen target	Fluoro-phore	Host species	Dilution	Incubation	Supplier	Catalogue number
Mouse	Alexa 680	Goat	1:10,000	1 hour, room temp.	Invitrogen	A21057
Rabbit	Alexa 800	Goat	1:10,000	1 hour, room temp.	VWR	ROCK611-132-122

Table 2.7.3.5 Secondary antibodies, and their suppliers, used in Western blot analysis.

2.7.4 Confirmation of TSPO genotype by PCR

Unfixed liver tissue from the high-fat fed TSPO +/+ and -/- mice were collected and stored at -80 °C. Equal-sized samples were taken and added to Eppendorf tubes containing 0.5 mL DNA digestion buffer (Table 2.7.4.1) with 0.5 mg/mL proteinase K (Table 2.1). These were incubated at 55 °C overnight, after which 0.7 mL of Phenol:Chloroform:Isoamyl alcohol (Table 2.1) was added. The lysates were allowed to mix for 1 hour at 4 °C on an Eppendorf rotating rack. The tubes were then centrifuged at 14,000 RPM for 5 minutes and 0.5 mL of the supernatant was transferred into clean Eppendorf tubes. DNA was precipitated by addition of 1 mL 100% ethanol, centrifuged at 14,000 RPM for 5 minutes to pellet the DNA and the supernatant discarded. To wash the pellet, 0.5 mL of ice-cold 70% ethanol was then added to the tubes and then they were centrifuged again. The supernatant was discarded, and the DNA pellet left to air-dry overnight until there was no ethanol remaining. Once dry, pellets were re-suspended in 200 µL Tris-EDTA buffer (Table 2.7.4.1) and incubated at 65 °C for 15 minutes. The DNA yield was measured using the NanoDrop (Table 2.2) and diluted in Tris-EDTA buffer to 50-100 ng/µL.

Buffer	Components
DNA digestion	50 mM Tris-HCl (pH 8.0), 100 mM EDTA (pH 8.0), 100 mM NaCl, 1% SDS in distilled water
Tris-EDTA	10 mM Tris, 1 mM EDTA in distilled water (pH 8.0)

Table 2.7.4.1 Buffers used for extraction of liver DNA for TSPO mouse genotyping.

For PCR, reaction mix was prepared for the digests (Table 2.7.4.2) and cycling conditions optimised for the TSPO -/- allele (Table 2.7.4.3). A water-only negative control was included, with lysate replaced with DNA-free water, plus known TSPO +/+ and -/- samples for reference. The lysates were then separated by electrophoresis on a 1.5% agarose gel made in Tris-acetate-EDTA with 5 µL of GelRed nucleic acid stain (Table 2.1). 5 µL of Generuler DNA ladder (Table 2.1) and 5 µL of samples and control were loaded per lane. Samples were run at 90 V for 70 minutes, and imaged using a GelMax Imaging system (Table 2.2).

Component	Volume (µL)
DreamTaq PCR master mix	10
DNA-free water	6
5’ arm primer 5’>3’ [AGCAGAAGTAGGAAGAAGGTG] (10 pmol/µL)	1
3’ arm primer 5’>3’ [GTCAACCCATCACTGCCTTCA] (10 pmol/µL)	1
LAR3 primer 5’>3’ [CAACGGGTTCTTCTGTTAGTCC] (10 pmol/µL)	1
DNA digest (50-100 ng)	1

Table 2.7.4.2 Reaction mix for PCR in TSPO genotyping.

Temperature (°C)	Time	Number of cycles
95	5 minutes	1
94	30 seconds	39
65	45 seconds	
72	45 seconds	
72	10 minutes	1
4	hold	1

Table 2.7.4.3 PCR cycling conditions for TSPO genotyping.

2.8 Image acquisition and analysis

Images were captured with the Leica fluorescent or confocal microscopes (Table 2.2) unless stated otherwise. Images for display purpose were captured using confocal microscopy. HC PL APO CS2 20x/0.75 dry objective and HC PL APO CS2 63x/1.40 oil objective were used to capture images at for 20x and 63x magnification, respectively. Two photomultiplier tubes, which were sensitive to wavelengths between 597nm - 644nm and 763nm - 768nm, were used to detect emission peaks corresponding to Alexa Fluor 488, 568 and 594 dyes. A hybrid photodetector (Leica) was used to detect the emission peak corresponding to DAPI dye. For image capturing, pinhole size was kept at 95.5 µm, or 1 airy unit, and image resolution was consistently 1024 by 1024 pixels which equated to 0.18 µm pixel-to-voxel size ratio. Image files were exported and processed for analysis using FIJI ImageJ (Table 2.3).

2.8.1 Analysis of TSPO-immunoreactivity distribution in the mouse brain

The distribution of TSPO-immunoreactivity in the mouse brain was assessed qualitatively using standard upright fluorescent microscopy (Table 2.2). This used a HC PL FLUOTAR 10x/0.30 dry objective, with a numerical aperture of 0.3, and a Leica L5 cube with a bandpass 480/40 excitation and 527/30 suppression filter. TSPO was identified in brain regions through comparison of sections to figures in the Mouse Brain in Stereotaxic Coordinates (381). Delineation of sub-region within nuclei was generally avoided except in cases of absolute clarity, for

instance the lateral septal nuclei. The intensity of immunoreactivity was qualitatively graded per brain region across sections for each animal (Table 2.8.1.1). The values attributed to each region were averaged within brain nuclei for animals of the same sex. Co-immunoreactivity with neural cell markers, and TSPO immunoreactivity in TSPO -/- mice, was assessed qualitatively in both male and female mice but the images presented here are taken from male mice.

TSPO immunoreactivity	Description (brain region)	Grade
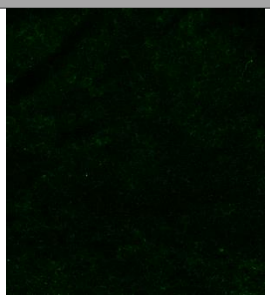	No immunoreactivity (Zona incerta)	0
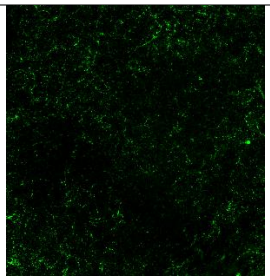	Light, punctate immunoreactivity (Ventromedial hypothalamic nucleus)	+
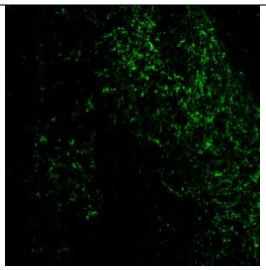	Light, punctate immunoreactivity and visible projections (Lateral septal nucleus, intermediate part)	++
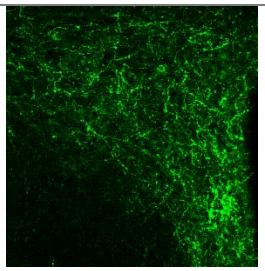	Mostly projection-like immunoreactivity (Paraventricular hypothalamic nucleus)	+++
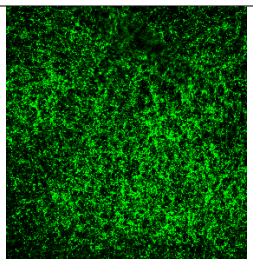	Dense projection-like immunoreactivity (Dorsomedial hypothalamic nucleus)	++++

Table 2.8.1.1 Scale used for qualitative assessment of TSPO immunoreactivity.

For display purpose, 20x magnification images were captured using confocal microscopy (Table 2.2) with tile scanning and multiple z-slices. Tile scans were automatically merged by the Leica Application Suite (Table 2.3). Final images were formed from an average intensity projection of five z-slices using ImageJ (Table 2.3). One z-slice was captured for each image taken at 63x magnification. In order to assess potential co-localisation of TSPO with cell-markers, 10 z-slices were captured to assess coincidence of immunoreactivity but only one representative z-slice was used for display purpose.

2.8.2 Assessment of TSPO regulation by dietary exposure using immunohistochemistry

In brain sections of mice exposed to acute and chronic high-fat diet, as well as food deprivation, immunohistochemical processing was used to semi-quantitatively assess changes in TSPO expression. Confocal microscopy and exposure settings for image acquisition were maintained within each cohort. FIJI ImageJ (Table 2.3) was used for measurement of intensity of anti-TSPO fluorophore-labelled immunoreactivity. Region of interest (ROI) was drawn around the brain nuclei assessed – DMH and Arc, as well as the wall of the third ventricle– in which intensity of immunohistochemical staining was measured. A ROI was measured outside of the brain nuclei of interest of the same slide, in which no immunoreactivity was detected, and this value was subtracted from the primary measurement to control for background fluorescence (Figure 2.8.2.1). This was performed on 1 slide per animal in each cohort, ensuring that the images were taken at the same coordinate of -1.70 mm from bregma.

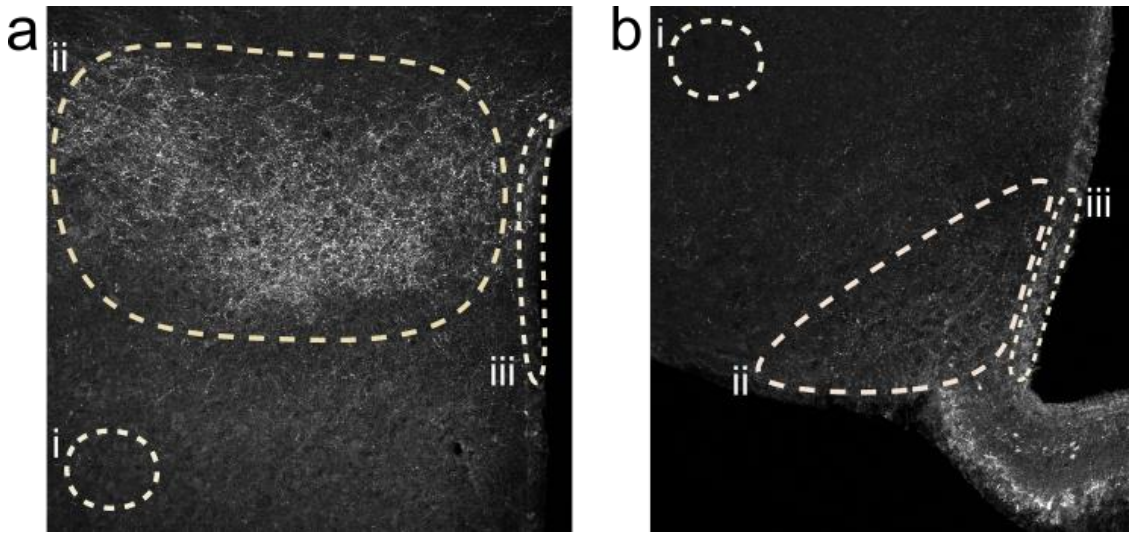

Figure 2.8.2.1 The regions of interest used in semi-quantification of TSPO immunoreactivity.

TSPO-positive immunoreactivity was semi-quantified in the dorsomedial (a) and the arcuate nucleus (b) of the hypothalamus. The regions of interest (ROI) were selected out of the nuclei to provide background fluorescence measurements (i). This was subtracted from the measurements made in the nuclei ROI (ii) and also in the wall of the third ventricle (iii). Images captured at 20x magnification.

2.8.3 Analysis of GFAP-positive astrocyte morphology using immunohistochemistry

Immunohistochemically processed brain sections of mice exposed to dietary manipulation were used to assess potential changes in GFAP expression – a marker for astrocytes. Measurements were made of cell counts and analysis of morphology, performed on the same sections of -1.70 mm from bregma as those used in the TSPO-immunoreactivity analysis. The cell counter plugin in FIJI ImageJ was used to measure the number of GFAP-expressing cells in a representative section per animal from each cohort. Inclusion criteria for the GFAP-expressing cells to be counted was to contain an observable cell body as well as cell processes.

The ImageJ plugin, ‘Simple Neurite Tracer’ (383), was used to quantify morphology of five randomly selected GFAP-expressing cells per section and animal. The data acquired from the ‘Simple Neurite Tracer’ plugin is based on the linear quantitative analysis designed by Sholl (384). Sholl’s linear method measures the distribution of crossings made by cell processes at concentric

circles expanding from the cell body (383,384). This is used to characterise the morphology of the cell. In this research, the number of intersections of GFAP-positive processes at each concentric circle were measured (Fig 2.5.3.1). Concentric circles were made at intersections of 3 μm. This data was averaged between the 5 selected cells for each circle of increasing radius by 3 μm. The average values were inputted to GraphPad Prism for analysis (Table 2.3), corresponding to each animal of dietary treatment and to each 3 μm radius.

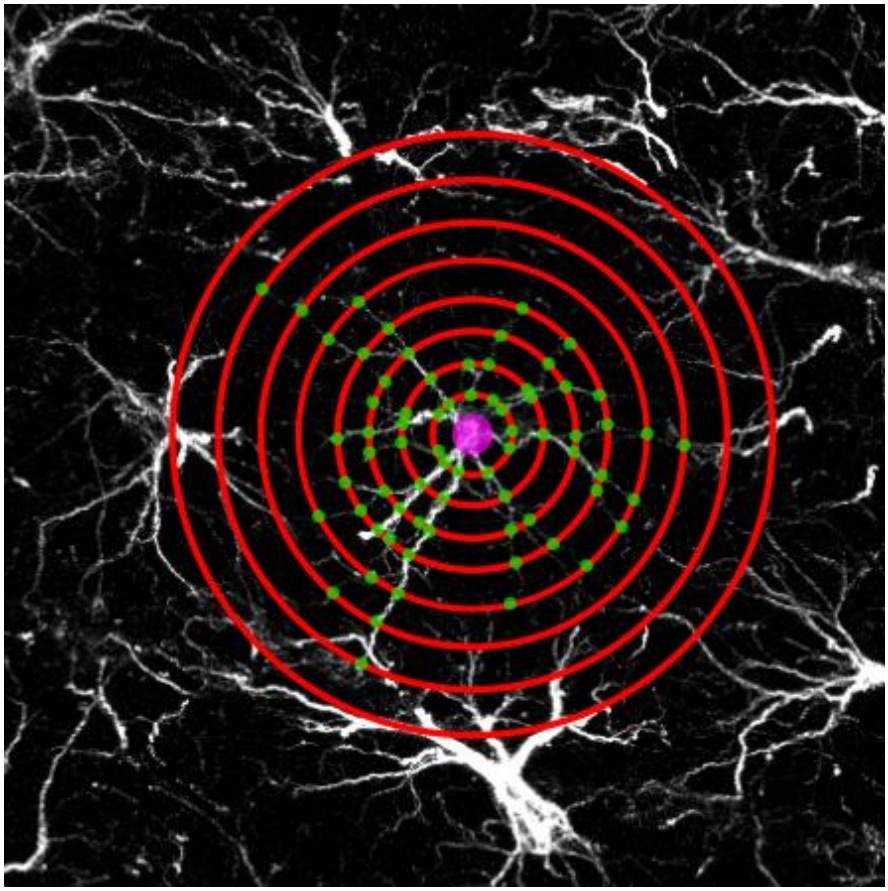

Figure 2.8.3.1 Representation of data collection from 'Simple Neurite Tracer' analysis of GFAP-expressing astrocytes.

The cell body (pink) is centre of concentric circles of 3 μm apart. Data is extracted from the number of cell processes passing each expanding radius (green). Image taken at 20x magnification and digitally maximised.

2.8.4 Analysis of white adipose tissue structure from immunohistochemical processing

WAT structure was imaged at 20x magnification using the Leica confocal microscope (Table 2.2), and z-stacks were collected. A range of 6 z-stacks were processed using ImageJ and set to 'maximum projection', in order to visualise entire cells across the image. Using the ImageJ 'Measure' feature, the area of each adipocyte was measured in one image of WAT section per animal. The area of adipocytes was averaged per animal.

The number of F4/80-positive macrophages was measured in the same image, per animal, using the 'Cell Counter' plugin of ImageJ.

2.8.5 Analysis of liver tissue structure from haematoxylin & eosin histological processing

Three images per liver sample were captured using light microscopy (Table 2.2). In ImageJ, images were converted to 8-bit and a threshold applied to convert them to black-and-white representations of the tissue structure. The same threshold adjustments were applied to all images. The images were inverted so that the stained area appeared black, and the 'Analyse particles' feature of ImageJ was applied. This provided information including the average area of black particles, which corresponded to the size of vacuolarised sites in the liver tissue. This was averaged again for each of the three images taken per animal and plotted accordingly.

2.8.6 Analysis of TSPO and GFAP protein expression measured by Western Blot

The membranes for TSPO and GFAP quantification were probed with Total Protein stain (Table 2.1). This was measured on the Image Studio Lite software (Table 2.3) and used to normalise densitometry of TSPO and GFAP bands.

2.9 Data presentation and statistical analysis

Data were processed using Microsoft Excel 2013 (Table 2.3). Graphs were produced and statistical analysis was performed using GraphPad Prism versions 8 and 9 (Table 2.3). Data were presented as individual points – where possible – with error bars indicating the range of standard error from the mean. Data were tested for normal distribution and the appropriate parametric or non-parametric statistical tests were applied. Where comparisons were made between treatment groups over time, two-way analysis of variance (ANOVA) tests with repeated-measures were applied – and the non-parametric versions if data had unequal variances. For example, in cases where data collection at time points were missed or inaccurately recorded, a mixed-effects analysis model was used instead. An Area Under Curve (AUC) analysis was applied to measurements of glucose tolerance, where the analysis parameters included peaks greater than the baseline of “0” and ignored peaks that were less than 10% of the total distance from baseline to the maximum Y-value. In this case, where there were multiple comparisons across three groups (for example genotype, diet and sex in glucose tolerance AUC measurements), three-way ANOVA tests were applied using GraphPad Prism.

Chapter 3: Characterisation of TSPO expression in the healthy mouse brain

3.1 Introduction

Enhanced neural expression of the mitochondrial translocator protein of 18 kDa (TSPO) is associated with neuroinflammation. This is attributed to up-regulation of TSPO in reactive astrocytes and microglia (228,240,298,370). TSPO is a target in the clinical setting to survey neuroinflammation, typically through positron emission tomography (PET) imaging (385). However, TSPO function in the healthy brain – human or rodent – is not well characterised. In addition to glia, TSPO has been identified in the vascular and ependymal cells (284), but also some neurons (300). In the context of PET imaging for clinical assessment of neuroinflammation, it is important to acknowledge that there are brain regions that have high levels of TSPO even in absence of an underlying pathology. For example, previous studies have identified TSPO expression in the dentate gyrus, olfactory bulb, choroid plexus as well as the neural vasculature system in healthy mouse models (284,325,369). Moreover, a more detailed understanding of the location of TSPO in the brain may provide an idea of the functions of this protein.

The purpose of this study was to characterise the expression of TSPO using immunohistochemistry in the healthy adult mouse brain. To achieve this, three main objectives were investigated:

- To examine the distribution of TSPO expression
- To identify the cellular sources of TSPO localisation
- To validate specificity of the anti-TSPO antibody in a knock-out mouse model

3.2 Results

3.2.1 Distribution of TSPO immunoreactivity in regions of the mouse brain involved in energy homeostasis

Single fluorescence immunohistochemistry was performed on formaldehyde-fixed free-floating brain sections. I examined the distribution of TSPO immunoreactivity throughout the brain in both male and female mice (Table 3.2.1.1). I focused on brain regions that are known to be involved in regulating energy homeostasis. Levels of immunoreactivity were qualitatively assessed according to a number scale of 0 to 4; in which 4 indicated the densest levels of immunoreactivity (Chapter 2, Table 2.8.1.1). The results of this semi-quantified immunoreactivity were averaged across three animals in both sexes.

Tissue was examined from both sexes, to consider sexual dimorphism in neuroendocrine function (135,386–390). While the vast majority of TSPO immunoreactivity was very similar between male and female C57BL/6J mice, there were some small differences in immunoreactivity density. In some cases immunoreactivity was identified in brain regions of one sex and not in the other (Tables 3.2.1.1). For example, TSPO immunoreactivity was detected in the striohypothalamic nucleus in the female mice and not in the males, while immunoreactivity was observed in the septohypothalamic nucleus in the males only.

In all animals the strongest levels of TSPO immunoreactivity were seen in the dorsomedial hypothalamic nucleus (DMH), median eminence (ME), and choroid plexus (Tables 3.2.1.1). High levels of TSPO-immunoreactivity were also seen in non-hypothalamic regions that are considered to be involved in energy homeostasis, such as the bed nucleus of the stria terminalis (BNST) (84,391–393), the lateral septal nuclei (LSN) (92,114), and the nucleus of the solitary tract (NTS) (38,82,106,110) (Table 3.2.1.1). Other regions in which TSPO immunoreactivity was observed include the preoptic region, choroid plexus, subfornical organ (SFO), and amygdala (Table 3.2.1.1). The relative distribution of TSPO immunoreactivity in different brain regions will be described in more detail in the next sections.

3.2.1.1 TSPO immunoreactivity in the hypothalamus

Throughout the hypothalamus, TSPO immunoreactivity was detected within the periventricular nucleus (Pe; Fig 3.2.1.1) surrounding the third ventricle (3V). The density of the observed immunoreactivity was variable throughout the coronal sections. Labelling in the Pe was in addition to the high levels of TSPO-positive immunoreactivity seen in the 3V wall. TSPO immunoreactivity was also seen in the paraventricular hypothalamic nucleus (PVH; Fig 3.2.1.1). TSPO immunoreactivity followed the transitions in the wing-like structure of the PVH in the coronal plane, from -0.58 to -1.22 mm from bregma (Table 3.2.1). TSPO immunoreactivity also spread lateral of the PVH, towards the lateral hypothalamic nuclei and within the tuber cinereum (Fig 3.2.1.1). Immunoreactivity was also observed dorsal of the PVH, defined to a single focal point at the base of the reuniens thalamic nucleus either side of the 3V (Fig 3.2.1.1).

As aforementioned, dense TSPO immunoreactivity was recorded throughout the DMH of both male and female mice (Fig 3.2.1.2). Minimal immunoreactivity was seen in the ventromedial hypothalamic nucleus (VMH; Fig 3.2.1.2). Moderate TSPO immunoreactivity was identified within the arcuate nucleus (Arc) of both male and female mice (Fig 3.2.1.2). Immunoreactivity here encompassed the entire nucleus and followed the trajectory by the 3V from anterior to posterior. TSPO immunoreactivity extended into the ME at the base of the 3V (Fig 3.2.1.2), of which strong immunoreactivity was observed particularly at the external layer.

Weak TSPO immunoreactivity was noted in both the anterior and the lateral hypothalamic regions of male and female mice (Table 3.2.1.1). Here, immunoreactivity did not fill the entire nuclei. Within the lateral hypothalamic nucleus, immunoreactivity was mostly confined to the peduncular portion. TSPO immunoreactivity was also absent-to-weak in the ventrolateral hypothalamus. Light immunoreactivity was also reported within the septohypothalamic nucleus in the brains of male mice, and weak to moderate immunoreactivity in the females (Table 3.2.1.1). Weak to moderate immunoreactivity was observed in the striohypothalamus in female mice only (Table 3.2.1.1).

Brain region	Sub-region	Distance from Bregma (Observed)	Protein density: Males	Protein density: Females
Cortex	Peduncular, dorsal	0.38 to 1.78	+	+
Nucleus Accumbens	Shell	1.18 to 1.98	+	+
	Shell	0.74 to 1.18	+++	++
	Core	1.98 to 0.74	+, +/-	++
Corpus Collosum		0.14 to 1.70	+	+
Vertical Limb of the Diagonal Band		0.74 to 1.34	0	+
Septohippocampal Nucleus		0.74 to 1.18	+	+
Lateral Septal Nucleus	Dorsal	0.38 to 1.42	+	+
	Intermediate	0.14 to 0.98	++	+, +/-
	Ventral	0.14 to 1.18	++	++
Bed Nucleus of the Stria Terminalis	Dorsal	0.02 to 0.62	+	++
	Ventral	0.62 to -0.34	+++	+++
	Medial	-0.46 to 0.02	+	+, +/-
	Lateral	-0.10	0	++
Medial Preoptic Area		-0.46 to 0.74	+	+, +/-

Brain region	Sub-region	Distance from Bregma (Observed)	Protein density: Males	Protein density: Females
Vascular Organ of the Lamina Terminalis		0.26 to 0.62	+++	+++
Periventricular Hypothalamic Nucleus		-1.94 to 0.38	++	++
Striohypothalamic Nuclei		-0.10 to 0.62	0	++
Septohypothalamic Nuclei		0.02 to 0.62	+	0
Subfornical Organ		-0.58 to 0.02	++, +/-	++
Paraventricular Hypothalamic Nucleus		-1.22 to -0.46	+++	++
Thalamus	Para-ventricular, Paratenial, Reuniens, Mediodorsal, Paraxiphoid	-2.06 to -0.22	+	+
Anterior Hypothalamic Area		-1.94 to -0.34	+, +/-	+, +/-

Brain region	Sub-region	Distance from Bregma (Observed)	Protein density: Males	Protein density: Females
Retrochiasmatic Nucleus		-1.34 to 0.94	0	+
Ventromedial Hypothalamic Nucleus		-2.06 to -1.34	+	+
Supraoptic Area	Nucleus; decussation	-1.70 to -0.58	+, +/-	0
Arcuate Nucleus		-2.54 to -1.06	++, +/-	++, +/-
Dorsomedial Hypothalamic Nucleus		-2.18 to -1.34	++++	++++
Amygdala	Medial Amygdaloid Nucleus, posterodorsal part	-2.06 to -1.70	+	+
Median Eminence		-2.30 to -1.58	++++	++++
Choroid Plexus			+++, +/-	++++
Tubero/ Retromammilary Nucleus		-2.70 to -2.54	++	+

Brain region	Sub-region	Distance from Bregma (Observed)	Protein density: Males	Protein density: Females
Parabrachial Nucleus	Lateral external, ventral part	-5.34	0	+. +/-
Locus Coeruleus		-5.34 to -5.52	++, +/-	+
Tegmental Nucleus	Laterodorsal	-5.40	0	+
Medial Vestibular Nucleus	Posterior part	-5.80	+	0
Parvicellular Reticular Nucleus	Alpha part	-6.36	++	0
Pre-Botzinger Complex		-7.08	0	+
Rostral Ventral Respiratory Group		-7.20 to -7.32	++, +/-	0
Raphe Pallidus Nucleus		-7.20 to -7.76	++	+
Raphe Obscurus Nucleus		-7.32 to -7.64	+	+

Brain region	Sub-region	Distance from Bregma (Observed)	Protein density: Males	Protein density: Females
Nucleus of the Solitary Tract	Medial, dorsomedial, dorsolateral, commissural, ventral parts	-7.08 to -7.92	+, +/-	++
Dorsal Motor Nucleus of the Vagus Nerve		-7.08 to -7.92	++	++, +/-
C1 adrenergic & A1 noradrenergic cells		-7.56 to -7.92	+, +/-	+, +/-
Pyramidal Tract		-7.92	+, +/-	++
A2 noradrenergic cells		-8.24	+	+

Table 3.2.1.1 Semi-quantitative distribution of TSPO-immunoreactivity in the male mouse brain.

Density of TSPO immunoreactivity was semi-quantified in the adult male and female mouse brain (n = 3), with a focus on neuroendocrine regions.

Scale: 0 (no immunoreactivity), + (little immunoreactivity), ++ (moderate immunoreactivity), +++ (dense immunoreactivity), ++++ (very dense immunoreactivity).

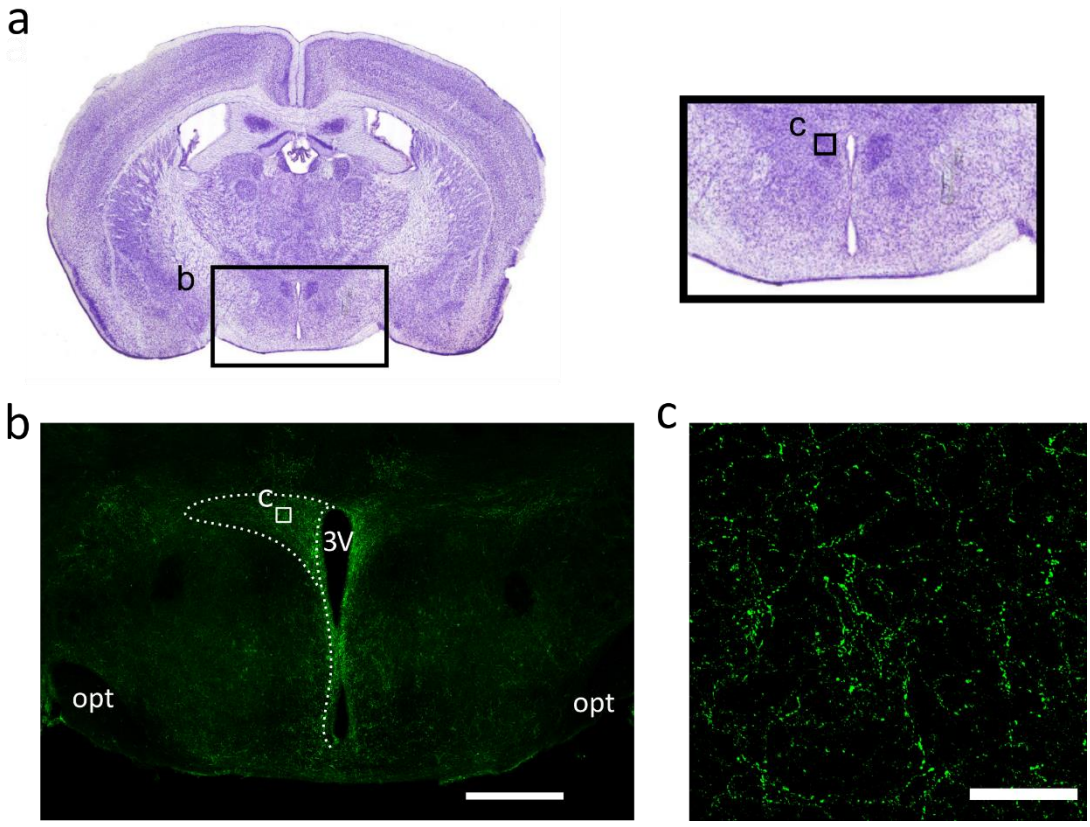

Figure 3.2.1.1 TSPO immunoreactivity around the third ventricle of brain tissue from a female C57BL/6J mouse, including the paraventricular nucleus of the hypothalamus.

A coronal diagram (a), taken from the Mouse Brain atlas (381) at -1.06 mm from bregma, labelled to correspond with the captured images (b-c). Representative image capturing TSPO immunoreactivity (green) in the periventricular hypothalamic nucleus around the third ventricle (outlined) and paraventricular nucleus of the hypothalamus (outlined) (b). A magnified image taken within the paraventricular nucleus of the hypothalamus (outlined by the white box), showing TSPO immunoreactivity in the green (c). Images captured at 20x (b) and 63x (c) magnification, with scale bars representing 200 µm and 50 µm respectively.

Key: Third ventricle (3V); optic tract (opt).

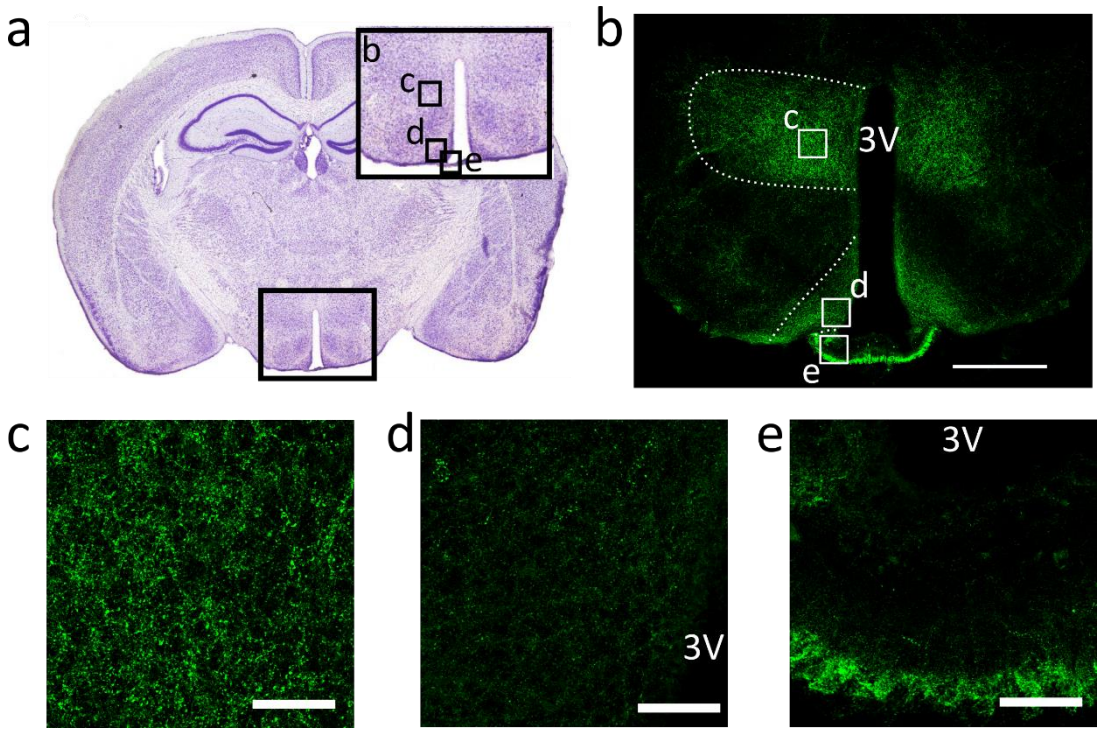

Figure 3.2.1.2 TSPO immunoreactivity around the third ventricle of brain tissue from a female C57BL/6J mouse, including the dorsomedial and mediobasal hypothalamic nuclei.

A representative diagram, from the Mouse Brain atlas (381) at -1.70 mm from bregma, labelled to correspond with the captured images (a). Dense TSPO immunoreactivity (green) is observed around the third ventricle (b) and particularly within the hypothalamic dorsomedial nucleus (c), arcuate nucleus (d) and median eminence (e). Scale bar represents 200 μm in image captured at 20x magnification (b), and 50 μm in images taken at 63x magnification (c-e).

Key: Third ventricle (3V).

3.2.1.2 TSPO immunoreactivity in non-hypothalamic regions that are involved in regulating energy homeostasis

The BNST makes reciprocal connections with hypothalamic nuclei, of which some are able to influence food intake (394,395). TSPO immunoreactivity was variable within the BNST in all animals (Fig 3.2.1.3). Immunoreactivity was strongest in the ventral region (BNSTv), below the anterior commissure (acc). Immunoreactivity was not observed in the lateral BNST (BNSTl) in brains taken from male mice, but was observed at moderate intensity in female mice. Weak to moderate immunoreactivity was noted in the dorsal and medial parts of the BNST in all animals.

Moderate immunoreactivity was also observed within the nucleus accumbens (NAcc; Table 3.2.1.1); mostly within the shell, but also in the core as the coronal sections moved caudally. The NAcc is involved in energy homeostasis, as well as implicated in modulating the reward response to sugar and fat intake (113).

The NTS received input from the gastrointestinal tract, via the vagus nerve, regarding food intake and relays this to the hypothalamus to revoke feeding (106,110). TSPO immunoreactivity was also documented within the NTS (Fig 3.2.1.4). This was found throughout the nucleus at moderate intensity – though weaker in brain sections from male mice compared to female. In many sections, immunoreactivity was identified at or across the border to the dorsal motor nucleus of the vagus nerve (DMV) in both sexes (Fig 3.2.1.4).

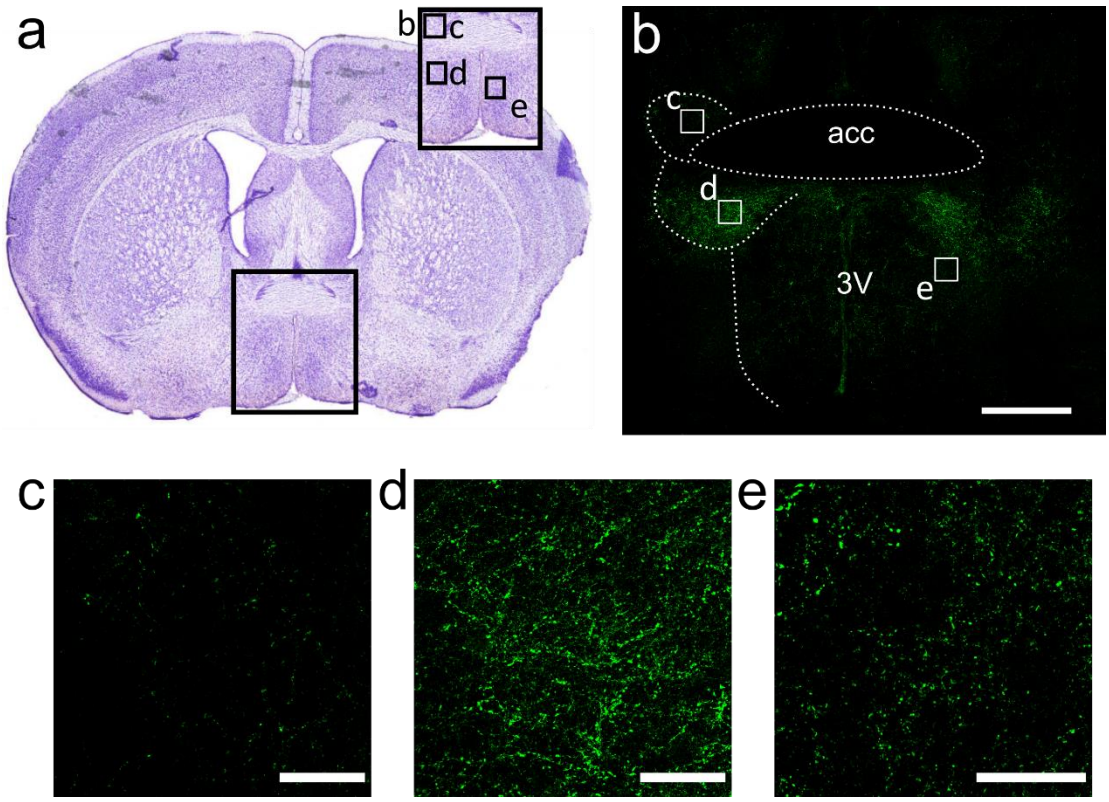

Figure 3.2.1.3 TSPO immunoreactivity around the anterior commissure, in the bed nucleus of the stria terminalis and in the medial preoptic area of brain tissue from a female C57BL/6J mouse.

A representative coronal diagram (a), taken from the Mouse Brain atlas (381), highlighting the regions observed corresponding to 0.14 mm from bregma. TSPO immunoreactivity was dense below the anterior commissure and around the third ventricle (b). Immunoreactivity was also detected in the bed nucleus of the stria terminalis, above the anterior commissure (c), though reactivity was most dense below in the ventral region (d) and also in the medial preoptic area (e). Images taken at 20x (b) and 63x (c-e) magnification with scale bars representing 200 μm and 50 μm, respectively.

Key: Third ventricle (3V), anterior commissure (acc).

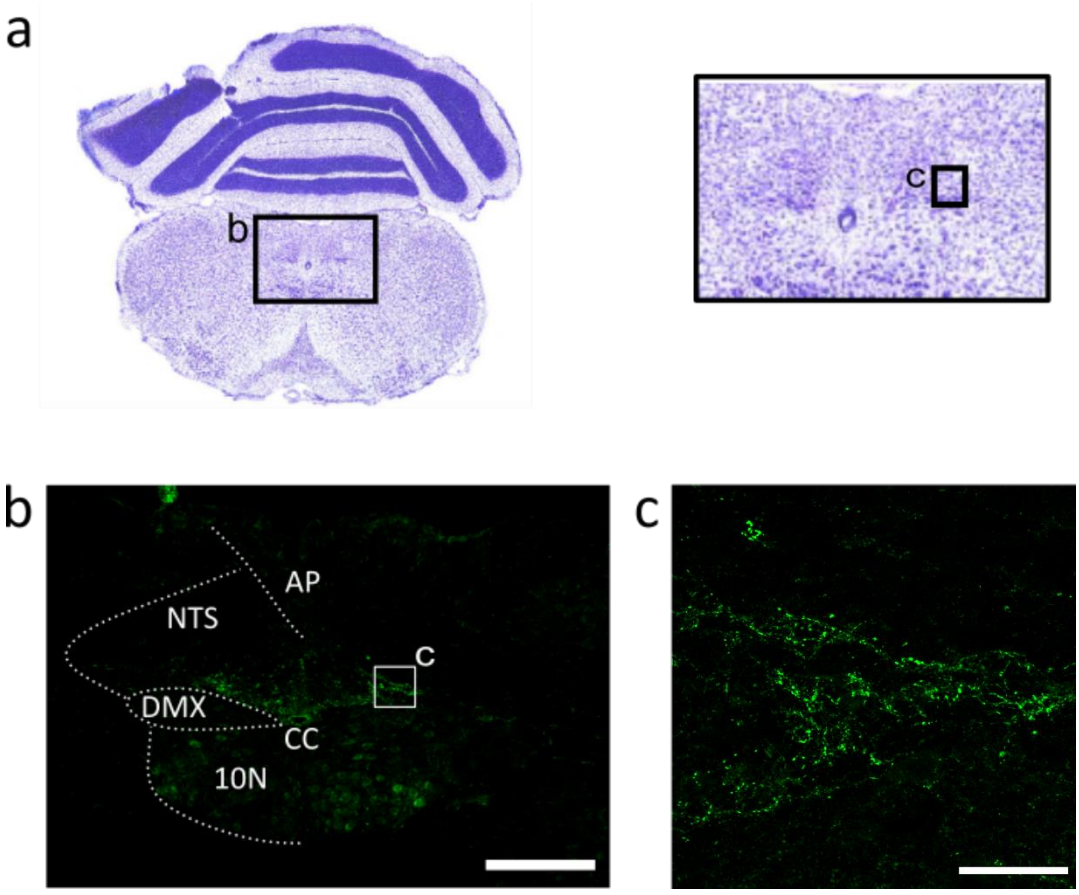

Figure 3.2.1.4 TSPO immunoreactivity around the central canal of hindbrain tissue taken from a male C57BL/6J mouse.

A representative coronal image, taken from the Mouse Brain atlas (381), labelling the regions corresponding to -7.76 mm from bregma at which the images were captured (a). TSPO immunoreactivity was observed around the central canal (b), and densely in the ventral part of the nucleus of the solitary tract (c) adjacent to the dorsal motor vagal nucleus. Images taken at 20x magnification contain a scale bar representing 200 µm (b), and taken at 63x the scale bar represents 50 µm (c-e).

Key: Hypoglossal nucleus (10N); Area postrema (AP); central canal (CC) dorsal motor nucleus of the vagus nerve (DMX); nucleus of the solitary tract (NTS).

3.2.1.3 TSPO within circumventricular organs

TSPO immunoreactivity was detected in multiple circumventricular organs. As previously described, strong immunoreactivity was noted in the ME (Fig 3.2.1.2), but was weak-to-absent in the area postrema (AP; Fig 3.2.1.4). In addition, dense immunoreactivity was observed in the SFO (Table 3.2.1.1, Fig 3.2.2.2) and in the vascular organ of the lamina terminalis (VOLT; Table 3.2.1.1, Fig 3.2.2.9). The SFO contained TSPO immunoreactivity, of notably a 'speckled' pattern, to a moderate degree in brain slices from mice of both sexes. There were sex-differences noted in TSPO immunoreactivity at the VOLT. Medium-level immunoreactivity was most notable in male animals (Table 3.2.1.1), while much more variable in brain tissue from female mice (Table 3.2.1.2). The subcommissural organ showed no TSPO immunoreactivity. The pituitary and the pineal gland were not immunohistochemically processed for TSPO.

3.2.1.4 TSPO in other brain regions

TSPO immunoreactivity was also observed in regions not known to be involved in energy homeostasis. Of most notable was strong immunoreactivity within the choroid plexus (Table 3.2.1.1). Immunoreactivity was also seen throughout the medial preoptic area (Fig 3.2.1.3) with weak to moderate intensity in both male and female mice. The same was observed in thalamic regions. With both of these areas, however, it was difficult to distinguish between sub-regions. Weak immunoreactivity was noted within a small region of the amygdala, which is considered to be within the posterior part of the medial amygdaloid nucleus (Table 3.2.1.1). Dense immunoreactivity was also identified in the noradrenaline/adrenaline cell group (C1/A1) of the hindbrain in both sexes (Table 3.2.1.1).

3.2.1.5 Controls for detection of TSPO immunoreactivity

TSPO immunoreactivity was compared to sections, taken from the same mouse brain, which underwent an identical immuno-processing technique minus the primary antibody. The purpose of this was to identify non-specific binding of the secondary antibody used, for which none was identified in any of the brain regions observed (Fig 3.2.1.5). Western blot processing of mouse ventral hypothalamic

tissue also identified a band at the predicted molecular weight of TSPO (18 kDa; Fig 3.2.1.6)

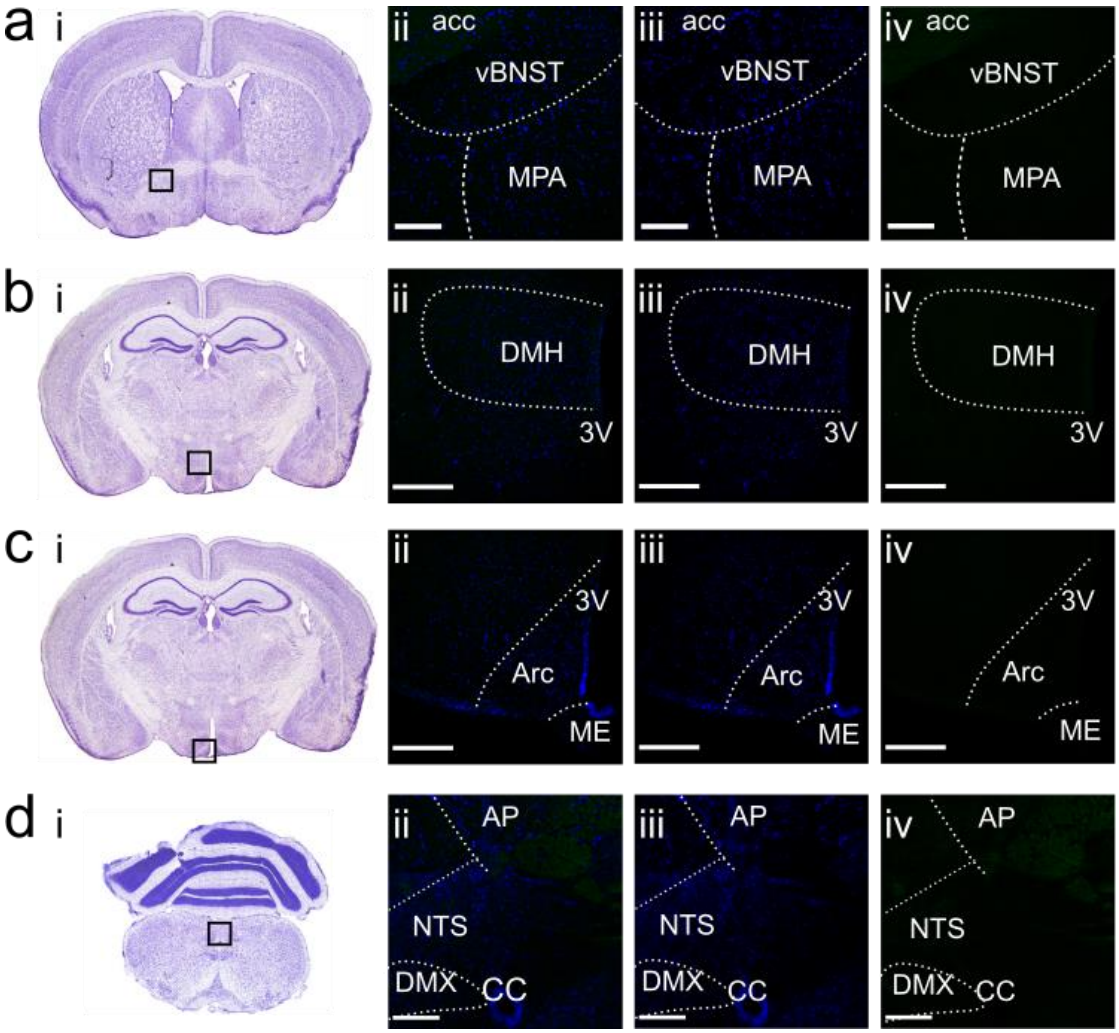

Figure 3.2.1.5 Validation of TSPO immunoreactivity in the mouse brain by immunohistochemical processing with secondary antibody only.

Figures taken from the Mouse Brain in Stereotaxic Coordinates (381), indicating the regions in which the corresponding images are taken (i). Anti-rabbit^{488} immunofluorescence in the absence of primary rabbit anti-TSPO (ii), showing DAPI nuclear staining (iii; blue) and anti-rabbit^{488} binding (iv; green). Images depict the bed nucleus of the stria terminalis (a; image 0.26 mm from bregma), the dorsomedial (b; image -1.70 mm from bregma) and arcuate (c; image -1.70 mm from bregma) nuclei of the hypothalamus, and in the dorsal vagal complex (d; image -7.48 from bregma). Images taken at 20x magnification, scale bars represent 100 μm.

Key: Third ventricle (3V); anterior commissure (acc); area postrema (AP); central canal (CC); hypothalamic arcuate nucleus (Arc); hypothalamic dorsomedial nucleus (DMH); dorsal motor nucleus of the vagus nerve (DMX); median eminence (ME); medial preoptic area (MPA); nucleus of the solitary tract (NTS); bed nucleus of the stria terminalis, ventral portion (vBNST).

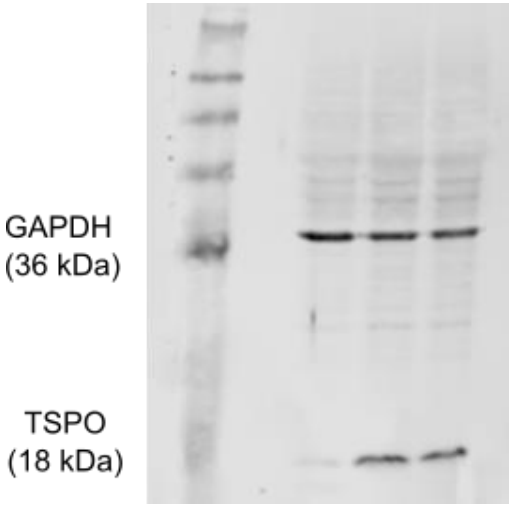

Figure 3.2.1.6 Validation of TSPO antibody in Western blot.

Western blot analysis of TSPO protein expression – indicated by a band identified at 18 kDa - in the ventral portion of the hypothalamus of male C57BL/6J mice. Presence of GAPDH acts as a loading control. N=3

3.2.2 Cellular identity of TSPO immunoreactivity

After identifying the regions of the male and female mouse brain with dense TSPO immunoreactivity, I then used dual-label immunohistochemistry to identify the cell type location within the brain. As glial cells are well documented to be responsible for most TSPO immunoreactivity (172,227,228,284), I used antibodies against common glial markers – glial fibrillary acidic protein (GFAP), ionised calcium binding adaptor molecule 1 (IBA1) and vimentin - to identify astrocytes, microglia and tanycytes respectively. However, considering the pattern of TSPO immunoreactivity and previous reports of TSPO in neurons (300), I also used transgenic reporter mice to label neuropeptide-expressing neurons.

3.2.2.1 TSPO in GFAP-positive astrocytes

I used dual-immunohistochemistry on forebrain sections from male C57BL/6J mice, to identify immunoreactivity of TSPO and of GFAP – a commonly used marker for astrocytes. GFAP is a cytoskeletal protein, and so antibodies label the astrocytic processes as well as the cell soma. GFAP expression is largely restricted to astrocytes and some tanycytes, but is not expressed by neurons. The activation state of astrocytes influences the level of GFAP expressed (396).

Extensive immunoreactivity of TSPO was observed in the hypothalamus (Table 3.2.1.1, Fig 3.2.1.1-2). Hypothalamic astrocytes have been implicated in regulating energy balance (204,207,219,397), as well as being activated in response to nutritional state (125,180,182,187,198,202). Minimal GFAP immunoreactivity was detected within the PVH, DMH or VMH. No coincidence of co-immunoreactivity of GFAP with TSPO was observed in the PVH nor the DMH. There was minor overlap of immunoreactivity observed within the VMH (Fig 3.2.2.1). At first glance, TSPO and GFAP immunoreactivity appeared to overlap at the base of the Arc (Fig 3.2.2.1). However, at greater magnification the incidences of immunoreactivity are observed to be in apposition to each other.

Potential occurrences of co-localisation between GFAP and TSPO were observed outside of the hypothalamus. Coincidence of immunoreactivity between GFAP and TSPO was identified within the SFO, but the majority of TSPO immunoreactivity did not co-localise with GFAP (Fig 3.2.2.2). There was

extensive GFAP immunoreactivity in the cortex, which did appear to coincide with TSPO (Fig 3.2.2.3). However, this was only visible if intensity of fluorescence was increased considerably compared to imaging of other brain regions. TSPO and GFAP immunoreactivity were also detected around vasculature throughout the brain, but with minimal co-localisation (Fig 3.2.2.3).

Immuno-processing of brain sections with the secondary fluorescent antibodies, in absence of primary antibodies, confirmed their specificity for the TSPO and GFAP antibodies (Fig 3.2.2.4).

3.2.2.2 TSPO in IBA1-positive microglia

IBA1 is a cell marker for microglia. Its expression, as with GFAP, can be influenced by the reactive state of the cell (398,399). IBA1 is also specific to microglia, and labels cell bodies as well as projections.

No co-localisation of TSPO and IBA1 immunoreactivity was detected in the PVH, DMH or VMH. IBA1-positive cells were abundant within the Arc and appeared to co-express TSPO, but at greater magnification the immunoreactivity was concluded to be in apposition (Fig 3.2.2.5). Specificity of secondary antibodies were confirmed with immuno-processing in absence of anti-TSPO and anti-IBA1 antibodies (Fig 3.2.2.6).

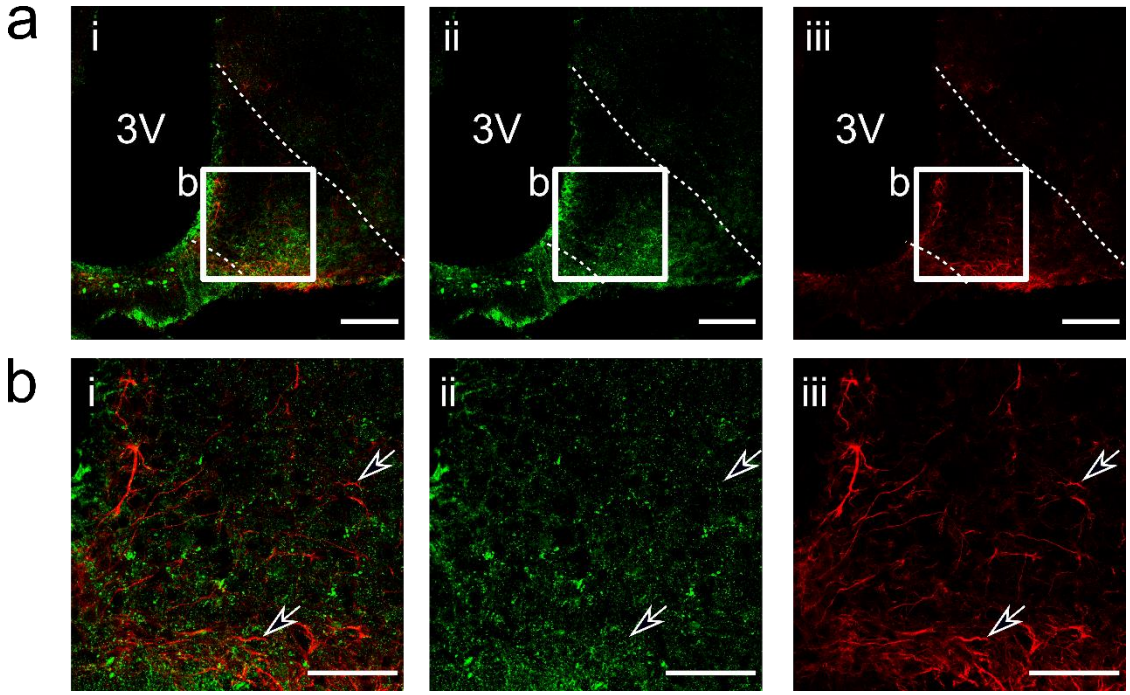

Figure 3.2.2.1 TSPO and GFAP immunoreactivity in the hypothalamic arcuate nucleus and median eminence of a male C57BL/6J mouse brain.

TSPO (ii; green) and GFAP (iii; red) immunoreactivity did not coincide in neither the hypothalamic arcuate nucleus nor median eminence (a-i; merge). Image taken at 20x magnification, and scale bars represent 100 µm. GFAP immunoreactivity was strongest in the arcuate nucleus around the median eminence (b). Images here were taken at 63x magnification, and scale bars represent 50 µm.

Key: Third ventricle (3V).

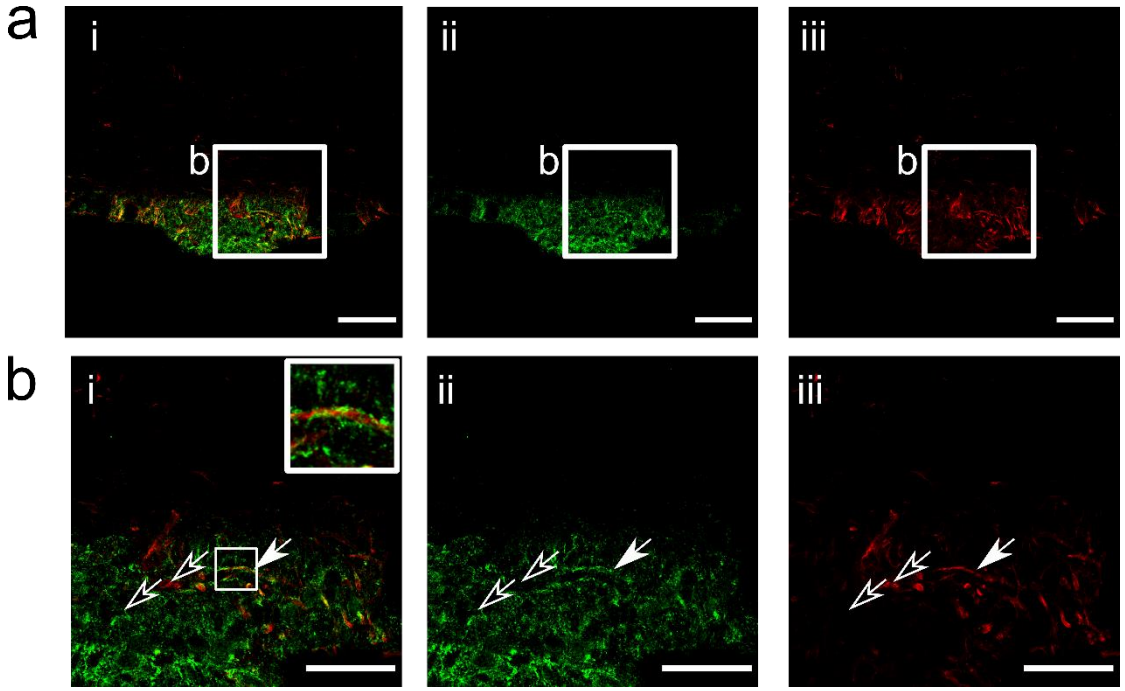

Figure 3.2.2.2 TSPO and GFAP immunoreactivity in the mouse subfornical organ of tissue taken from a male C57BL/6J mouse.

TSPO (ii; green) and GFAP (iii; red) immunoreactivity was detected within the subfornical organ (a-i). There appeared to be coincidences of immunoreactivity detected at higher magnification, as indicated by the white filled arrow versus the empty arrows, and insert of digital zoom image (b). Images taken at 20x (a) and 63x (b) magnification with scale bars representing 100 μm and 50 μm, respectively.

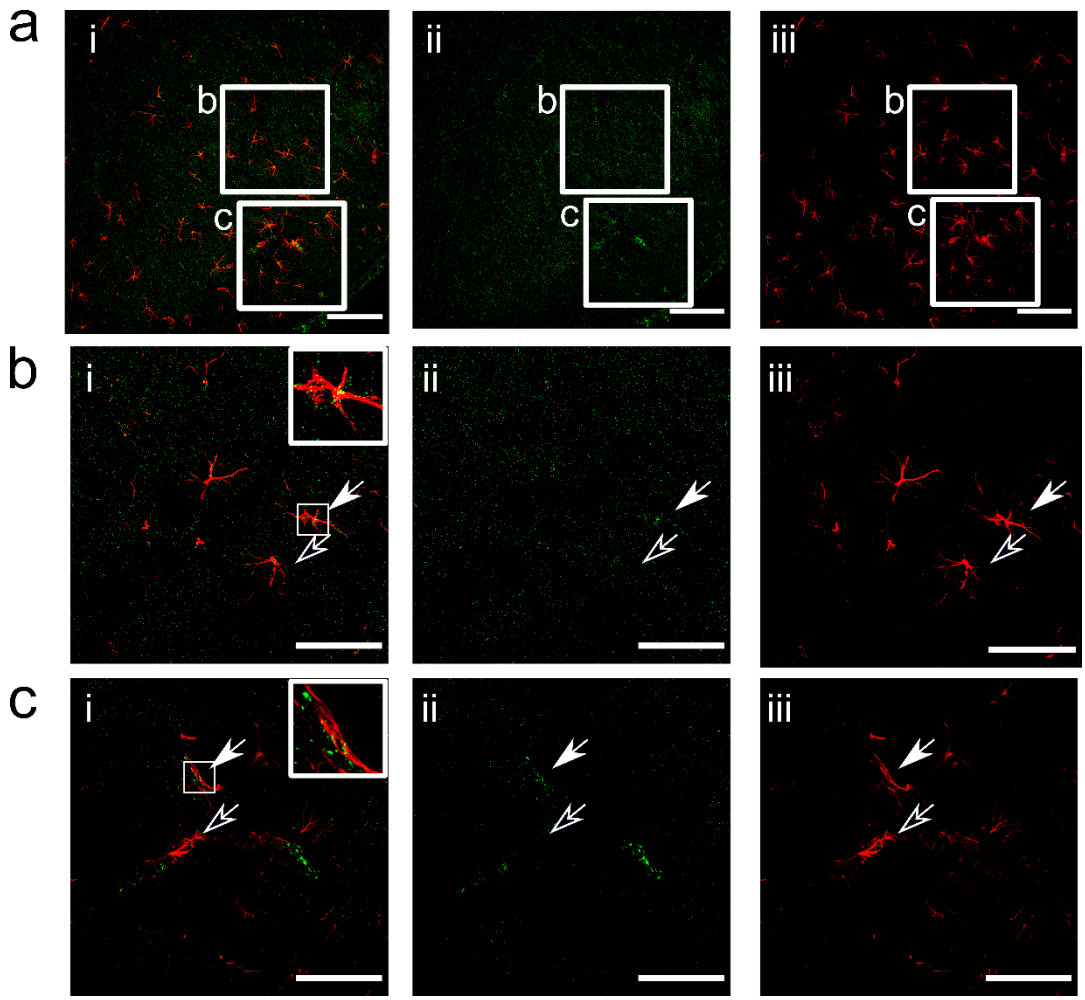

Figure 3.2.2.3 TSPO and GFAP immunoreactivity in the mouse cortex.

TSPO (ii; green) and GFAP (iii; red) immunoreactivity were both observed in the mouse cortex (a-i; merge). Image captured at 20x magnification, and scale bar represents 100 µm. Co-localisation of immunoreactivity was detected in some GFAP-positive astrocyte cells (b), as indicated by the white filled versus the empty arrows. Insert on merged image shows digital zoom of potential colocalisation. GFAP immunoreactivity was also observed around TSPO-positive immunoreactivity in the vasculature (c). Images here were captured at 63x magnification, with scale bar representing 50 µm.

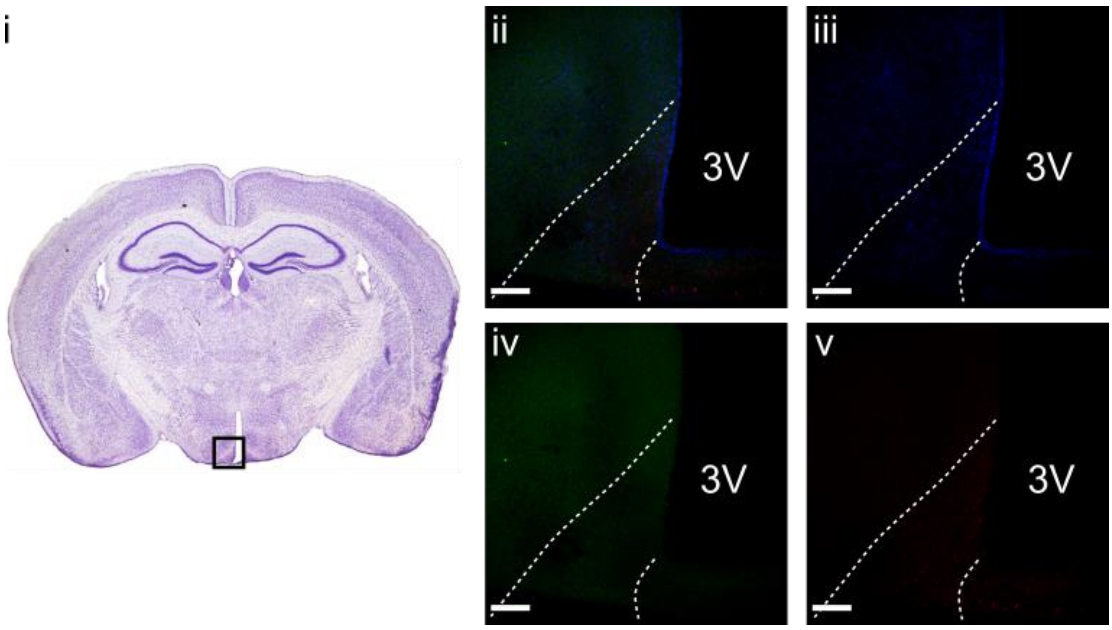

Figure 3.2.2.4 Immunohistochemistry in absence of TSPO and GFAP antibodies in the mouse brain.

Figure from the Mouse Brain in Stereotaxic Coordinates (381) at -1.70 mm from bregma indicating the brain region from which the images are displayed (i). Image of the hypothalamic arcuate nucleus (outlined) showing secondary antibody non-specific binding (ii; merge) and DAPI nuclear staining (iii; blue) in the absence of TSPO (iv; green) and GFAP (v; red) antibodies. Images taken at 20x magnification and scale bars represent 100 µm.

Key: Third ventricle (3V).

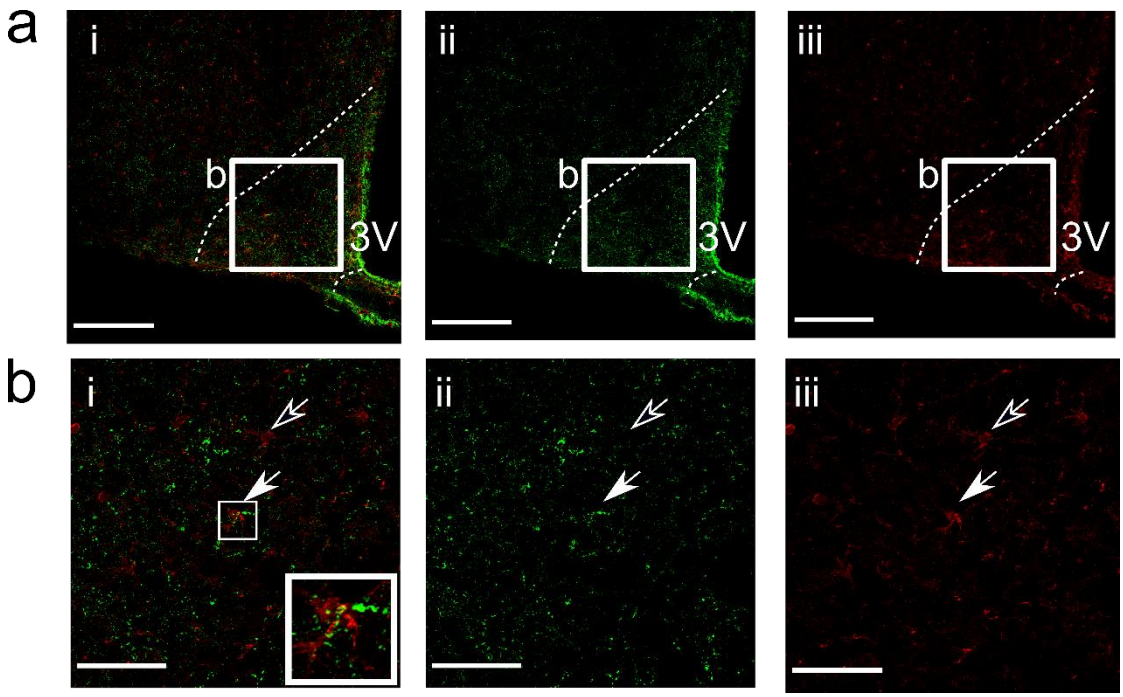

Fig 3.2.2.5 TSPO and IBA1 immunoreactivity in the hypothalamic arcuate nucleus and median eminence of a male C57BL/6J mouse.

TSPO (ii; green) and IBA1 (iii; red) immunoreactivity were both detected within the arcuate nucleus of the hypothalamus (a-i; merge). There was coincidence of immunoreactivity detected at higher magnification, as depicted by the white filled arrows and the digital zoom insert (outlined) (b). The empty arrows indicate TSPO-negative GFAP-positive cell. Images taken at 20x magnification (a) and 63x magnification (b), with scale bars representing 100 µm and 50 µm respectively.

Key: Third ventricle (3V)

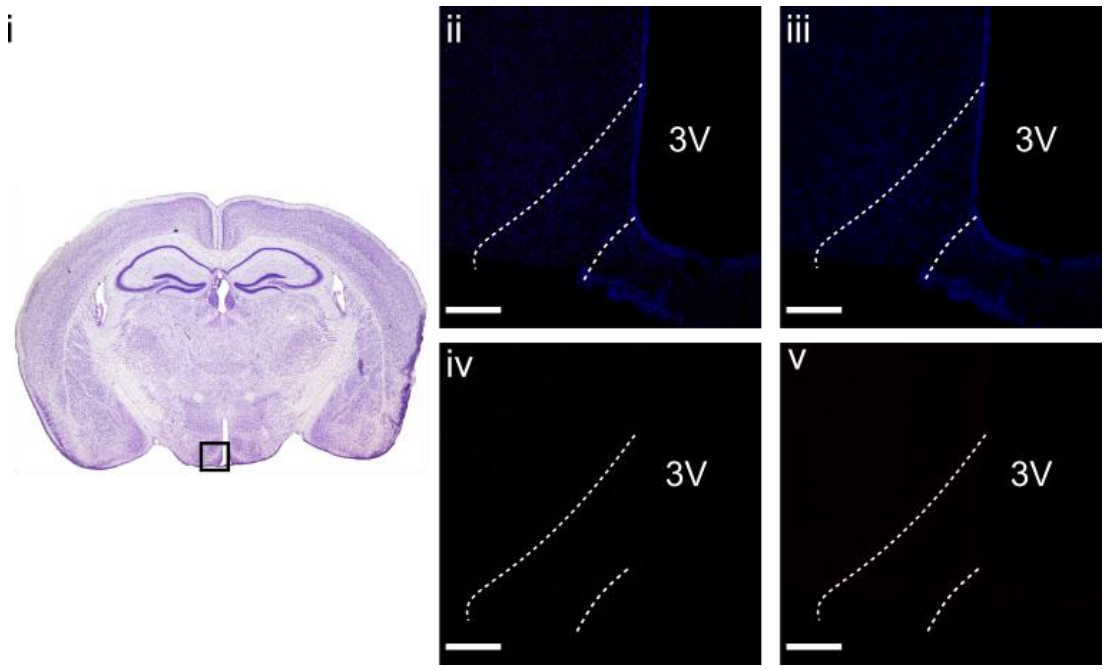

Figure 3.2.2.6 Immunohistochemical processing in absence of TSPO and IBA1 antibodies in the mouse brain.

Representative figure of -1.70 mm from bregma, taken from the Mouse Brain in Stereotaxic Coordinates (381), depicting the region in which the images were taken (i). Immunohistochemical processing in the hypothalamic arcuate nucleus as outlined by the white dashed line (ii; merge) with DAPI nuclear staining (iii; blue), in absence of TSPO (iv; green) and IBA1 (v; red) antibodies. Images taken at 20x magnification and scale bars represent 100 µm.

Key: Third ventricle (3V).

3.2.2.3 TSPO in vimentin-positive tanycytes

I used dual immunohistochemistry on forebrain sections from male C57Bl/6J mice; processing for TSPO and vimentin, a commonly used cell marker for tanycytes. Tanycytes are an ependymal-like cell that line the ventricles of the brain and are present in the circumventricular organs (153,400). Vimentin is a type-3 intermediate filament protein that is expressed in mesenchymal cells (401,402), and can also be expressed by mature astrocytes and ependymal cells (403).

As expected, vimentin immunoreactivity was observed around the 3V throughout the brain in male and female mice (Fig 3.2.2.7-8). I found that TSPO immunoreactivity was mostly expressed in the 3V lining that is adjacent to the MBH compared to the level of the DMH (Fig 3.2.2.7). Co-localisation was also most prominent in the tanycyte layer next to the Arc (Fig 3.2.2.7c). There was a little co-immunoreactivity between TSPO and vimentin in the tanycytes at the base of the 3V (Fig 3.2.2.7d). Similarly, in the tanycytic layer adjacent to the DMH, no TSPO immunoreactivity was co-detected with vimentin (Fig 3.2.2.7b).

Vimentin-positive cells were also identified around the 3V, further anterior in the mouse brain, at the level of the VOLT (Fig 3.2.2.8). As identified previously, this region has dense TSPO immunoreactivity and strong overlap of TSPO and vimentin immunoreactivity was observed across the region.

Vimentin-labelled cells were also identified around the lateral ventricle (LV) of the mouse forebrain (Fig 3.2.2.9). Both TSPO and vimentin Immunoreactivity was only identified in the dorsal and lateral sides of the ventricles – where they appeared to co-localise. TSPO immunoreactivity was found throughout the LSN. Although it did not appear to extend from the ventricles, some vimentin immunoreactivity was identified in the LSN.

The secondary antibody used in this immuno-processing was confirmed to be specific in immunohistochemistry in absence of TSPO and vimentin antibodies (Fig 3.2.2.10).

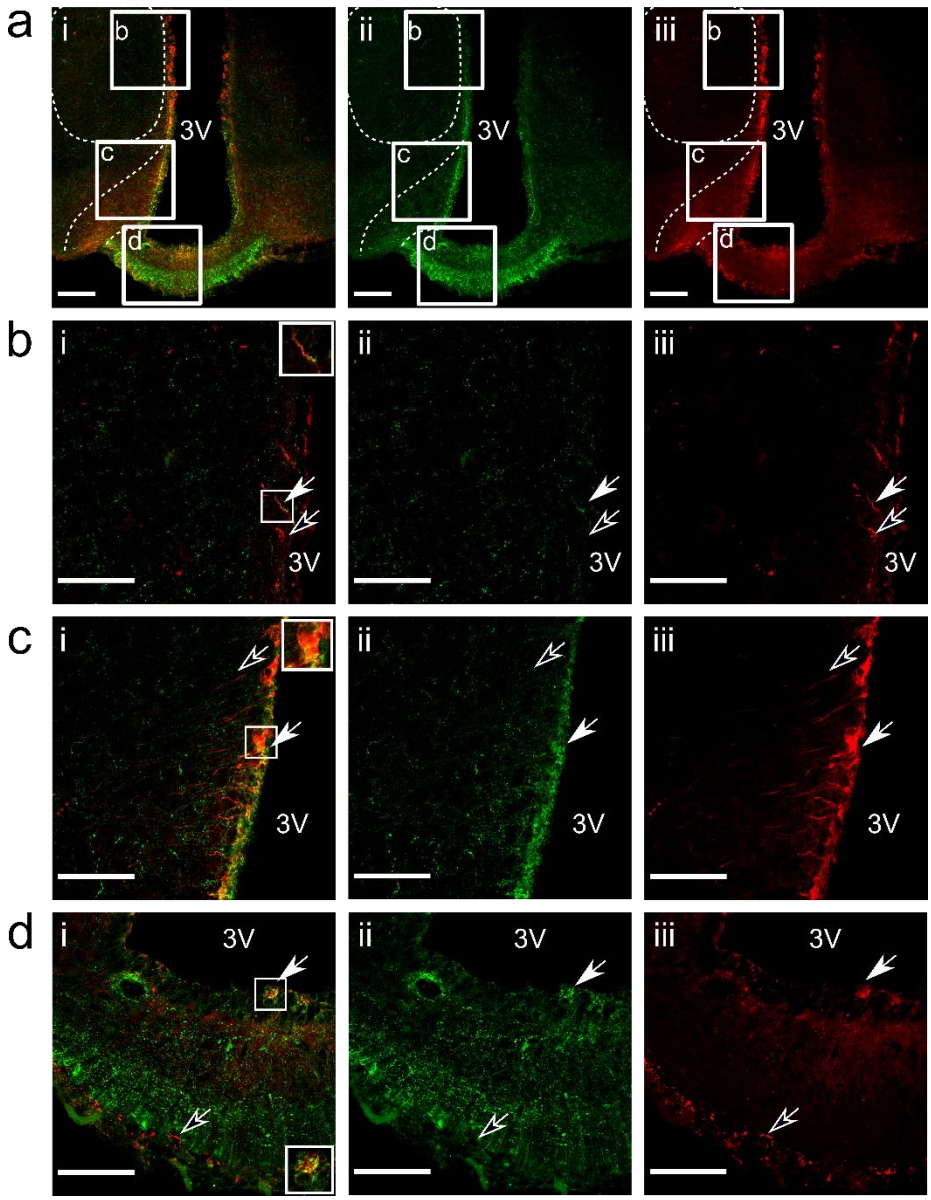

Figure 3.2.2.7 Vimentin and TSPO immunoreactivity coincide at the third ventricle adjacent to the hypothalamic arcuate nucleus in tissue from a male C57BL/6J mouse.

TSPO (ii; green) and vimentin (iii; red) labelling occurred around the third ventricle in the hypothalamus (a-i; merge). There was minimal incidence of TSPO and vimentin co-immunoreactivity in the region adjacent to the dorsomedial hypothalamus (b), as denoted by the white filled arrows versus empty arrows digital zoom insert (outlined). There was considerably greater coincidence of immunoreactivity at the ventricle wall adjacent to the arcuate nucleus (c). There was little colocalisation of vimentin and TSPO above the median eminence (d). Images taken at 20x magnification with scale bars representing 100 µm (a). Images taken at 63x magnification and scale bars representing 50 µm (b-d).

Key: Third ventricle (3V).

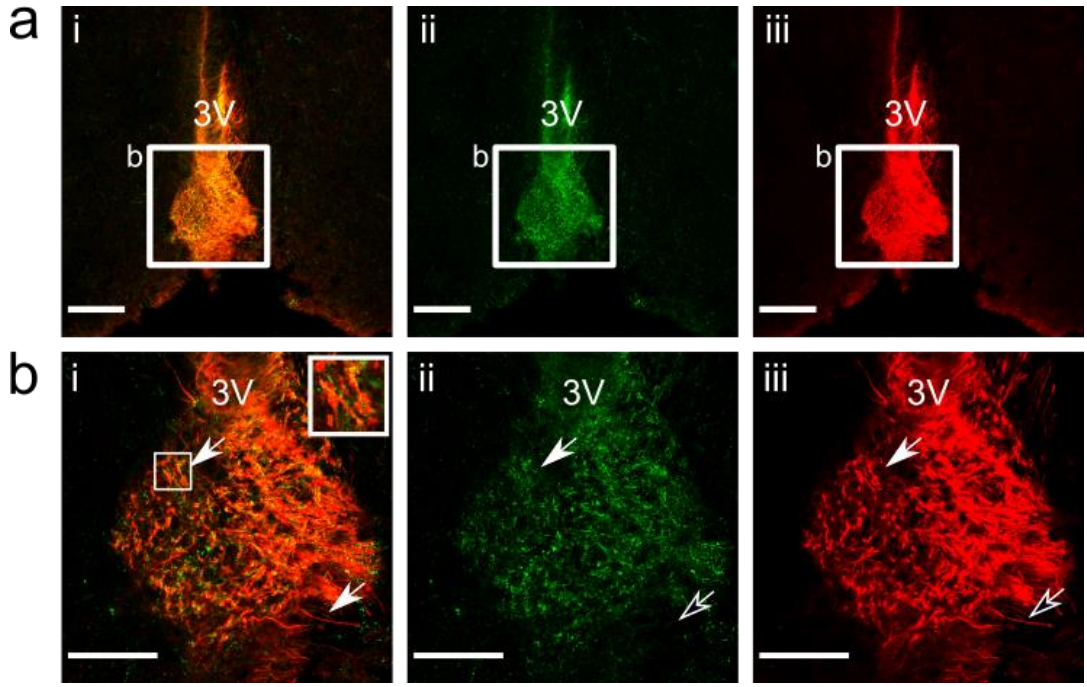

Figure 3.2.2.8 TSPO and vimentin immunoreactivity in the vascular organ of the lamina terminalis, in brain tissue taken from a male C57BL/6J mouse.

TSPO (ii; green) and vimentin (iii; red) immunoreactivity were observed in the vascular organ of the lamina terminalis around the third ventricle (a-i; merge). The majority of immunoreactivity appeared to coincide (b), as noted by the white filled arrows versus empty arrows and the digital zoom insert (outlined). Images taken at 20x magnification, with scale bars representing 100 µm (a), and at 63x magnification with scale bars representing 50 µm (b).

Key: Third ventricle (3V).

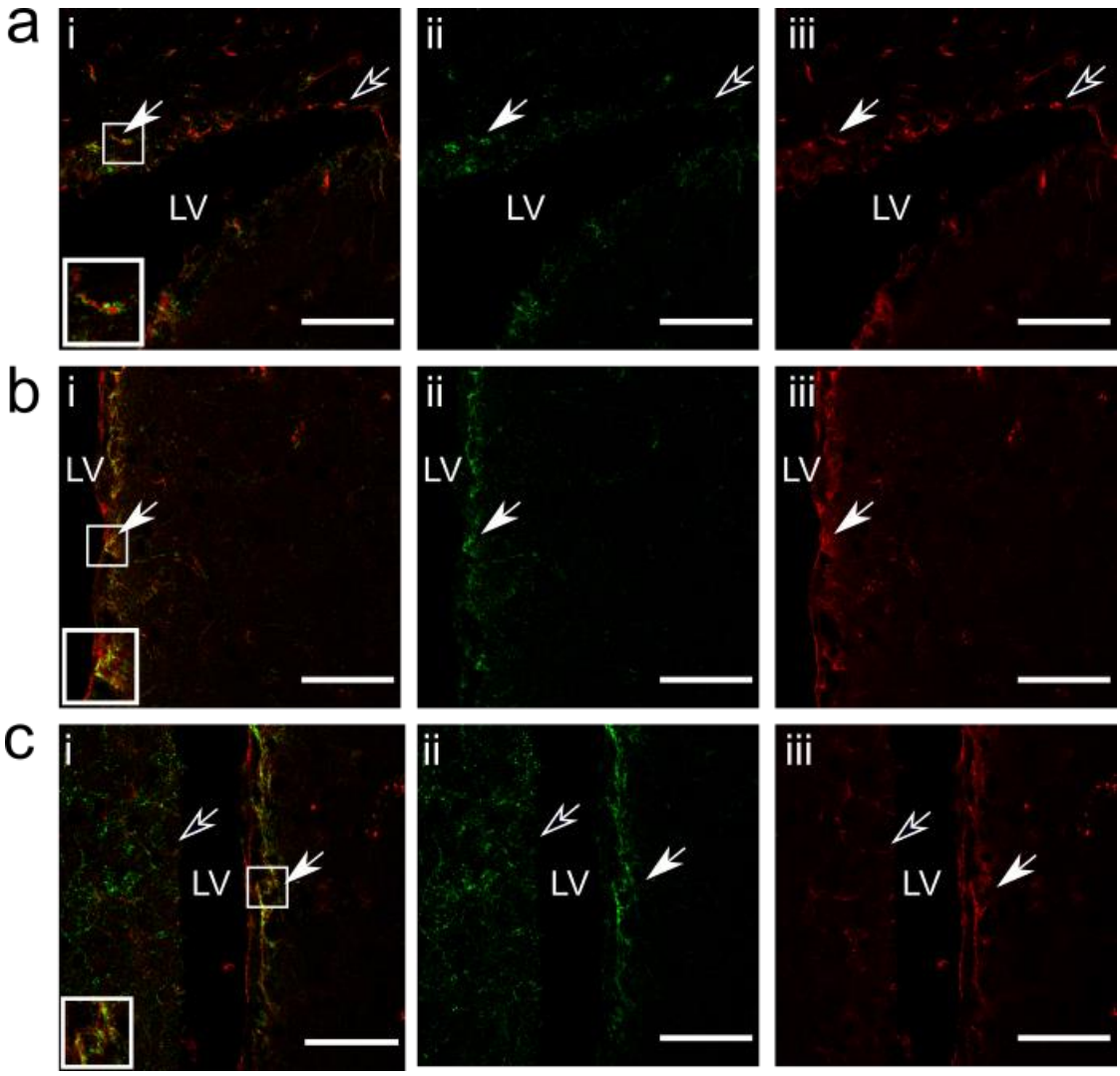

Figure 3.2.2.9 TSPO and vimentin immunoreactivity around the lateral ventricle in brain tissue taken from a male C57BL/6J mouse.

TSPO (ii; green) and vimentin (iii; red) immunoreactivity were observed in the lining of the lateral ventricle (i; merge). The majority of immunoreactivity appeared to coincide at the wall adjacent to the lateral septal nucleus in the dorsal (a), intermediate (b) and ventral parts (c). Incidences of co-immunoreactivity are noted by the white filled arrows versus empty arrows, and the digital zoom insert (outlined). Images taken at 63x magnification with scale bars representing 50 μm.

Key: Third ventricle (3V).

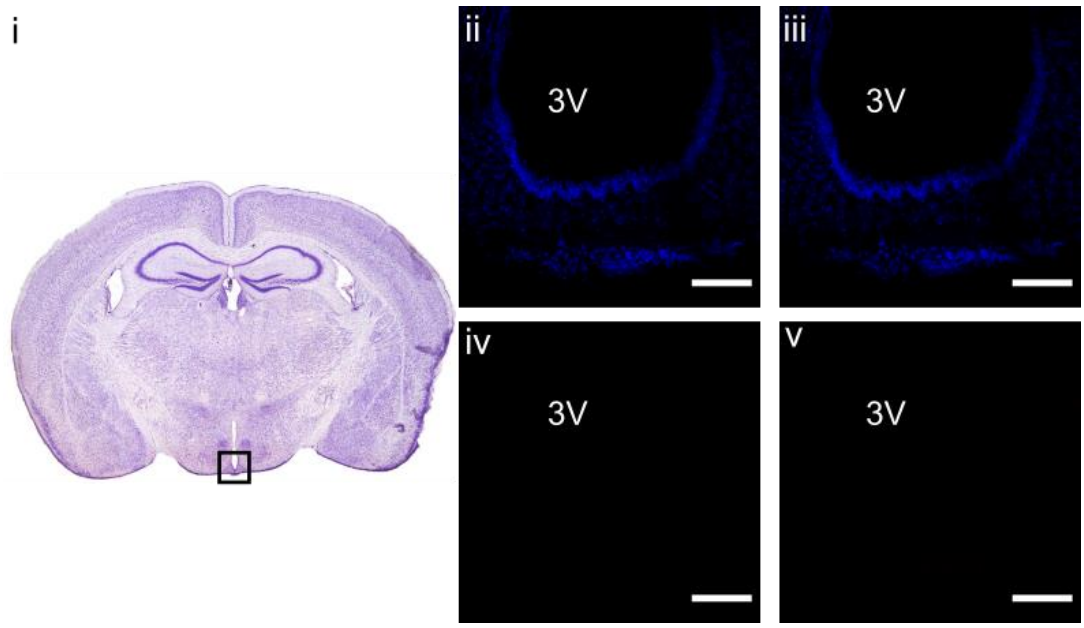

Figure 3.2.2.10 Immunohistochemical processing in absence of TSPO and vimentin antibodies in the mouse brain.

Figure taken from the Mouse Brain in Stereotaxic Coordinates (381) indicating the brain region at -1.58 mm from bregma in which the images were taken (i). Immunohistochemical processing at the median eminence (ii; merge) with DAPI nuclear staining (iii; blue), in the absence of TSPO (iv; green) and vimentin (v; red) antibodies. Images taken at 20x magnification and scale bars represent 100 µm.

Key: Third ventricle (3V).

3.2.2.4 TSPO immunoreactivity in TRH-positive neurons

I used dual immunohistochemistry to identify TSPO and GFP immunoreactivity in brain sections taken from TRH-eGFP reporter mice. Thyrotropin-releasing hormone (TRH) is synthesised primarily within neurons of the PVH, of which the axons project down to the ME. While TRH neurons are important in release of thyrotropin and prolactin from the pituitary gland, the interest of relevance to this study is their distribution within the PVH (87). As previously described, dense TSPO immunoreactivity was observed in the PVH which looked neuronal in appearance rather than glial (Fig 3.2.1.1). Furthermore, the characterised location of TRH-expressing neurons in the PVH matches with the pattern of TSPO immunoreactivity (87). TRH is also expressed in neurons outside of the hypothalamus, and has been shown to be expressed in reactive astrocytes (404).

I identified a low level of co-localisation of TSPO immunoreactivity with that of GFP, a proxy marker of TRH neurons, within the paraventricular hypothalamus (Fig 3.2.2.11). TRH-eGFP immunoreactivity was mostly concentrated in the medial part of the PVH, while co-localisation was observed primarily in the lateral and dorsal regions of the PVH. The pattern of TRH-eGFP immunoreactivity formed mostly cell bodies and axons. TRH-eGFP immunoreactivity was noted within the medial zone of the ME (Fig 3.2.2.12). Surprisingly, this did not overlap with TSPO immunoreactivity, which was primarily contained within the external layer of the ME. TRH-eGFP immunoreactivity was, however, expressed in the DMH and this did coincide with TSPO immunoreactivity (Fig 3.2.2.13). TRH-eGFP formed some cell bodies within the DMH, as well as processes.

Other regions within the murine brain that both expressed GFP, as a proxy to TRH, and TSPO were the BNST and the SFO. Within the BNST, TRH-eGFP immunoreactivity took the form of processes rather than cell bodies – indicative of either dendrites or axons passing through these areas (Fig 3.2.2.14). Moderate coincidence of immunoreactivity was noted in the ventral portion of the BNST (Fig 3.2.2.14). TRH-eGFP immunoreactive cell bodies and processes were observed within the SFO, but these did not overlap with TSPO immunoreactivity (Fig 3.2.2.15).

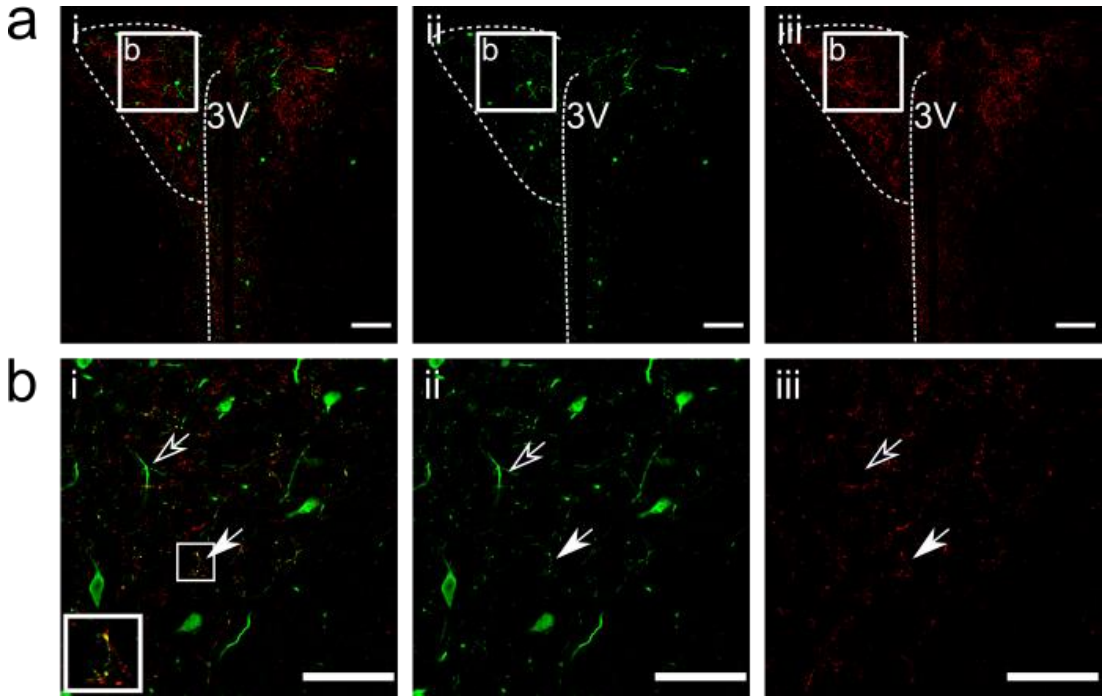

Figure 3.2.2.11 TSPO and TRH-eGFP immunoreactivity are detected within the paraventricular hypothalamus of male mice.

Both TSPO (ii; red) and TRH-eGFP (iii; green) immunoreactivity was detected in the paraventricular hypothalamus (a-I; merge). Image captured at 20x magnification, and the scale bar marks 100 µm. At 63x magnification (b), very little overlap of immunoreactivity was evident as depicted by the white filled arrows and the digital zoom insert versus the empty arrows. Scale bar represents 50 µm.

Key: Third ventricle (3V).

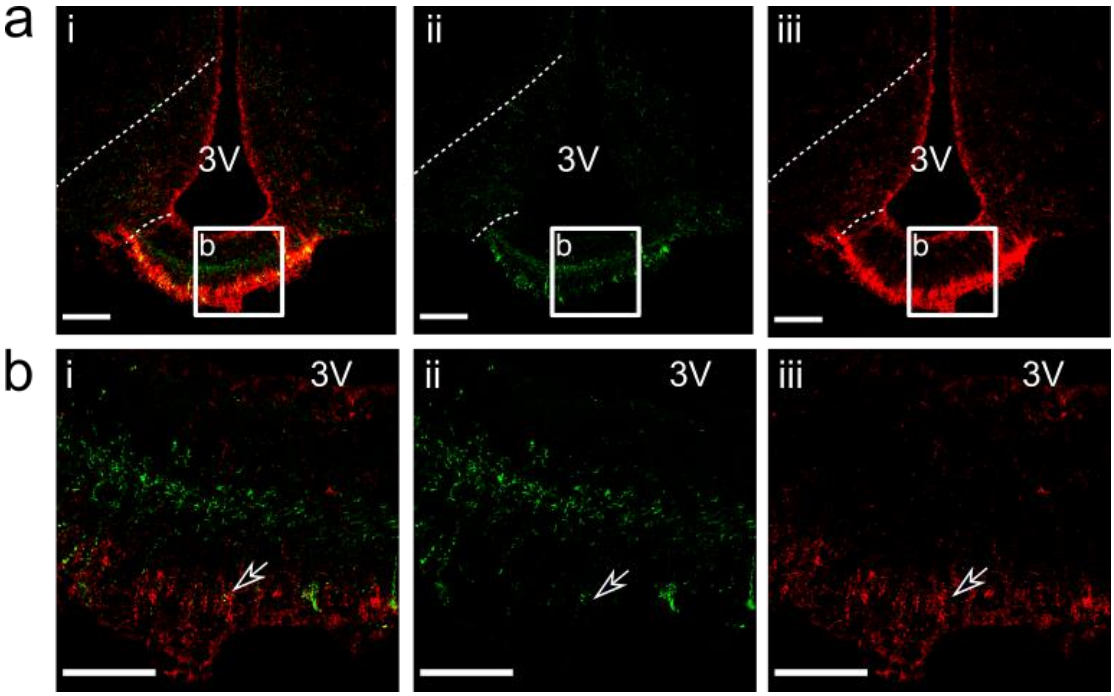

Figure 3.2.2.12 TSPO and TRH-eGFP immunoreactivity at the arcuate hypothalamic nucleus of male mice.

TSPO (ii; red) and TRH-eGFP (iii; green) immunoreactivity were both detected within the median eminence, but not the arcuate nucleus, of the hypothalamus (a-i; merge). Image captured at 20x magnification, with the scale bar representing 100 μm. No coincidence of immunoreactivity, as noted by the empty arrows, was detected in the median eminence at 63x magnification (b). Scale bars here represents 50 μm.

Key: Third ventricle (3V).

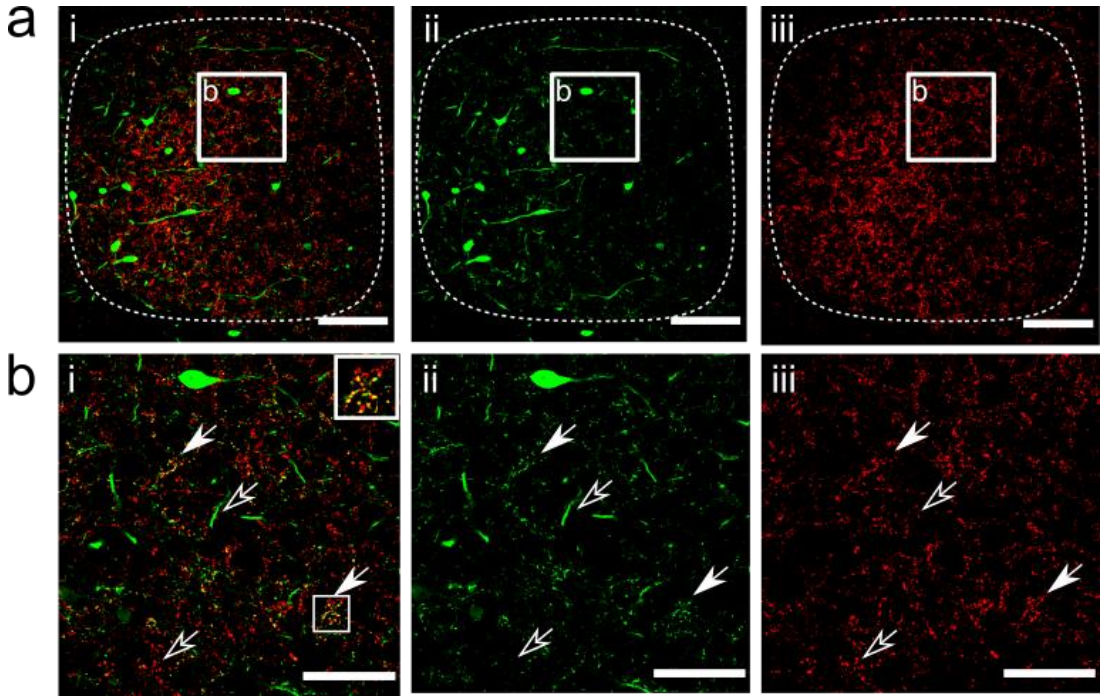

Figure 3.2.2.13 TSPO and TRH-eGFP immunoreactivity in the dorsomedial hypothalamus of a male mouse.

Dense TSPO (ii; red) and TRH-eGFP (iii; green) immunoreactivity was observed in the dorsomedial hypothalamus (a-i; merge). Image was taken at 20x magnification and the scale bar represents 100 µm. Incidences of potential co-localisation were observed and noted by the white arrows versus the empty arrows and the digital zoom insert (outlined) (b). Images were taken at 63x magnification with scale bars marking 50 µm.

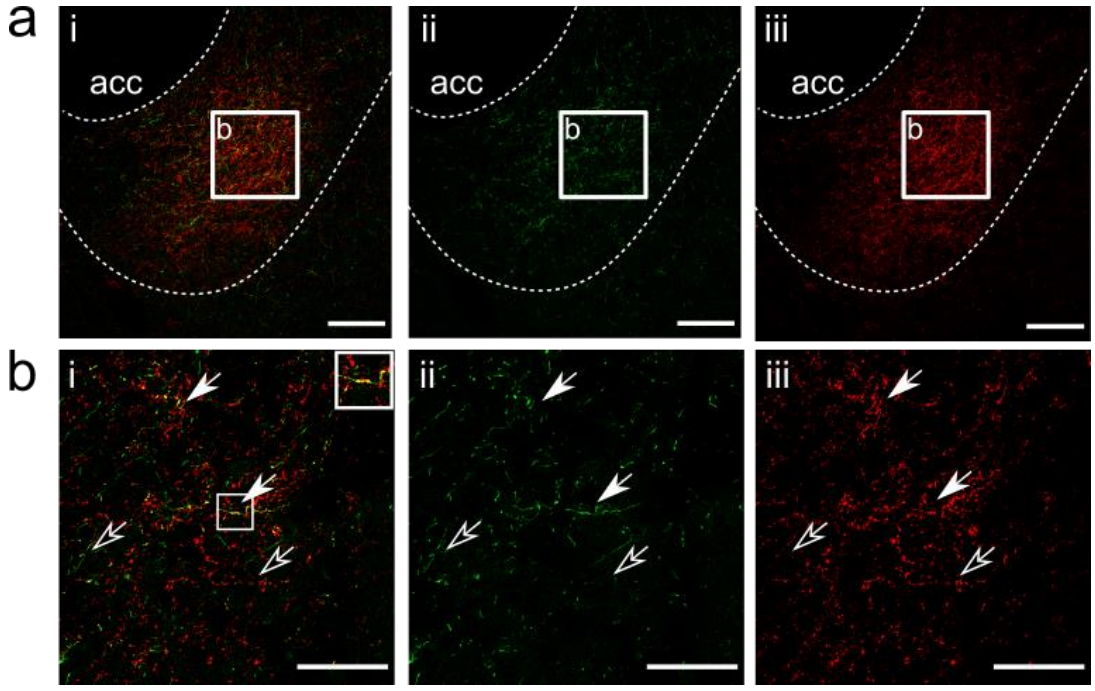

Figure 3.2.2.14 TSPO and TRH-eGFP immunoreactivity in the ventral portion of the bed nucleus of the stria terminalis of a male mouse.

TRH-eGFP immunoreactivity (ii; green) formed projection-like structures alongside TSPO (iii; red) immunoreactivity in the ventral bed nucleus of the stria terminalis (a-i; merge). There was a little overlap in immunoreactivity observed at high magnification, as noted by the filled arrows versus the empty arrows and the digital zoom insert (outlined) (b). Images taken at 20x (a) and 63x (b) magnification, with scale bars representing 100 µm and 50 µm respectively.

Key: anterior commissure (acc).

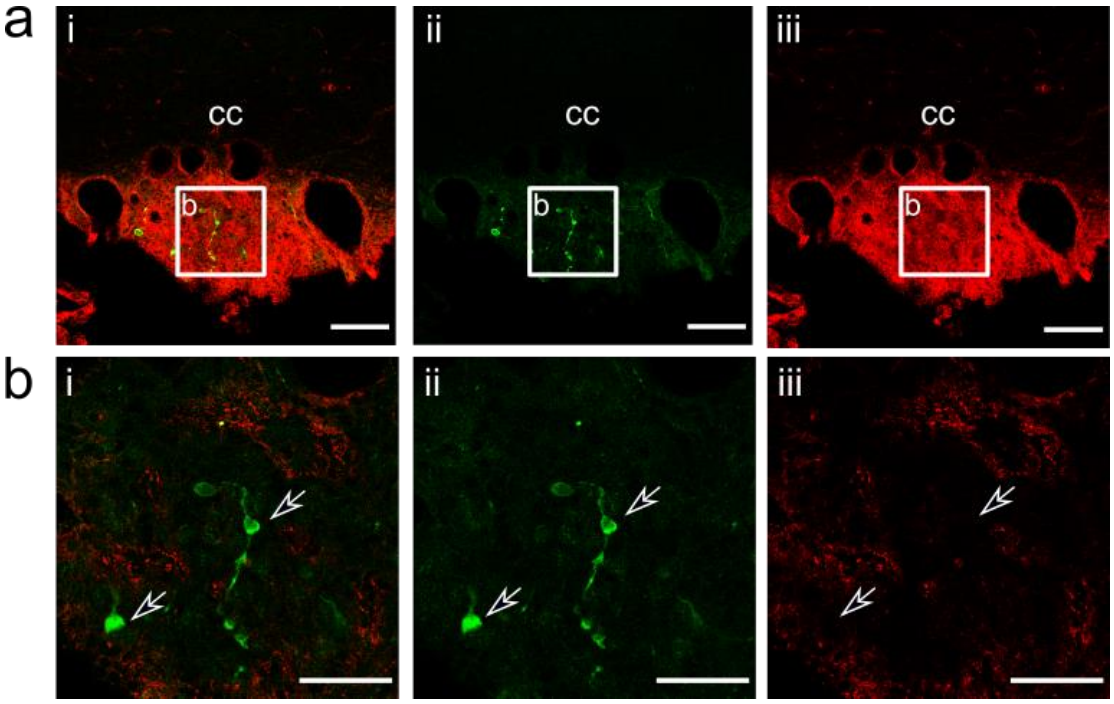

Figure 3.2.2.15 TSPO and TRH-eGFP immunoreactivity within the subfornical organ of a male mouse.

Both TRH-eGFP (ii; green) and TSPO (iii; red) immunoreactivity were observed in the subfornical organ (a-i; merge). No coincidence of immunoreactivity was observed as denote by the empty arrows (b). Images taken at 20x (a) or 63x (b) magnification with scale bars representing 100 μm and 50 μm, respectively.

Key: Corpus callosum (cc).

3.2.2.5 TSPO immunoreactivity in CRH-positive neurons

Corticotrophin-releasing hormone (CRH) is expressed within the parvocellular cells of the PVH, interspersed with TRH-expressing neurons. These neurons also project to the ME (87,405). CRH-positive neurons are important in regulating the neuroendocrine response to stress (405). CRH is also documented to be expressed in non-hypothalamic brain regions that are also associated with stress, such as the BNST and the amygdala (406,407). Furthermore, TSPO ligand Ro5-4864 induces CRH production in *ex vivo* rat hypothalamic slices (408). I applied immunohistochemistry to forebrain brain tissue from mice that express eYFP in CRH-positive neurons to investigate co-immunoreactivity with TSPO.

There was an overlap of immunoreactivity between TSPO and eYFP (labelled with GFP, as a proxy for CRH-expressing neurons) within the PVH (Fig 3.2.2.16). CRH-eYFP immunoreactivity formed mostly cell bodies in the parvocellular PVH, as expected, but processes were discernible in the dorsal portion of the PVH. TSPO immunoreactivity overlapped with that of CRH, albeit to a minor extent, in both the cell bodies and in the projections. TSPO immunoreactivity covered a greater area of the PVH than that of CRH-eYFP.

Sparse CRH-eYFP labelled cell bodies were also observed in the DMH, though these did not contain any TSPO immunoreactivity. CRH-eYFP labelled projections were observed within the ME, which were dense within the external layer (Fig 3.2.2.17b). Images taken at 63x magnification indicated that TSPO and CRH-eYFP immunoreactivity were in apposition to each other at the external layer of the ME.

There was coincidence of TSPO and CRH-eYFP immunoreactivity in the VOLT, immediately surrounding the 3V (Fig 3.2.2.18). The CRH-eYFP immunoreactivity formed mostly cell bodies plus some projections.

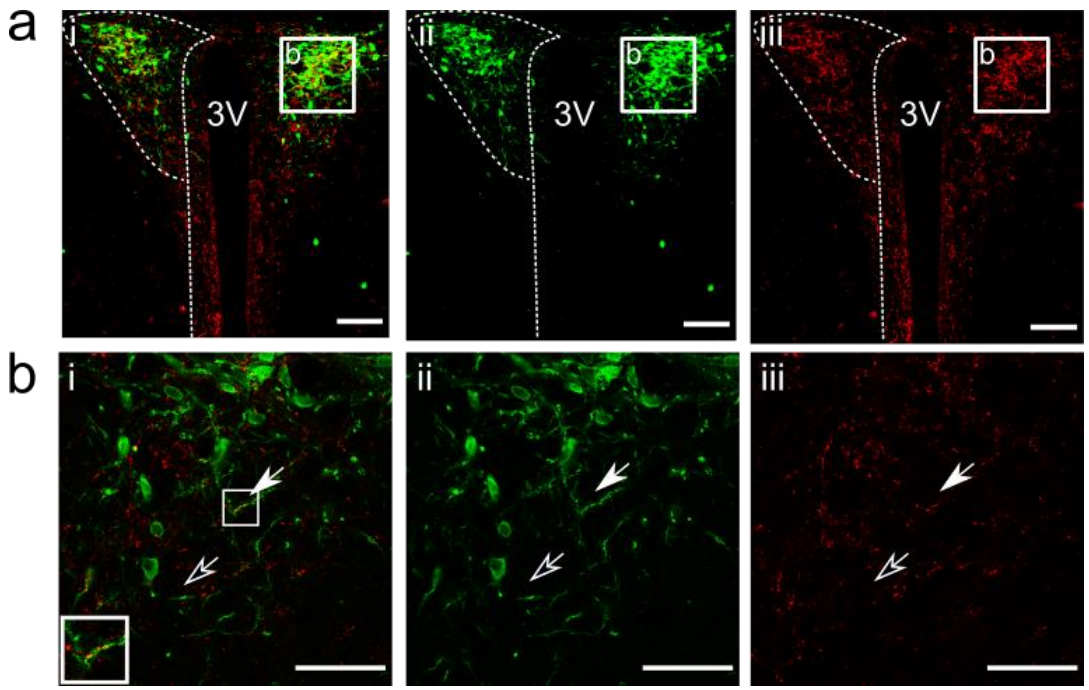

Figure 3.2.2.16 TSPO and CRH-eYFP immunoreactivity in the paraventricular and periventricular regions of the hypothalamus of a male mouse.

Dense CRH-eGFP (ii; green) and TSPO (iii; red) immunoreactivity was observed in the paraventricular hypothalamic nucleus (a-i; merge). Overlap of immunoreactivity was identified in the ventral portion of the paraventricular hypothalamus, as denoted by the filled arrows versus empty arrows and the digital zoom insert (outlined) (b). Images taken at 20x (a) and 63x magnification (b), with scale bars representing 100 µm and 50 µm respectively.

Key: Third ventricle (3V).

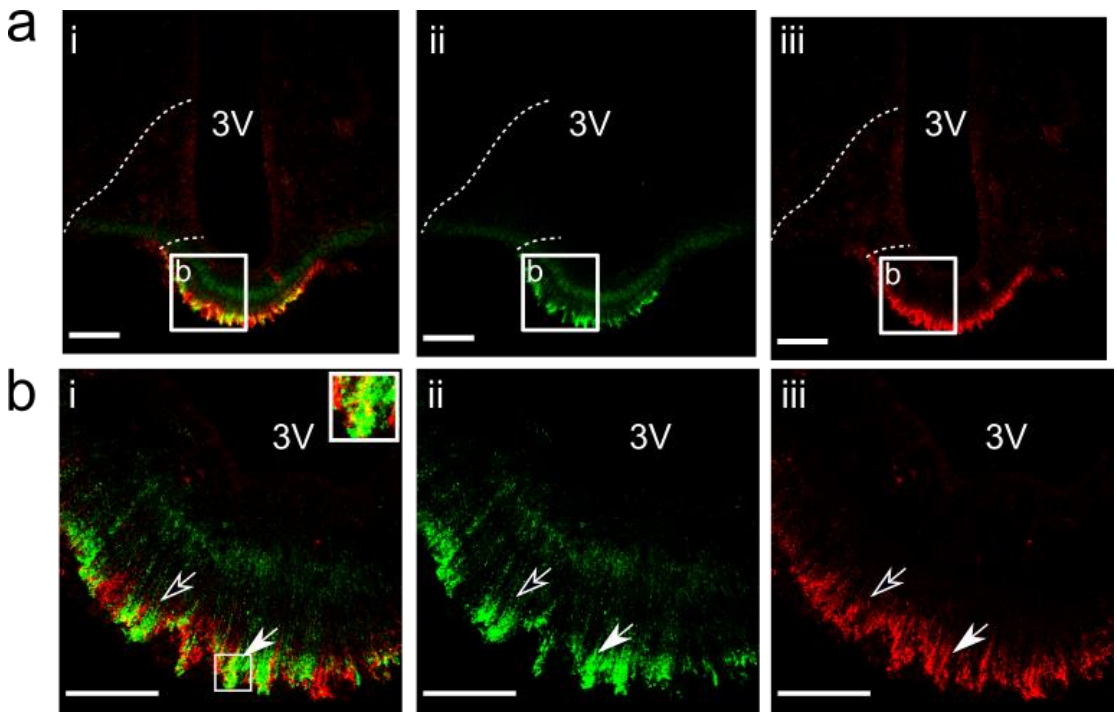

Figure 3.2.2.17 TSPO and CRH-eYFP immunoreactivity in the ventral part of the hypothalamus of a male mouse.

CRH-eYFP immunoreactivity (ii; green) was detected alongside that of TSPO (iii; red) in the median eminence (a-i; merge). There were little incidences of co-localisation detected in the external layer of the median eminence, as noted by the filled arrows and digital zoom insert (outlined), but the vast majority of reactivity occurred in apposition – exemplified by the empty arrows (b). Images taken at 20x (a) and 63x magnification (b), with scale bars representing 100 µm and 50 µm respectively.

Key: Third ventricle (3V).

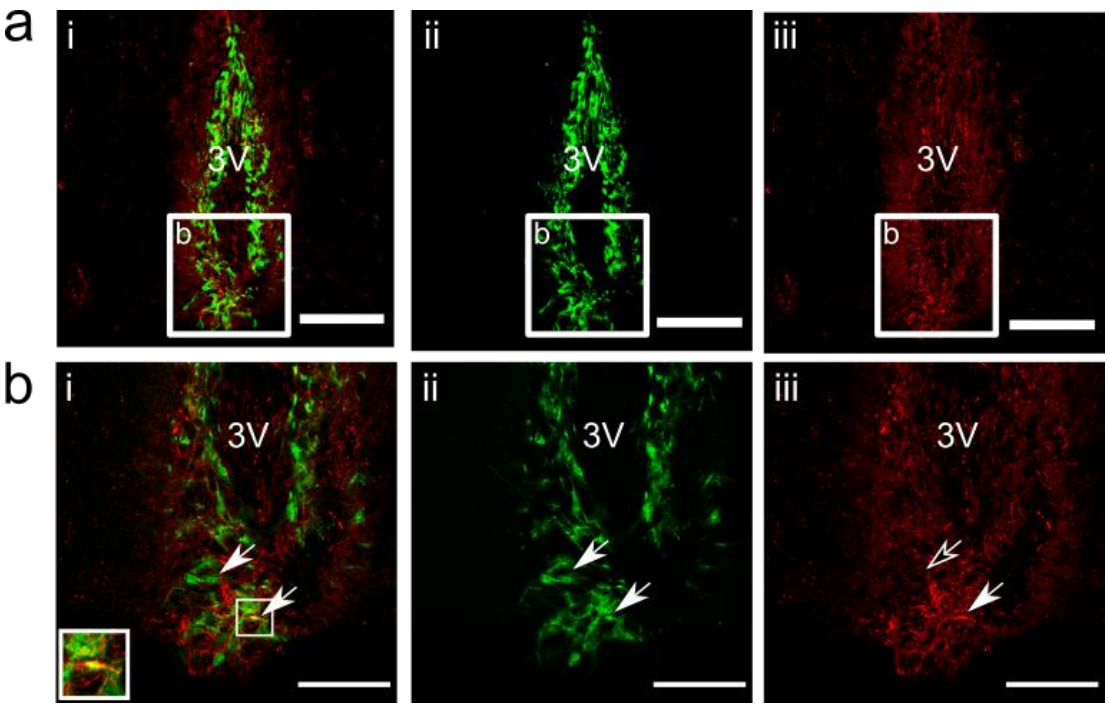

Figure 3.2.2.18 TSPO and CRH-eYFP immunoreactivity around the third ventricle in the vascular organ of the lamina terminalis of a male mouse.

CRH-eYFP (ii; green) & TSPO (iii; red) immunoreactivity were detected in the vascular organ of the lamina terminalis (a-i; merge). At higher magnification, a few incidences of co-reactivity were detected – defined by the white filled arrows versus the empty arrows and the digital zoom insert (outlined) (b). Images taken at 20x (a) and 63x magnification (b), with scale bars representing 100 µm and 50 µm respectively.

Key: Third ventricle (3V).

3.2.2.6 TSPO immunoreactivity in GAD65-expressing neurons

Glutamate decarboxylase (GAD) is an enzyme, expressed in both the CNS and in the pancreas, that catalyses the decarboxylation of glutamate to γ-aminobutyric acid (GABA) and carbon dioxide (409). It exists as two isoforms, either GAD65 or GAD67, and each have distinct functions (410). GAD65 is primarily used in neuronal terminals and synapses of the neuroendocrine system, where it synthesises GABA for release as a neurotransmitter. Furthermore, the central benzodiazepine receptor is structurally similar to TSPO and has high affinity to GABA (411). TSPO ligands are also capable of modulating GABA secretion (412). To investigate TSPO expression in GAD65-positive neurons, I immunohistochemically processed brain sections taken from transgenic GAD65-GFP mice for TSPO immunoreactivity.

GAD65-positive neurons were identified within the DMH (Fig 3.2.2.19). These formed mostly cell bodies, and immunoreactivity did not coincide with that of TSPO. GAD65-GFP immunoreactivity was also observed within the Arc, but this was not identified to co-localise with that of TSPO (Fig 3.2.2.20).

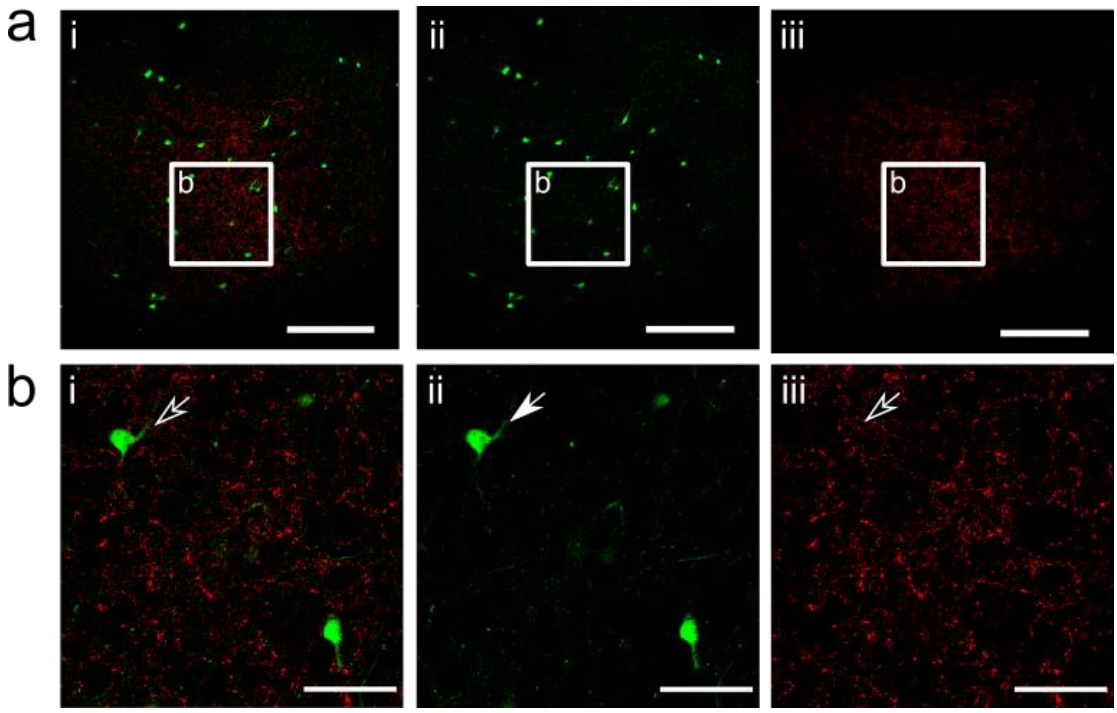

Figure 3.2.2.19 TSPO and GAD65-eGFP immunoreactivity within the dorsomedial hypothalamus of a male mouse.

TSPO (iii; red) immunoreactivity was detected around GAD65-eGFP-positive (ii; green) cell bodies in the dorsomedial hypothalamus (a-i; merge). No coincidence of overlap was detected at higher magnification, indicated by the empty arrows (b). Images taken at 20x (a) and 63x magnification (b), with scale bars representing 100 µm and 50 µm respectively.

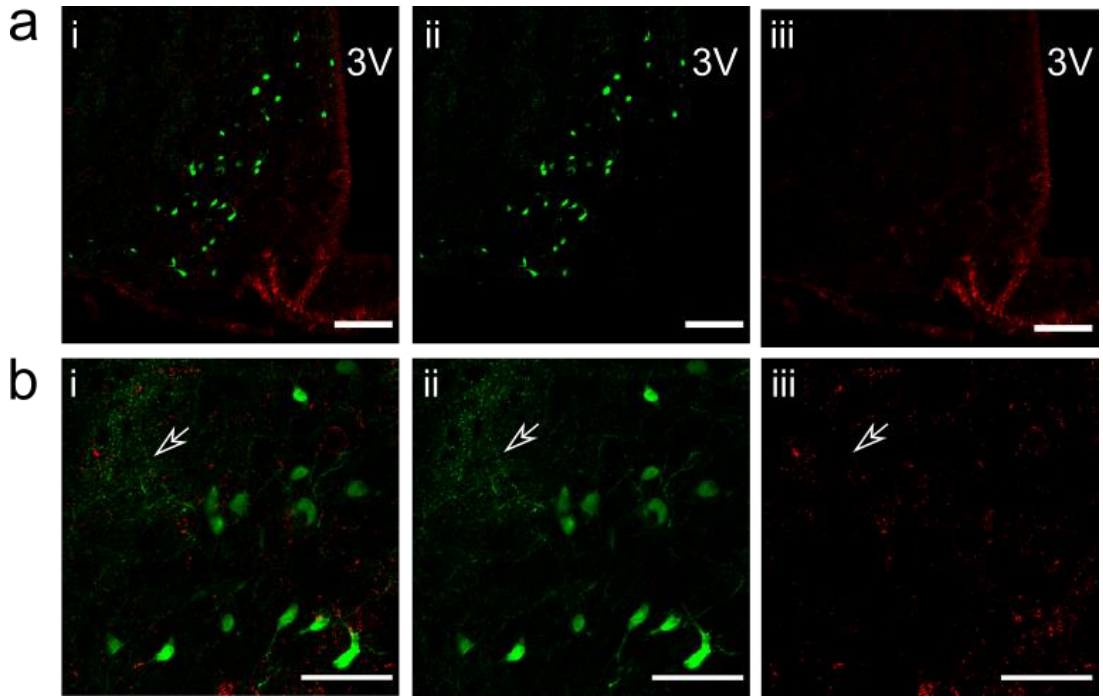

Figure 3.2.2.20 TSPO and GAD65-eGFP in the hypothalamic arcuate nucleus of a male mouse.

GAD65-eGFP (ii; green) and TSPO (iii; red) immunoreactivity was detected in the arcuate nucleus of the hypothalamus (a-i; merge). No coincidences of immunoreactivity were detected in the arcuate nucleus, as exemplified by the empty arrows (b). Images taken at 20x (a) and 63x magnification (b), with scale bars representing 100 μm and 50 μm respectively.

Key: Third ventricle (3V).

3.2.3 Verification of immunoreactivity detected by rabbit anti-TSPO antibody in TSPO knock-out mice

It was important to validate the antibody that targeted TSPO in order to confirm the distribution of TSPO in the mouse brain and the significance of the antibody's immunoreactive product. This was performed by repeating the immunohistochemical process on brain sections obtained from TSPO wild-type (+/+) and knock-out (-/-) mice. Unfortunately, despite the antibody being knock-out validated by its production company, I was still able to detect TSPO-positive immunoreactivity within the brain tissue from the TSPO -/- mice (Figs 3.2.3.2-5). Western blot analysis with the same antibody identified a band at 18 kDa, which corresponds to TSPO (Fig 3.2.1.6). Immunocytochemical processing of cortical primary astrocytes, cultured from litters of TSPO +/+ and -/- mice, confirmed absence of immunoreactivity in the astrocytes of TSPO -/- litters (Fig 3.2.3.1). In brief, these cultured cortical astrocytes were isolated as described by Schildge *et al* (413), seeded at 1 brain per flask and maintained in supplemented in Dulbecco's modified Eagle Medium as described by Vlachaki Walker *et al* (414). For immunocytochemical processing, the mouse primary astrocytes were plated at a density of 1 x 10^5 cells per coverslip, fixed with 4% paraformaldehyde solution and permeabilised by lysine block prior to staining with rabbit anti-TSPO (Table 2.7.1.1) and donkey anti-rabbit^{488} (Table 2.7.1.2) at the same concentrations and incubation times as described in this thesis. Considering the results obtained from these experiments, I consequently deduce that there is cross-reactivity between the TSPO antibody and an unknown antigen in mouse brain tissue – which is not present in primary astrocyte cell culture. I immunohistochemically processed forebrains from TSPO +/+ and -/- mice to investigate any differences in immunoreactivity identified by the TSPO antibody.

First, it was important to look into the hypothalamic regions in which dense TSPO immunoreactivity was observed. Within the DMH, immunoreactivity was similar if not more intense in the TSPO -/- mice compared TSPO +/+ (Fig 3.2.3.2). Conversely, immunoreactivity within the Arc seemed to be reduced in TSPO -/- animals (Fig 3.2.3.2). This may have been due to the absence of TSPO immunoreactivity in the ependymal/tanycytes layer of the 3V in the TSPO -/- animals. There was no TSPO immunoreactivity that formed "tanycyte-like" projections away from the 3V in the TSPO -/- mice compared to that in TSPO +/+.

There was also reduced TSPO immunoreactivity within the ME, though not completely absent, in the TSPO -/- brains (Fig 3.2.3.2).

Loss of TSPO-targeted immunoreactivity in circumventricular organs was observed in the TSPO -/- mice. In the VOLT, immunoreactivity was drastically reduced in brains from TSPO -/- animals compared to TSPO +/+ (Fig 3.2.3.3). However, immunoreactivity was not entirely absent and so expression of the unknown protein that cross-reacts with the antibody must also be present in the VOLT. Immunoreactivity was reduced in the SFO of TSPO -/- compared to TSPO +/+ mice (Fig 3.2.3.4). Within the choroid plexus, immunoreactivity was entirely absent in brains from TSPO -/- mice (Fig 3.2.3.5). The genotype of the mice, from which brain tissue was immunohistochemically processed, was confirmed using PCR (Fig 3.2.3.6).

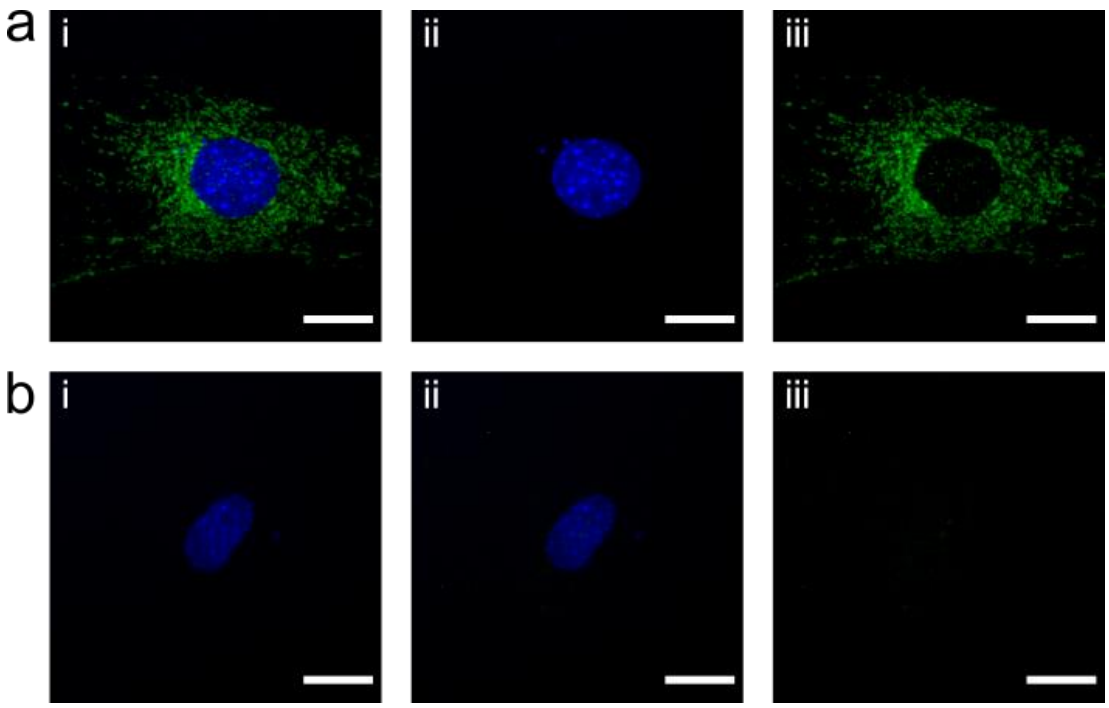

Figure 3.2.3.1 TSPO immunoreactivity in primary cultured astrocytes of TSPO +/+ and -/- mice.

TSPO immunoreactivity was present in primary astrocytes, cultured from < 5 day old mouse pups, of TSPO +/+ (a) and -/- (b) litters. Channels are merged (i) from DAPI nuclear staining (ii; blue) and TSPO immunoreactivity (iii; green). Images captured at 20x magnification, and scale bars represent 25 μm. Image courtesy of Dr. Josie Robb, University of Exeter (415).

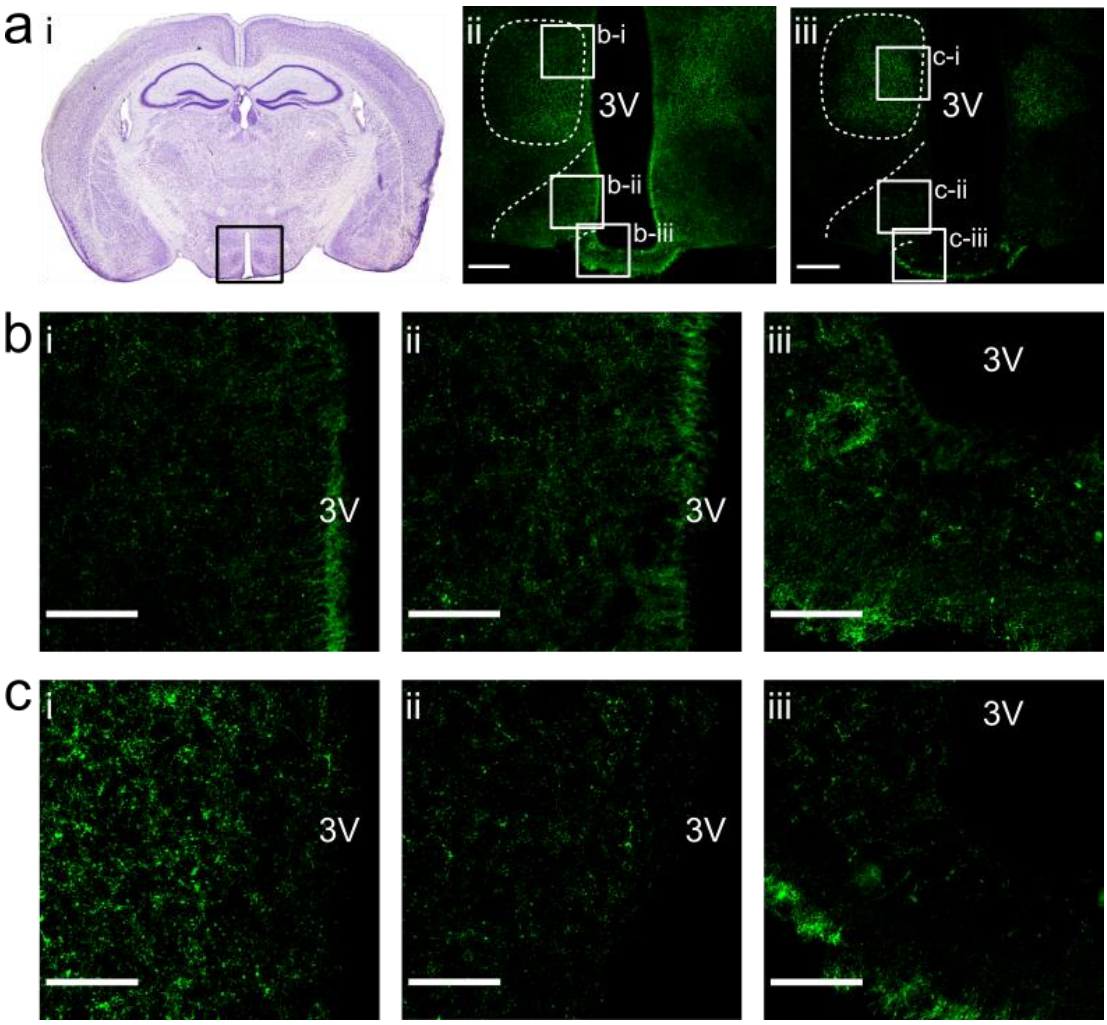

Figure 3.2.3.2 TSPO immunoreactivity in the dorsomedial and mediobasal hypothalamus of TSPO +/+ and -/- mice.

Figure taken from the Mouse Brain in Stereotaxic Coordinates (381), outlining the region at -1.70mm from bregma where the images were taken (a-i). TSPO immunoreactivity was lower in the mediobasal hypothalamus and in the layer of the third ventricle of TSPO -/- (a-iii) compared to TSPO +/+ mice (a-ii). Immunoreactivity imaged at 63x magnification in the dorsomedial hypothalamic nucleus (i), arcuate nucleus (ii) and median eminence (iii) of TSPO +/+ (b) and -/- (c) mice. Scale bars represent 200 μm at 20x magnification (a), 50 μm at 63x magnification (b, c).

Key: Third ventricle (3V).

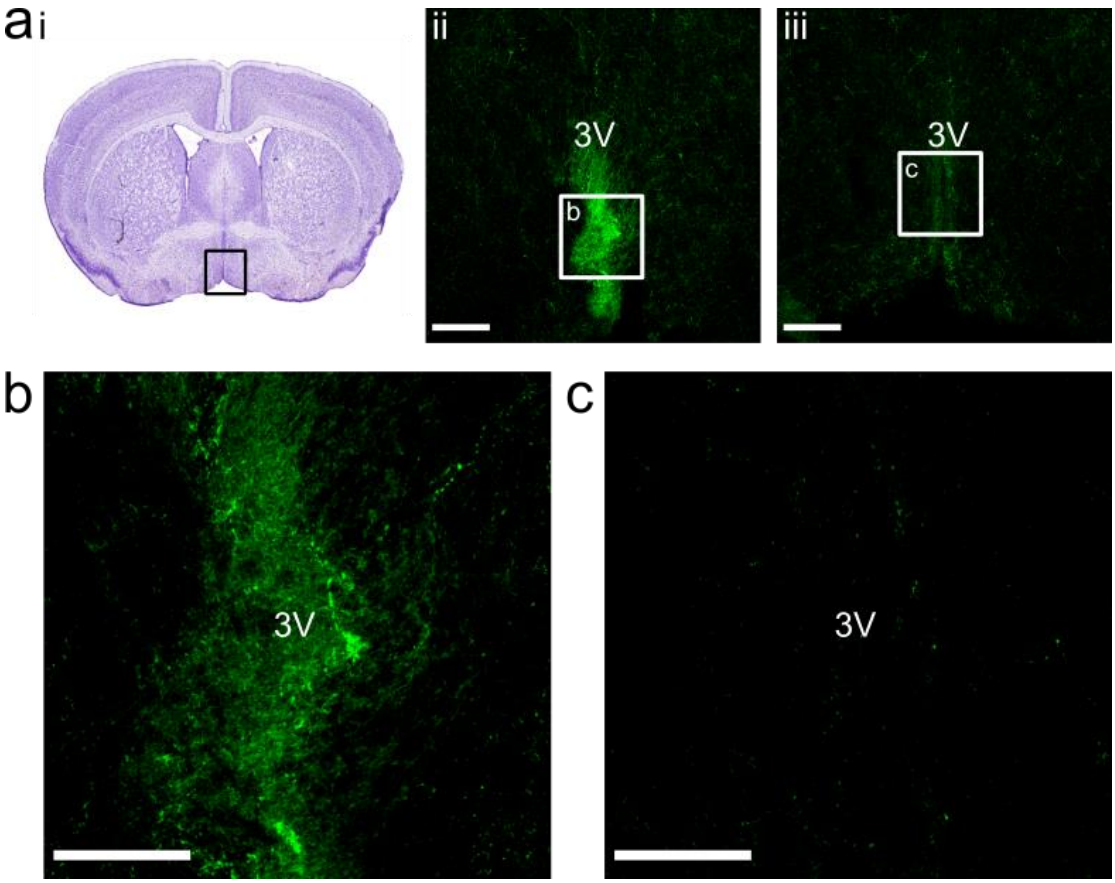

Figure 3.2.3.3 TSPO immunoreactivity around the vascular organ of the lamina terminalis of TSPO +/+ and -/- mice.

A representative figure, taken from the Mouse Brain in Stereotaxic Coordinates (381), indicating the region in which the images were taken at 0.28 mm from bregma (a-i). TSPO immunoreactivity in the vascular organ of the lamina terminalis of TSPO +/+ (a-ii) and -/- (a-iii) mice. Images taken at 63x magnification show high levels of immunoreactivity in TSPO +/+ tissue (b) compared to tissue taken from -/- mice (c). Scale bars represent 100 μm at 20x magnification (a) and 50 μm at 63x magnification (b, c).

Key: Third ventricle (3V).

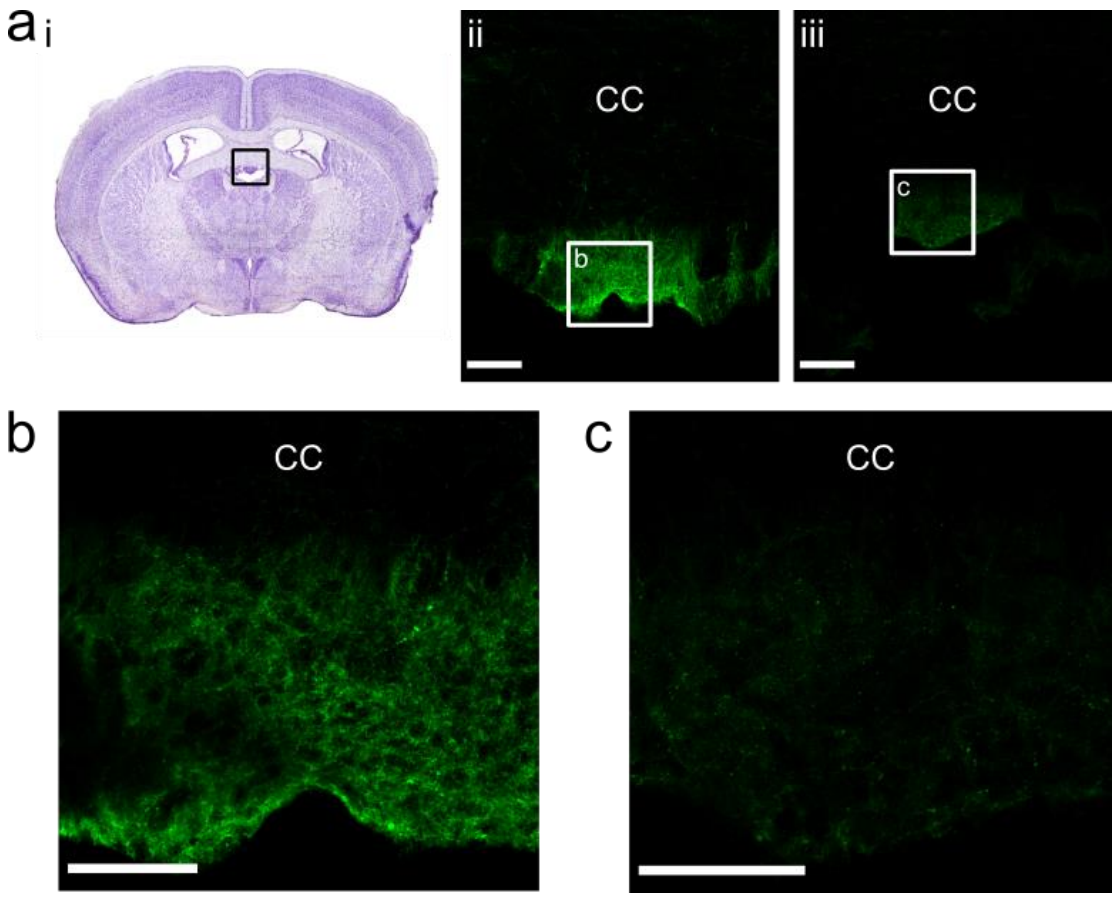

Figure 3.2.3.4 TSPO immunoreactivity in the subfornical organ (SFO) in TSPO +/+ and -/- mice.

Figure of the mouse brain at -0.70 mm from bregma, taken from the Mouse Brain in Stereotaxic coordinates (381), indicating the region in which the images were taken (a-i). TSPO immunoreactivity in the brain tissue of TSPO +/+ (a-ii) and -/- mice (a-iii). TSPO-targeted immunoreactivity is reduced, but not absent, in the SFO in TSPO -/- mice (c) compared to TSPO +/+ mice (b). Scale bars represent 100 µm at 20x magnification (a), 50 µm at 63x magnification (b, c).

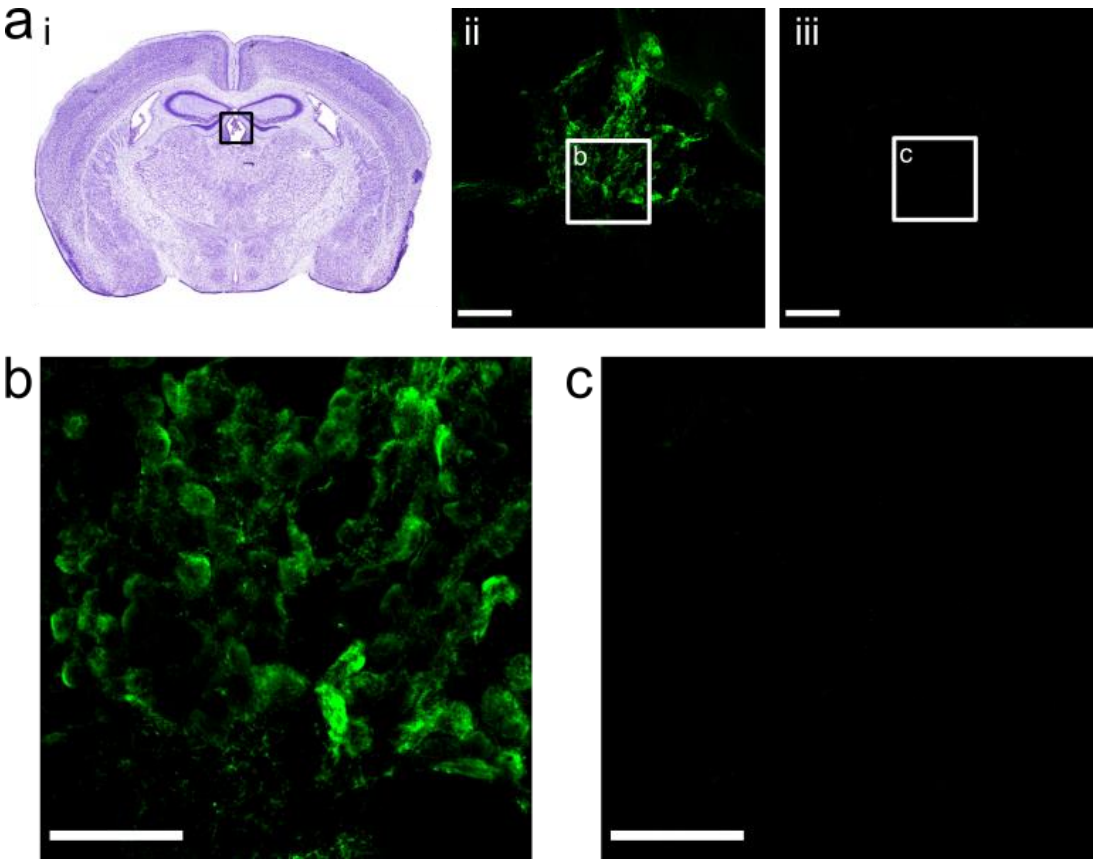

Figure 3.2.3.5 TSPO immunoreactivity within the choroid plexus of TSPO +/+ and -/- mice.

Figure of the mouse brain at -1.22 mm from bregma, taken from the Mouse Brain in Stereotaxic Coordinates (381), indicating the region in which the images were taken (a-i). TSPO immunoreactivity is observed in the choroid plexus of brain tissue taken from TSPO +/+ mice (a-ii), but not TSPO -/- mice (a-iii). Images taken at 63x magnification show strong immunoreactivity in tissue from TSPO +/+ animals (b) which is absent in TSPO -/- tissue (c). Scale bars represent 100 µm at 20x magnification (a), 50 µm at 63x magnification (b, c).

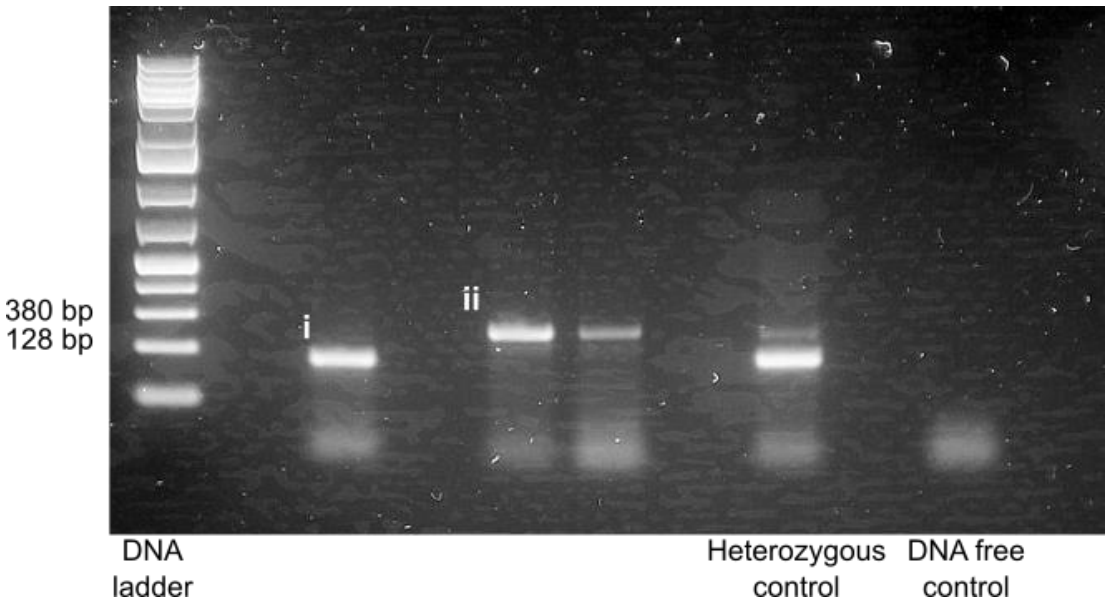

Figure 3.2.3.6 Confirmation of genotype of TSPO +/+ and -/- mice used for antibody validation.

A gel displaying the TSPO +/+ (i) and TSPO -/- (ii) alleles from tail samples of the mice used for immunohistochemical validation of the TSPO antibody.

3.3 Discussion

3.3.1 Summary of findings and conclusions

Uncovering the pattern of expression of proteins within an organ can help elucidate their role. In regionally heterogeneous organs such as the brain, this has been helpful to determine the roles of neuropeptides from the distribution of their expression. Using the hypothalamus as an example, novel peptides that are expressed in the Arc are likely (but not necessarily) to be involved in regulating feeding behaviour (77). TSPO is a mitochondrial protein that has been implicated in a variety of roles, as such linking its distribution to function may prove to be complex. In the clinical setting, non-invasive brain imaging such as PET is used to identify changes in TSPO expression in disease pathology. Techniques such as PET do not yet have the resolution to identify specific brain nuclei in which TSPO is highly expressed. There have been a few papers published which have characterised TSPO expression in the mouse brain, but these have all focussed primarily on the hippocampus and cortex (284). However, given that TSPO is expressed in other brain regions, this leaves potential CNS functions unresolved.

Until very recently, there has been limited published work on TSPO expression and function in hypothalamic regions. There is good reason for hypothalamic TSPO expression to be investigated: TSPO is well-documented to be expressed in activated glia (172,284,294), and hypothalamic gliosis is known to be involved in the physiological response to high-fat intake (125,180,416). It seems sensible to expect that TSPO is expressed within the hypothalamus and, if not, this would remain interesting and provide evidence of glia heterogeneity. There are also non-hypothalamic regions that have been identified to be involved in appetite control and energy homeostasis. While the focus of this series of experimental studies in this chapter was in regions of the brain controlling energy balance, TSPO expression was also observed in these other brain areas.

The purpose of this study was to identify regions in the mouse brain that contain detectable TSPO levels, even in absence of disease pathology and/or experimental intervention. This then has potential to provide a basis for understanding imaging of TSPO levels in the clinical setting; it is important to consider regional differences where high expression levels are considered normal or abnormal, and vice versa.

When using an antibody to investigate and describe protein expression in tissue, it is crucial to ensure that the antibody binding within the tissue is specific to the target antigen. Here, I performed the same immunohistochemical processing procedure in the brains of mice with a germline deletion of TSPO. The expectation was that the distribution of immunoreactivity, detected with the TSPO antibody, would be absent in the TSPO -/- mice. This was not the case, and the mice were confirmed as TSPO -/- using PCR and gel electrophoresis.

I compared the immunoreactivity between TSPO +/+ and -/- mice, to investigate if there were any disparities in antibody binding. Differences in TSPO immunoreactivity between TSPO +/+ and -/- mice were noted in some circumventricular and secretory organs of the brain. These included brain regions where TSPO immunoreactivity co-localised with vimentin in TSPO +/+ tissue. This provides evidence that TSPO is relevant in some nuclei that are involved in – but not limited to – energy homeostasis. Furthermore, knock-out validated immuno-labelling was performed by immunocytochemistry in primary astrocyte culture. These observations collectively indicate that there is likely specificity of the antibody in glia, tanycytes and ependymal cells.

TSPO immunoreactivity was observed in the cell layer surrounding the 3V, which also co-localised with vimentin – a cell marker for tanycytes. These cells are essential for the communication of nutrients and signals from the cerebrospinal fluid to the surrounding hypothalamic nuclei (153,155–157,160,161,163). A high level of expression in these cells indicates a potential role for TSPO in nutrient sensing. At the time of the experiments, there had been no mention in the literature of TSPO expression within tanycytes. Since the research was conducted, a study has been published which investigated the functional role of TSPO expression in β-tanycytes (301). The research I presented here agrees with the authors regarding the distribution of TSPO expression around the 3V: that TSPO expression is was mostly confined to the ventral portion of the 3V, adjacent to the Arc and ME, in the β-tanycyte cell layer. As well as proposing a role for TSPO in tanycytic integration of nutrient sensing to hypothalamic function, this restricted expression of TSPO in a sub-population of tanycytes is also an example of glial heterogeneity – a notion that is recently becoming acknowledged for its importance (417–419). Importantly, this study used the same antibody as was used in my work and also saw the same pattern of potentially “non-specific”

staining in the PVH and DMH; however, this was not noted as “non-specific” by the authors.

In the studies described in this chapter, TSPO and vimentin immunoreactivity also co-localised in other areas of the mouse brain, in which was also validated by its absence in the TSPO -/- mice. Co-expression was observed in the VOLT, which surrounds the 3V anterior of the hypothalamus, and along the cell layer lining the lateral ventricles. TSPO expression in vimentin-positive cells of the ventricles may a play similar role to that in tanycytes despite differences in location of expression.

3.3.2 Limitations of experimental approach

Qualitative studies that rely on immunohistochemistry are limited by the quality and validity of the antibodies used. The validation of the TSPO antibody I performed as part of this study was purely for precautionary reasons; the antibody had been used and published by a variety of research groups and the reputable supplier of the antibody, Abcam, had performed in-house knock-out validation. Differences in antibody-antigen binding can be a result of technical approaches, and upon discussion with an Abcam representative I discovered such differences in our methods to validate the antibody. Abcam used peroxidase immunohistochemical labelling with an antigen-retrieval step – as recommended on the antibody product description. The advantage of using peroxidase activity to label immunoreactivity as opposed to fluorescence is that it negates obscuring positive-signal by autofluorescence in the tissue. That being said, I used secondary-only antibody labelling on tissue as an internal control for tissue autofluorescence and I did also perform peroxidase immunochemical labelling with the same antibody and observed the same pattern of immunoreactivity. At the time I did not see any need to perform antigen-retrieval as the immunoreactive signal was so strong, and the purpose of the retrieval is to unmask antigens. However, this technical difference may be useful to investigate further if the project were to continue. Furthermore, the “non-specific” TSPO labelling was identified in multiple laboratories and in a variety of mouse strains by myself and by colleagues. This also applied to multiple batches of the antibody. In addition, the pattern of immunoreactivity around the DMH and Arc has been included in published work (301). Consequently, it is unlikely that the “non-specific”

immunoreactivity occurred as a result of mouse strain genetics or histochemical techniques.

A further point taken from the correspondence with a representative for Abcam is that the heterogeneity of TSPO expression must be considered when validating the targeting antibody. The images of the TSPO antibody validation provided by Abcam show a region of the hypothalamus, but with no labels so it is difficult to determine which nucleus of the hypothalamus is shown. As depicted in this chapter, while there is strong immunoreactivity within hypothalamic regions this is restricted to particular nuclei and there are some hypothalamic nuclei without any TSPO targeted labelling. One such example is the suprachiasmatic nucleus, which I think is the hypothalamic nucleus depicted in the Abcam image. During the correspondence, the Abcam representative also referred to a figure that used the antibody in Western blot analysis of a variety of tissues from both TSPO +/+ and -/- mice (420). However, there was no band indicating expression in brain tissue of either TSPO +/+ and -/- mice. On the contrary, I had identified TSPO expression in brain tissue of TSPO +/+ mice using the same antibody (Fig 3.2.1.6). The key differences here were that the researchers used whole-brain tissue while I used micro-dissected hypothalamic tissue. This would influence the strength of the signal identified by the antibody, as it would be dampened by the inclusion of brain regions absent of TSPO in whole-brain tissue compared to hypothalamus only. Furthermore, the loading control of GAPDH is noticeably weaker in the lanes corresponding to the brain tissue compared to the other tissue samples taken (420). This indicates a lower level of protein was loaded from the brain compared to other samples, which would also reduce the antibody signal. I concluded that the antibody validation performed and sourced by Abcam were not adequate to rule out non-specific binding, especially in light of my immunohistochemical staining. However, my complaints were dismissed by the Abcam representative I spoke to.

While the glial cell markers applied in this study are commonly used in immunohistochemistry and other applications, this does not mean that they are the most appropriate for this purpose. Both GFAP and IBA1 are regulated by their respective cellular active state (396,398,399). Consequently, it may be the case that these glial markers are not expressed to a substantial extent in the healthy brain limiting their detection using immunohistochemistry in this context. This

would influence the observations in coincidence of TSPO-targeted immunoreactivity with either cell marker. Another important note to consider in the case of astrocytes is that GFAP is a cytoskeletal protein. As a cytoskeletal protein, GFAP-immunoreactivity does not reveal the complete three-dimensional size and shape of astrocytes – which is more complex than the characteristic star-like shape (421). Therefore, we would not necessarily expect to see GFAP and mitochondrial proteins to co-localise. In addition, it is critical to make note of other cell types identifiable by the cell marker. GFAP is not specific to astrocytes, and so dual labelling around the vasculature is likely to have identified ependymal cells or tanycytes. In such cases, application of multiple cell markers could provide assurance to the cellular localisation.

3.3.3 Future perspectives and outstanding questions

Distribution of TSPO expression in the healthy mouse brain still remains to be fully understood. The studies outlined here would benefit from supporting data with additional methodologies. For example, employing different tissue acquisition and immunohistochemical processing approaches. This could be snap-freezing of dissected brain tissue to replace formaldehyde fixation, and peroxidase-labelled immunohistochemistry instead of fluorescence. The complete cellular localisation of TSPO is also still to be determined. Immunohistochemical co-labelling is an appropriate approach. However, considering the limitations mentioned above, for confidence that a protein is expressed within a particular cell type a more detailed sub-cellular approach may be beneficial – such as electron microscopy.

The identity of the “non-specific” immunoreactivity could be informed by further examination of TSPO structure. There are proteins that are structurally similar to TSPO, namely TSPO-2 and TSPO-associated protein (422–424). It is possible that the “non-specific” antibody binding seen in the PVH and DMH is to an antigen expressed in neurons as the labelling, which formed a ‘projection’-like pattern and co-localised with neuropeptides, was still visible in TSPO -/- tissue. Therefore, the unknown antigen could be expressed in the neurons as identified in the dual-immunohistochemistry experiments – namely TRH- and CRH-expressing neurons. These neurons are important regulators of neuroendocrine function, indicating a potential involvement of the unknown antigen. The company that

produced the antibody refused to disclose the antigen sequence used in its generation, so I was unable to pursue this further.

Irrespective of the outcome of antibody validation, measuring differences in protein expression would benefit from additional approaches due to the qualitative nature of the methodology applied here. Western blot analysis of protein quantification is one prospect, but it alone lacks the spatial resolution of immunohistochemistry. *In situ* hybridisation is an alternative technique to assess distribution of expression, though of mRNA instead of protein

To conclude, I characterised the distribution and cellular location of binding of a TSPO antibody in the mouse brain. Unfortunately, the majority of TSPO-positive immunoreactivity described in this study is likely a result of non-specific binding of the antibody to an unknown antigen. However, the techniques used provided information on the validity of the antibody. From comparison of immunoreactivity in TSPO +/+ and -/- brain tissue, I am confident that the TSPO-positive labelling at the walls of the ventricles is valid. Considering the insights of dual-immunohistochemistry with TSPO and vimentin, I can conclude that the TSPO expression at the ventricles is contributed to by tanycytes of the 3V. Identifying the cellular location of TSPO has provided an insight to its function: that TSPO may be involved in nutrient sensing and communication between the cerebrospinal fluid (CSF) and the hypothalamus. This conclusion has since been strengthened by published work (301).

Chapter 4: Dietary regulation of hypothalamic TSPO expression

4.1 Introduction

Exposure to a high-fat and high-sugar diet is associated with widespread systemic low grade inflammation in rodents (122,123,125,367). Within the central nervous system, this is characterised by proliferation of glial cells (125,174,178,180,181,184); alterations in glial morphology (125,180); increased secretion of cytokines and reactive oxygen species (122,125,367,416,425–427); and infiltration of peripheral macrophages (123). Diet-induced gliosis is thought to occur in two separate temporal phases: the first following acute exposure, which then subsides but returns ensuing chronic high-fat diet intake (125). The reasons behind the temporal changes in gliosis are unknown – perhaps due to initial adaptation which becomes negated in chronic high-fat intake. Upregulation in glial mRNA, but not protein expression, is observable from one day of high-fat exposure (125). Excessive intake of energy-dense foods can lead to weight gain, if not balanced by energy expenditure. Obesity is a risk factor to other health problems, including cognitive deficits and neurodegeneration (178,181,223,224) - both of which are also associated with neuroinflammation (428–432). Investigation of the inflammatory pathways that follow high-fat feeding and into obesity may unveil the mechanisms that invoke susceptibility to other neurological disease.

In diet-induced obesity, excessive fat intake causes impaired lipid storage and so results in a higher level of free fatty acids (FFAs) in the circulation (119,433,434). Previous work has indicated that exposure to saturated fatty acids (SFAs) acts as a pro-inflammatory stimulus in glial cells (187). Attenuation of fatty acid (FA) signalling prevents FA-induced gliosis (435). Consequently, it is assumed that reactive gliosis in response to energy excess is in part caused by an increased level of circulating FAs.

Nutrient availability is not the only energy-associated signal that hypothalamic glia respond to. Interestingly, an increase in hypothalamic glial protein expression is observed after food deprivation in mice (202). Weight-loss in diet-induced obese mice also evokes hypothalamic reactive gliosis (182). This possibly indicates that reactive gliosis is triggered by a multitude of factors, and not restricted to excess nutrients. On the other hand, negative energy balance may cause release of free FAs (FFAs) from fat stores in the body – resulting in increased FFA availability and consequently hypothalamic gliosis. In cancer-associated cachexia in mice, increased gliosis was observed in the mediobasal hypothalamus (MBH) (190). The gliotic response observed here was proposed to be beneficial and protective against cachexia and weight loss. Consequently, there is much yet to be understood in the glial reactive response to calorie deficit.

The tanycyte cells – specialised ependymal cells that line the ventricles of the brain – of the third ventricle (3V) are key in sensing and communication of FFA availability (121,163). Ablation of these cells adjacent to the MBH exacerbates diet-induced obesity (191). Interestingly, disruption of lipid uptake in hypothalamic astrocytes also contributes to diet-induced obesity (218). Furthermore, there is recent evidence to suggest that tanycytes can mediate inflammatory-associated effects on food intake via the NF-κB pathway (436). This complements the previous finding that NF-κB signalling is essential in the reactive astrocytic response to diet-induced obesity (216). These collection of studies make it apparent that tanycytes are essential for reactive astrogliosis to occur in the hypothalamus in response to high-fat diet.

The mitochondrial translocator protein of 18 kDa (TSPO) is expressed in glia, and upregulated in reactive gliosis (172,227,228,284,293–295,350,385,437). The importance of TSPO function in activated glia is not yet understood, but TSPO up-regulation is selective to cells in a pro-inflammatory phenotype (228,438). Nonetheless, there are temporal and cell-dependent effects in neural TSPO expression. In a rat model of brain damage in the hippocampus, reactive microglia did not upregulate TSPO until 14 days after damage was induced (172). Meanwhile, TSPO expression was increased in reactive astrocytes at all times during the experiment. Furthermore, TSPO up-regulation is detectable in pro-inflammatory astrocytes in rat striatum even while nearby microglia remain in a resting state (227). These studies have focussed on striatal and hippocampal

regions, while less is known on TSPO up-regulation specifically in hypothalamic glia.

There is little research to date that has examined TSPO expression and function in the context of diet-induced inflammation. Published work has shown TSPO expression to be moderately greater in the hippocampus and choroid plexus of the leptin-deficient *ob/ob* mouse compared to wild-type (439). However, a diet-induced obese mouse model did not replicate this data (369). Regulation of hypothalamic TSPO in different states of energy balance is yet to be elucidated.

The experiments in this chapter investigated the following hypothesis: changes in TSPO expression would be observed in hypothalamic regions of mice exposed to deviations in energy balance. This would be attributed to, in part, increases in hypothalamic glial fibrillary acidic protein (GFAP) expression – a marker for astrocytes – which indicates astrocytic proliferation and morphological changes (149,440). It is important to note that this hypothesis was formed and investigated before the problems with the TSPO antibody were realised. With this in mind, at the time of this study I anticipated that hypothalamic TSPO expression would be upregulated alongside that of GFAP. However, as diet-induced gliosis occurs in both positive (125,174,178,180,181,184) and negative (182,202) energy states it is possible that gliosis-induced up-regulation of protein is dependent on the stimulus rather than the activated state itself. Since there is a time-dependent effect on diet-induced gliosis as well as in TSPO up-regulation (125,172), the response to high-fat intake was examined in an acute and chronic scenario.

The following questions were addressed in order to investigate the hypothesis above:

- How are hypothalamic TSPO and GFAP regulated in response to acute high-fat diet exposure?
- Are hypothalamic expression of TSPO and GFAP influenced by acute food deprivation?
- Does 3-month chronic high-fat exposure regulate hypothalamic expression of TSPO and GFAP?

4.2 Results

4.2.1 Western blot analysis of TSPO and GFAP protein expression in the hypothalamus of mice exposed to positive and negative energy balance.

The primary aim of the following experiments was to observe whether an acute manipulation of energy balance influenced hypothalamic TSPO expression alongside GFAP. The dorsomedial hypothalamic nucleus (DMH) and arcuate hypothalamic nucleus (Arc) – the latter of which also contained the median eminence (ME) - were micro-dissected from the brains of mice that were maintained on standard chow, or exposed to high-fat diet or food deprivation for 12 hours. These brain regions were selected for study due to the dense TSPO-targeted immunoreactivity, under the knowledge at the time regarding the antibody as described in Chapter 3, and as important regions in energy homeostasis. Protein expression was semi-quantified by Western blot analysis.

To confirm that any changes in protein expression were due to energy intake, body weights and food intake of the mice were recorded. The weight of food pellets consumed was no different between mice fed high-fat diet or maintained on standard chow (Fig 4.2.1.1a; $p = 0.1261$). The high-fat chow pellets were more calorific than the standard chow, so even with a similar weight of food intake the high-fat fed mice consumed significantly more energy (Fig 4.2.1.1b; $p < 0.0001$). There were no differences in the body weights of the mice on the evening before dietary manipulation (Fig 4.2.1.1c; $p = 0.1207$).

Samples containing the Arc and ME were collected in the coronal plane at the base of the 3V using a micropunch (Fig 4.2.1.2a). These samples likely included a ventral portion of the ventromedial hypothalamic nucleus (VMH). TSPO expression within the Arc/ME samples was unchanged across dietary manipulation (Fig 4.2.1.2b; $p = 0.8373$). Meanwhile, there was a significant effect of dietary treatment on GFAP expression (Fig 4.2.1.2c; $p = 0.0207$) for which multiple comparisons analysis identified a significant increase in GFAP expression in Arc/ME tissue from high-fat fed mice compared to control ($p = 0.0335$).

The DMH samples were also micro-dissected from the coronal plane using the micropunch technique (Fig 4.2.1.3a). Due to the sampling technique, it is possible

that a portion of the paraventricular hypothalamic nucleus (PVH) or the VMH were also collected. DMH TSPO expression was decreased by dietary manipulation ($p = 0.0384$), with statistical significance achieved between the high-fat fed group with control (Fig 4.2.1.3b; $p < 0.05$). The appearance of double TSPO-positive bands in the Western blot indicated it to be in a dimeric or phosphorylated form (Fig 4.2.1.3e). GFAP expression in the DMH was not affected by dietary exposure (Fig 4.2.1.3c; $p = 0.3216$).

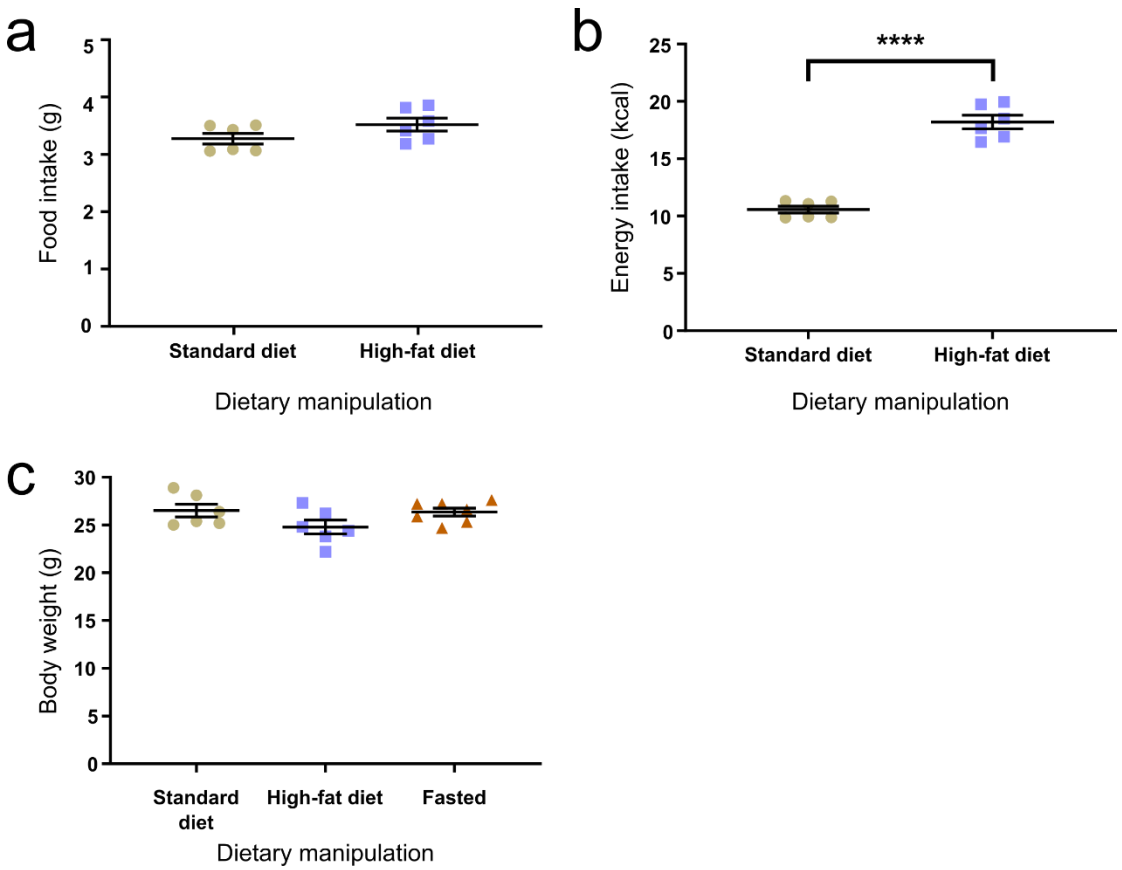

Figure 4.2.1.1 There was no difference in body weights of mice that were randomly assigned to the standard chow, high-fat diet or food deprivation conditions.

Mice that were provided with high-fat diet during the dark phase did not eat significantly more grams of food than the mice that were maintained on standard chow (a; p = 0.1261, n = 6). However, the mice on high-fat chow did have a significantly greater calorie intake (b; p < 0.0001, n = 6). The body weights of the mice on the day prior to diet manipulation did not significantly differ across groups (c; $F_{2,16}$ = 2.42, p = 0.1207, n = 6-7). Statistical analysis was conducted using unpaired Student's t-test (a-b) or one-way ANOVA with multiple comparisons (c). Data are expressed as mean ± standard error.

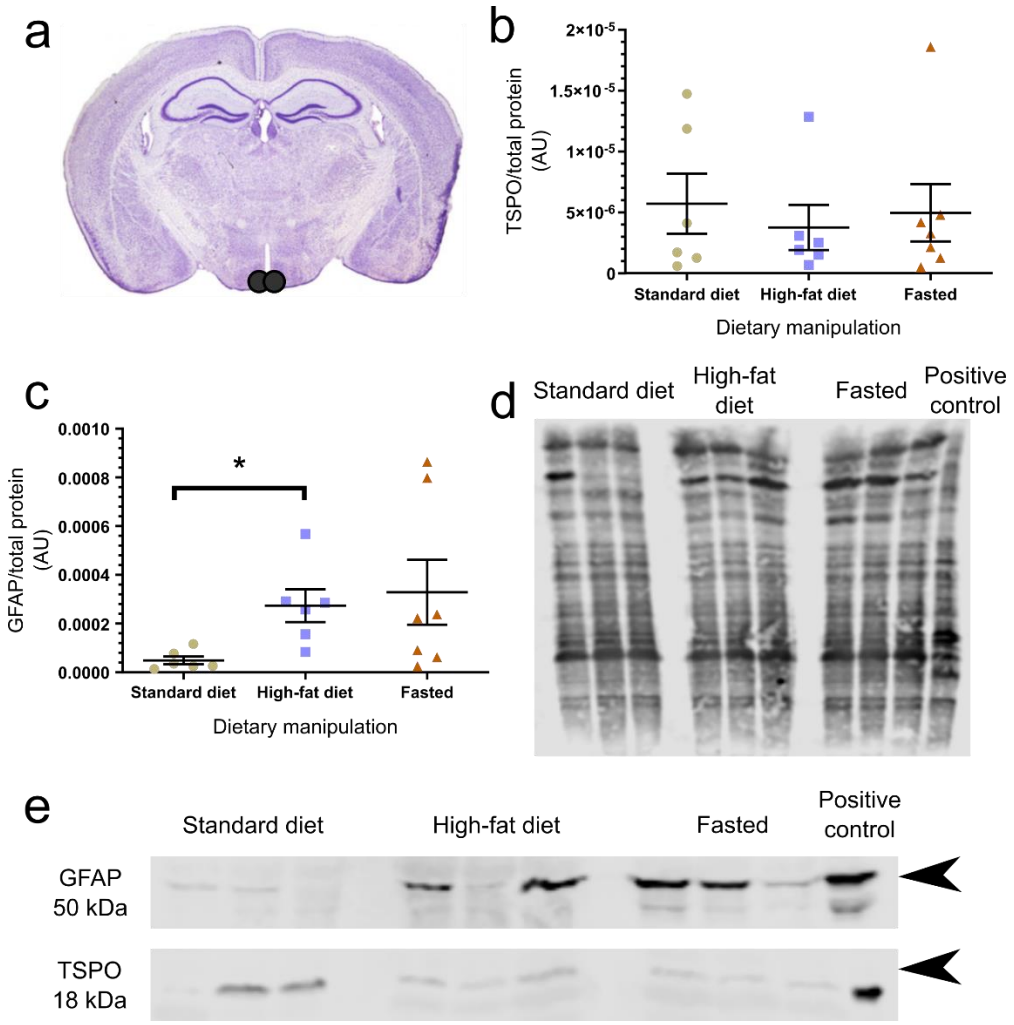

Figure 4.2.1.2 GFAP, but not TSPO, protein expression is altered in hypothalamic arcuate nucleus-containing samples from mice that were exposed to positive or negative energy balance.

An image, taken from The Mouse Brain atlas (381), depicting the location at -1.70 mm from bregma at which the protein samples were taken (a). TSPO expression was not altered by exposure to high-fat diet nor fasting (b; p = 0.8373, $F_{2,16}$ = 0.1795, n = 6-7). GFAP expression was statistically significantly affected by dietary manipulation (c; p = 0.0207, $F_{2,7}$ = 6.646, n = 6-7). Multiple comparisons indicated a significant difference of GFAP expression from mice fed high-fat diet compared to control (*, p = 0.0335), but not between fasted expression and control. Protein expression was quantified relative to total protein (d). The black filled arrows indicate the band from which GFAP and TSPO protein expression was quantified (e). The positive control was protein lysate from primary cultured mouse cortical astrocytes (d, e). Statistical analysis was performed by one-way ANOVA (b) or Welch's ANOVA test (c) with Dunnett's multiple comparisons test. Data are expressed as mean ± standard error.

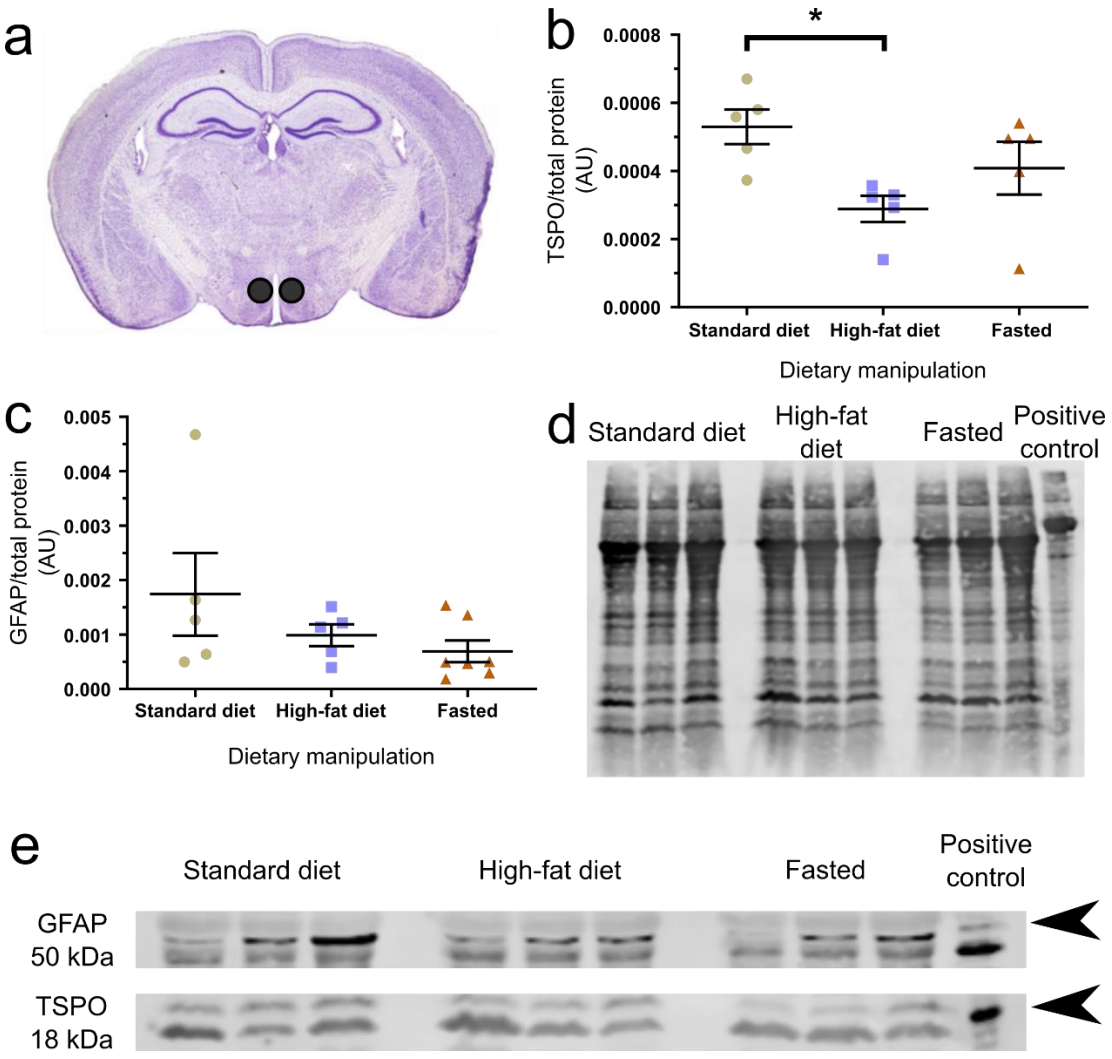

Figure 4.2.1.3 TSPO, but not GFAP, protein levels in the dorsomedial hypothalamic area are influenced by energy state.

An image, taken from The Mouse Brain atlas (381), depicting the location at -1.70 mm from bregma at which the DMH protein samples were taken (a). TSPO expression was statistically significantly altered by dietary manipulation (b; $p = 0.0384$, $F_{2,12} = 4.328$, n = 5-7). Multiple comparisons indicated statistical significance in TSPO expression of mice fed high-fat diet compared to standard chow (*, $p = < 0.05$). DMH GFAP expression was not affected by dietary manipulation (c; $p = 0.3216$, $F_{2,7} = 1.393$, n = 5-7). Total protein was used to quantify relative expression of TSPO and GFAP (d). The black filled arrows indicate the bands from which protein expression was measured (e). Protein lysate from primary cortical astrocytes was used to confirm binding of the antibodies (d, e). Statistical analysis was performed using either one-way ANOVA with Bonferroni's multiple comparisons test (b) or Welch's ANOVA test (c). Data are expressed as mean ± standard error.

4.2.2 Immunohistochemical analysis of brain tissue from mice that were exposed to either high-fat diet or standard chow for 12 hours.

To complement the protein quantification data acquired from Western blot, qualitative immunohistochemical examination was performed on hypothalamic sections from mice exposed to a high-fat diet for 12-hours. Male mice were fed either a high-fat diet or maintained on standard chow for a 12-hour period during the dark phase. Body weights and food intake were measured followed by euthanasia and transcardial perfusion for brain tissue collection.

In mice of either dietary group, there was no difference in weight of food pellets consumed (Fig 4.2.2.1a; p = 0.4981). Since the high-fat pellets contain more calories per gram than standard chow, these mice consumed a significantly greater amount of energy (Fig 4.2.2.1b; p = 0.0011). Despite random allocation of mice to groups, the average body weight of mice in the control group was significantly higher than the mice in the high-fat group (Fig 4.2.2.1c; p = 0.012).

Sections were immunohistochemically processed to examine TSPO and GFAP immunoreactivity (Fig 4.2.2.2). Semi-quantitative measures of TSPO immunoreactivity intensity in the Arc revealed no difference in TSPO expression between the two diet groups (Fig 4.2.2.3b; p = 0.709). The number of GFAP-immunoreactive cells was also not influenced by acute exposure to high-fat diet (Fig 4.2.2.3c; p = 0.7336), nor was the number of processes on GFAP-positive cells (Fig 4.2.2.3d; p = 0.9172). Expression of TSPO at the 3V lining was also measured by intensity of immunoreactivity and number of TSPO-immunoreactive projections extending from the 3V into the hypothalamus (as discussed in Chapter 3). In both cases, there was no difference in measurements between diet groups (Fig 4.2.2.3e, p = 0.5029; 3f, p = 0.7973).

Diet-induced inflammation in the DMH is not well characterised compared to the response within the Arc. However, as described in Chapter 3, dense immunoreactivity which was thought to bind to TSPO was detected in the DMH. TSPO and GFAP immunoreactivity was assessed in the DMH following acute exposure to high-fat diet (Fig 4.2.2.4). Measurement of TSPO immunoreactivity intensity indicated that TSPO expression was unaffected by acute high-fat diet feeding (Fig 4.2.2.5b; p = 0.2306). The number of GFAP-immunoreactive cells was also not different in the DMH of high-fat fed mice compared to control (Fig 4.2.2.5c; p = 0.263). There was no difference between dietary groups in the

number of processes of GFAP-immunoreactive cells (Fig 4.2.2.5d; p = 0.7481). Semi-quantification of TSPO immunoreactivity in the wall of the 3V also revealed no differences between high-fat fed mice and control (Fig 4.2.2.5e, p = 0.6717; 5f, p = 0.316).

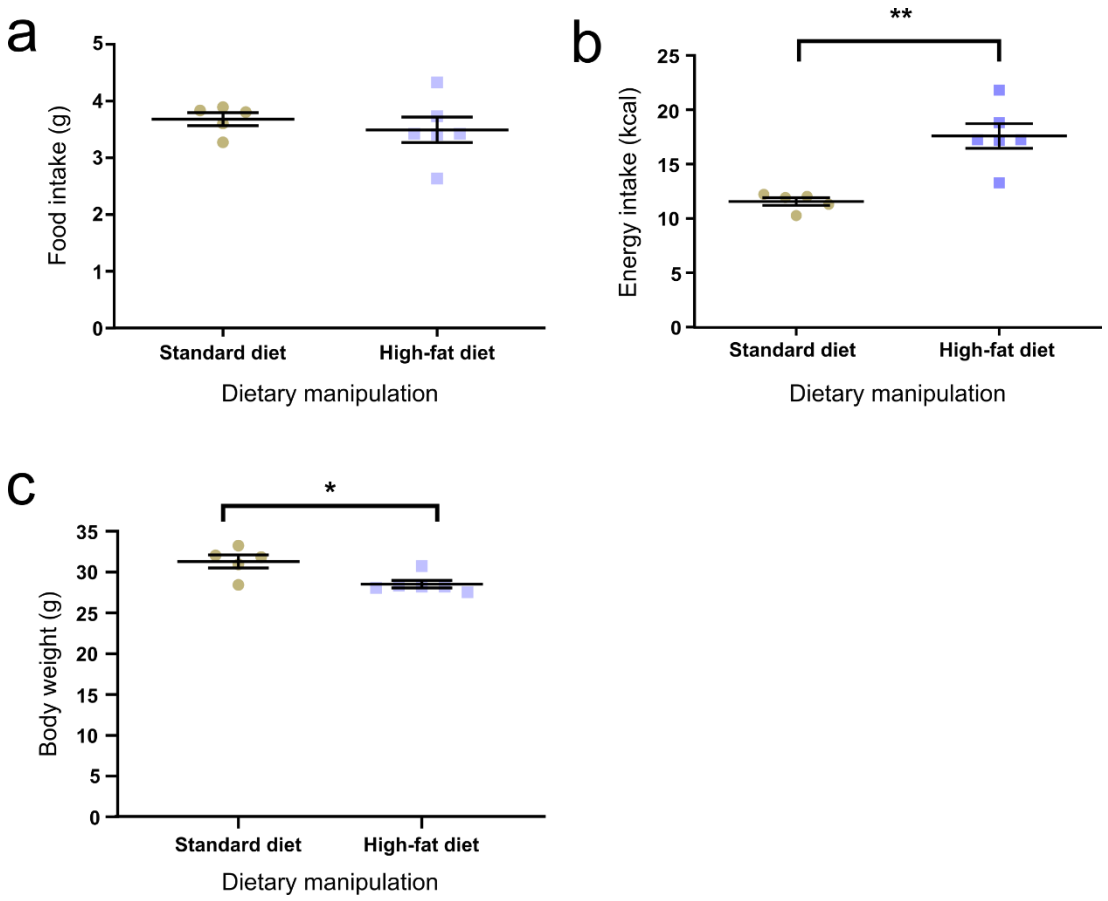

Figure 4.2.2.1 Mice that were exposed to high-fat diet for 12 hours consumed more energy in calories than their littermate controls.

Mice that were provided with high-fat diet for 12 hours did not eat a greater mass of food compared to mice kept on standard chow diet (a; p = 0.4981). However, these mice consumed more energy due to the higher caloric density of the food (b; **, p = 0.0011). The experimental cohort of mice randomised to the high-fat diet group was statistically significant lower in body weight compared to control mice (c; *, p = 0.012). N = 5-6. Statistical analysis performed using Student's unpaired t-test. Data are expressed as mean ± standard error.

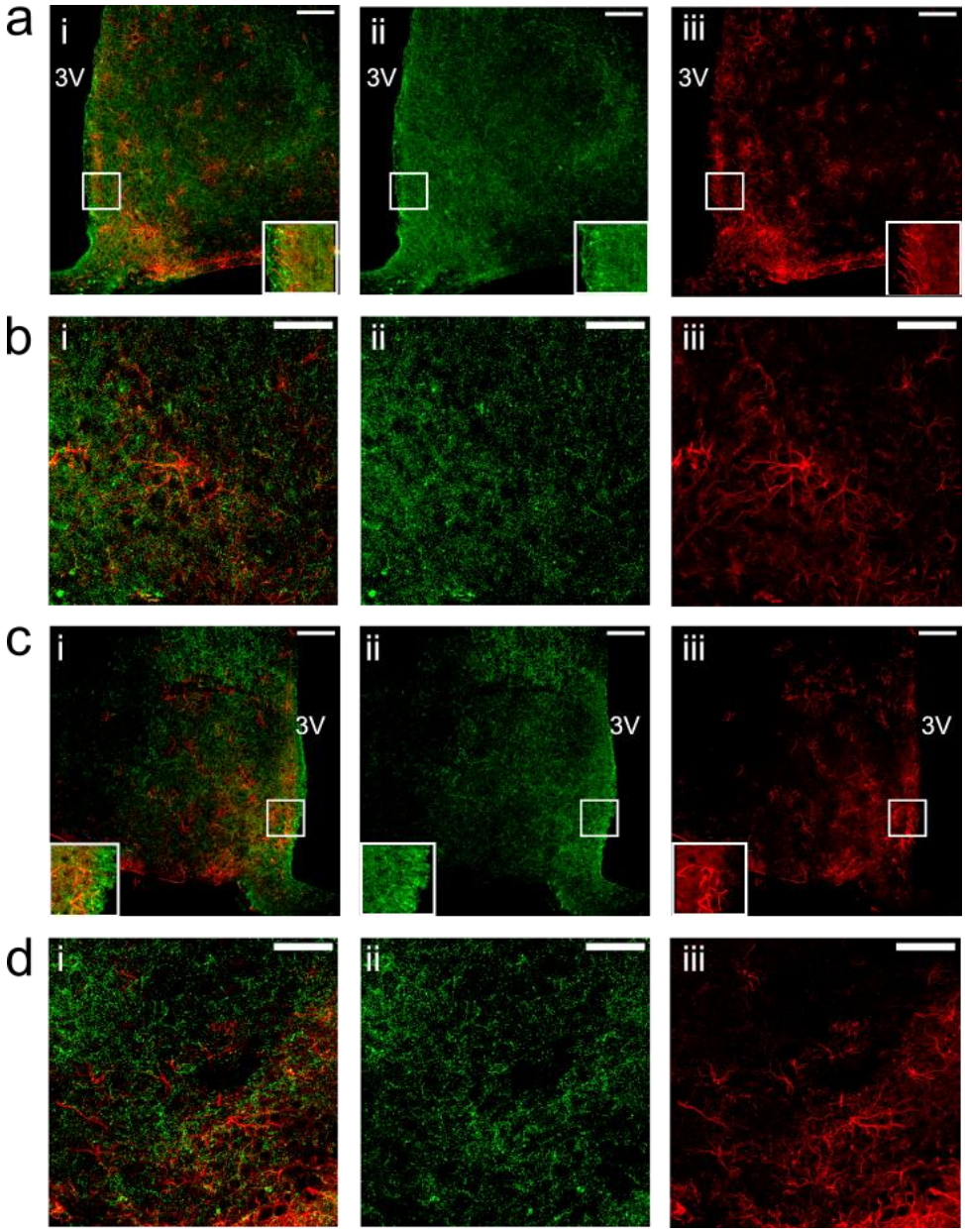

Figure 4.2.2.2 TSPO and GFAP immunoreactivity in the hypothalamic arcuate nucleus of mice following acute exposure to high-fat diet.

Images, taken at 20x magnification, indicating immunoreactivity for TSPO (ii; green) and GFAP (iii; red) in the arcuate nucleus of male mice fed either standard chow (a-i; merge) or high-fat diet (c-i) for 12 hours in the dark phase. Insets indicate TSPO and GFAP in the lining of the third ventricle following digital zoom. The same regions were captured at 63x magnification, for mice fed standard chow (b) and high-fat diet (d). Scale bars represent 100 μm in images taken at 20x magnification, and 50 μm in images taken at 63x magnification.

Key: Third ventricle (3V)

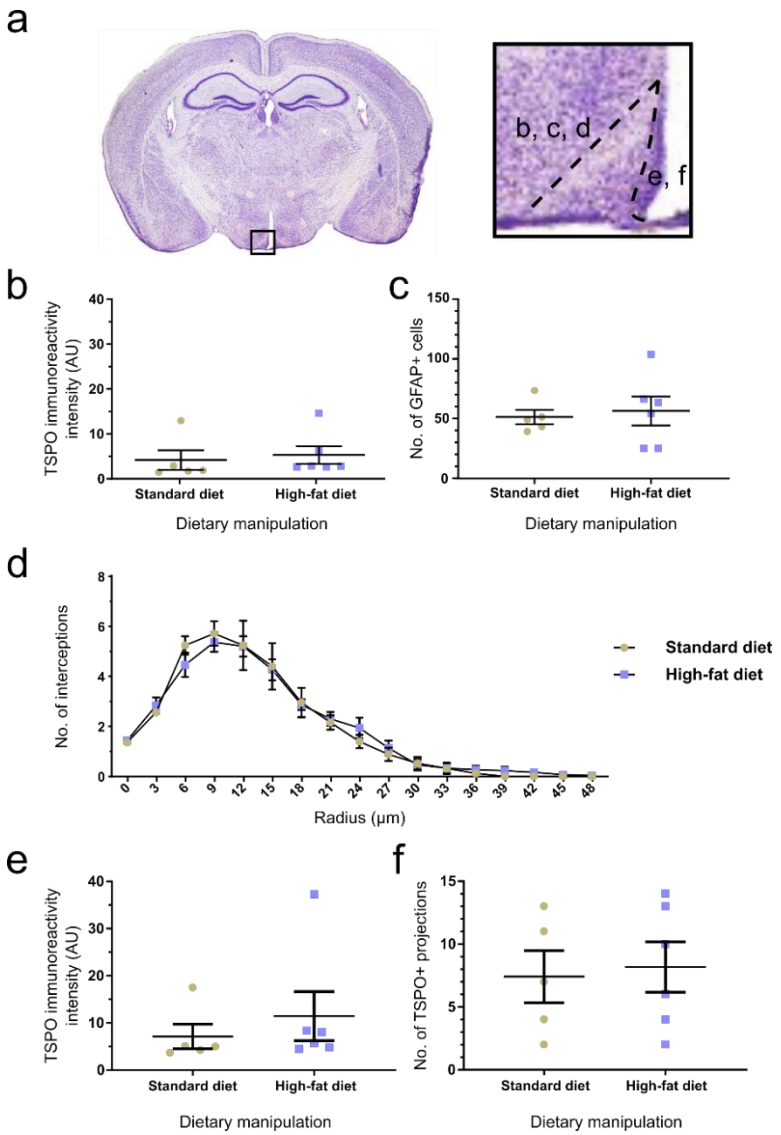

Figure 4.2.2.3 TSPO and GFAP immunoreactivity in the male mouse hypothalamic arcuate nucleus was not influenced by a 12-hour exposure to high-fat diet.

Image of coronal section (381), at -1.70 mm from bregma, indicating the region in which image analysis was performed (a). Semi-quantitative analysis of TSPO immunoreactivity intensity (b; p = 0.709) and number of GFAP-positive cells (c; p = 0.7336) did not differ between diet groups. Morphological tracing analysis of GFAP-positive cells did not show any difference following dietary manipulation (d; diet: p = 0.9172, $F_{1,9}$ = 0.0114; interaction of diet and radius: p = 0.966, $F_{16,144}$ = 0.4489) TSPO immunoreactivity intensity (e; p = 0.5029) and number of TSPO-positive cell projections (f; p = 0.7973), in the ependymal layer of the third ventricle at the level of the arcuate nucleus, did not differ in mice exposed to high-fat diet for 12 hours compared to mice maintained on standard chow. N = 5-6 animals. Statistical analysis performed with Student's unpaired t test (b, c, e, and f) and two-way ANOVA with repeated measures (d). Data are expressed as mean ± standard error.

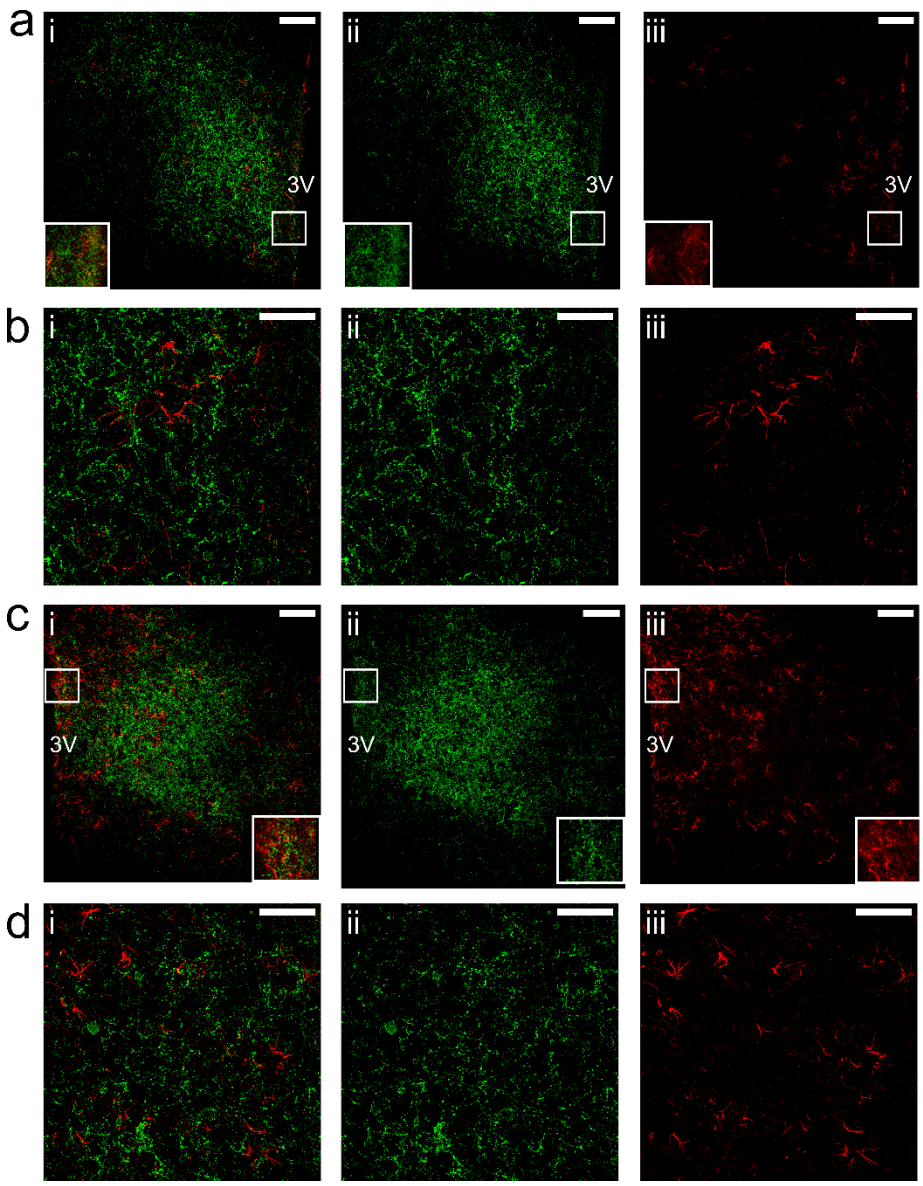

Figure 4.2.2.4 TSPO and GFAP immunoreactivity in the dorsomedial hypothalamus of high-fat and standard chow fed male mice.

Images taken at 20x magnification of TSPO (ii; green) and GFAP (iii; red) immunoreactivity in the dorsomedial hypothalamus from mice fed either standard chow (a-i; merge) or high-fat diet (c-i) for 12 hours overnight. Insets indicate digital zoom of TSPO and GFAP immunoreactivity at the third ventricle lining. The same regions were captured at 63x magnification in the mice fed standard chow (b) and high-fat diet (d). Scale bars represent 100 μm in images taken at 20x magnification, and 50 μm at 63x. Key: Third ventricle (3V).

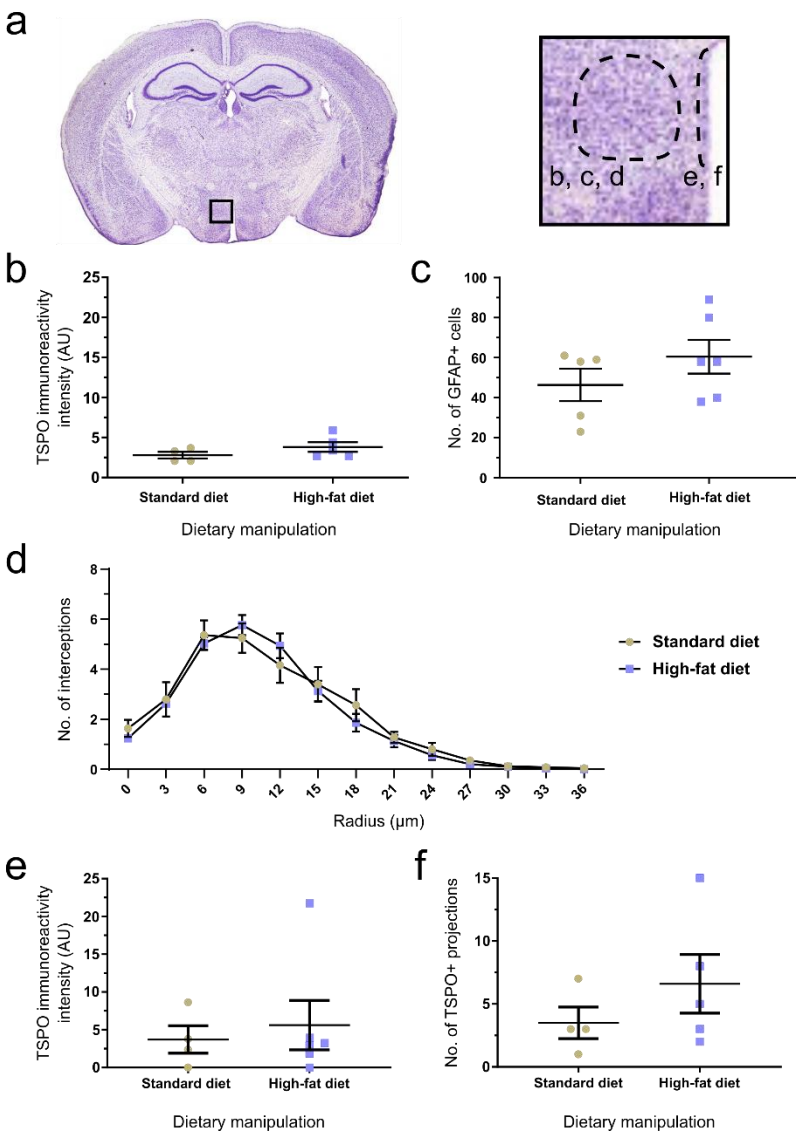

Figure 4.2.2.5 TSPO and GFAP immunoreactivity in the dorsomedial hypothalamic nucleus was unaffected by acute exposure to high-fat chow in male mice.

Image of coronal section (381), at -1.70 mm from bregma, indicating the region in which image analysis was made (a). Semi-quantitative analysis of TSPO immunoreactivity intensity (b; $p = 0.2306$, n = 4-5) and number of GFAP-positive cells (c; $p = 0.263$, n = 5-6) did not differ between diet groups. There was also no impact of dietary manipulation on morphological tracing analysis of GFAP-immunoreactive cells (d; diet: $p = 0.7481$, $F_{1,9} = 0.1097$; interaction of diet and radius: $p = 0.732$, $F_{12,108} = 0.7171$, n = 5-6). TSPO immunoreactivity intensity (e; $p = 0.6717$, n = 4-6) and number of TSPO-positive cell projections (f; $p = 0.316$, n = 4-5) in the wall of the third ventricle did not differ with dietary manipulation. Statistical analysis performed with students' unpaired t test (b, c, e, and f) and two-way ANOVA with repeated measures (d). Data are expressed as mean ± standard error.

4.2.3 Immunohistochemical analysis of brain tissue taken from mice that were exposed to 12-hour food deprivation compared to satiated mice.

Cachexia or weight loss in obese mice can result in hypothalamic inflammation (182,190). Western blot analysis indicated that GFAP expression in the Arc was regulated by food deprivation (Fig 4.2.1.2). Therefore, I qualitatively examined immunoreactivity of TSPO and GFAP in hypothalamic brain regions of mice that were fasted for 12-hours compared with mice that were maintained on standard laboratory chow. There was no difference in body weights of mice randomly allocated to either the fasted or fed experimental group (Fig 4.2.3.1; $p = 0.6702$).

Immunoreactivity of TSPO and GFAP were assessed within the Arc and the adjacent 3V wall (Fig 4.2.3.2). There was no difference in intensity of TSPO immunoreactivity in the Arc of the fed and the fasted mice (Fig 4.2.3.3b; $p = 0.0947$), in the number of GFAP-positive cells (Fig 4.2.3.3c; $p = 0.154$) nor in the number of GFAP-immunoreactive projections (Fig 4.2.3.3d; $p = 0.0893$). Measurements of TSPO immunoreactivity in the 3V wall adjacent to the Arc revealed no impact of fasted status on TSPO-immunoreactivity intensity and cell processes (Fig 4.2.3.3.e, f; $p = 0.0947, 0.1093$).

GFAP immunoreactivity increased within the DMH of food deprived mice, while TSPO immunoreactivity remained unchanged between experimental groups (Fig 4.2.3.4). These observations were reflected in the semi-quantification of immunoreactivity. Intensity of TSPO immunoreactivity was not affected by overnight food deprivation (Fig 4.2.3.5b; $p = 0.433$). Meanwhile, the number of GFAP-positive cells were significantly greater in the DMH of fasted mice compared to fed (Fig 4.2.3.5c; $p = 0.0217$). However, the measurement of GFAP-immunoreactive cell projections indicated no differences between experimental groups (Fig 4.2.3.5d; $p = 0.9531$). Semi-qualitative measures of TSPO immunoreactivity at the 3V wall, adjacent to the DMH, demonstrated no change in immunoreactivity intensity and in number of TSPO-immunoreactive cell processes (Fig 4.2.3.5e, $p = 0.1884$; 5f, $p = 0.1648$).

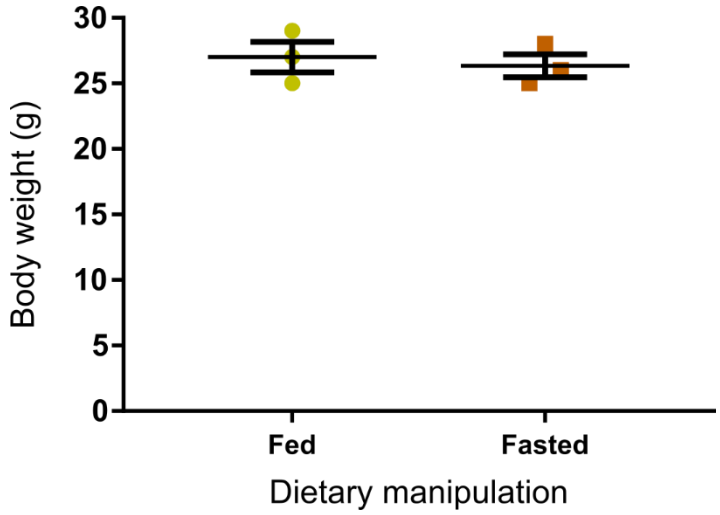

Figure 4.2.3.1 There were no differences in body weight of mice prior to dietary manipulation.

There were no differences in the body weight of mice randomly assigned to food deprivation or control groups (p = 0.6702, n = 3). Statistical analysis was performed using Student's t test. Data are expressed as mean ± standard error.

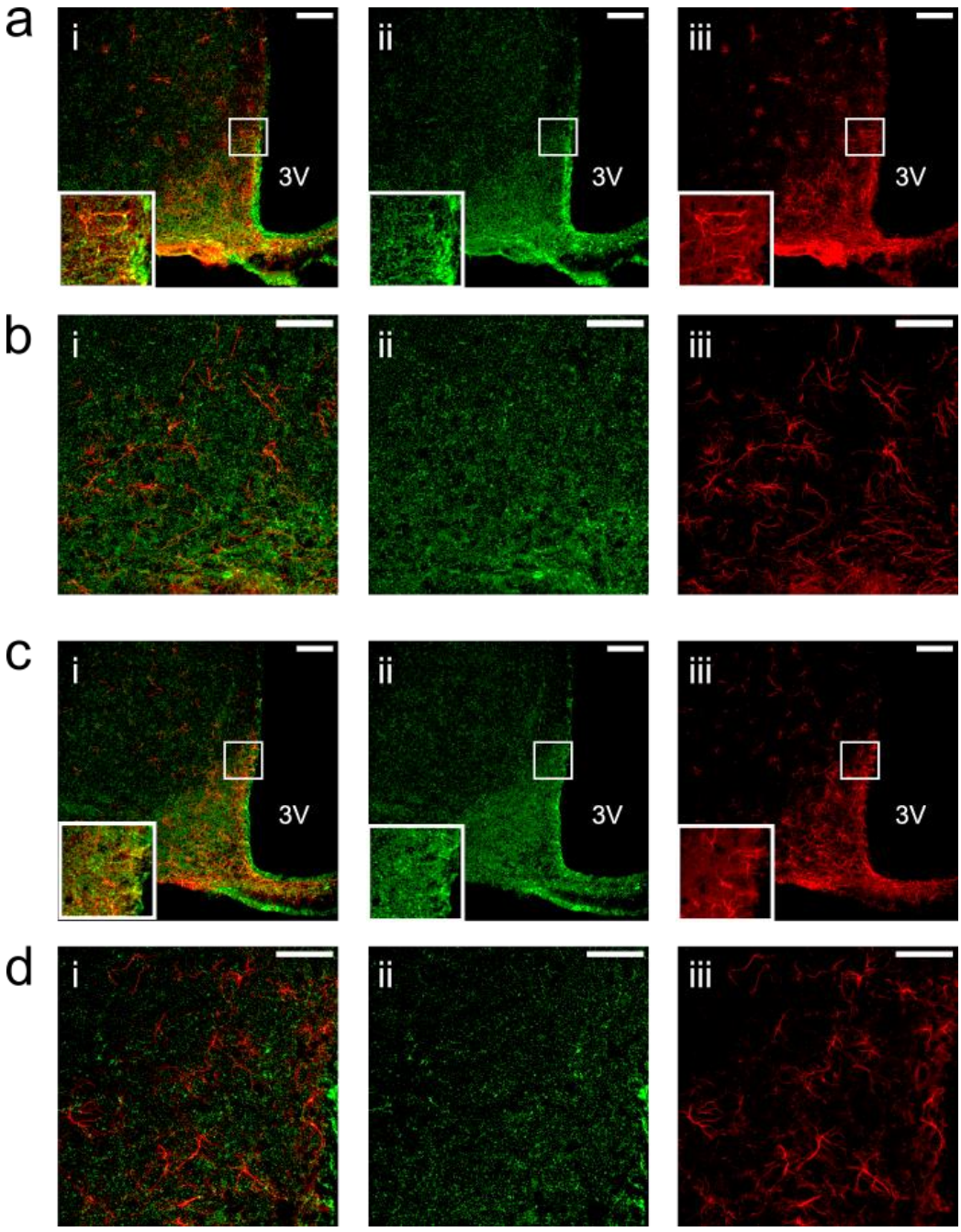

Figure 4.2.3.2 TSPO and GFAP immunoreactivity in the hypothalamic arcuate nucleus of food deprived male mice.

TSPO (ii; green) and GFAP (iii; red) immunoreactivity in the arcuate nucleus from mice fed either standard chow (a-i; merge) or food-deprived (c-i; merge) during the dark phase. Insets indicate digital zoom images of TSPO and GFAP staining in the layer of the third ventricle. Images taken at 20x (a, c) and 63x (b, d) magnification with scale bars representing 100 μm and 50 μm, respectively.

Key: Third ventricle (3V).

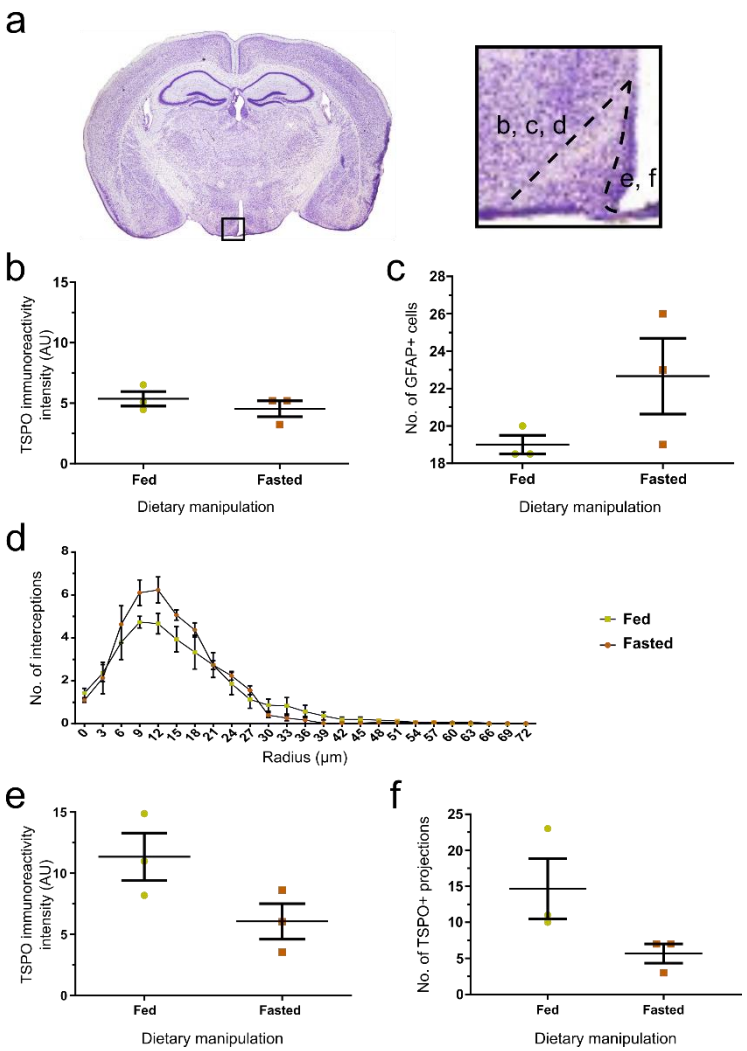

Figure 4.2.3.3 TSPO and GFAP immunoreactivity in the hypothalamic arcuate nucleus is influenced by food deprivation in male mice.

Image of coronal section (381), at -1.70 mm from bregma, indicating the regions in which image analysis was performed (a). Semi-quantitative analysis of TSPO immunoreactivity intensity did not differ between groups (b; $p = 0.0947$). The number of GFAP-positive cells was no different in the food-deprived compared to fed mice (c; $p = 0.154$). Morphological tracing analysis of GFAP-immunoreactive cells indicated no statistically significant difference in number of processes (d; diet: $p = 0.0893$, $F_{1,100} = 2.943$; interaction of diet and radius: $p = 0.0951$, $F_{24,100} = 1.472$). TSPO immunoreactivity intensity (e; $p = 0.0947$) and number of TSPO-positive cell projections (f; $p = 0.1093$), in the third ventricle wall by the arcuate nucleus were not influenced by food deprivation. N = 3 animals per group. Statistical analysis performed by Student's unpaired t test (b, c, e, and f) and repeated measures two-way ANOVA with Sidak's multiple comparisons (d). Data are expressed as mean ± standard error.

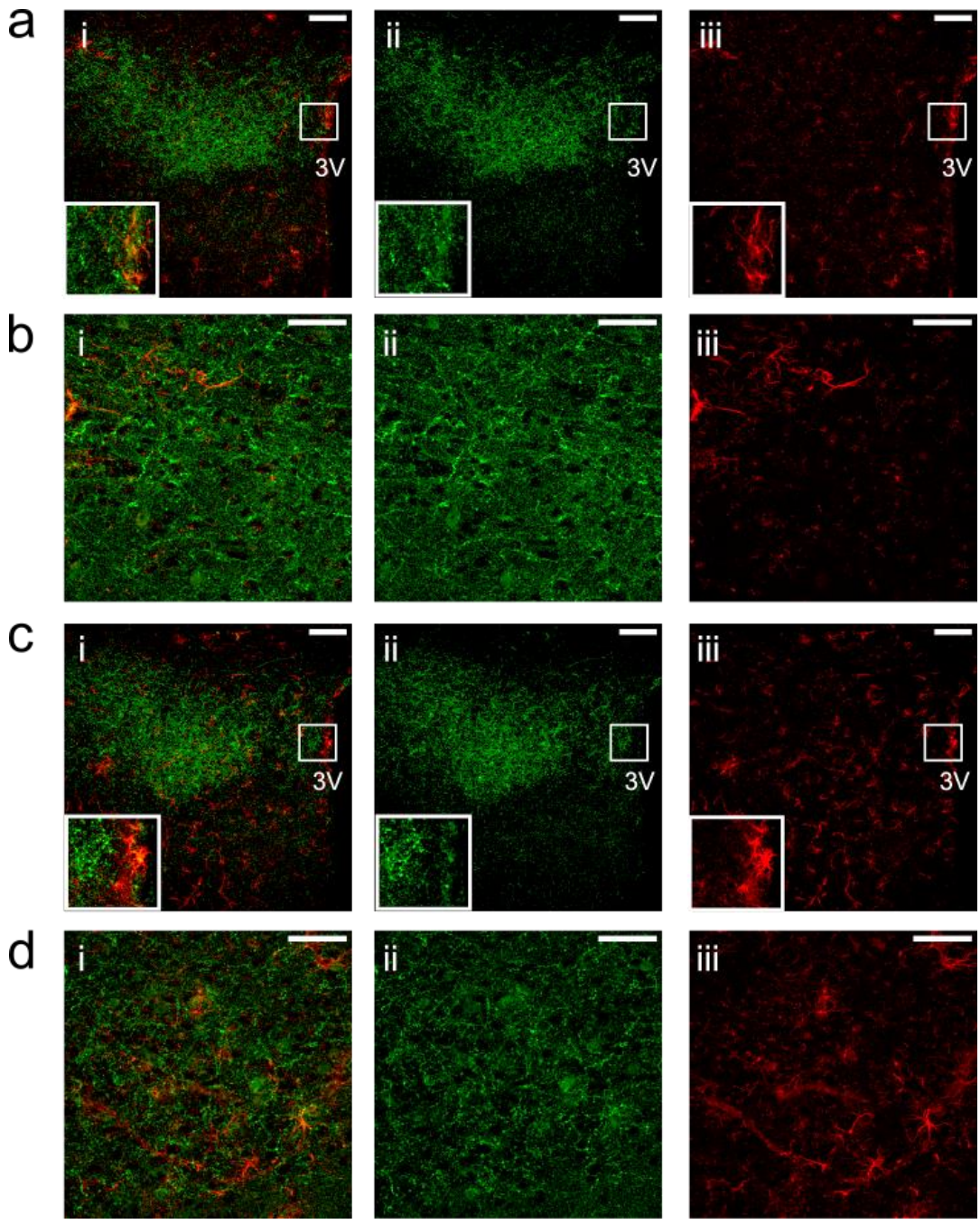

Figure 4.2.3.4 TSPO and GFAP immunoreactivity in the dorsomedial hypothalamic nucleus in satiated and food deprived male mice.

TSPO (ii; green) and GFAP (iii; red) expression in the dorsomedial hypothalamic nucleus from mice fed either standard chow (a-i; merge) or food-deprived (b) during the dark-phase. Insets indicate digital zoom images of TSPO and GFAP staining at the third ventricle lining. Images taken at 20x (a, c) and 63x (b, d) magnification with scale bars representing 100 μm and 50 μm, respectively.

Key: Third ventricle (3V).

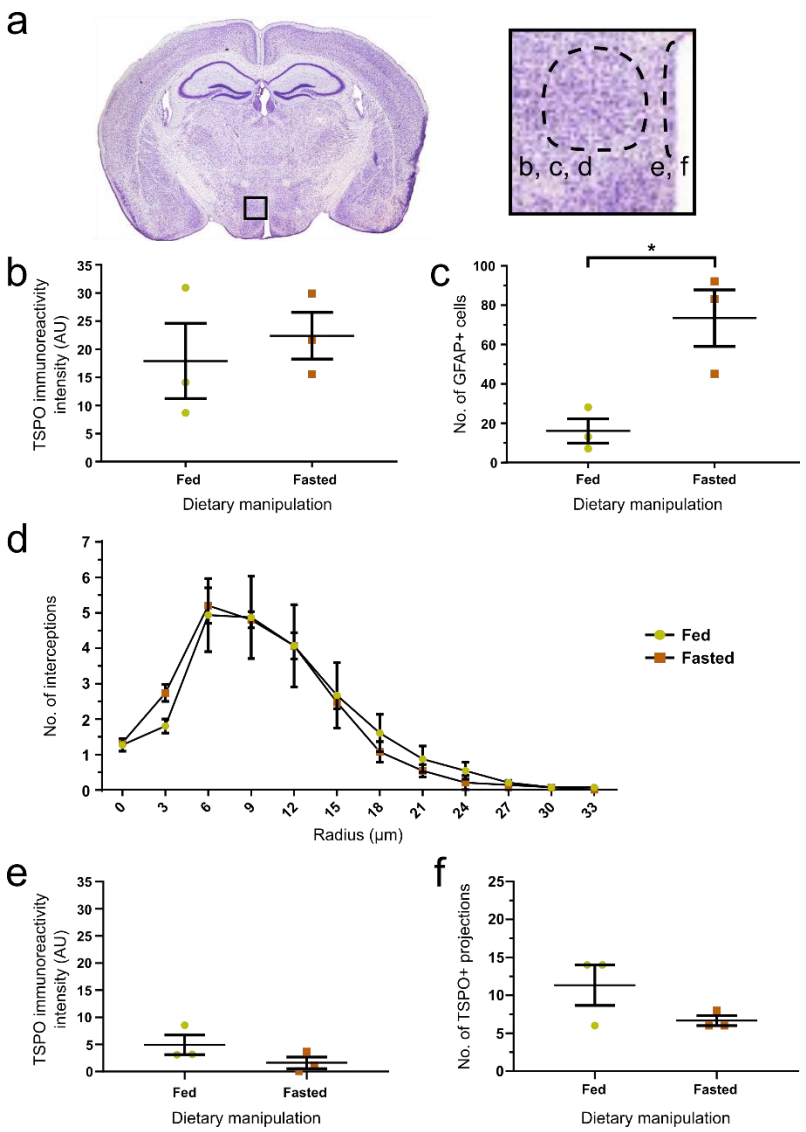

Figure 4.2.3.5 GFAP, but not TSPO, immunoreactivity in the dorsomedial hypothalamic nucleus is influenced by acute food deprivation in male mice.

Image of coronal section (381), at -1.70 mm from bregma, indicating the region used for image analysis (a). Semi-quantitative measurements of TSPO immunoreactivity intensity did not differ between dietary treatments (b; $p = 0.433$). The number of GFAP-positive cells was significantly greater in the dorsomedial hypothalamic nucleus of food-deprived, compared to fed, mice (c; $p = 0.0217$). Morphological tracing analysis of GFAP-immunoreactive cells indicated no differences of GFAP-positive cell morphology in the dorsomedial hypothalamus of fasted or fed mice (d; diet: $p = 0.9531$, $F_{1,4} = 0.0039$; interaction of diet and radius: $p = 0.9379$, $F_{11,44} = 0.4226$). TSPO immunoreactivity intensity (e; $p = 0.1884$) and number of TSPO-positive projections (f; $p = 0.1648$), in the wall of the third ventricle adjacent to the dorsomedial hypothalamic nucleus, were no different in fasted mice compared to fed. N = 3 animals. Statistical analysis performed by students' unpaired t test (b, c, e, f) and repeated measures two-way ANOVA (d). Data are expressed as mean ± standard error.

4.2.4 Investigating the impact of diet-induced obesity on hypothalamic expression of TSPO and GFAP.

The purpose of this experiment was to determine the effect of chronic high-fat diet intake on the expression of TSPO alongside that of GFAP. Male C57BL/6J mice (wild-type GFP-negative offspring of NPY-hrGFP mice on a C57BL/6J background) were provided with either high-fat diet or maintained on standard chow for a period of 12 weeks. The mice were then euthanised and transcardially perfused to collect brain tissue for immunohistochemical analysis.

The body weight of mice in both groups did not significantly differ at the start of the experimental timeline. The mice fed high-fat diet gained significantly more weight than their littermate controls, which remained at a steady weight throughout (Fig 4.2.4.1a; $p = 0.0003$). Prior to euthanasia the body weights of the high-fat fed mice were significantly greater than that of the standard chow fed controls (Fig 4.2.4.1b; $p = 0.0001$). This confirmed diet-induced obesity in the mice provided with high-fat chow.

TSPO and GFAP immunoreactivity were assessed within the Arc (Fig 4.2.4.2). TSPO immunoreactivity was no different in the mice that were diet-induced obese compared to control (Fig 4.2.4.3b; $p = 0.2618$). The number of GFAP-labelled cells (Fig 4.2.4.3c; $p = 0.2062$) and morphological tracing analysis of GFAP immunoreactivity (Fig 4.2.4.3d; $p = 0.8995$) were also not different between experimental groups. Measurements of TSPO immunoreactivity at the ventral 3V layer – intensity and number of TSPO-positive cell projections – were also unaffected by dietary manipulation (Fig 4.2.4.3e, $p = 0.5955$; 3f, $p = 0.2584$).

TSPO and GFAP immunoreactivity was observed in the DMH of diet-induced obese and control mice (Fig 4.2.4.4). No differences in TSPO immunoreactivity were detected between diet groups (Fig 4.2.4.5b; $p = 0.977$), nor in the number of GFAP-positive cells (Fig 4.2.4.5c; $p = 0.1070$). There were also no differences in morphological tracing analysis of GFAP-immunoreactive cells between mice of the experimental groups (Fig 4.2.4.5d; $p = 0.4454$). No difference was measured in TSPO intensity in the 3V wall, adjacent to the DMH (Fig 4.2.4.5e, $p = 0.5768$; 5f, $p = 0.2708$).

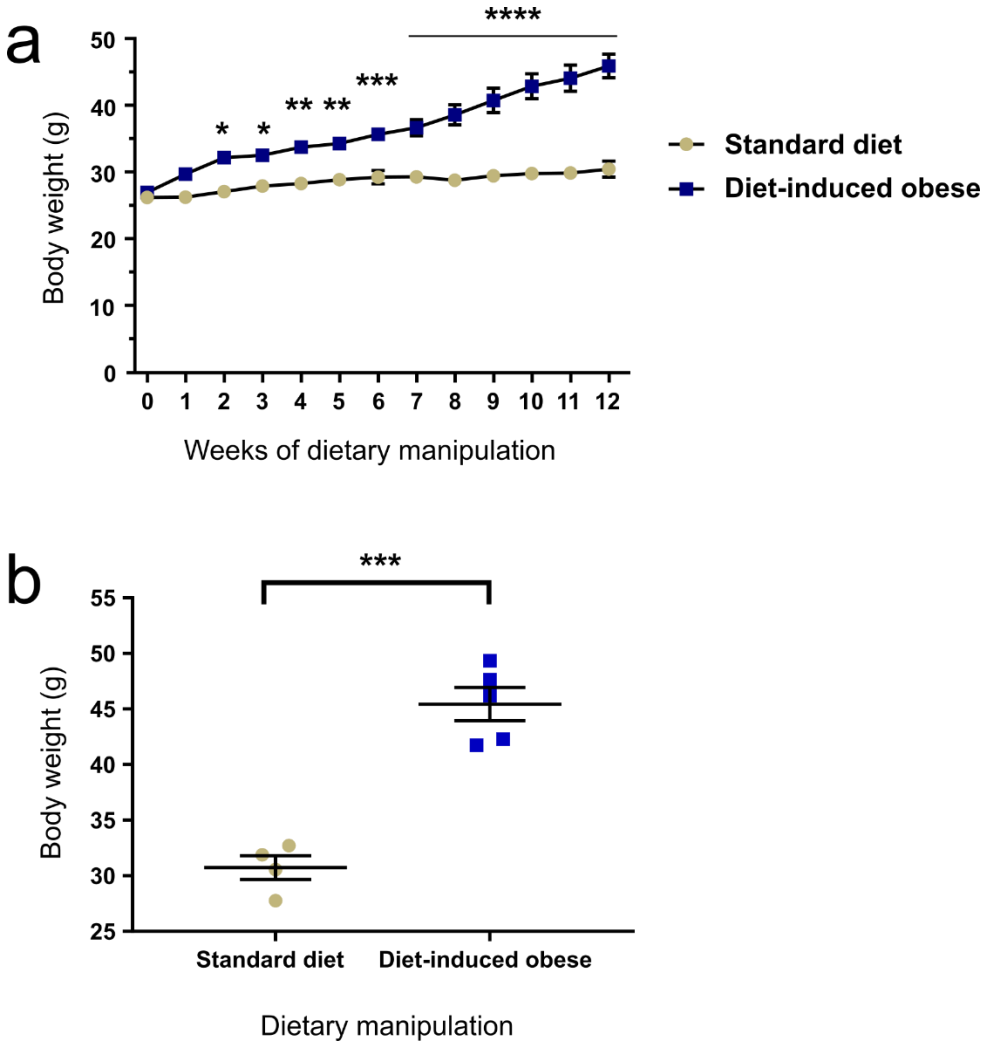

Figure 4.2.4.1 Mice with prolonged exposure to high-fat diet gained significantly more weight than their littermates that were maintained on standard chow.

The body weights of the mice throughout the study, with Week 0 being the point at which dietary manipulation was commenced. There was a statistical significant increase in body weight of mice fed high-fat diet over the experimental timeframe (a; diet: $p = 0.0003$, $F_{12,84} = 50.56$; interaction of diet and time: $p < 0.0001$, $F_{12,84} = 20.78$). Multiple comparisons test indicated statistical significance at time points 2, 3 (*, $p < 0.05$), 4, 5 (**, $p < 0.01$), 6 (***, $p < 0.001$) and 7 to 12 (****, $p < 0.0001$) weeks. The body weights between the mice in each treatment group were significantly different at the week of euthanasia (b; ***, $p = 0.0001$). N = 4-5 animals. Statistical analysis was performed with repeated measures two-way ANOVA with Sidak's multiple comparisons test (a) and Student's t test (b). Data are expressed as mean ± standard error.

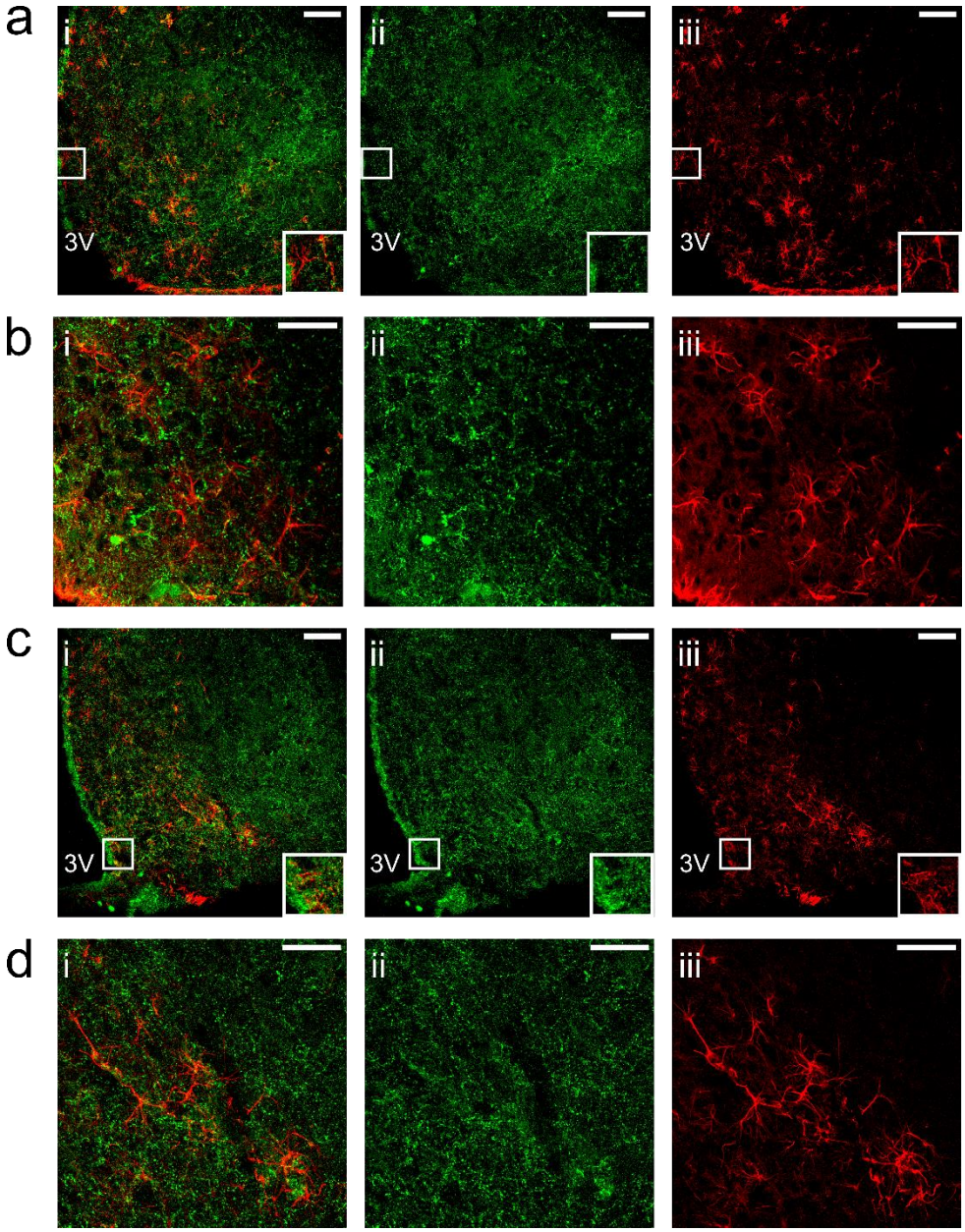

Figure 4.2.4.2 TSPO and GFAP immunoreactivity within the hypothalamic arcuate nucleus of male mice fed standard chow or high-fat diet for 12 weeks.

A representative image taken at 20x magnification depicting TSPO (ii; green) and GFAP (iii; red) immunoreactivity within the hypothalamic arcuate nucleus of male mice maintained on standard (a-i; merge) or high-fat chow (c) for 12 weeks. Insets show digital zoom images of TSPO and GFAP at the wall of the third ventricle. Images taken at 63x magnification display a similar pattern of immunoreactivity in brains from standard chow (b) and high-fat (d) mice. Scale bars represent 100 µm in images taken at 20x magnification (a, c), and 50 µm at 63x magnification (b, d).

Key: Third ventricle (3V).

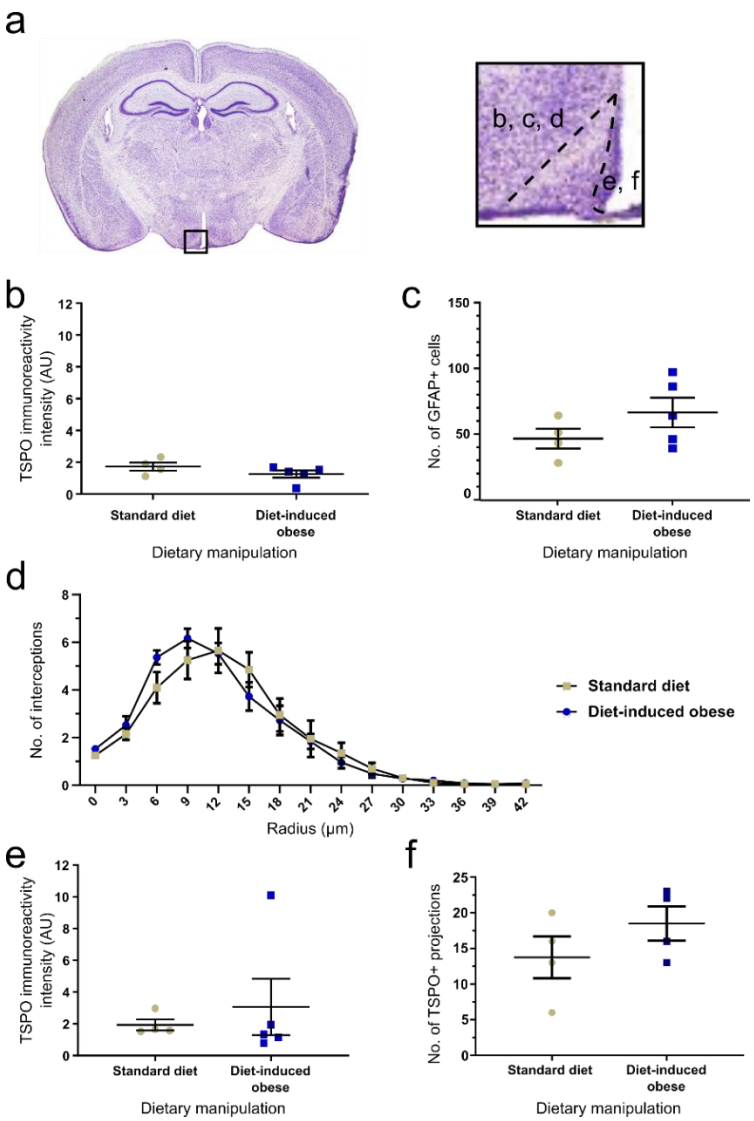

Figure 4.2.4.3 Chronic high-fat diet exposure did not alter TSPO or GFAP immunoreactivity in the hypothalamic arcuate nucleus of male mice.

Image of coronal section (381), at -1.70 mm from bregma, indicating the region used for image analysis (a). Semi-quantitative analysis of TSPO immunoreactivity intensity did not differ in the arcuate nucleus of diet-induced obese compared to control mice (b; $p = 0.2168$). The number of GFAP-immunoreactive cells also did not differ between dietary manipulation groups (c; $p = 0.2062$; n = 5-6), and there was no difference in number of GFAP-immunoreactive cell processes between diet groups (d; diet: $p = 0.8995$, $F_{1,7} = 0.0171$; interaction of diet and radius: $p = 0.1625$, $F_{14,98} = 1.411$, n = 5-6). There was no difference between dietary manipulations in TSPO immunoreactivity intensity (e; $p = 0.5955$, n = 5-6) or in number of TSPO-positive cell projections (f; $p = 0.2584$, n = 4) at the third ventricle layer beside the arcuate nucleus. Statistical analysis performed by Student's unpaired t test (b, d, e, and f) and repeated measures two-way ANOVA (c). Data are expressed as mean ± standard error.

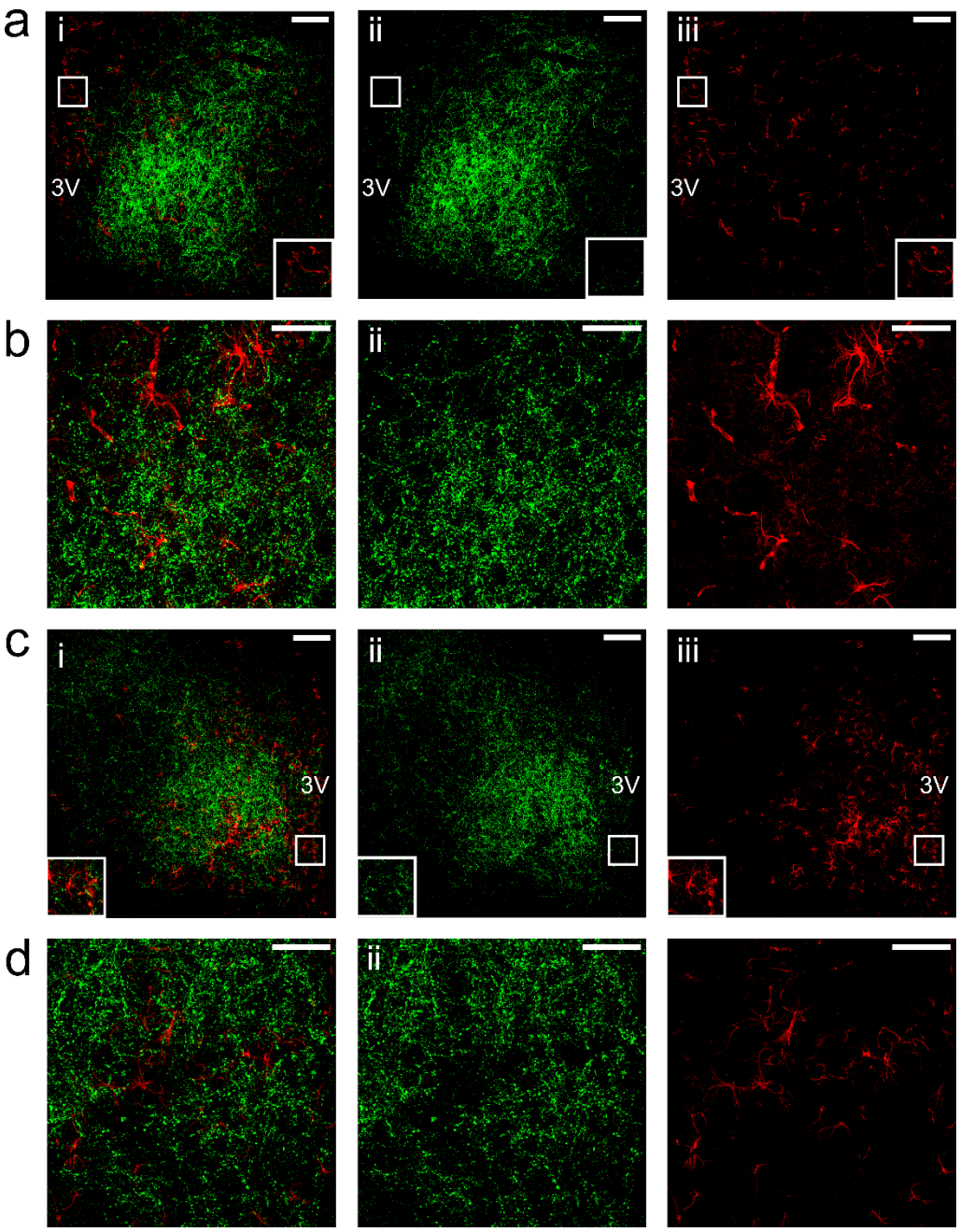

Figure 4.2.4.4 TSPO and GFAP immunoreactivity in the dorsomedial hypothalamic nucleus in diet-induced obese male mice compared to mice fed standard chow.

TSPO (ii; green) and GFAP (iii; red) immunoreactivity in the dorsomedial hypothalamic nucleus in mice fed standard chow (a, b) and high-fat diet (c, d) for 12 weeks. Images were captured at 20x magnification (a, c) and 63x magnification (b, d). Scale bars represent 100 μm at 20x magnification, and 50 μm at 63x.

Key: Third ventricle (3V).

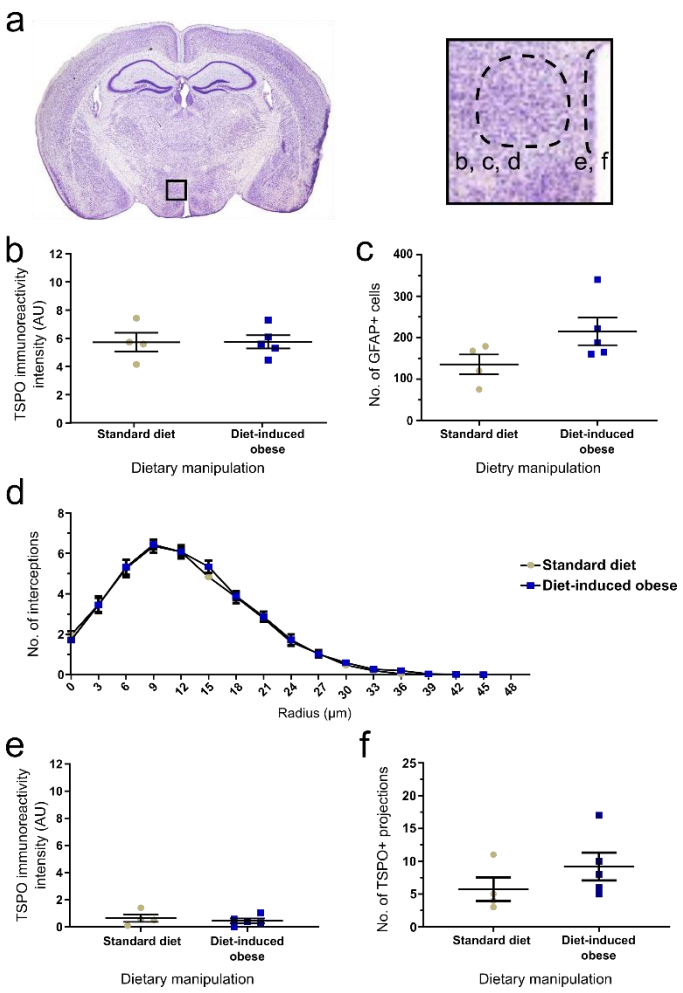

Figure 4.2.4.5 Diet-induced obesity did not influence TSPO or GFAP immunoreactivity in the dorsomedial hypothalamic nucleus of male mice.

Coronal image (381), take at -1.70 mm from bregma, depicting the dorsomedial hypothalamic nucleus in dotted lines where quantitative analysis was performed (a). Semi-quantitative analysis of TSPO immunoreactivity intensity within the dorsomedial hypothalamic nucleus did not differ with dietary manipulation (b; p = 0.977). The number of GFAP-immunoreactive cells in the dorsomedial hypothalamus of obese mice were no different to that of control mice (c; p = 0.1070). Analysis of GFAP-positive cell processes within the dorsomedial hypothalamus did not indicate any differences between mice of either dietary group (d; diet: p = 0.4554, $F_{1,112}$ = 0.5611, interaction of diet and radius: p = 0.9987, $F_{15,112}$ = 0.2342). TSPO immunoreactivity intensity (e; p = 0.5768) and number of TSPO-immunoreactive projections (f; p = 0.2708), in the third ventricle wall adjacent to the dorsomedial hypothalamic nucleus, also did not differ in diet-induced obese mice compared to control. N = 4-5 animals. Statistical analysis performed by students' unpaired t test (b, c, e, f) and two-way ANOVA with repeated measures (d). Data are expressed as mean ± standard error.

4.3 Discussion

4.3.1 Summary of findings and conclusions

The goal of this study was to investigate whether hypothalamic TSPO expression was regulated in the mouse brain by changes in energy balance, alongside GFAP, a common cell marker for astrocytes. TSPO regulation by diet has been documented in a few tissues: mouse adipose tissue, including adipose tissue macrophages (310), and in the human placenta (441). With regards to the brain, the leptin-deficient *ob/ob* mice show an up-regulation of TSPO in the hippocampus and choroid plexus (439). However, this has not been replicated in high-fat fed mice (369). No attempts to identify regulation within the hypothalamus have been published. Consequently, this research is novel and its findings are important contributions to knowledge.

TSPO expression in the DMH, as measured by Western blot, was downregulated in acute high-fat diet exposure. Although DMH GFAP expression was not regulated, this coincided with an upregulation of GFAP in the MBH - indicative of diet-induced gliosis. The acute high-fat fed group did not eat significantly more pellets by weight but did consume more calories than the standard chow-fed group. This suggests that the results observed were unlikely to be influenced by gastric stretch but are probably due to excess calories and nutrients of the high-fat chow. The body weights of the mice were the same prior to dietary manipulation, so could not have been a confounding factor. However, the absence of specificity of the TSPO immunoreactivity in the mouse brain (described in chapter 3) is still a concern and further investigation is recommended. Furthermore, although only one band was quantified, the TSPO antibody identified two bands in Western blot at the relevant molecular weight in the DMH samples. This could be a result of TSPO existing in a dimeric form (442), or may be an artefact from the lack of specificity of the antibody.

Complementary to the Western blot analysis, TSPO-immunoreactivity at the 3V wall was lower in fasted mice; this site of TSPO-immunoreactivity was validated in a TSPO-knockout mouse as specific in Chapter 3. However, the effect was not statistically significant, which could be due to lack of power in the sample size. The number of GFAP-positive cells in the DMH was higher in the fasted group.

This finding complements that of protein expression quantified by Western blot. If the sample number was increased, then a significant reduction of TSPO immunoreactivity may be observable at the 3V. This finding would be further enhanced by additional experimental approaches.

In contrast to high-fat diet, the impact of food deprivation on glial reactivity is relatively under-studied; however, negative energy balance also induces reactive gliosis (202). While this initially appears contradictory, considering high-fat diet also induces gliosis, it is important to note that reactive gliosis is a process induced by a variety of stimuli. In addition, a role for TSPO in food deprivation has not previously been investigated. One possibility arising from this study is that downregulation of TSPO expression may reflect a modulation of metabolic flexibility. Upon reactive gliosis, cellular energetic requirements can change and this requires a shift in substrate use (226,443,444). Downregulation of TSPO could complement the energetic needs of the hypothalamic glia, in both positive and negative energy balance. Tanycytes are not known to be inflammatory cells, so tanycytic TSPO expression may serve a different purpose involving metabolic flexibility. Considering that tanycyte FA sensing is a key factor for diet-induced reactive astrogliosis (121,163,191), tanycytic TSPO expression may be important for nutrient sensing at the 3V and downregulated in nutrient deprivation.

4.3.2 Limitations of the study

I applied two experimental approaches in this study to assess protein expression: immunohistochemistry and Western blotting. Immunohistochemical visualisation of cells enables analysis of morphology and cell number as a proxy for glial reactivity. Morphological tracing analysis based on Sholl's linear model – a method of quantifying neuronal morphology (384,445) - was performed to measure the ramification of GFAP-positive astrocytes (184). Semi-quantification of protein expression was performed by Western blot analysis. Unfortunately, after the study had been conducted it was realised that the TSPO antibody applied did not bind exclusively to TSPO in mouse brain tissue (see Chapter 3). This means that the majority of the TSPO analysis needs to be interpreted with extreme caution – with the exception of binding at the ventricle layers, which was validated in TSPO -/- brain tissue (see Chapter 3). Specificity of the antibody in

Western blot analysis has been validated in whole brain tissue (420), and also in primary cultured astrocytes and TSPO -/- astrocytes cells in our laboratory.

There were inconsistencies in the results presented here, between immunohistochemistry compared to Western blot analysis. One such example was GFAP expression analysis in the Arc of high-fat fed mice. Western blot analysis indicated upregulation of GFAP in the MBH of high-fat fed mice, which is consistent with what is reported in the literature (125,180). Immunohistochemical processing did not identify any change in cell number or morphology, both of which can allude to increased GFAP protein levels in the tissue. There are a few potential reasons for this. Firstly, despite random allocation, the mice in the high-fat diet group were significantly lighter in body weight than the control mice. This could have masked any effect; the heavier weight of the control mice may have led to a higher number of resident astrocytes in the Arc. Nonetheless, diet-induced gliosis is attributed to diet rather than weight-gain: gliosis occurs before weight-gain in high-fat fed mice (125), and the obese *ob/ob* mouse model does not display increased Arc reactive gliosis unless fed a high-fat diet (446). Reactive gliosis is also associated with aging (447,448) and the mice of the immunohistochemical cohort were much older than those used for Western blot analysis (18-24 weeks versus 9-13 weeks old). Therefore, the basal level of astrogliosis in the older mice may have masked any effect from acute high-fat diet exposure in immunohistochemical analysis.

Although not also quantified by Western blot, immunohistochemical analysis of GFAP immunoreactivity in diet-induced obese mice did not indicate any differences between experimental groups. This finding also contradicts what is reported in the literature (125,180,181,184). The mouse cohort that was maintained on high-fat diet for 12-weeks gained significantly more weight than the standard chow fed mice, demonstrating that the diet-induced obese model was valid. A potential confounding factor that can underlie differences in results of studies investigating metabolism is the composition of the high-fat and control diet (449–452). However, this is unlikely to be the case here. I used a diet made consisting of 60% calories from fat – the same diet as used in the Thaler *et al* publication (125). Similarly, there were only small differences in diet composition in the other comparative studies (180,181,184). The discrepancy in my results is

most likely due to a different variable, such as duration of the experiment or age of the animals.

The study presented here differed in time-points examined, compared to previous studies that investigated obesity on hypothalamic gliosis (125,180). In the study by Thaler *et al* (125), astrogliosis in response to diet-induced obesity declines after 3 weeks of exposure but returns by the 8 month mark. Elsewhere, hypothalamic markers of astrogliosis are observed after 2 months and 5 months of high-fat diet intake – depending on the study (174,176,177). It is clear that, even considering bimodal wave, markers of reactive gliosis in chronic high-fat feeding are observed at different time points by different research groups. In my study presented here, 3 months of high-fat exposure may have not been sufficient to allow the second wave of diet-induced gliosis to occur. This would explain the absence of any differences in markers of astrogliosis in the diet-induced obese model used here.

4.3.3 Future perspectives and outstanding questions

Considering the lack of specificity of the common TSPO antibody, the experiments detailed here would benefit from additional methodologies to measure protein expression. For example, quantification of mRNA by *in situ* hybridisation is an alternative route for to confirm regulation of TSPO gene expression in response to dietary manipulation, including in the tanycyte layer of the 3V. Another approach to measure TSPO expression in this experimental scenario would be to use slice autoradiography with TSPO ligands. This study would also benefit with additional age-matched cohorts, and additional time points during high-fat exposure. For instance, changes in protein expression may be measurable at 3 to 7 days exposure and at 8 months as seen by Thaler *et al* (125) . It is important to consider the dynamic nature of glia through the lifespan, and how this may influence results.

To conclude, this study (considering the assumption at the time that the TSPO antibody was specific) provides evidence to support the hypothesis that TSPO is regulated in the hypothalamus by energy imbalance. TSPO expression in the DMH, as measured by Western blot, was downregulated by acute high-fat

exposure. No effects were seen in the Arc. Down-regulation was also observed in TSPO at the 3V which, considering the findings of Chapter 3, is likely expressed by tanycytes. If these findings hold true with further experimentation, TSPO may promote metabolic flexibility in the different reactive states of glia. Furthermore, TSPO expression is unlikely to be solely related to reactive state of astrocytes as it was not co-regulated alongside GFAP in these studies. This study also supports previous work showing that negative energy balance can induce markers of reactive astrocytes (182,202). There may be a common downstream factor below sensing of both positive and negative energy imbalance that influences gliosis.

Chapter 5: Inhibition of TSPO-mediated signalling

5.1 Introduction

Experiments that used genetic and pharmacological manipulation of TSPO have indicated a potential role in metabolism (311,324,325,329,330,347,359,362,363,379,453). While *in vitro* experiments can provide useful insight into the molecular mechanisms underlying TSPO-mediated signalling, *in vivo* studies are needed to determine the physiological impact. As both approaches have their limitations, a combination of experimental methodologies is ideal for investigating protein function. In this chapter, I will present a series of data from different studies using pharmacological and genetic manipulation to investigate a potential role for TSPO in regulating systemic metabolism in C57BL/6 mice.

Genetically manipulation of TSPO in cell culture reveals a role in mitochondrial metabolism. Knock-down of TSPO expression in cultured steroidogenic testicular Leydig cells increases fatty acid oxidation (FAO) (330) and alters lipid homeostasis (359). This indicates a shift in energy substrate preference from glucose to fatty acids. Furthermore, isolated microglia from TSPO knock-out (-/-) mice produce less ATP in culture than microglia taken from TSPO wild-type (+/+) controls (325). These studies demonstrate that alterations in TSPO expression can result in changes in cellular metabolism.

Pharmacological targeting of TSPO in cell culture, on the other hand, has revealed varying effects on mitochondrial bioenergetics. Application of a range of TSPO ligands – XBD173, Ro5-4864 and PK11195 – enhances mitochondrial respiration in mouse BV-2 microglia cell culture (329). This was inconsistent, depending on the ligand, reflecting potential activation/inhibition actions. The same conclusions were drawn from human neuroblastoma (SH-SY5Y) cells (453). These studies suggest that exogenous TSPO ligands exert different functions depending on dose, and may exhibit non-specific binding. Moreover, at the doses used the off-target effects from these ligands were also observed in

TSPO knock-down BV-2 cells (329), therefore solid conclusions cannot be obtained from such studies.

Studies in which TSPO expression is deleted in mice have strengthened the evidence from *in vitro* work that TSPO is involved in metabolism. Upon the discovery that global germ-line deletion of TSPO mice are viable (420), it has been determined that these mice appear to have normal growth rate, food intake, behaviour and blood composition - at least when fed a standard chow diet (325). However, mice with targeted TSPO deletion in steroidogenic factor 1 (SF-1) positive cells display higher basal blood glucose levels than the control animals (363). This was only observed in male mice and no such alterations in resting blood glucose were seen in the females. Lipid storage was altered in both male and female SF-1 TSPO -/- mice, with increased storage in the gonads; liver; and testes (362). A comparison between these studies suggests a role for TSPO in mediating glucose homeostasis and lipid storage that is specific for its function in steroidogenic tissues.

In addition to genetic manipulation, pharmacological targeting of TSPO in mice has also revealed effects on whole-body metabolism and glucose regulation. In food deprived C57BL/6 mice up-regulation of mRNA of metabolic enzymes is observed in the liver, an effect that is enhanced after treatment with the TSPO ligand PK11195 (347). The targets examined included glucose-6-phosphatase (*G6p*), carnitine palmitoyltransferase 1a (*Cpt1a*), and phosphoenolpyruvate carboxykinase 1 (*Pck1*) – which are all involved in glucose or lipid metabolism. Meanwhile, in diet-induced obese C57BL/6 mice, treatment with PK11195 was protective against hyperglycaemia and also reduced hepatic steatosis (347). This study implies that TSPO is involved in compensatory responses to changes in energy balance – such as food deprivation and excessive nutrient intake. Administration of TSPO ligands can influence the role of TSPO in tissue metabolism (301,347), which may provide protection against the maladaptive effects of energy imbalance. However, further investigation along with replication of these observed effects is required before conclusions are made.

Comparing the discoveries from genetic and pharmacological manipulation studies of TSPO highlights gaps in knowledge of its function. There are differences between *in vivo* investigations of TSPO function in whole-organism physiology that require clarity. For instance, SF-1 specific cell knock-out of TSPO

resulted in hyperglycaemia that was not observed in global knock-out mice (325,363). The SF-1 TSPO -/- mice also had altered lipid deposits (362), which was not investigated in the global knock-out mice and so comparisons are difficult to make. Pharmacological manipulation of TSPO *in vivo* hints at influence in physiological metabolic state in response to negative and positive energy balance. For example, in the case of energy excess, targeting TSPO signalling was protective in diet-induced obese mice (347). Meanwhile, TSPO knock-out in SF-1 cells resulted in a pre-diabetic phenotype irrespective of dietary manipulation (362,363). Regarding food deprivation, only gene expression of key metabolic enzymes was examined and so the physiological impact of targeting TSPO in negative energy states remains to be fully understood. Further experiments are required to answer these outstanding questions.

The hypothesis underlying the study presented here is as follows: whole-body manipulation of TSPO-mediated signalling will alter the animals' energy homeostasis. A shift in substrate preference for metabolism will occur in the affected cells, favouring fatty-acid oxidation as a fuel source over glycolysis. A change in energy substrate, due to absence of TSPO, will lead to a different physiological compensation to energy imbalance. I proposed that, in TSPO deficient mice, this will manifest as protection against the negative effects of chronic high-fat diet consumption: improved glucose tolerance; reduced body weight gain; and reduced markers of obesity-associated impairment in organs crucial for systemic metabolism. In regard to negative energy balance, as PK11195 induces upregulation of hepatic metabolic enzymes, this may be observed to reduce food-intake in fasted TSPO -/- mice. This study used both genetic global TSPO -/- mice along with pharmacological experiments with the TSPO ligand PK11195.

The key questions used to investigate this hypothesis were:

- Does absence of TSPO reduce food intake and body weight gain when mice are maintained on high-fat diet?
- Does absence of TSPO protect against the negative effects of chronic high-fat feeding in mice?
- Does modulation of TSPO signalling impact systemic glucose tolerance?
- Does modulation of TSPO signalling alter food intake post-food deprivation?

5.2 Results

5.2.1 Investigating differences in energy homeostasis in TSPO -/- mice

The TSPO -/- and TSPO +/+ littermate control mice arrived at the biological services unit at ages 6-9 weeks old. Upon arrival, the mice were de-identified and randomised before being individually housed. Weekly measurements of food intake and body weight were made for 12 weeks. No measurements of food intake were taken in experimental week 5 due to the fasting intervention taking place. The investigators were blinded to the genetic identity of the mice for the entire study.

The mice gained weight at a gradual and steady rate over this portion of the study. (Fig 5.2.1.1a & c). The male mice gained more weight than their female counterparts. The male TSPO -/- mice gained slightly more weight than their littermate controls over the experimental time-frame, which achieved statistical significance (Fig 5.2.1.1a; p = 0.0359). There was no difference between genotypes in body weight gain in the female mice (Fig 5.2.1.1c; = 0.3909). There was no genotypic influence in food intake in the male (Fig 5.2.1.1b; p = 0.3121) and female mice (Fig 5.2.1.1d; p = 0.3909). Food intake was also comparable between the male and female cohorts.

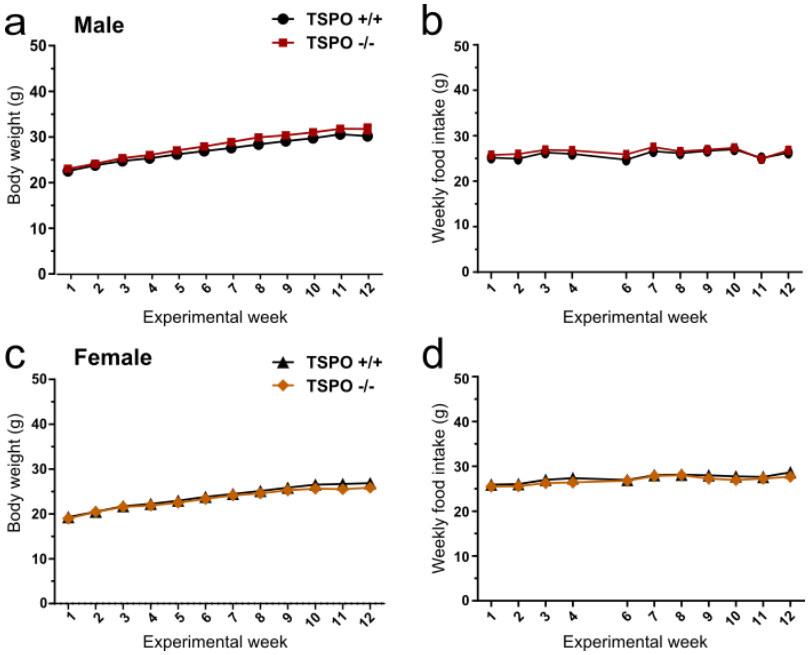

Figure 5.2.1.1 Male TSPO -/- mice gained slightly more weight than TSPO +/+ controls, while growth of female mice and food intake of both sexes showed no genotypic differences.

Male mice of both genotypes gained weight over the experimental time-course (a; Week: $p < 0.0001$, $F_{1,45} = 399.1$, n = 12-14) but TSPO -/- mice gained significantly more weight than their TSPO +/+ counterparts over the period (a; Interaction: $p = 0.0359$, $F_{11,263} = 1.93$). *Post-hoc* multiple comparisons analysis did not identify any statistical differences at any time point during the experiment. There was no significant impact of genotype alone (a; $p = 0.2561$, $F_{1,24} = 1.354$). There was no impact of genotype (b; $p = 0.3121$, $F_{1,24} = 1.066$, n = 12-14) nor interaction of genotype and time (b; $p = 0.7472$, $F_{10,239} = 0.675$) on weekly food intake in the male mice maintained on standard chow, but there was a significant effect of time (b; $p < 0.0001$, $F_{5,131} = 10.01$). In female mice, there was no effect of genotype (c; $p = 0.3643$, $F_{1,25} = 0.854$, n = 13-15) nor an interaction between genotype and time (c; $p = 0.5288$, $F_{11,275} = 0.9124$) on cumulative body weight gain between genotypes when kept on standard chow. Both genotypes gained weight over the experimental period (c; $p < 0.0001$, $F_{2,50} = 173$). There was no influence by genotype (d; $p = 0.3909$, $F_{1,25} = 0.7624$, n = 13-15), or an interaction with experimental time (d; $p = 0.9587$, $F_{10,249} = 0.3698$) on weekly standard chow food intake between female TSPO -/- and +/+ mice. There was a significant effect of experimental time on food intake in the female cohort (d; $p < 0.0001$, $F_{5,139} = 10.55$). Statistical analysis was performed using two-way ANOVA with repeated measures or mixed-effects analysis when appropriate. Data are expressed as mean ± standard error.

Pharmacological modulation of TSPO in fasted mice enhances the fast-induced up-regulation of mRNA for hepatic gluconeogenic enzymes and lowers blood glucose (347). This would likely cause homeostatic changes in food intake to recover the loss of energy. However, no such role of TSPO in homeostatic energy regulation has been published. To investigate this, I conducted a fast-induced re-feeding experiment in TSPO +/+ and -/- mice. This produced two measurements: day-time food intake following the 12-hour overnight fast, alongside corresponding body weight changes in response to fasting and re-feeding. These measures reflect the homeostatic compensation for the food deprivation, and the ability of the animals to sense and recover body mass after state of negative energy balance. There was no impact of TSPO absence on the ability to retain body weight in the fasting period in the male mouse cohort (Fig 5.2.1.2a; p = 0.2686), nor in cumulative food intake during the fast-induced re-feeding (Fig 5.2.1.2b; p = 0.9414). Furthermore, no differences were observed in the loss of or recovery in body weights (Fig 5.2.1.2c; p = 0.3939) or in refeeding (Fig 5.2.1.2d; p = 0.1064) between female TSPO +/+ and -/- mice.

The loss of TSPO signalling on the response to positive energy imbalance was investigated by exposing the TSPO +/+ and -/- mice to an obesogenic diet. Following the 12 weeks on standard chow diet, mice were provided with high-fat diet (HFD; 60% calories from fat) as their only source of food, while their food intake and body weights were continued to be monitored. Daily measurements of food intake were taken during the first week, followed by weekly recordings in the weeks following. During this transition to a HFD, male TSPO -/- mice had significantly lower food intake than TSPO +/+ mice over the experimental period which came to a significant difference at day 7 (Fig 5.2.1.3a; p = 0.0078). The female TSPO +/+ and -/- mice displayed no significant differences in daily food intake during the initial exposure to the high-fat diet (Fig 5.2.1.3b; p = 0.2765). At day 7 of high-fat diet exposure, both cohorts of mice had increased their daily chow intake compared to previous days. However, both the female TSPO +/+ and -/- mice consumed more chow on day 7 than the male cohort. Greater variability in the female cohort was observed, due to the female mice shredding and hoarding the chow.

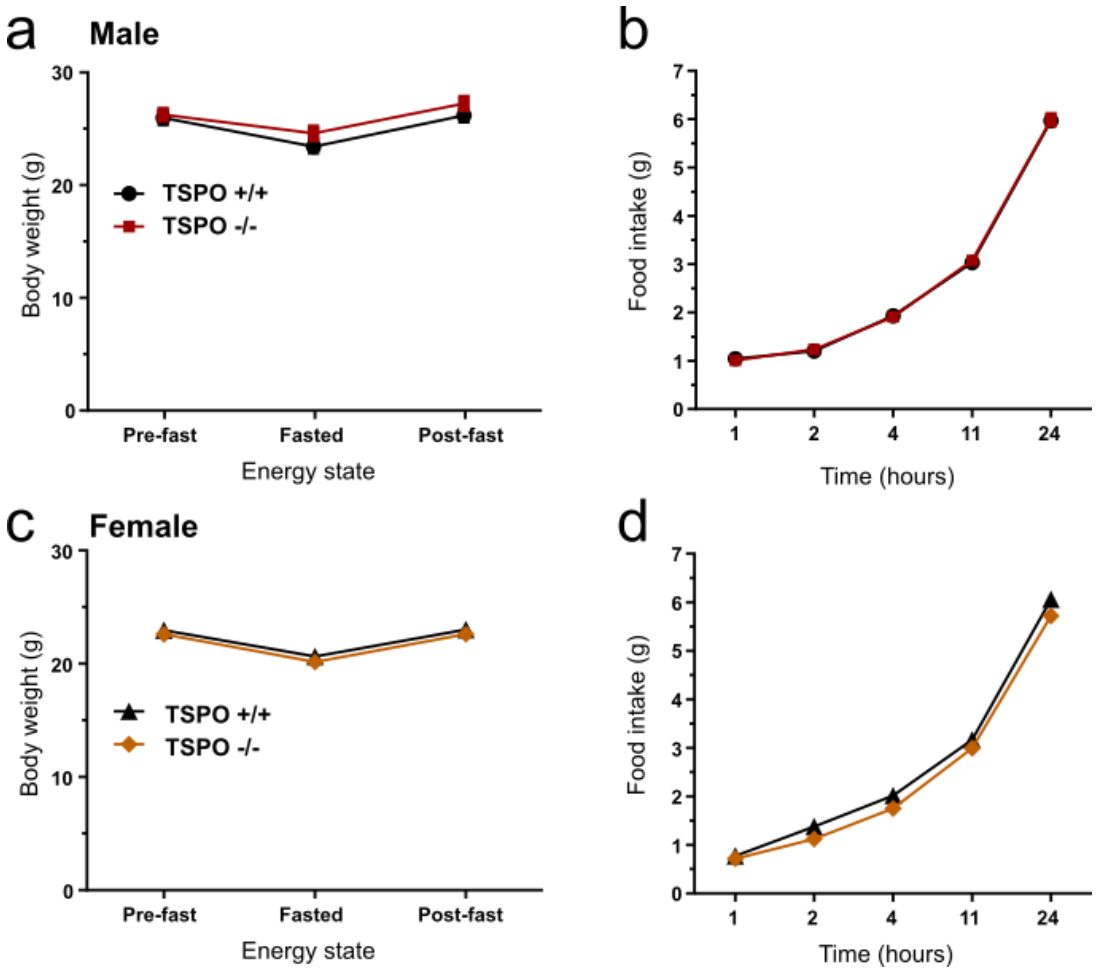

Figure 5.2.1.2 Absence of TSPO did not impact the homeostatic feeding response to negative energy balance.

No differences in fasting induced body weight loss were observed in male TSPO -/- compared to TSPO +/+ mice (a; Genotype: p = 0.2686, $F_{1,24}$ = 1.283; Interaction of genotype and energy state: p = 0.2201, $F_{2,48}$ = 1.563, n = 12-14). Compensatory food intake of male TSPO -/- mice was no different to that of TSPO +/+ mice following refeeding after 12 hours of overnight food deprivation (b; Genotype: p = 0.9414, $F_{1,120}$ = 0.0054; Interaction of genotype and time: p = 0.9855, $F_{4,120}$ = 0.0898, n = 12-14). There was no effect of genotype on body weight change from before to after fasting in female TSPO +/+ and -/- mice (c; Genotype: p = 0.3939, $F_{1,26}$ = 0.7517; Interaction of genotype and energy state: p = 0.7115, $F_{2,52}$ = 0.3426, n = 13-15). Fast-induced refeeding was also unaffected by genotype in the female TSPO +/+ and -/- mice (d; Genotype: p = 0.1064, $F_{1,26}$ = 2.797; Interaction of genotype and time: p = 0.3089, $F_{4,104}$ = 1.215, n = 13-15). Statistical analysis was performed with two-way ANOVA with repeated measures. Data are expressed as mean ± standard error.

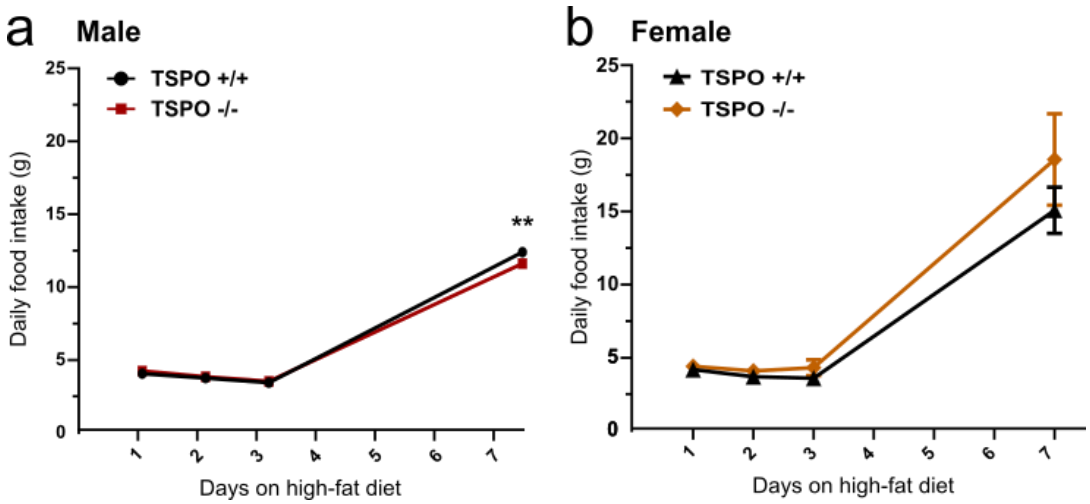

Figure 5.2.1.3 High-fat diet intake in TSPO +/+ and -/- mice over 1 week.

Male TSPO -/- mice ate a slightly, but significant, lower amount of high-fat chow than TSPO +/+ mice across the first week of high-fat exposure (a; Interaction of genotype and time: p = 0.0078, $F_{3,72}$ = 4.272, n = 12-14). Sidak's multiple comparisons test indicated a significant difference at experimental day 7 (**, p = 0.0093). However, there was no significant effect of genotype alone (a; p = 0.5245, $F_{1,24}$ = 0.4172). Acute measurements of food intake in the first week of exposure to high-fat diet in female TSPO +/+ and -/- mice did not identify any genotypic differences (b; Genotype: p = 0.2765, $F_{1,25}$ = 1.238; Interaction of genotype and time: p = 0.5032, $F_{3,75}$ = 0.7901, n = 13-15). Statistical analysis was performed with two-way ANOVA with repeated measures. Data are expressed as mean ± standard error.

The TSPO +/+ and -/- mice were maintained on high-fat diet for 6 weeks. The subtle difference in body weight of male TSPO +/+ and -/- mice observed when the mice were fed standard chow, was lost and there was no significant effect of genotype on body weight (Fig 5.2.1.4a; p = 0.5432). Food (Fig 5.2.1.4b; p = 0.8045) and energy (Fig 5.2.1.4c; p = 0.8671) intake of the male mouse cohort displayed no genotypic differences. In both measurements, intake was lower at after 1 week of high-fat diet compared to standard chow (week 0) but had recovered and stabilised by week 3. Female TSPO -/- mice had a slightly lower rate of cumulative body weight gain than the TSPO +/+ littermates, but this did not reach statistical significance (Fig 5.2.1.4d; p = 0.061). In this portion of the study, both mouse cohorts gained weight and the sex difference in body weights reduced (Fig 5.2.1.4a & d). There was no influence of genotype in food (Fig 5.2.1.4e; p = 0.7465) or energy (Fig 5.2.1.4f; p = 0.7587) intake in the female mice. Comparable to the male mouse cohort, the first week of high-fat diet exposure resulted in lower food and energy intake compared to week 0. However, the female mice consumed more food and energy by week 3 than observed in the male cohort – which then reduced and stabilised by week 4.

Maintenance on an obesogenic diet leads to impaired glucose sensing and handling (46,119), which can be replicated in mouse models (374,454). This is reflected by reduced glucose clearance from the blood following an intra-peritoneal bolus injection of glucose in a glucose tolerance test (GTT). The purpose of this experiment was to observe whether absence of TSPO alter the ability of the animals to clear glucose in the GTT in animals on a standard chow or high-fat diet. Accordingly, this procedure was performed prior to dietary manipulation and repeated following 5 weeks exposure to the high-fat diet. While maintained on standard chow, there was no genotypic difference in blood glucose levels in response to the GTT in the male mouse cohort (Fig 5.2.1.5a; p = 0.9521). Following exposure to high-fat diet, there was still no genotypic effect on blood glucose levels (Fig 5.2.1.5b; p = 0.2802). In both genotypes, basal blood glucose – as measured at time 0 (the time of injection) – was only slightly elevated following high-fat feeding (Fig 5.2.1.5b; mean = 13.8 mMol/L) compared to when maintained on standard chow (Fig 5.2.1.5a; mean = 11.8 mMol/L). Blood glucose of both high-fat fed mice did not return to basal measures during the experimental time-course (Fig 5.2.1.5b). Similarly, in the female mouse cohort, there were also

no genotypic differences on blood glucose levels of mice fed standard chow (Fig 5.2.1.5c; p = 0.8032) or when fed high-fat diet (Fig 5.2.1.5d; p = 0.5259). In similarity to the males, blood glucose of high-fat fed female mice did not return to baseline levels during the experimental period.

Female mammals are less susceptible to the negative consequences of consuming a high-fat diet than the males of the species, and female C57BL/6 mice are no exception (386–388,455). The discrepancy between the sexes is likely due to differences in adipose mass and distribution, as well as differences in circulating sex hormones. The differences result in a lower rate of body weight gain and improved glucose tolerance, compared to male mice. To detect how sexual dimorphism influenced glucose handling in TSPO +/+ and -/- mice, the area under the curve was calculated for each graph in figure 5.2.1.5 and the data from both sexes were pooled together (Fig 5.2.1.5e). Comparisons of area under the curve of the changes in blood glucose levels during the glucose tolerance time-course test in both male and female mice indicated that, as expected, sex had a statistically significant effect on blood glucose levels during the GTT (Fig 5.2.1.5e; p = 0.0006). The three-way analysis of the pooled data also indicated a statistically significant effect of dietary manipulation on blood glucose (Fig 5.2.1.5e; p < 0.0001), and confirmed no effect of genotype (Fig 5e; F (1, 51) = 0.02, p = 0.877). There were also no significant interactions between genotype, sex and diet.

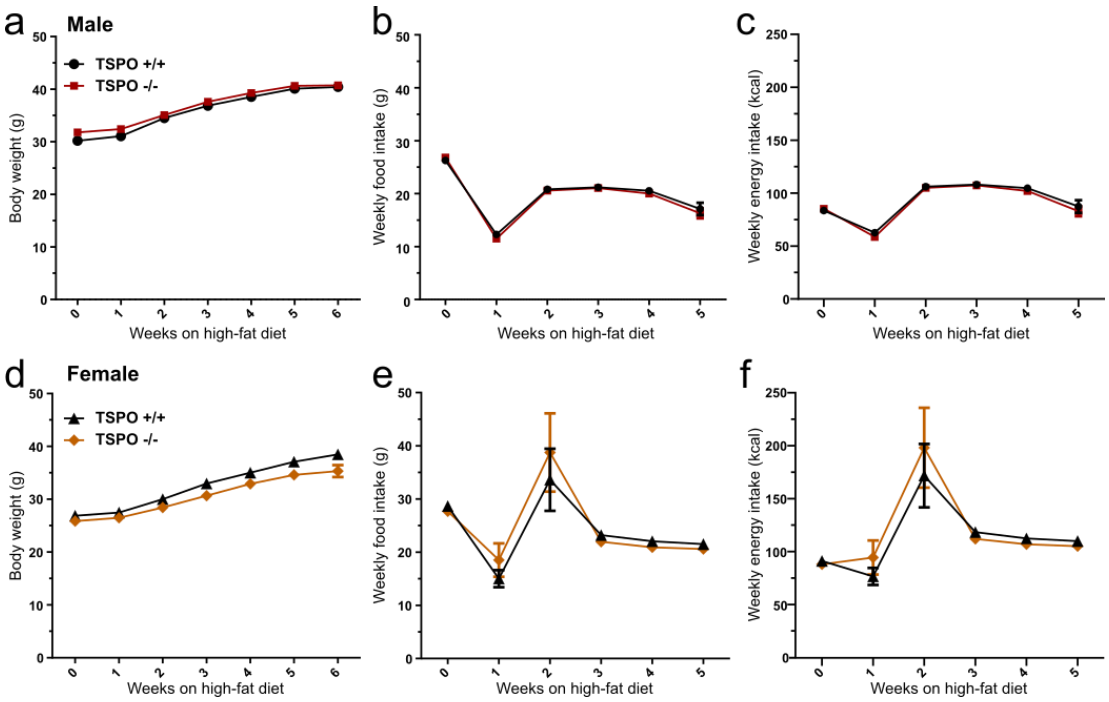

Figure 5.2.1.4 High-fat diet resulted in increased body weight and altered food intake compared to standard chow, but with no differences between genotype. Access to high-fat diet lead to a steady increase in body weight in both genotypes of male mice, compared to when mice were fed standard chow (Week 0) (a; p <0.0001, $F_{2,53}$ = 320.9, n = 12-14). There was no interaction between genotype with regard to weight gain on high-fat diet (a; p = 0.5432, $F_{6,143}$ = 0.8371, n = 12-14). Measures of food intake were also unaffected by genotype in male mice (b; p = 0.8045, $F_{5,120}$ = 0.4611, n = 12-14). Weekly energy intake was also no different between genotype (c; p = 0.8671, $F_{5,120}$ = 0.3718, n = 12-14). Female TSPO -/- mice gained body weight at a lower rate than their TSPO +/+ counterparts while on high-fat diet, but this did not reach statistical significance (d; p = 0.061, $F_{6,150}$ = 2.062, n = 13-15). In both genotypes, body weight did increase over time (d; p <0.0001, $F_{3,75}$ = 226.4, n = 13-15). Weekly measures of high-fat chow intake did not differ between genotype in female mice (e; p = 0.7465, $F_{5,124}$ = 0.5388, n = 13-15). Weekly energy intake of mice was also unaffected by genotype (f; p = 0.7587, $F_{5,124}$ = 0.5227, n = 13-15). Statistical analysis was performed with two-way ANOVA with repeated measures or mixed-effects analysis as applicable. Data are expressed as mean ± standard error.

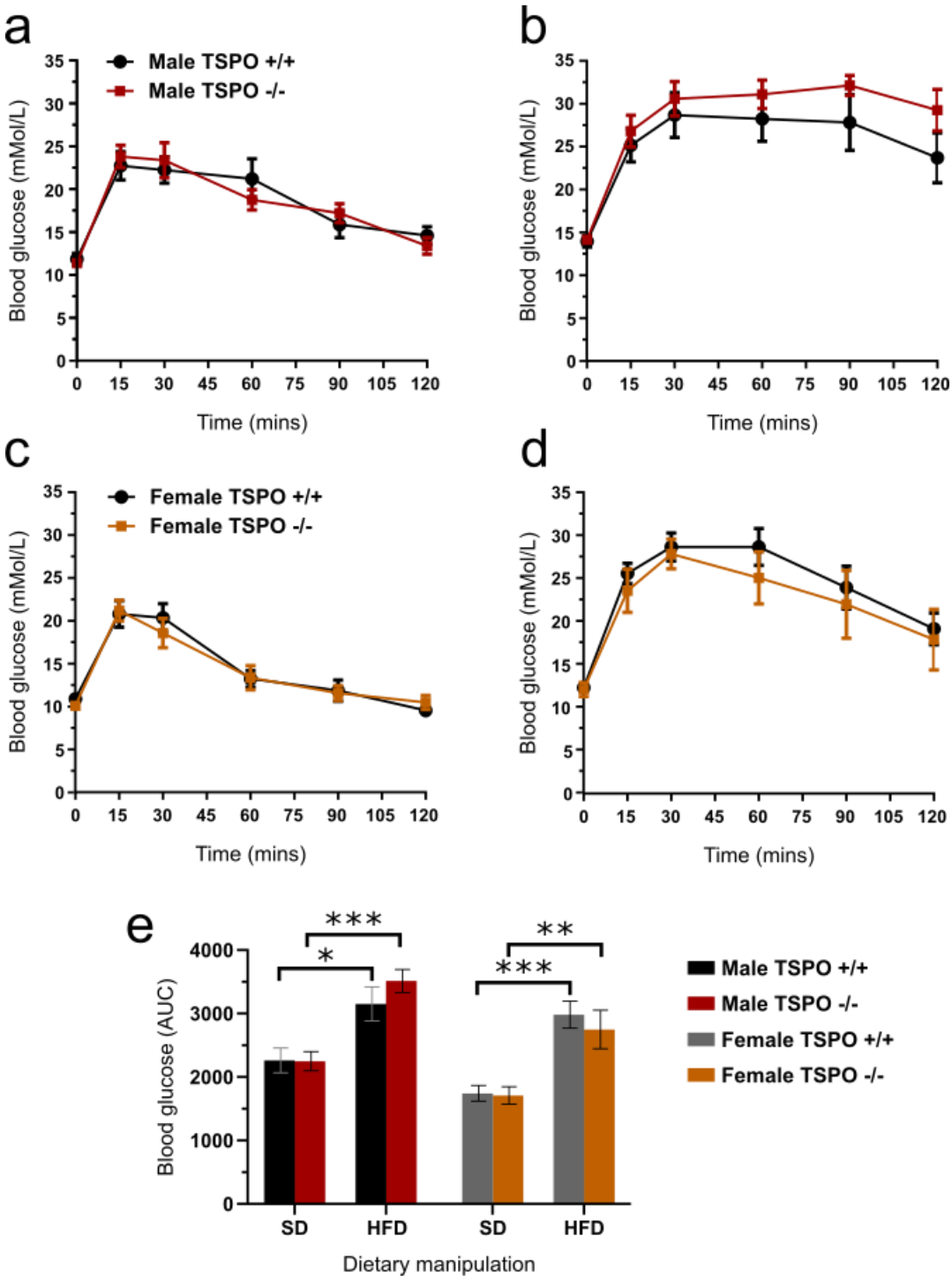

Figure 5.2.1.5 Exposure to high-fat diet resulted in reduced glucose tolerance in TSPO +/+ and -/- mice with a sex-dependent effect, but with no significant differences seen between genotypes.

There was no difference in blood glucose levels over time, following an intra-peritoneal injection of 2 g/kg glucose at time 0, in male TSPO +/+ and -/- mice fed standard chow (a; Genotype: $p = 0.9521$, $F_{1,14} = 0.0037$; Interaction of genotype and time: $p = 0.3683$, $F_{5,70} = 1.1$, n = 8). Following 5 weeks of high-fat feeding, blood glucose levels of TSPO -/- mice were slightly higher than that of TSPO +/+ mice but this did not reach statistical significance (b; Genotype: $p = 0.2802$, $F_{1,11} = 1.29$; Interaction of genotype and time: $p = 0.3818$, $F_{5,55} =$

1.08, n = 6-7). Similarly, there was no genotypic difference between standard chow fed female TSPO mice in blood glucose levels following a glucose challenge (c; Genotype: p = 0.8032, $F_{1,15}$ = 0.0644; Interaction of genotype and time: p = 0.8503, $F_{5,75}$ = 0.3957, n = 8). After 5 weeks of high-fat diet, female TSPO -/- mice still exhibited no difference in blood glucose levels during the tolerance test compared to their TSPO +/+ littermates (d; Genotype: p = 0.5259, $F_{1,11}$ = 0.429; Interaction between genotype and time: p = 0.9185, $F_{5,55}$ = 0.2866, n = 6-7). Three-way comparison of area under the curve also indicated no effect of genotype on blood glucose (e; p = 0.8772, $F_{1,51}$ = 0.0241, n = 6-7) while both sex (e; p = 0.0006, $F_{1,51}$ = 13.28) and diet (e; p < 0.0001, $F_{1,51}$ = 65.71) had a statistically significant influence on blood glucose levels. There was no statistically significant interaction between genotype and sex (e; p = 0.2619, $F_{1,51}$ = 1.287) nor between genotype and diet (e; p = 0.745, $F_{1,51}$ = 0.1069). Sidak's multiple comparisons test indicated a significant difference in blood glucose area under the curve in comparisons of measurements taken before and after high-fat diet exposure in all cohorts (Male TSPO +/+: p = 0.0313, Male TSPO -/-: p = 0.0002, female TSPO +/+: p = 0.0002, female TSPO -/-: p = 0.0064). Statistical analysis was performed with two-way ANOVA with repeated measures (a-d) and three-way ANOVA (e). Data are expressed as mean ± standard error.

Key: High-fat diet (HFD); standard chow diet (SD).

In the 6th week of high-fat diet exposure, the mice were euthanised and their primary metabolic tissues were extracted for analysis. Immunohistochemistry was performed on the peri-gonadal white adipose tissue (WAT) to investigate TSPO expression and the presence of macrophages – using the macrophage marker F4/80. In WAT extracted from male mice, TSPO immunoreactivity was expressed throughout TSPO +/+ tissue and absent in WAT from TSPO -/- mice (Fig 5.2.1.6). A low level of background fluorescence is visible in the green channel in tissue of TSPO -/- mice captured at 63x, but not 20x, magnification (Fig 5.2.1.6c & d). TSPO was localised to F4/80-positive macrophages in WAT of TSPO +/+, but not TSPO -/-, mice (Fig 5.2.1.6b & d).The absence of TSPO had no influence on the weight of WAT in the male mouse cohort (Fig 5.2.1.7a; $p = 0.8421$). Image analysis of immunoreactivity in the WAT of male mice did not indicate that there were genotypic differences in adipocyte size (Fig 5.2.1.7b; $p = 0.7493$) nor the number of F4/80-positive macrophages identified in the tissue (Fig 5.2.1.7c; $p = 0.6182$).

Immunohistochemical staining of WAT dissected from female TSPO +/+ and -/- mice also exhibited TSPO immunoreactivity throughout the TSPO +/+ tissue (Fig 5.2.1.8a-b). TSPO staining was absent in tissue from the TSPO -/- mice, though auto-fluorescent was again visible in images taken at 63x magnification (Fig 5.2.1.8c-d). TSPO immunoreactivity co-localised with F4/80-positive macrophages in the TSPO +/+ tissue. The weight of the WAT dissected from female TSPO -/- mice did not differ from that taken from TSPO +/+ mice, although it did exhibit more variation between individuals (Fig 5.2.1.9a; $p = 0.1829$). Dissected WAT weight was also similar between sexes. There were no genotypic differences in average adipocyte size (Fig 5.2.1.9b; $p = 0.6867$) nor in the number of F4/80-positive cells (Fig 5.2.1.9c; $p = 0.1747$) per image within the female mouse cohort. The average adipocyte size was smaller in female mice compared to males, irrespective of genotype, while the average number of infiltrating F4/80-positive cells was similar in both cohorts.

The specificity of the secondary antibodies used in the WAT immunohistochemical analysis were assessed with the same procedure in absence of anti-TSPO and anti-F4/80. This was applied to WAT taken from female mice of the TSPO transgenic line that were fed standard chow (Fig 5.2.1.10). Any observable fluorescence was either auto-fluorescence within the

tissue or by non-specific binding of the secondary antibodies. Both TSPO-negative and F4/80-negative fluorescence was absent. Images were taken at 20x magnification only.

Histology was assessed in the liver tissue dissected from the high-fat fed TSPO +/+ and -/- mice. The purpose here was to investigate lipid droplet accumulation in the liver tissue, which occurs in diet-induced obesity. It was previously reported that 5-weeks treatment with the TSPO ligand, PK11195, protects against hepatic lipid accumulation in diet-induced obese mice (347). Haematoxylin and eosin (H&E) staining was applied to identify vacuolarised (non-stained) areas within the tissue, as a proxy for presence of lipid droplets. No differences in liver weight at time of dissection (Fig 5.2.1.11a; $p = 0.9021$) nor average vacuolarised space (Fig 5.2.1.11b; $p = 0.3286$) were observed between high-fat fed male TSPO +/+ and -/- mice. Representative images of the H&E stained liver sections from male TSPO +/+ (Fig 5.2.1.11c) and TSPO -/- (Fig 5.2.11d) mice were captured with light microscopy. There were no genotypic difference in the weights of liver tissue extracted from female TSPO +/+ and -/- mice (Fig 5.2.1.12a; $p = 0.3269$). Liver weights of the female cohort were slightly lower than that taken from the males, which likely reflects the lighter body weight of the female mice. No differences in average vacuolarised area were observed between the female TSPO +/+ and -/- mice (Fig 5.2.1.12b; $p = 0.7416$). Average vacuolarised area was also similar between the female and male mice, regardless of genotype. Representative images of H&E staining of the liver were taken by light microscopy from female TSPO +/+ (Fig 5.2.1.12c) and TSPO -/- (Fig 5.2.1.12d) mice.

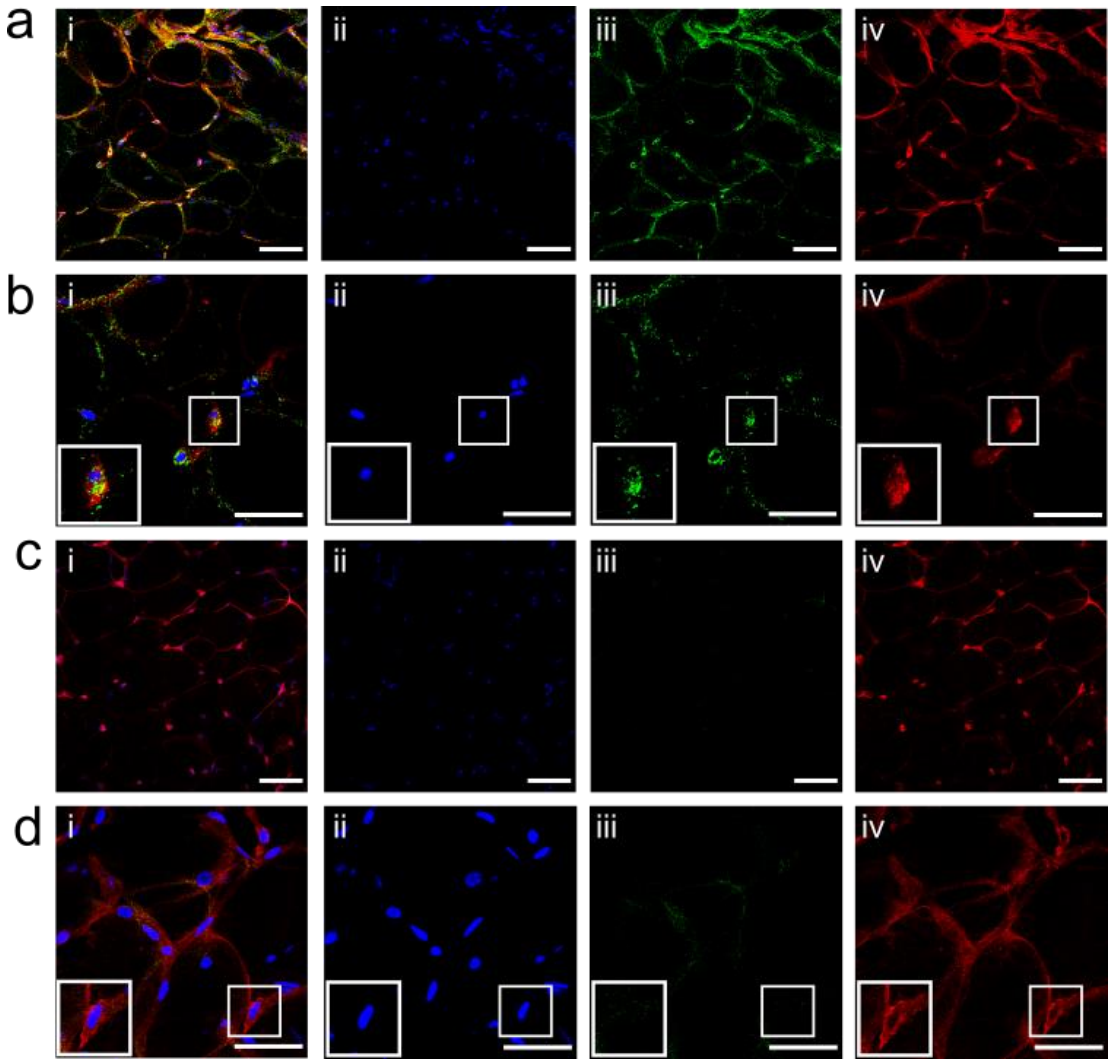

Figure 5.2.1.6 TSPO and F4/80 immunoreactivity in epididymal white adipose tissue taken from male TSPO +/+ and -/- mice fed high-fat diet.

A representative 20x magnification image of white-adipose tissue from a TSPO +/+ mouse (a-i) - depicting DAPI-positive nuclear staining (ii, blue), TSPO (iii, green) and F4/80 (iv, red) immunoreactivity. The same tissue is displayed at 63x magnification (b). Adipose tissue from a TSPO -/- mouse confirms absence of TSPO immunoreactivity, at 20x (c) and 63x (d) magnification. TSPO +/+ (b) and TSPO -/- (d) F4/80-positive macrophages are shown in digital zoom in the inset images. Scale bars represent 100 μm (a, c) and 50 μm (b, d).

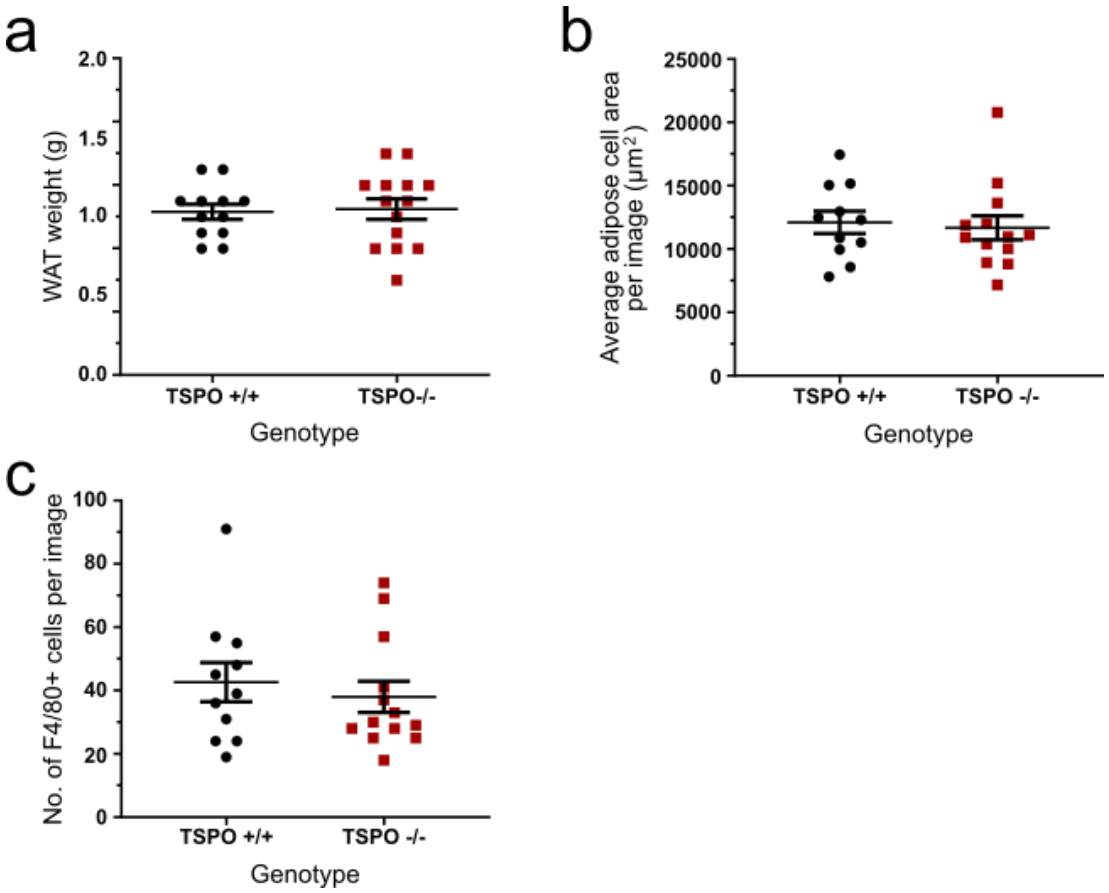

Figure 5.2.1.7 Absence of TSPO signalling did not impact adipocyte size or macrophage infiltration into epididymal white adipose tissue in high-fat fed male mice.

The weight of peri-gonadal white adipose tissue did not differ between high-fat fed male TSPO -/- and +/+ mice (a; p = 0.8421, n = 11-13). The average size of adipocyte captured by microscopic image was also not distinct between genotypes (b; p = 0.7493, n = 11-13). TSPO absence also had no genotypic effect on the number of F4/80-positive macrophages captured by image (c; p = 0.6182, n = 11-13). Statistical analysis assessed by Student's (a, b) and Mann Whitney unpaired t test (c). Data are expressed as mean ± standard error.

Key: White adipose tissue (WAT).

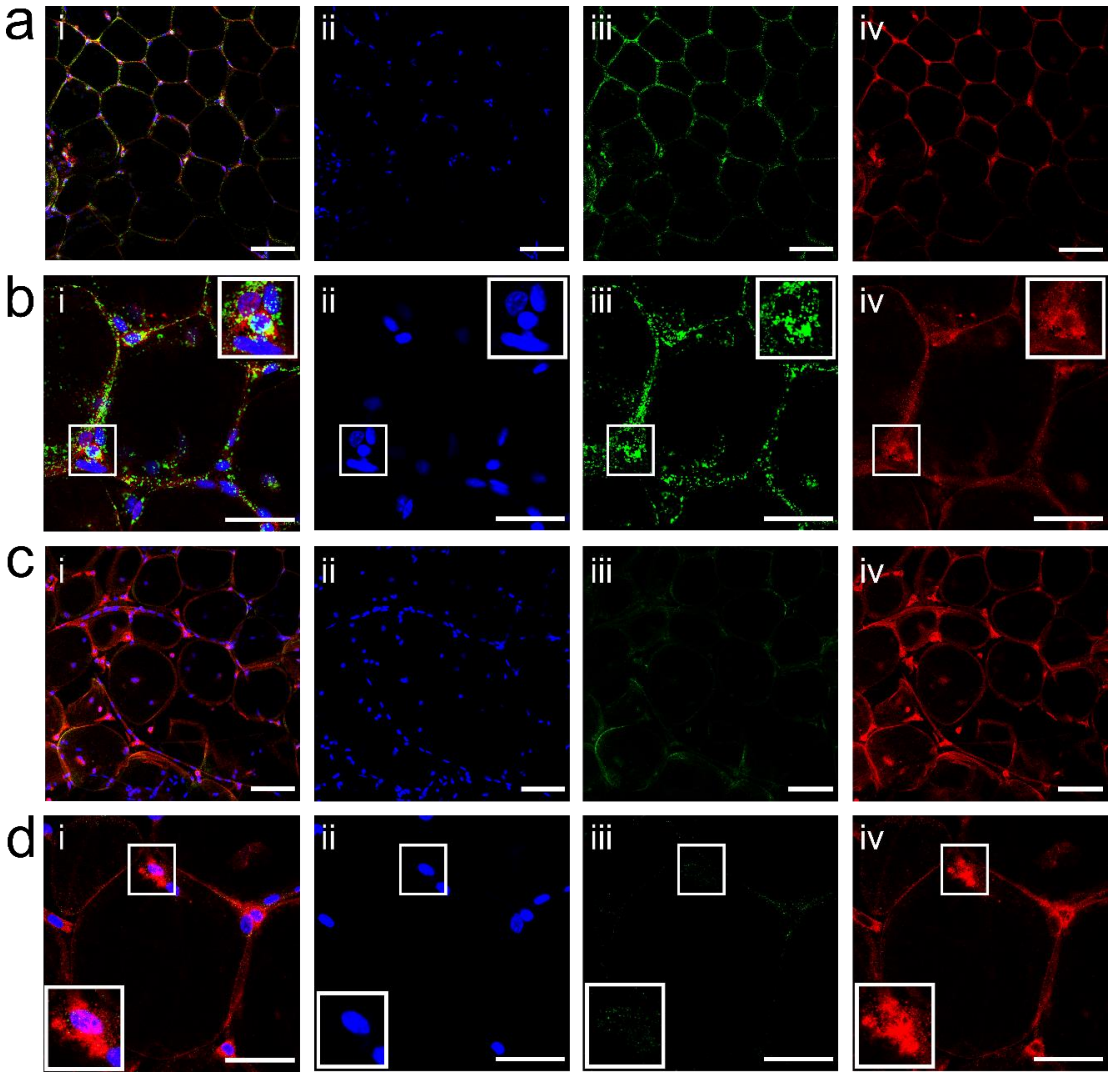

Figure 5.2.1.8 TSPO and F4/80 immunoreactivity in peri-gonadal white adipose tissue of female TSPO +/+ and -/- mice fed high-fat diet.

A representative 20x magnification image of white adipose tissue from a female TSPO +/+ mouse (a-i) - depicting DAPI-positive nuclear staining (ii, blue), TSPO (iii, green) and F4/80 (iv, red) immunoreactivity. The same tissue is displayed at 63x magnification (b). Adipose tissue from a TSPO -/- mouse confirms absence of TSPO immunoreactivity, at 20x (c) and 63x (d) magnification. Digital zoom images of TSPO +/+ (b) and TSPO -/- (d) F4/80-positive macrophages are shown in the insets. Scale bars represent 100 μm (a, c) and 50 μm (b, d).

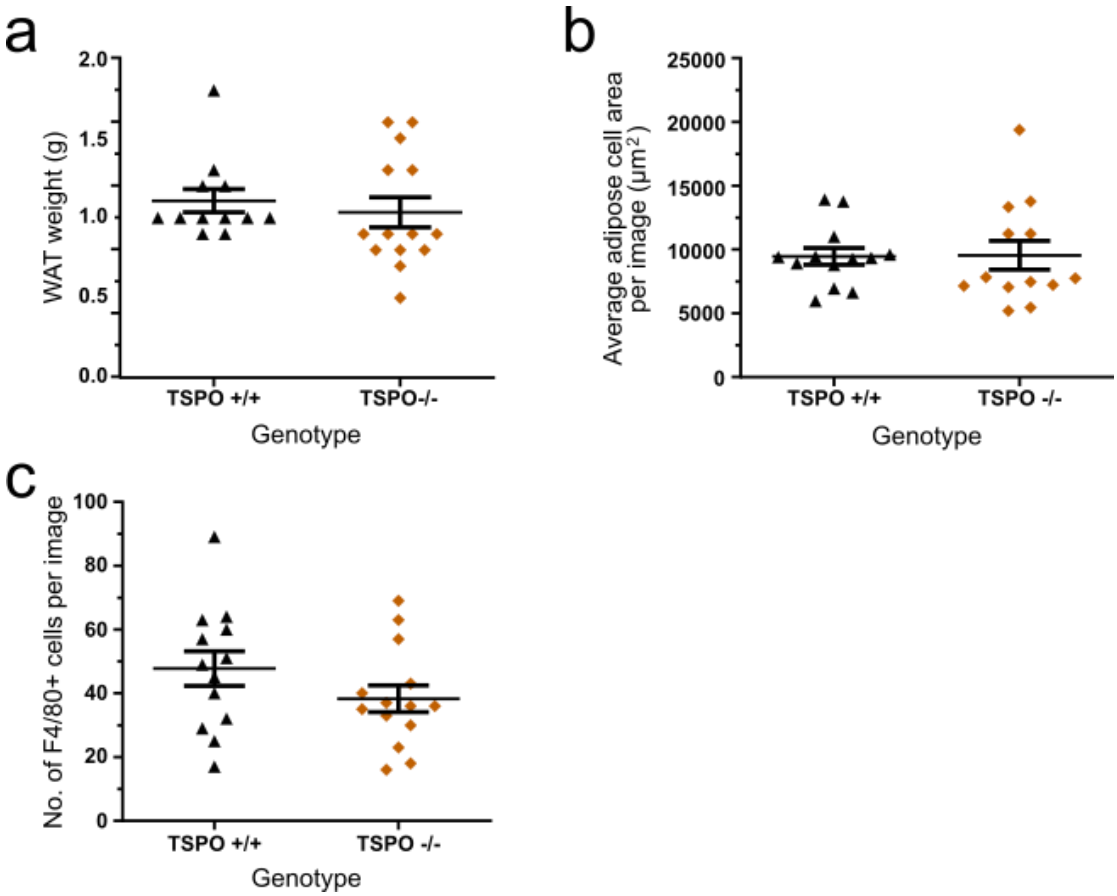

Figure 5.2.1.9 Absence of TSPO signalling did not impact adipocyte size or macrophage infiltration in the white adipose tissue of high-fat fed female mice. The weight of peri-gonadal white adipose tissue did not differ between high-fat fed female TSPO +/+ and -/- mice (a; $p = 0.1829$, n = 12-14). The average size of adipocyte captured by microscopic image was also no different between genotypes in female mice (b; $p = 0.6867$, n = 13). Female TSPO -/- also exhibited no difference on the number of F4/80-positive macrophages captured by image compared to TSPO +/+ controls (c; $p = 0.1747$, n = 13-14). Statistical analysis assessed by Mann Whitney test (a, b) and Student's unpaired t test (c). Data are expressed as mean ± standard error. Key: White adipose tissue (WAT).

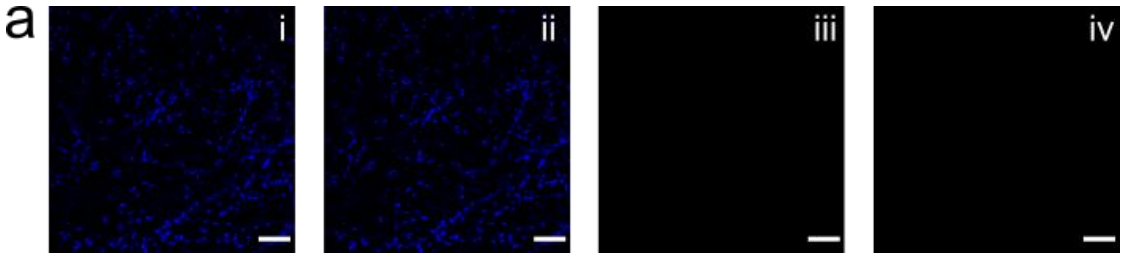

Figure 5.2.1.10 Non-specific immunoreactivity in peri-gonadal white adipose tissue of a female TSPO +/+ mouse.

An image of non-specific secondary antibody immunoreactivity in sub-cutaneous white adipose tissue, in absence of primary antibodies, taken from a female TSPO +/+ mouse (a-i). DAPI nuclear staining (ii, blue) is still applied and visible, while TSPO (iii, green) and F4/80 (iv, red) immunoreactivity is absent. Images captured at 20x magnification with scale bars representing 100 μm.

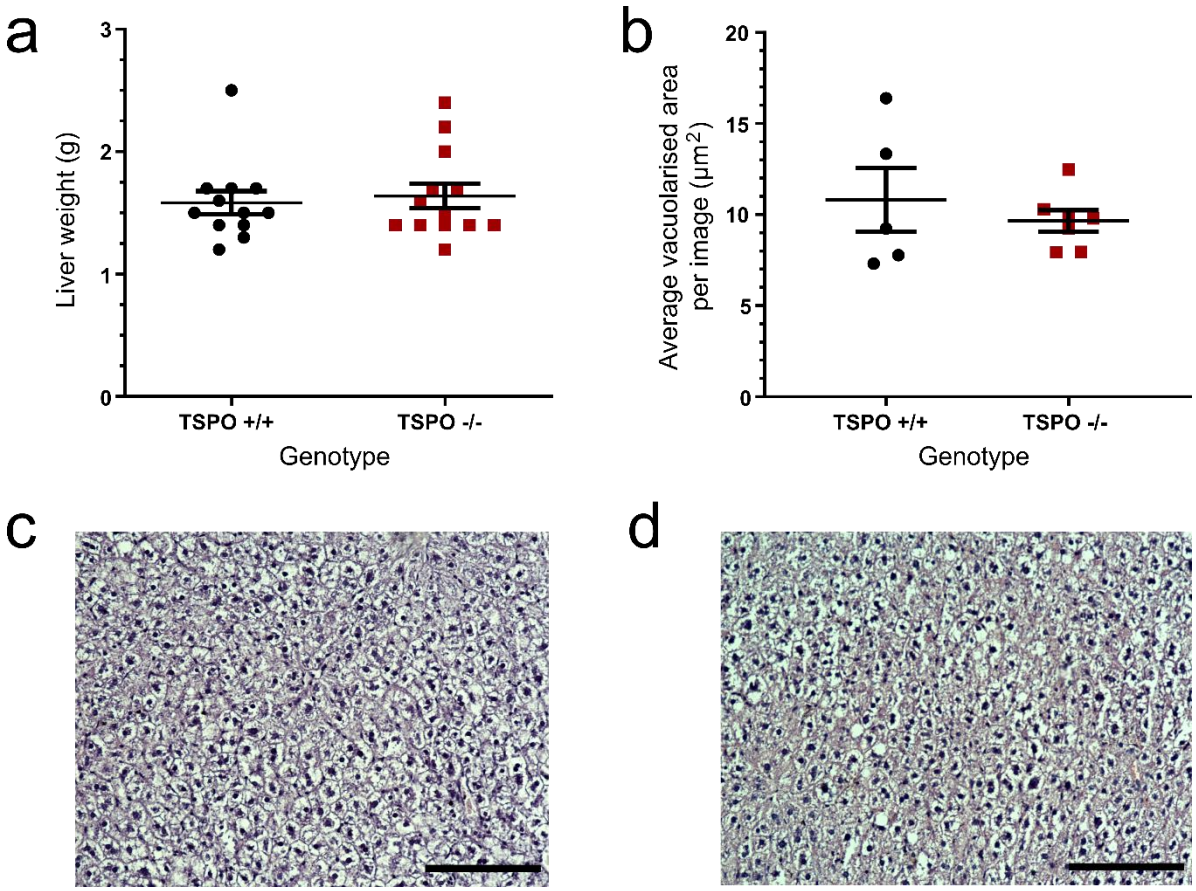

Figure 5.2.1.11 Male high-fat fed TSPO +/+ and TSPO -/- mice exhibited no differences in gross liver weight or histology were observed between.

There was no difference in liver tissue weight taken from male TSPO +/+ and TSPO -/- mice that were fed high-fat diet for 6 weeks (a; p = 0.9021, n = 12-13). The average vacuolarised area was not different between the genotypes (b; p = 0.3286, n = 6-7). Statistical analysis was performed using Mann Whitney (a) and Student's unpaired t test (b). Data are expressed as mean ± standard. Representative haematoxylin and eosin stained images of liver tissue from TSPO +/+ (c) and -/- (d) male mice, captured at 20x magnification. Scale bars represent 100 µm.

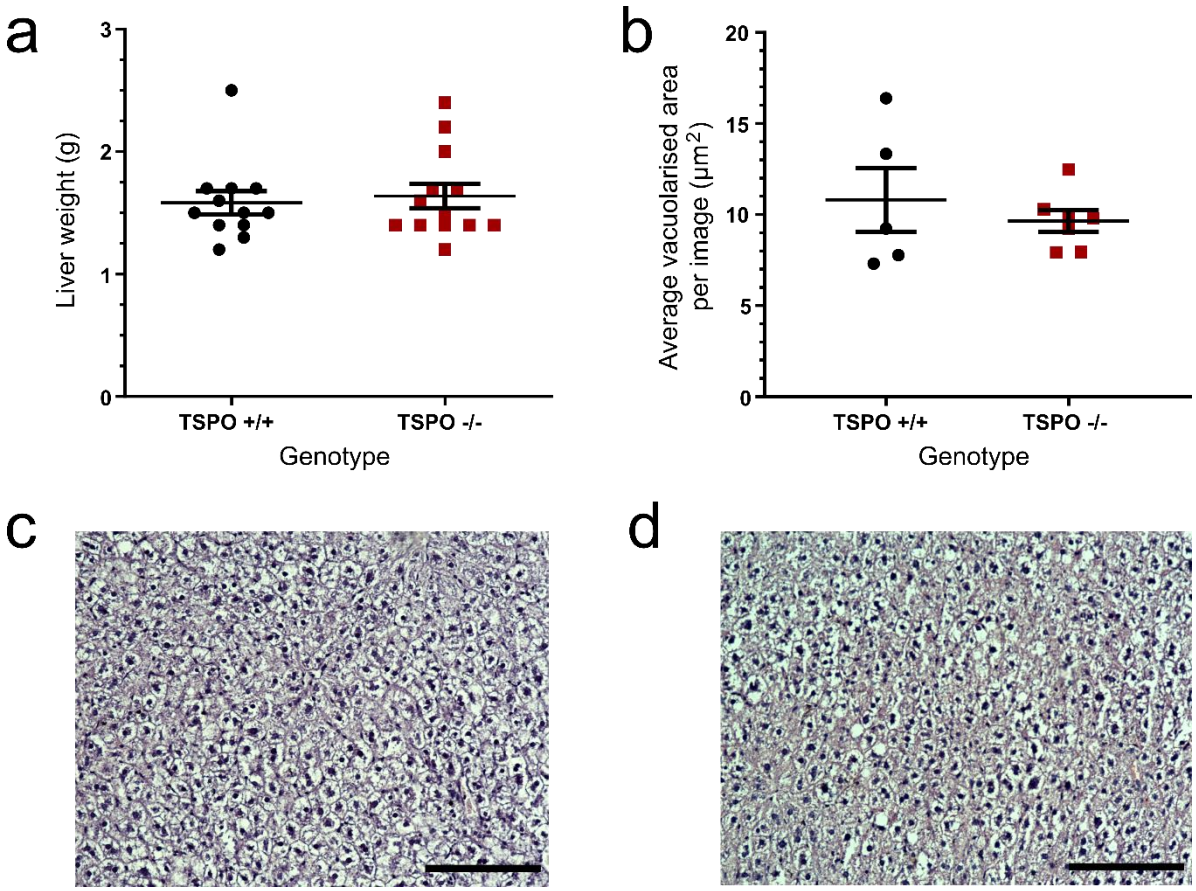

Figure 5.2.1.12 High-fat fed female TSPO +/+ and TSPO -/- mice exhibited no differences were observed in gross liver weight or histology from.

There were no differences in liver tissue weight taken from TSPO -/- mice compared to TSPO +/+ littermates following 6-week maintenance on high-fat diet (a; p = 0.3269, n = 13-14). The average vacuolarised area was not different between the genotypes (b; p = 0.7416, n = 6-7). Statistical analysis was performed using Student's unpaired t test. Data are expressed as mean ± standard error. Representative haematoxylin and eosin stained images of liver tissue structure from TSPO +/+ (c) and -/- (d) female mice, captured at 20x magnification. Scale bar represents 100 µm.

5.2.2 Investigating the effects of the TSPO ligand, PK11195, on feeding behaviour and analysis

To complement the studies in TSPO -/- mice, I assessed the effect of a well-studied TSPO ligand on energy homeostasis in a cohort of C57BL/6J mice. To first assess the impact of the drug on normal mouse feeding behaviour, two experimental protocols were performed. These consisted of measuring food intake in the nocturnal phase – when mice consume the majority of their daily energy intake - and at the beginning of the light phase when the mice are typically satiated and sleeping. Male and female mice were single-housed for at least a week prior to the experimental day. Intra-peritoneal administration of 1 mg/kg PK11195 had no impact on nocturnal (Fig 5.2.2.1a; p = 0.115) nor on satiated food intake in male mice (Fig 5.2.2.1b; p = 0.911). The same experiments were repeated in female C57BL/6J mice, where no effect of the ligand on nocturnal feeding was observed (Fig 5.2.2.1c; p = 0.1769). PK11195 treatment appeared to reduce food intake in the light phase, but this is likely a reflection of the scale of the graph axis and did not reach statistical significance (Fig 5.2.2.1d; p = 0.0602).

The same fast-induced refeeding protocol, that was applied to investigate the effect of negative energy balance in TSPO -/- mice, was repeated in C57BL/6J mice treated with PK11195. The published work prior to this experiment also used PK11195 at similar doses (347). Therefore, as well as accompanying the experiment performed in TSPO -/- mice, this portion of the study also acted to replicate previous findings. As with the TSPO -/- cohort, body weight prior to and after food deprivation was measured as well as post-fast food intake. Male and female mice were individually housed for at least one week prior to the experiment. The mice were food deprived for 12-hours, from onset of the dark phase, and treated with either 1 mg/kg PK11195 or vehicle as food was returned to the respective cages. Neither body weight change (Fig 5.2.2.2a-i; p = 0.3482) nor cumulative food intake (Fig 5.2.2.2a-ii; p = 0.1454) differed between the male mice administered 1 mg/kg PK11195 or vehicle. Although there was no impact of treatment on body weight change, the body weights of the PK11195-treated mice were slightly higher than that of the controls. Due to random allocation of the mice to the treatment group, this effect was likely due to chance. In the female mice, injection of 1 mg/kg PK11195 also had no influence on body weights (Fig

5.2.2.2b-i; p = 0.7726) or cumulative food intake (Fig 5.2.2.2b-ii; p = 0.2433). To determine whether the lack of any observed effect was related to the dose of the drug used, a greater dose of PK11195 at 5 mg/kg was given to an additional cohort of male mice. Change in body weights over the experiment were not influenced by PK11195 administration (Fig 5.2.2.2.c-i; p = 0.5993), as was the case with cumulative food intake (Fig 5.2.2.2c-ii; p = 0.2733). Here, the well-defined TSPO ligand PK11195 did not influence homeostatic feeding behaviour in response to a negative energy state.

As with the TSPO +/+ and -/- cohort of mice, glucose tolerance was also tested in male and female C57BL/6J mice treated with PK11195. However, in this study the protocol was only performed on standard chow fed mice and a small sample size that limited statistical analysis. In this experiment, mice received 5 mg/kg PK11195 or vehicle in the same intra-peritoneal injection as the bolus dose of 2 g/kg glucose used for the GTT. There was no observable effect of drug treatment on peak blood glucose levels in either male (Fig 5.2.2.3a) or female mice (Fig 5.2.2.3b). The response to the glucose tolerance test was not different in PK11195-treated male mice compared to vehicle (Fig 5.2.2.3a), nor in the female mice (Fig 5.2.2.3b).

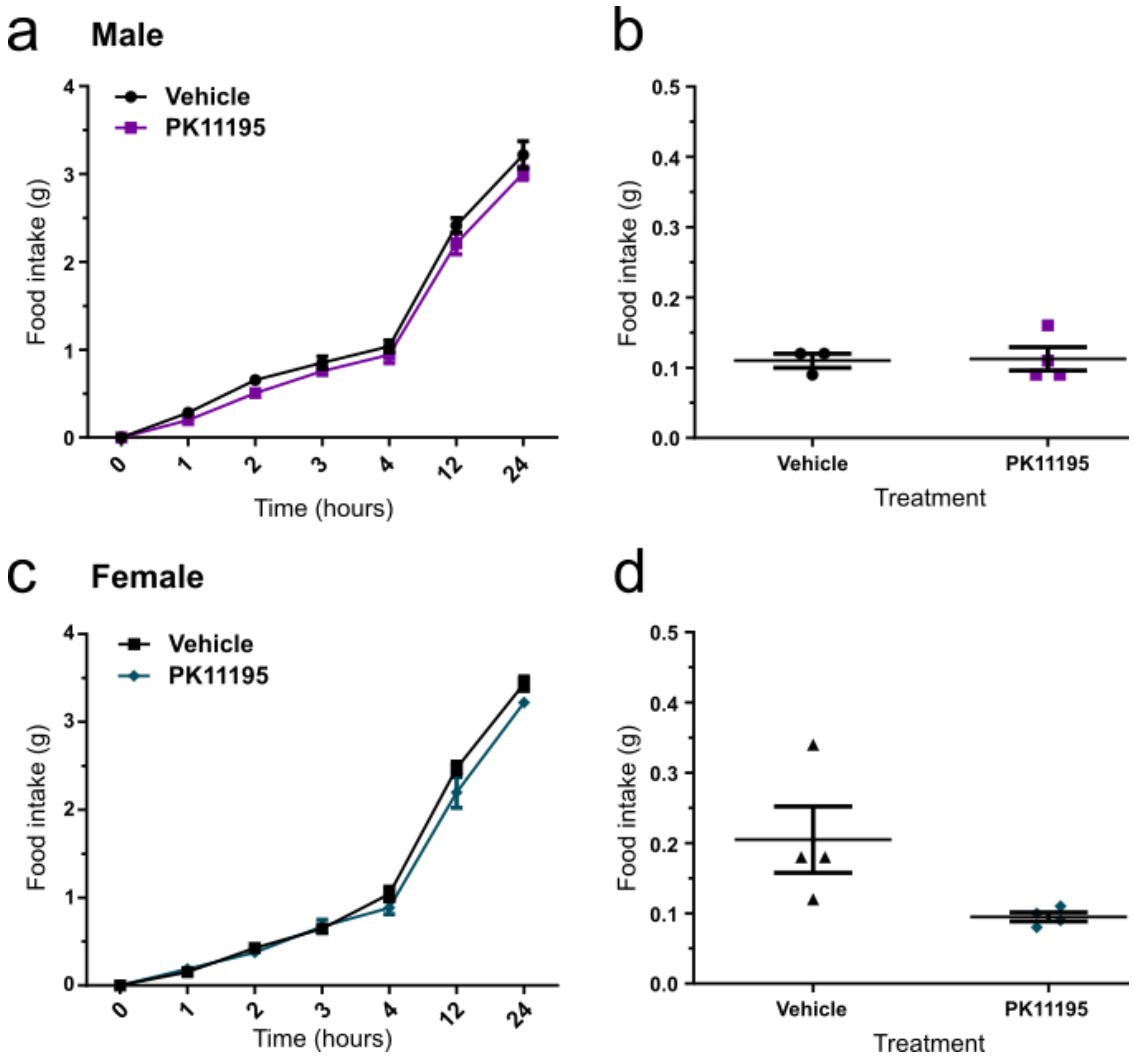

Figure 5.2.2.1 Pharmacological targeting of TSPO signalling did not disrupt normal feeding behaviour.

Male C57BL/6J mice, administered with 1 mg/kg PK11195 at the start of the dark phase, did not display altered nocturnal feeding compared to vehicle injected mice (a; Treatment: $p = 0.115$, $F_{1,8} = 3.127$; Interaction of treatment and time: $p = 0.6694$, $F_{6,48} = 0.6762$, n = 5). No difference in food intake was measured 90 minutes following intra-peritoneal injection of 1mg/kg PK11195 or vehicle at the start of the light phase in satiated male mice (b; $p = 0.911$, n = 3-4).There was also no effect of 1 mg/kg PK11195 administration in nocturnal feeding in female mice (c; Treatment: $p = 0.1769$, $F_{1,7} = 2.255$; Interaction of treatment and time: $p = 0.1102$, $F_{6,42} = 1.862$, n = 4-5). Injection of 1 mg/kg PK11195 at lights-on induced a slight, but not significant, reduction in food intake in female mice compared to vehicle-injected mice (d; $p = 0.0602$, n = 4). Statistical analysis was assessed by two-way ANOVA with repeated measures (a, c) and Student's unpaired t test (b, d). Data are expressed as mean ± standard error.

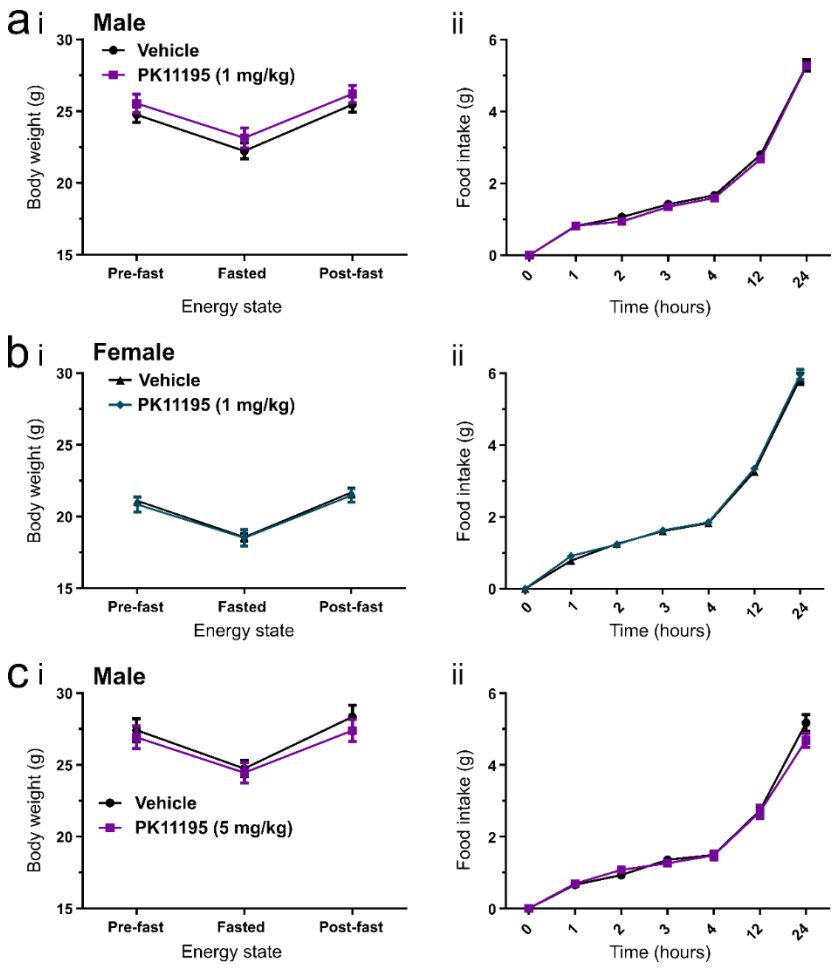

Figure 5.2.2.2 Pharmacological targeting of TSPO signalling did not impact the homeostatic response to acute food deprivation.

Intra-peritoneal injection of 1 mg/kg PK11195 in male C57BL/6J mice had no effect on the recovery of body weight after fasting (a-i; Treatment: p = 0.3484, $F_{1,25}$ = 0.914; Interaction of treatment and energy state: p = 0.6896, $F_{2,50}$ = 0.3743, n = 13-14). Cumulative post-fast re-feeding was also not affected by PK11195 treatment (a-ii; Treatment: p = 0.1454, $F_{1,175}$ = 2.139; Interaction of treatment and time: p = 0.941, $F_{6,175}$ = 0.2902, n = 13-14). There was no influence of 1mg/kg PK11195 on post-fast body weight recovery (b-i; Treatment: p = 0.7726, $F_{1,25}$ = 0.0853; Interaction of treatment and energy state: p = 0.4958, $F_{2,50}$ = 0.7115, n = 13-14) or re-feeding (b-ii; Treatment: p = 0.2433, $F_{1,245}$ = 1.368; Interaction of treatment and time: p = 0.9593, $F_{6,245}$ = 0.2493, n = 13-14) in female C57BL/6J mice. A dose of 5 mg/kg PK11195 in male mice also did not impact body weight regulation (c-i; Treatment: p = 0.5993, $F_{1,8}$ = 0.2992; Interaction of treatment and energy state: p = 0.1427, $F_{2,16}$ = 2.204, n = 5) or fast-induced refeeding (c-ii; Treatment: p = 0.2733, $F_{1,116}$ = 1.212, Interaction of treatment and time: p = 0.36, $F_{6,116}$ = 1.111, n = 5). Statistical analysis was performed using two-way ANOVA with repeated measures. Data are expressed as mean ± standard error.

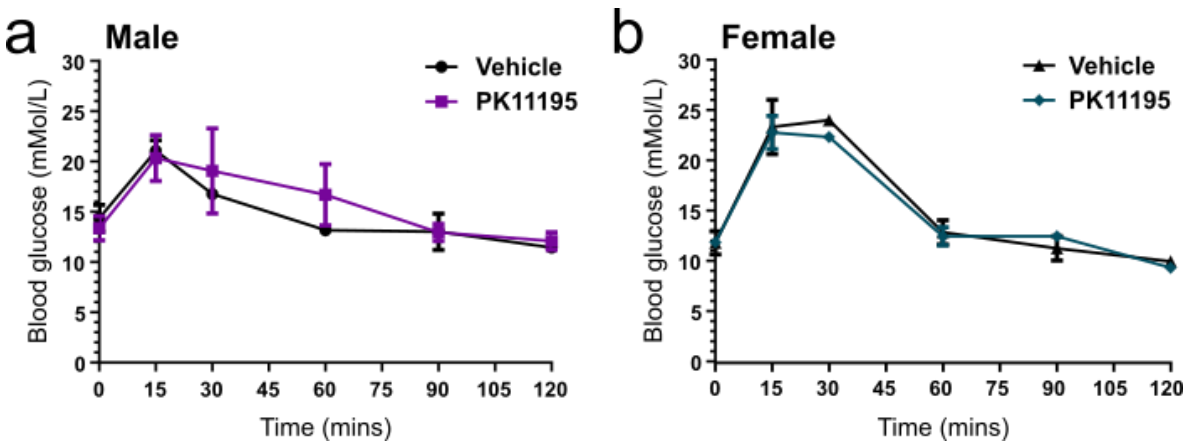

Figure 5.2.2.3 Administration of the TSPO ligand, PK11195 (5 mg/kg), did not affect glucose tolerance in male or female C57BL/6J mice.

There was no difference in blood glucose levels in either male (a; n = 2-3) or female (b; n = 2) C57BL/6J mice after intra-peritoneal administration of 5mg/kg PK11195 with 2 g/kg glucose, compared to vehicle-injected mice. Data are expressed as mean ± standard error.

5.3 Discussion

5.3.1 Summary of findings and contribution to the literature

The aim of the studies presented here was to characterise the whole-body metabolic response of TSPO -/- mice in response to deviations in energy balance. Previous research has examined the impact of loss of TSPO signalling on normal growth, but critically did not explore the potential effect of physiological challenge (325). Growth curves of TSPO -/- mice used in my studies did not deviate from that of TSPO +/+ mice, in both males and females. The data presented in this chapter confirms that of Banati *et al* (325), and complements the literature with measurements of weekly food intake. Furthermore, Banati *et al* reported no genotypic differences in basal blood glucose in either sex (325). The same observations were made in the study presented here, with additional measurements reflecting glucose tolerance in the animals when fed standard and high-fat chow. No influence of genotype was observed in either male or female mice, echoing the published work (325). Collectively these studies suggest that there is no role for TSPO in modulating normal body weight gain or blood glucose in male or female mice. I investigated whether there may be sex-specific functions for TSPO in female mice with regards to glucose handling, which would align with known sex-specific differences in metabolism (386–388,455), but my data supports the null hypothesis.

The series of experiments presented here indicate that there is no role of TSPO in the whole-body homeostatic regulation of energy balance, at least using the approaches employed. This is a remarkably consistent conclusion amongst what is quite a controversial literature (301,325,347,363,379). The phenotypic characterisation of germ-line TSPO -/- mice to deviations in energy balance had not been explored before, and so this study is an important contribution to the literature. These findings are distinct from the results of previous studies, which used cell-type specific knock-outs (301,362,363). Using a germ-line/whole body deletion may result in developmental adaptation/compensation that mask some of the effects of deleting the gene from specific cell-types. This can be bypassed in future studies by use of inducible knock-out models.

Glucose handling is sensitive to activity of the hypothalamic-pituitary-adrenal (HPA) axis, which is also a research area in which modulation of TSPO signalling

has been studied. A conditional TSPO -/- mouse line was recently generated where TSPO was deleted specifically from cells that produce steroidogenic factor 1 (SF-1) (363). Consequently, the steroid-producing organs of these mice – the gonads and the adrenals – had a modest reduction in *Tspo* gene expression (362). The male TSPO -/- mice of the cohort had significantly higher basal glucose in serum samples compared to the TSPO +/+ mice, while no differences were exhibited in the female mice (363). Linking this study with that of Banati *et al* (325) and the experiments presented above, it can be concluded that TSPO is not directly involved in mediating glucose homeostasis. However, there are likely downstream effects on blood glucose levels via TSPO absence in steroidogenic organs. This may also explain the sex differences in blood glucose of the SF-1 conditional TSPO -/- mice (363), which was not the case in my global TSPO -/- mouse line. The SF-1 TSPO -/- mice also have altered secretion of adrenaline and corticosterone (362,363), and adrenaline is known to raise blood glucose levels (456,457). The lack of an overall effect on glucose levels in the global TSPO -/- mice may be due to compensatory effects occurring across organs.

While this research project was ongoing, a conditional TSPO -/- mouse line - with manipulation specific to the β-tanycytes of the third ventricle (3V) - was published (191). Similar to the study presented here and in the Banati *et al* (325) paper, there were no differences in body weight and cumulative food intake between TSPO tanycytic -/- and TSPO +/+ mice. However, when the mice were placed on a high-fat diet for 4 weeks, the TSPO tanycytic -/- mice gained less body weight and had reduced food intake compared to controls (191). In my study, while the male TSPO -/- mice did eat slightly less high-fat chow than controls in the first seven days of dietary manipulation, the general trends I observed contradicted with that of the tanycytic TSPO -/- mouse line. Differences in high-fat diet composition and genetic background of the mice cannot explain the contrast in results, as diet composition between studies is very similar and genetic background is experimentally controlled. Furthermore, tanycyte-specific TSPO -/- mice also displayed no difference in glucose tolerance to that of TSPO +/+ mice even after high-fat diet exposure (191). This echoes that of the data described here in the global TSPO -/- mice. The β-tanycytes lie adjacent to the mediobasal hypothalamus (MBH), which contains the hypothalamic arcuate nucleus (Arc) and median eminence (ME). Consequently, any alteration in tanycytic function

would be immediately relayed to appetite and energy regulatory regions of the brain. Despite the tanycyte-specific TSPO -/- mice exhibiting subtle resistance to diet-induced obesity, the fact that they are not resistant to diet-induced glucose intolerance indicates a distinct role for TSPO in the tanycytes from the rest of the organism. This may be in nutrient sensing pertaining to fatty acids, but not glucose.

The feeding studies with global TSPO -/- were replicated with a pharmacological intervention of intra-peritoneal injection with the TSPO ligand PK11195. This ligand is thought to act to oppose TSPO function (319,458–462). While the findings were consistent within my studies, they did differ to recently published work that also used PK11195 (301). Intra-cerebroventricular administration of PK11195 to mice resulted in a reduction in body weight and food intake when the mice were fed either standard chow or high-fat diet (301). The route of treatment is likely responsible for the difference in effects; intra-cerebroventricular injection will primarily target the TSPO-expressing tanycytes of the 3V. As described above, genetic modulation of tanycytic TSPO influences feeding behaviour (301). Meanwhile, although PK11195 in the periphery can cross the blood-brain barrier (BBB), its primary target will be TSPO-expressing organs such as the liver and the adrenal glands. The doses of PK11195 used in these studies was also different. My studies presented in this chapter used a greater dose of 1-5 mg/kg PK11195 than Kim *et al* administered to experimental animals with 2 nMol (301). This is also lower than the dissociation constant of PK11195 at 2.4 nMol. This considering, the greater dose of PK11195 administered via the peritoneum is likely to target TSPO in a wider range of tissues than intra-cerebroventricular injection at a lower dose.

I also tested manipulation of TSPO-mediated signalling – through both genetic and pharmacological techniques – on recovery from negative energy balance. To date, no such research had been published. The reasoning behind these experiments followed those by Gut *et al,* who demonstrated an enhanced upregulation of gluconeogenic enzyme mRNA in fasted mice that were treated with PK11195 (347). In the study of Gut *et al*, intra-peritoneal PK11195 also lowered fasted glucose levels in the mice (347). Any impact on food intake in these mice were not reported, and so I anticipated that feeding behaviour would be reduced. I also sought to replicate the effect of PK11195 on fasted basal blood

glucose and extend these studies by performing intra-peritoneal glucose tolerance tests. My experiments involving the TSPO -/- and PK11195-treated mice did not reveal any effects on body weight, fast-induced refeeding or blood glucose levels. This may be explained by the duration of the fast; I exposed the mice to a 12-hour fast prior to refeeding and body weight measurements, which may not have been sufficient to induce hepatic gluconeogenesis. A 16- to 24-hour fast is substantial to induce gluconeogenesis in mice (463,464). However, in the study by Gut *et al*, the mice were fasted for 8 hours which was sufficient to see enhanced transcription of the gluconeogenic enzyme mRNA and 24 hours for reduction in blood glucose levels (347). In my glucose tolerance test, mice were only fasted for 6 hours during the day. This would have minimal impact on hepatic gluconeogenesis, as the mice would not typically consume much food during the day. Consequently, a prolonged fast duration may be required for effects of PK11195 on food intake and response to a bolus injection of glucose to be observed. Daily treatment with PK11195 for 4 weeks also alleviated glucose intolerance in diet-induced obese mice (347). No effect was observed in glucose levels during my TSPO -/- experiments of this chapter. In both studies - the PK11195 treatment by Gut *et al* (347) and my TSPO -/- experiment - the mice were fasted for 6 hours, and so it is possible that the different experimental approaches resulted in disparity between results.

As well as a role in metabolism, TSPO expression is upregulated in pro-inflammatory states of multiple cell types (227,286,290,291,310,350,353). High-fat feeding is associated with adipocyte expansion and macrophage infiltration into the WAT and lipid accumulation in the liver (3,57,64,66). Furthermore, increased TSPO expression in macrophages of WAT has been observed in obese mice compared to lean controls (310). In high-fat fed TSPO -/- mice, no phenotypic differences were observed in either the WAT or liver tissue compared to the TSPO +/+ mice in any of the parameters examined. These findings complement the absence of a genotypic effect on weight gain and glucose tolerance observed *in vivo.*

5.3.2 Limitations of the study

The studies presented in this chapter combined two experimental approaches to tackle the hypothesis that attenuation of TSPO-mediated signalling in mice will

alter their ability to maintain energy homeostasis. Comparison between the two approaches led to complementary findings: that systemic manipulation of TSPO-signalling does not influence energy homeostasis in mice. The respective strengths and weaknesses of each experimental approach must be critiqued in reference to this study.

The choice of mouse strain and its respective genetic background is important when comparing between studies that use more than one strain. The TSPO -/- mouse line used here was on the C57BL/6N subset, contrasting to the pharmacological studies that used mice on a 6J subset background. There are differences in metabolism identified between the N and the J subsets. In the case of the study presented here, both the genetic and pharmacological inhibition of TSPO signalling resulted in the same conclusions. In addition, appropriate controls were used in line with the difference in strain subset. Therefore, it is safe to assume that the differences in C57BL/6 mouse backgrounds used did not influence these results.

Global germ-line deletion of a gene can result in compensatory effects, as key proteins can exhibit genetic robustness (465). Compensation can occur at the transcriptional or signalling level. For example, in global TSPO -/- models there may be an upregulation of proteins with a similar function and/or distribution. Alternatively, proteins that are involved in the same signalling network as TSPO may increase their activity in response to its loss (466,467). Use of conditional and or inducible knock-outs can overcome these effects. Phenotypes resulting from global deletion of a gene can differ to the phenotype of conditional knock-out. For example, liver-specific deletion of sirtuin-1 (SIRT1) in mice leads to fatty liver while mice with global knock-out of SIRT1 exhibit healthy livers (468). A form of regulatory compensation is likely to have happened in the global TSPO -/- studies. This would explain the absence of a different response to high-fat feeding (reported in this chapter) compared with the subtle reduction in high-fat diet-induced weight gain following tanycytic-specific TSPO ablation (301), as well as the lower basal blood glucose levels in the SF-1 conditional TSPO -/- mice that was not observed with the global TSPO -/- model (363).

Observations resulting from pharmacological inhibition of a protein can be dose-dependent; an administration of excess drug could have off-target or toxic effects, while a too low dose may be insufficient to detect any impact. The dissociation

constant for PK11195 is 2.4 nMol. I used a dose (1-5 mg/kg) greater than the dissociation constant that was also in line with the experiments performed by Gut *et al* – which showed an effect of PK11195 on blood glucose levels (347). This dose is also compatible with other *in vivo* studies (233,281,292). Off-target effects have been seen in cell culture with treatment of 100 nMol PK11195 (283). Clearly, it is important to rely on not one technique with regards to TSPO function. My study here benefits from using genetic manipulation as well as pharmacological approaches.

Route of administration of pharmacological agents can also lead to variability in results. For example, an intra-cerebroventricular injection will directly target the brain and may not reach the periphery. Meanwhile, an intra-peritoneal dose will reach the liver; spleen; and GI system and – depending on the drug – may not pass the blood-brain barrier. PK11195 was injected to the peritoneum in my experiments. Peripheral injection of PK11195 can cross the blood-brain barrier, as demonstrated by PK11195-radioligand binding for use in positron emission tomography (PET) (289,469–471). However, the drug would primarily target TSPO expression in peripheral organs such as the liver and adrenal glands. The integration of two or more experimental approaches, with critique and comparison of results, aims to bypass these listed problems and motivated the experimental design used for the experiments described in this chapter.

5.3.3 Future perspectives and outstanding questions

As covered in the limitations of this study above, some of the experiments described here would benefit from replication. For example, due to the potential off-target effects of PK11195 it would be insightful to repeat these experiments with another TSPO ligand. Conversely, it would also be useful to consider the impact of treatment with a ligand that is considered to enhance TSPO function, and whether it shows the anticipated effects based on the literature. TSPO pharmacology is an ever-developing aspect of the field, and crucial to approach TSPO experiments with the most appropriate ligand.

There was data that was not included in this thesis, as analysis could not be sufficiently completed due to lockdown restrictions of the Covid-19 pandemic. These were to assess the same histological markers in liver and WAT tissue of

female TSPO +/+ and -/- mice which were maintained on standard chow. Since these experiments, data has been published from another group that shows lower lipid accumulation in liver tissue from standard chow-fed TSPO -/- mice compared to control (379). If replicable, then this suggests a role for TSPO in hepatic fatty acid metabolism outside of energy homeostasis.

To unravel the role of TSPO across the organism, additional conditional knock-out lines could reveal TSPO function pertaining to that specific tissue. Knock-down of TSPO in hepatic cells could confirm a role of TSPO in glucose homeostasis at the level of the liver. In addition, the generation of inducible global TSPO -/- animal models may avoid any compensatory developmental effects. Regardless of model used, it is important to consider the results in accordance to what has been reported in the literature from other knock-out animals. TSPO is expressed throughout the body, and this should be appreciated accordingly.

My studies presented in this chapter also leave questions for further investigation. For instance, to connect the published data from the SF-1-dependent TSPO -/- mice with that presented here (363), it would be of interest to measure the circulating levels of adrenaline in the global TSPO -/- mice. This would provide insight as to whether the effect of SF-1 TSPO -/- is maintained in the global TSPO -/- model. One of the actions of adrenaline is to enhance hepatic glucose production by gluconeogenesis (472,473). If adrenaline is higher in global TSPO -/- mice, then the action of adrenaline in the liver may have negated the effect of absent hepatic TSPO expression on lowering glucose production. Considering that SF-1 TSPO -/- also had differential effects on production of other steroid hormones – including sex-associated steroids – this sex-dependent influence may also be present and effective in the global TSPO -/- mice (135,386,387,474,475). A repeat comparison of glucose tolerance in male and female TSPO -/- mice would also benefit from increased power.

In conclusion, this study combines genetic and pharmacological approaches to demonstrate that absence of TSPO signalling does not result in an altered response to energy imbalance. TSPO -/- mice were not protected against the negative consequences of diet-induced obesity in comparison to TSPO +/+ controls, nor did they display altered feeding in response to food deprivation.

These data were complemented with pharmacological targeting of TSPO in lean mice. The results observed here contrast with published findings from conditional TSPO -/- models (301,362,363,379). Therefore, this study provides novel insight to the importance of experimental approach to study TSPO function. It is likely that TSPO function differs between organs and that global inhibition results in compensatory responses.

Chapter 6: General Discussion

6.1 Summary of findings and contribution to the literature

The hypothesis underlying this project was that the mitochondrial translocator protein of 18 kDa (TSPO) is involved in cellular metabolic flexibility, and could be manipulated to influence energy homeostasis. Metabolic flexibility is crucial for function of certain cell types, such as immune-associated cells. In these cells, the transition in inflammatory states occurs alongside a shift in substrate utilization (476–481). Furthermore, nutrients for energy production - such as saturated fatty acids (SFAs) – may themselves trigger an inflammatory response (123,125,180,367,427,482). TSPO is implicated in both mitochondrial metabolism and pro-inflammatory phenotypes in different cell types (227,281,286,291,297,298,301,303,311,319,324,327,330,342,350,453,483). Henceforth, I investigated whether TSPO is involved in regulation in energy balance in the whole organism.

6.1.1 Distribution of TSPO immunoreactivity in the healthy mouse brain

The first study (Chapter 3) investigated the distribution of TSPO expression in the mouse brain, along with it its cellular localisation. This was important to investigate since TSPO upregulation in the brain is commonly used as a biomarker for neuroinflammation, both in research and the clinical setting (227,248,273,277,278,288,289,293,300,312,325,369,385,437,439,441,484–495). Still, the distribution of TSPO in the healthy brain is relatively unknown (294,300,301,303). I observed and semi-quantified dense TSPO immunoreactivity in multiple brain regions, in the male and female mouse, that are known to be involved in energy homeostasis. However, upon comparison to brain sections taken from TSPO knock-out (-/-) mice, I confirmed the dense immunoreactivity was not specific for TSPO. The antigen for the off-target binding was unable to be identified due to being proprietary of Abcam. However, it appeared to colocalise with markers of neuroendocrine neurons such as

thyrotropin-releasing hormone (TRH). Intense immunoreactivity within the walls of the ventricles was suspected to be specific for TSPO, as it was absent in the TSPO -/- brain tissue. Following dual immunohistochemical analysis, this immunoreactivity colocalised with vimentin – a tanycytic marker. The low level of immunoreactivity throughout the brain was also absent in the TSPO -/- tissue.

This study identified TSPO expression within tanycytes and ependymal cells of the brain ventricles, and provided evidence against the brain tissue specificity of a commonly used antibody against TSPO. This has implications for the extent of TSPO expression in healthy and diseased mouse brain tissue, as previously published research on this topic has relied on this particular antibody (296,306,322,325,362,369,379,420,496–511). While I confirmed that the antibody selectively binds to TSPO in mouse white adipose tissue (WAT) – and my colleagues confirmed specificity in cultured glia – we cannot rule out that there may be non-specific binding in other tissues and in other species. Furthermore, although I could not identify the antigen that causes the non-specific binding, it is possible that it is a protein structurally related to TSPO – such as TSPO-2 (422) or TSPO associated protein (424) – and remains of interest to research on hypothalamic control of energy balance.

6.1.2 Regulation of hypothalamic TSPO by energy balance

The second study of this thesis (Chapter 4) explored regulation of neural TSPO expression by energy state, alongside that of an astrocyte marker to confirm the presence of reactive gliosis. These experiments were conducted prior to the knowledge that the TSPO antibody lacked specificity in the mouse brain. Two methodologies were used, immunohistochemistry and Western blot, to provide both quantitative and qualitative measures.

Western blot analysis identified downregulation of TSPO protein level in the dorsomedial hypothalamic nucleus (DMH) of high-fat fed male mice. Assessment of GFAP protein levels by densitometry confirmed presence of diet-induced changes in astrocyte number or morphology. This was also observed in high energy state and localised to the arcuate hypothalamic nucleus (Arc) of the mice. There are very few studies that report dietary regulation of TSPO – and none have considered negative energy balance (310,369,439,441). Published works

also focus largely on TSPO expression in hippocampal and cortical regions of the brain, not the hypothalamus.

The downregulation of TSPO in positive energy states complements findings which indicate that knock-out of TSPO enhances fatty acid oxidation (FAO) and lipid catabolism (301,330) in cells. Following acute high-fat feeding, circulating fatty acids (FAs) would be elevated and so cells may respond with a shift in substrate utilisation from glucose to FAs. Therefore, expression of TSPO may be important for mitochondrial metabolic flexibility. Since TSPO is not expressed in all cells or tissues, if true, expression may be specific to cells that require such flexibility – such as inflammatory cells.

This study also provided additional evidence that hypothalamic astrogliosis can also occur in response to an acute fast. This has been previously demonstrated, but with few published studies to confirm the findings (202). It at first seems paradoxical in relation to similar observations from animals fed a high-fat diet (125,174,180), given that one state represents an excess of energy availability and the other insufficient energy. However, both energy states can involve circulating levels of pro-inflammatory SFAs to increase (187). Furthermore, reactive gliosis is a response to a range of different stimuli so there may be multiple factors involved.

The results from the immunohistochemical analysis of GFAP expression in diet-induced obese mice in this study did not reflect what has been reported in the literature (125,222). The mice were exposed to high-fat chow for 3 months and gained substantial weight compared to the control mice, so this discrepancy in the findings was surprising. However, considering the bimodal response of inflammation to chronic high-fat diet (125), this points to the importance of exposure time and age of the animals in studies such as these.

Considering the results and conclusions from this study, I propose that TSPO downregulation in the hypothalamus may be indicative of a role in mediating metabolic flexibility. Bearing in mind the non-specific immunolabelling of the antibody, the downregulation in the DMH may relate to a distinct but related protein. However, a report published since my studies were conducted has also identified a role for TSPO in tanycytic lipid metabolism at the 3V (301). In addition, glial physiology is dynamic and responsive to a range of factors – including

inflammatory stimuli, energy excess, and energy deprivation. Consequently, assessing gliosis in the setting of energy homeostasis requires control for or consideration to extraneous variables that can influence reactive gliosis.

6.1.3 Inhibition of TSPO-mediated signalling

The final part of this project (Chapter 5) looked to characterise the metabolic phenotype of mice with germ-line deletion of TSPO or pharmacological modulation of TSPO activity – including in response to both positive and negative energy states. This study, at the time of writing, was a novel and important contribution to the literature. The absence of differences in food intake, body weight, and blood glucose of TSPO +/+ and -/- mice when fed standard chow has been described previously (325). My work confirmed this, as well as providing new information regarding the physiological response to different levels of energy availability.

Absence of TSPO in mice with germ-line deletions did not alter body weight or feeding behaviour of mice exposed to acute food deprivation, or to acute and chronic high-fat feeding. This was replicated in mice that received an intra-peritoneal injection of the TSPO ligand, PK11195. Since I conducted these experiments, a paper was published demonstrating that both conditional TSPO -/- in tanycytes and intra-cerebroventricular injection of PK11195 in the 3V subtly reduced food intake and body weight of diet-induced obese mice (301). This is an interesting difference to my data described here, which is likely explained by the types of animal models. While administration of PK11195 to the periphery - such as intra-peritoneal injection, as in my study - can enter the brain, multiple organs will be impacted including the liver, adrenals and gonads. Injection of PK11195 to the 3V is unlikely to affect these organs, and predominantly target the surrounding hypothalamic nuclei and other peri-ventricular brain regions. Kim *et al* also specifically knocked-out TSPO expression in the tanycytes adjacent to the MBH, which replicated their results from PK11195 treatment (301). I did not observe this in the global TSPO -/- mice, presumably due to compensatory effects not present in the tanycyte specific TSPO -/- model.

In the study by Kim *et al* (301), glucose tolerance was not altered by tanycytic-specific TSPO -/- or PK11195 treatment which – despite the difference in

methodologies - is consistent with the findings in my project. However, in a different study intra-peritoneal PK11195 reduces basal blood glucose in acute fasted mice and sub-cutaneous PK11195 improves glucose tolerance with repeated treatment in diet-induced obese mice (347). Furthermore, knock-out of TSPO in the adrenal cortex of mice induces hyperglycaemia (363). These studies suggest tissue-specific differences in TSPO function, which could explain an absence of effect in global TSPO -/- mice.

I propose that TSPO function is tissue-specific, and this explains the discrepancy amongst the literature regarding its role in mitochondrial function. Consequently, with current technology the action of TSPO can only be studied in a snapshot. A global TSPO -/- model or peripheral administrations of ligands will target the different actions across the expressing tissues. Meanwhile, to distinguish the role of TSPO in different tissues, conditional knock-outs or localised drug administration will only highlight the roles of TSPO in the targeted tissues. A combination of and comparison between the above approaches will provide informed insight to the function of TSPO.

6.2 Technical limitations of the study

6.2.1 Limitations of immunolabelling methods

There are a number of advantages, as well as limitations, to immunohistochemical processing to examine protein expression. This was used in Chapter 3 to characterise the expression distribution of TSPO in the mouse brain. The limitations of this approach became apparent with use of the TSPO antibody in brain tissue from TSPO -/- mice, as I found that the antibody had off-target binding in the brain that had not been previously documented nor published. Consequently, this part of the project emphasised the need to validate use of antibodies independent of the supplier. Validation should be performed with the proposed technique and protocol for experimental use, using samples from an appropriate knock-out animal or cell-line or one with knock-down expression. In addition, tissue that is known to not express the protein of interest can be used as a negative control. For my studies, brain TSPO distribution could

also have be assessed/confirmed through a slice radioligand autoradiography binding study, although this method has limitations on its sensitivity.

Immunohistochemistry was also applied to investigate colocalisation of protein expression markers to indicate co-expression. Confocal microscopy was applied here in order to discern between apposition and colocalisation. This is not a confirmative method, and use of more powerful tools such as electron microscopy can provide more conclusive evidence.

Immunohistochemical labelling of astrocytes was used to assess astrogliosis in the hypothalamus of diet manipulated mice. This is a useful approach, in this scenario, to measure the number of astrocytes alongside the ramification of their morphology and could not be achieved by other methods. However, while GFAP is a common marker, heterogeneity amongst astrocytes has been identified and GFAP is not a universal marker of all astrocytes (512–514).

Western blot densitometry analysis provides more reliable quantification than fluorescent immunohistochemistry. However, quantification is only reflective of the sample processed and does not provide additional detail such as morphology or location. I used micropunch dissection to target specific hypothalamic nuclei. However, this can lead to subtle variability in the precise regions captured between animals. While Western blot can provide an accurate representation of quantitative protein expression, the multiple steps required for sample processing can lead to variation in the results.

6.2.2 Contrasts between animal models

This project used multiple mouse strains and models, each with their own limitations. As discussed previously, both the 6N and the 6J sub-strain of C57BL/6 mouse were used – which have different phenotypes with regards to metabolism. This was appropriately controlled for within my experiments. However, since the 6J sub-strain is more prone to diet-induced obesity than the 6N (371–373), generation of the global TSPO -/- mice on a 6J background might have yielded different results.

There were also differences in the results obtained in this project compared to those published with regards to PK11195 manipulation. While PK11195 can cross the blood-brain barrier (BBB), intra-peritoneal administration of PK11195

may not enter the brain and be sequestered instead by the dense TSPO expression in peripheral organs. This could explain the differences in my results compared to intra-cerebroventricular injection of PK11195 (301). Furthermore, *in vitro* studies have suggested that PK11195 has off-target effects and that its action at TSPO could be concentration-dependent (283). In this study, in which progesterone secretion was measured from MA-10 Leydig cells with and without TSPO expression, the dose of PK11195 that gave off-target effects was much lower than its dissociation constant. In my experiments of this project I used a much higher dose of PK11195 than these in vitro studies, which reflects other *in vivo* work with PK11195 (347). The pharmacology, and route of entry, of a ligand are important considerations and can introduce variability when attempting to reproduce previous conclusions.

Discrepancies in results obtained were found when comparing the global TSPO -/- mice of this study to those that used cell-specific knock-out models. The global TSPO -/- mice were generated by a germline deletion, which can result in compensatory effects during development. These could be avoided in future studies by the generation of mice with a global inducible TSPO deletion. For example, tamoxifen-inducible Cre-recombinase generated mouse models can allow for global and cell-type specific deletion of TSPO expression without developmental compensation. Injection of viral vectors expressing Cre-recombinase also enable site-specific knock-out.

6.3 Future perspectives & outstanding questions

TSPO expression and distribution in the healthy brain is still unconfirmed. It appears to be widespread at a low level, but particularly strong in some circumventricular regions as well as in the ventricle walls. Nonetheless, considering the lack of antibody-antigen binding specificity in these studies, these data would benefit replication via additional techniques such as radioligand binding and/or *in situ* hybridisation. Electron microscopy could also confirm colocalisation of TSPO in tanycytes as well as astrocytes and microglia. To clarify regulation of TSPO by energy balance in tanycytes, Western blot analysis does

not have the spatial resolution but quantitative data could be acquired from *in situ* hybridisation.

In these studies, the effect of modulation of TSPO-mediated activity on food deprivation and re-feeding was investigated. This was due to previous reports suggesting that hepatic gluconeogenic enzymes regulated by fasting are upregulated following PK11195 treatment (347). The same study demonstrated a PK11195-induced decrease in fasted basal blood glucose. I did not replicate this effect of PK11195 on either blood glucose levels or demonstrate an effect on fast-induced food intake, which may be due to differences in length of food deprivation used. Therefore, confirmatory measurement of the same gluconeogenic enzyme mRNA levels by quantitative PCR (qPCR) in PK11195-treated mice fasted for the shorter duration would provide further evidence of a potential function of TSPO in the liver and regulation of hepatic glucose production.

Global deletion of TSPO had no impact on mouse bodyweight or food intake when maintained on standard chow, but there may be differences in the structure of TSPO-expressing metabolic tissue. Recently, observations in another global TSPO -/- mouse strain were published which indicated a reduction in lipid droplets in the liver tissue of these mice maintained on standard chow (379). Whether a similar effect is seen in our TSPO -/- mice is yet to be shown.

TSPO is strongly expressed in the liver and adrenal glands, which are both key influencers of energy homeostasis. Cell-specific knock-out of TSPO in the adrenal cortex results in elevated adrenaline production, which may explain the elevated basal blood glucose levels in these mice (362,363). Adrenaline induces glucose production via hepatic gluconeogenesis (472,473). Conversely, treatment with the TSPO ligand PK11195 lowers blood glucose levels (347). The effects on hepatic glucose production from these two studies are contradictory, and this may explain the absence of any effect in the global TSPO -/- mice. Measurement of blood adrenaline levels in the global TSPO -/- mice could potentially discriminate the role of TSPO in these two organs. Furthermore, measurement of hepatic gluconeogenic enzymes from global TSPO -/- mouse tissue would elude to whether the absence of TSPO influences blood glucose and enzyme expression despite potential elevated adrenaline levels. Generation and characterisation of additional conditional and inducible TSPO -/- mice, in

comparison to the global TSPO -/- mouse line, will also provide insight to the differential roles of TSPO within different tissue types.

6.4 Conclusions of the study

The conclusion of this research project is that the function of TSPO is tissue-dependent (Fig 6.4.1). For example, in immune cells such as glia TSPO may be involved in mediating metabolic flexibility (286,310,318,324,326,484). This would then explain TSPO regulation in reactive gliosis (227,228,286), and also its potential downregulation in positive energy states within the hypothalamus (as reported in Chapter 4). Tissue-dependent function would result in a wide range of effects within the organism if pharmacologically targeted, including an overall null outcome from compensating actions in different tissues. Adrenal TSPO is involved in steroidogenesis (362,363) while hepatic TSPO regulates glucose homeostasis (347). These tissues have downstream effects on other functions – such as adrenal steroidogenesis impacting blood glucose – which complicates interpretation of the effects of TSPO manipulation. In addition, TSPO is unlikely to be an appropriate target for translational use clinically.

As well as providing information regarding TSPO function, these studies provide new insight into limitations of experimental approaches to investigate TSPO. I propose that the function of TSPO is flexible and dependent on the dynamic environment in which it is expressed. Multiple endogenous ligands are shown to bind to TSPO (235,244,317), and so this likely influences its activity in response to the respective levels of such ligands in TSPO-expressing cells. Furthermore, mitochondria are also highly dynamic (194,515,516) and TSPO forms complexes with other mitochondrial proteins (517–519) – which are likely to show tissue-dependent expression, such as the case with StAR (365,520,521). The access of the tissue to such ligands, and the tissue expression profile of mitochondrial proteins, may influence TSPO activity in a cell-type specific manner through tissue-specific binding or mitochondrial complex formation. This would explain the number of discrepancies within the TSPO literature regarding its function and ligand specificity in different cell types.

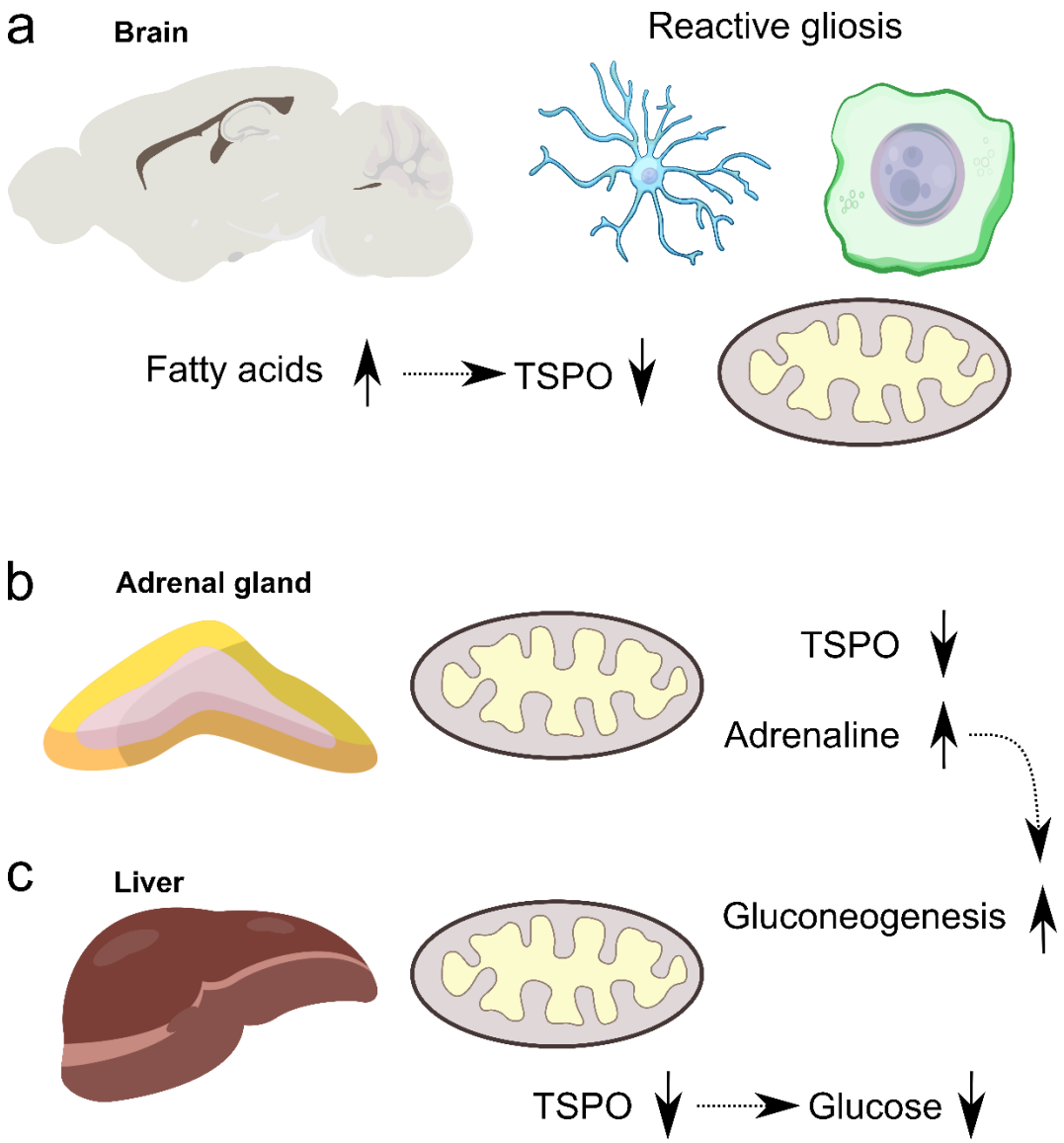

Figure 6.4.1 Visual summary of proposed TSPO function.

TSPO regulation in glia may reflect metabolic flexibility. Reactive glia utilise different energy sources compared to when in the resting state. Regulation of TSPO in relation to reactive gliosis may reflect this change in energy substrate preference (a). Reduction or absence of TSPO in the adrenal gland increases adrenaline secretion (b), which may in turn enhance gluconeogenesis in the liver (c). However, downregulation or knock-out of TSPO in the liver may reduce glucose production (c) – counteracting any changes in glucose homeostasis. Organ images are adapted from SciDraw (67).

Appendix

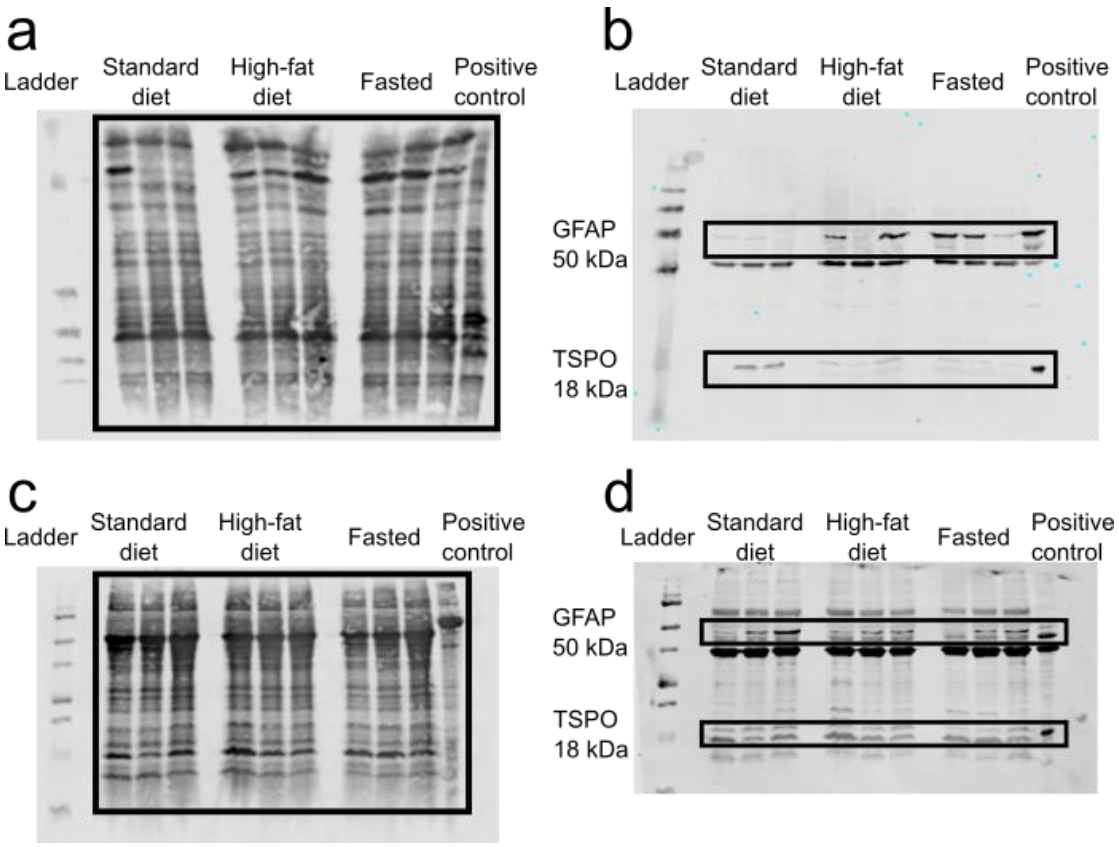

Appendix 1. Full representative immunoblots that were processed with anti-TSPO and anti-GFAP for semi-quantification of diet-induced regulation.

Blot showing total protein stain alongside ladder, of samples taken from the ventral portion of the hypothalamus of mice exposed overnight to high-fat chow or food deprivation or standard chow control (a). The same blot, but after total protein stain was washed off and instead probed with anti-GFAP and anti-TSPO (b). Blot showing total protein stain alongside ladder, of samples taken from the dorsomedial hypothalamic nucleus of the same mice exposed to overnight high-fat chow or food deprivation or control (c). The same blot, but after total protein stain was washed off and instead probed with anti-GFAP and anti-TSPO for analysis (d). In both blots, the positive control was protein lysate from primary cultured mouse cortical astrocytes. The black boxes represent the outline of the blot used in Figure 4.2.1.2 (a, b) and 4.2.1.3 (c, d).

Bibliography

1. World Health Organization. Controlling the global obesity epidemic. World Health Organ. 2015;
2. WHO (World Health Organization). WHO obesity and overweight fact sheet no 311. Obes Oveweight Fact Sheet. 2013;
3. Fischer IP, Irmler M, Meyer CW, Sachs SJ, Neff F, Hrabe De Angelis M, et al. A history of obesity leaves an inflammatory fingerprint in liver and adipose tissue. Vol. 42, International Journal of Obesity. 2018. p. 507–17.
4. Gaggini M, Morelli M, Buzzigoli E, DeFronzo RA, Bugianesi E, Gastaldelli A. Non-alcoholic fatty liver disease (NAFLD) and its connection with insulin resistance, dyslipidemia, atherosclerosis and coronary heart disease. Nutrients. 2013.
5. Ray I, Bhattacharya A, De RK. OCDD: An obesity and co-morbid disease database. BioData Min. 2017;10(1).
6. Howell S, Kones R. “Calories in, calories out” and macronutrient intake: The Hope, Hype, and Science of Calories. Am J Physiol - Endocrinol Metab [Internet]. 2017;ajpendo.00156.2017. Available from: http://ajpendo.physiology.org/lookup/doi/10.1152/ajpendo.00156.2017
7. ICD-11 [Internet]. [cited 2020 Jul 4]. Available from: https://icd.who.int/en
8. Bray GA, Kim KK, Wilding JPH. Obesity: a chronic relapsing progressive disease process. A position statement of the World Obesity Federation. Obes Rev. 2017 Jul 1;18(7):715–23.
9. 2017. Geneva: World Health Organization. Noncommunicable Diseases Progress Monitor. World Health Organization. 2017.
10. Fontaine KR, Redden DT, Wang C, Westfall AO, Allison DB. Years of life lost due to obesity. J Am Med Assoc. 2003;
11. De Gonzalez AB, Hartge P, Cerhan JR, Flint AJ, Hannan L, MacInnis RJ, et al. Body-mass index and mortality among 1.46 million white adults. N Engl J Med. 2010;
12. MacMahon S, Baigent C, Duffy S, Rodgers A, Tominaga S, Chambless L, et al. Body-mass index and cause-specific mortality in 900 000 adults: Collaborative analyses of 57 prospective studies. Lancet. 2009;
13. Blüher M. Obesity: global epidemiology and pathogenesis [Internet]. Vol. 15, Nature Reviews Endocrinology. Springer US; 2019. p. 288–98. Available from: http://dx.doi.org/10.1038/s41574-019-0176-8
14. Bentham J, Di Cesare M, Bilano V, Bixby H, Zhou B, Stevens GA, et al. Worldwide trends in body-mass index, underweight, overweight, and obesity from 1975 to 2016: a pooled analysis of 2416 population-based measurement studies in 128·9 million children, adolescents, and adults. Lancet. 2017 Dec 16;390(10113):2627–42.
15. Swinburn BA, Sacks G, Hall KD, McPherson K, Finegood DT, Moodie ML, et al. The global obesity pandemic: Shaped by global drivers and local environments. The Lancet. 2011.
16. Peeters A. Obesity and the future of food policies that promote healthy diets.

Nature Reviews Endocrinology. 2018.

17. Roberto CA, Swinburn B, Hawkes C, Huang TTK, Costa SA, Ashe M, et al. Patchy progress on obesity prevention: Emerging examples, entrenched barriers, and new thinking. The Lancet. 2015.

18. Wolfe BM, Kvach E, Eckel RH. Treatment of obesity [Internet]. Vol. 118, Circulation Research. Lippincott Williams and Wilkins; 2016 [cited 2020 Jul 4]. p. 1844–55. Available from: /pmc/articles/PMC4888907/?report=abstract

19. Lee PC, Dixon J. Pharmacotherapy for obesity. Aust Fam Physician [Internet]. 2017 Jul 1 [cited 2020 Jul 4];46(7):472–7. Available from: /pmc/articles/PMC4286660/?report=abstract

20. Mehta A, Marso SP, Neeland IJ. Liraglutide for weight management: a critical review of the evidence. Obes Sci Pract [Internet]. 2017 Mar 1 [cited 2020 Jul 4];3(1):3–14. Available from: /pmc/articles/PMC5358074/?report=abstract

21. Wilson JL, Enriori PJ. A talk between fat tissue, gut, pancreas and brain to control body weight. Mol Cell Endocrinol [Internet]. 2015;418:108–19. Available from: http://dx.doi.org/10.1016/j.mce.2015.08.022

22. Furness JB, Kunze WAA, Bertrand PP, Clerc N, Bornstein JC. Intrinsic primary afferent neurons of the intestine. Prog Neurobiol. 1998;

23. Mayer EA. Gut feelings: The emerging biology of gut-"brain communication. Nat Rev Neurosci [Internet]. 2011;12(8):453–66. Available from: http://dx.doi.org/10.1038/nrn3071

24. Furness JB. The enteric nervous system and neurogastroenterology. Nature Reviews Gastroenterology and Hepatology. 2012.

25. Dockray GJ. Cholecystokinin and gut-brain signalling. Regulatory Peptides. 2009.

26. Beck B. Neuropeptides and obesity. Nutrition. 2000;16(10):916–23.

27. West DB, Fey D, Woods SC. Cholecystokinin persistently suppresses meal size but not food intake in free-feeding rats. Am J Physiol - Regul Integr Comp Physiol. 1984;15(5).

28. Kojima M, Hosoda H, Date Y, Nakazato M, Matsuo H, Kangawa K. Ghrelin is a growth-hormone-releasing acylated peptide from stomach. Nature [Internet]. 1999 Dec 9 [cited 2020 Jul 5];402(6762):656–60. Available from: https://pubmed.ncbi.nlm.nih.gov/10604470/

29. Tschop M, Smiley DL, Heiman ML. Ghrelin induces adiposity in rodents. Nature [Internet]. 2000 Oct 19 [cited 2020 Jul 5];407(6806):908–13. Available from: www.nature.com

30. Müller TD, Nogueiras R, Andermann ML, Andrews ZB, Anker SD, Argente J, et al. Ghrelin. Vol. 4, Molecular Metabolism. Elsevier GmbH; 2015. p. 437–60.

31. Al Massadi O, López M, Tschöp M, Diéguez C, Nogueiras R. Current Understanding of the Hypothalamic Ghrelin Pathways Inducing Appetite and Adiposity. Vol. 40, Trends in Neurosciences. Elsevier Ltd; 2017. p. 167–80.

32. Smith GP, Jerome C, Norgren R. Afferent axons in abdominal vagus mediate satiety effect of cholecystokinin in rats. Am J Physiol - Regul Integr Comp Physiol. 1985;

33. Steffens AB, Van Der Gugten J, Godeke J, Luiten PGM, Strubbe JH. Meal-induced increases in parasympathetic and sympathetic activity elicit

simultaneous rises in plasma insulin and free fatty acids. Physiol Behav. 1986;37(1):119–22.

34. South EH, Ritter RC. Capsaicin application to central or peripheral vagal fibers attenuates CCK satiety. Peptides. 1988;

35. Williams G, Bing C, Cai XJ, Harrold JA, King PJ, Liu XH. The hypothalamus and the control of energy homeostasis: Different circuits, different purposes. Physiol Behav. 2001;74(4–5):683–701.

36. Williams EKK, Chang RBB, Strochlic DEE, Umans BDD, Lowell BBB, Liberles SDD. Sensory Neurons that Detect Stretch and Nutrients in the Digestive System. Cell [Internet]. 2016;166(1):209–21. Available from: http://dx.doi.org/10.1016/j.cell.2016.05.011

37. de Lartigue G, de La Serre CB, Raybould HE. Vagal afferent neurons in high fat diet-induced obesity; intestinal microflora, gut inflammation and cholecystokinin. Physiol Behav. 2011;

38. Schwartz GJ. The role of gastrointestinal vagal afferents in the control of food intake: Current prospects. In: Nutrition. 2000.

39. Travagli RA, Anselmi L. Vagal neurocircuitry and its influence on gastric motility. Nature Reviews Gastroenterology and Hepatology. 2016.

40. Browning KN, Travagli RA. Plasticity of vagal brainstem circuits in the control of gastrointestinal function. Autonomic Neuroscience: Basic and Clinical. 2011.

41. Rui L. Energy metabolism in the liver. Compr Physiol. 2014;4(1):177–97.

42. Wang PYT, Caspi L, Lam CKL, Chari M, Li X, Light PE, et al. Upper intestinal lipids trigger a gut-brain-liver axis to regulate glucose production. Nature. 2008;

43. Hackl MT, Fürnsinn C, Schuh CM, Krssak M, Carli F, Guerra S, et al. Brain leptin reduces liver lipids by increasing hepatic triglyceride secretion and lowering lipogenesis. Nat Commun. 2019 Dec 1;10(1).

44. Hodson L, Gunn PJ. The regulation of hepatic fatty acid synthesis and partitioning: the effect of nutritional state [Internet]. Vol. 15, Nature Reviews Endocrinology. Springer US; 2019. p. 689–700. Available from: http://dx.doi.org/10.1038/s41574-019-0256-9

45. Zhang Y, Proenca R, Maffei M, Barone M, Leopold L, Friedman JM. Positional cloning of the mouse obese gene and its human homologue. Nature. 1994;

46. Scheja L, Heeren J. The endocrine function of adipose tissues in health and cardiometabolic disease. Nat Rev Endocrinol [Internet]. 2019; Available from: http://dx.doi.org/10.1038/s41574-019-0230-6

47. Migliorini RH, Garofalo MAR, Kettelhut IC. Increased sympathetic activity in rat white adipose tissue during prolonged fasting. Am J Physiol - Regul Integr Comp Physiol [Internet]. 1997 [cited 2020 Jul 30];272(2 41-2). Available from: https://pubmed.ncbi.nlm.nih.gov/9124491/

48. Garofalo MAR, Kettelhut IC, Roselino JES, Migliorini RH. Effect of acute cold exposure on norpinephrine turnover rates in rat white adipose tissue. J Auton Nerv Syst. 1996;

49. Medina-Gómez G. Mitochondria and endocrine function of adipose tissue. Best Pract Res Clin Endocrinol Metab [Internet]. 2012;26(6):791–804. Available from: http://dx.doi.org/10.1016/j.beem.2012.06.002

50. Cannon B, Nedergaard J. Brown Adipose Tissue: Function and Physiological

Significance. Physiological Reviews. 2004.

51. Fenzl A, Kiefer FW. Brown adipose tissue and thermogenesis. Vol. 19, Hormone Molecular Biology and Clinical Investigation. 2014. p. 25–37.

52. Scheja L, Heeren J. Metabolic interplay between white, beige, brown adipocytes and the liver [Internet]. Vol. 64, Journal of Hepatology. Elsevier B.V.; 2016 [cited 2020 Jul 30]. p. 1176–86. Available from: https://pubmed.ncbi.nlm.nih.gov/26829204/

53. Jéquier E. Leptin signaling, adiposity, and energy balance. Ann N Y Acad Sci [Internet]. 2002;967:379–88. Available from: http://www.ncbi.nlm.nih.gov/pubmed/12079865

54. Frayn KN, Karpe F, Fielding BA, Macdonald IA, Coppack SW. Integrative physiology of human adipose tissue. International Journal of Obesity. 2003.

55. Stolarczyk E. Adipose tissue inflammation in obesity: a metabolic or immune response? Vol. 37, Current Opinion in Pharmacology. Elsevier Ltd; 2017. p. 35–40.

56. Trayhurn P. Hypoxia and adipose tissue function and dysfunction in obesity. Physiol Rev. 2013;93(1):1–21.

57. Rausch ME, Weisberg S, Vardhana P, Tortoriello D V. Obesity in C57BL/6J mice is characterized by adipose tissue hypoxia and cytotoxic T-cell infiltration. Int J Obes. 2008;32(3):451–63.

58. Geiger K, Leiherer A, Muendlein A, Stark N, Geller-Rhomberg S, Saely CH, et al. Identification of hypoxia-induced genes in human SGBS adipocytes by microarray analysis. PLoS One. 2011;

59. Mazzatti D, Lim FL, O'Hara A, Wood IS, Trayhurn P. A microarray analysis of the hypoxia-induced modulation of gene expression in human adipocytes. Arch Physiol Biochem. 2012;

60. Liu J, Divoux A, Sun J, Zhang J, Clément K, Glickman JN, et al. Genetic deficiency and pharmacological stabilization of mast cells reduce diet-induced obesity and diabetes in mice. Nat Med. 2009;

61. Lu J, Zhao J, Meng H, Zhang X. Adipose tissue-resident immune cells in obesity and type 2 diabetes [Internet]. Vol. 10, Frontiers in Immunology. Frontiers Media S.A.; 2019 [cited 2020 Jul 6]. p. 1173. Available from: www.frontiersin.org

62. Weisberg SP, McCann D, Desai M, Rosenbaum M, Leibel RL, Ferrante AW. Obesity is associated with macrophage accumulation in adipose tissue. J Clin Invest. 2003;

63. Xu H, Barnes GT, Yang Q, Tan G, Yang D, Chou CJ, et al. Chronic inflammation in fat plays a crucial role in the development of obesity-related insulin resistance. J Clin Invest. 2003;

64. Huh JY, Park YJ, Ham M, Kim JB. Crosstalk between adipocytes and immune cells in adipose tissue inflammation and metabolic dysregulation in obesity. Vol. 37, Molecules and Cells. 2014. p. 365–71.

65. Kawano Y, Nakae J, Watanabe N, Kikuchi T, Tateya S, Tamori Y, et al. Colonic Pro-inflammatory Macrophages Cause Insulin Resistance in an Intestinal Ccl2/Ccr2-Dependent Manner. Cell Metab. 2016;

66. Ellacott KLJ, Murphy JG, Marks DL, Cone RD. Obesity-induced inflammation in white adipose tissue is attenuated by loss of melanocortin-3 receptor signaling. Endocrinology. 2007;148(12):6186–94.

67. SciDraw | Scientific Drawings [Internet]. [cited 2020 Aug 4]. Available from: https://scidraw.io/?q=liver

68. Clarke IJ. Hypothalamus as an endocrine organ. Compr Physiol. 2015;5(1):217–53.

69. Broadwell RD, Brightman MW. Entry of peroxidase into neurons of the central and peripheral nervous systems from extracerebral and cerebral blood. J Comp Neurol. 1976;

70. Schneeberger M, Gomis R, Claret M. Hypothalamic and brainstem neuronal circuits controlling homeostatic energy balance. J Endocrinol. 2014;220(2).

71. Morita-Takemura S, Wanaka A. Blood-to-brain communication in the hypothalamus for energy intake regulation [Internet]. Vol. 128, Neurochemistry International. Elsevier Ltd; 2019 [cited 2020 Jul 30]. p. 135–42. Available from: https://pubmed.ncbi.nlm.nih.gov/31002894/

72. Rodríguez EM, Blázquez JL, Guerra M. The design of barriers in the hypothalamus allows the median eminence and the arcuate nucleus to enjoy private milieus: The former opens to the portal blood and the latter to the cerebrospinal fluid [Internet]. Vol. 31, Peptides. Peptides; 2010 [cited 2020 Jul 30]. p. 757–76. Available from: https://pubmed.ncbi.nlm.nih.gov/20093161/

73. Ramalho AF, Bombassaro B, Dragano NR, Solon C, Morari J, Fioravante M, et al. Dietary Fats Promote Functional and Structural Changes in the Median Eminence Blood/Spinal Fluid Interface-the Protective Role for BDNF. J Neuroinflammation. 2018 Jan 9;15(1).

74. Campbell JN, Macosko EZ, Fenselau H, Pers TH, Lyubetskaya A, Tenen D, et al. A molecular census of arcuate hypothalamus and median eminence cell types. Nat Publ Gr [Internet]. 2017;(July 2016). Available from: http://dx.doi.org/10.1038/nn.4495

75. Krashes MJ, Koda S, Ye CP, Rogan SC, Adams AC, Cusher DS, et al. Rapid, reversible activation of AgRP neurons drives feeding behavior in mice. J Clin Invest. 2011;

76. Tolle V, Low MJ. In vivo evidence for inverse agonism of agouti-related peptide in the central nervous system of proopiomelanocortin-deficient mice. Diabetes. 2008;

77. Cansell C, Denis RGP, Joly-Amado A, Castel J, Luquet S. Arcuate AgRP neurons and the regulation of energy balance. Front Endocrinol (Lausanne). 2012;3(DEC):1–7.

78. Horvath TL, Bechmann I, Naftolin F, Kalra SP, Leranth C. Heterogeneity in the neuropeptide Y-containing neurons of the rat arcuate nucleus: GABAergic and non-GABAergic subpopulations. Brain Res. 1997;

79. Lu D, Willard D, Patel IR, Kadwell S, Overton L, Kost T, et al. Agouti protein is an antagonist of the melanocyte-stimulating-hormone receptor. Nature [Internet]. 1994 [cited 2020 Aug 1];371(6500):799–802. Available from: https://pubmed.ncbi.nlm.nih.gov/7935841/

80. Yang Y-K, Ollmann MM, Wilson BD, Dickinson C, Yamada T, Barsh GS, et al. Effects of Recombinant Agouti-Signaling Protein on Melanocortin Action. Mol Endocrinol [Internet]. 1997 Mar 1 [cited 2020 Aug 1];11(3):274–80. Available from: https://academic.oup.com/mend/article/11/3/274/2754086

81. Yang Y, Fong TM, Dickinson CJ, Mao C, Li JY, Tota MR, et al. Molecular determinants of ligand binding to the human melanocortin-4 receptor.

Biochemistry [Internet]. 2000 Dec 5 [cited 2020 Aug 1];39(48):14900–11. Available from: https://pubs.acs.org/doi/full/10.1021/bi001684q

82. Wang D, He X, Zhao Z, Feng Q, Lin R, Sun Y, et al. Whole-brain mapping of the direct inputs and axonal projections of POMC and AgRP neurons. Front Neuroanat [Internet]. 2015;9(March):1–17. Available from: http://www.frontiersin.org/Neuroanatomy/10.3389/fnana.2015.00040/abstract

83. Sims JS, Lorden JF. Effect of paraventricular nucleus lesions on body weight, food intake and insulin levels. Behav Brain Res. 1986;

84. Kishi T, Aschkenasi CJ, Lee CE, Mountjoy KG, Saper CB, Elmquist JK. Expression of melanocortin 4 receptor mRNA in the central nervous system of the rat. J Comp Neurol. 2003;

85. Blevins JE, Schwartz MW, Baskin DG. Evidence that paraventricular nucleus oxytocin neurons link hypothalamic leptin action to caudal brain stem nuclei controlling meal size. Am J Physiol - Regul Integr Comp Physiol. 2004;

86. Balthasar N, Dalgaard LT, Lee CE, Yu J, Funahashi H, Williams T, et al. Divergence of melanocortin pathways in the control of food intake and energy expenditure. Cell. 2005;

87. Biag J, Huang Y, Gou L, Hintiryan H, Askarinam A, Hahn JD, et al. Cyto- and chemoarchitecture of the hypothalamic paraventricular nucleus in the C57BL/6J male mouse: A study of immunostaining and multiple fluorescent tract tracing. J Comp Neurol. 2012;

88. Garfield AS, Li C, Madara JC, Shah BP, Webber E, Steger JS, et al. A neural basis for melanocortin-4 receptor-regulated appetite. Nat Neurosci. 2015;18(6):863–71.

89. Kong D, Tong Q, Ye C, Koda S, Fuller PM, Krashes MJ, et al. GABAergic RIP-Cre neurons in the arcuate nucleus selectively regulate energy expenditure. Cell. 2012;

90. Dodd GT, Decherf S, Loh K, Simonds SE, Wiede F, Balland E, et al. Leptin and insulin act on POMC neurons to promote the browning of white fat. Cell. 2015;

91. Elmquist JK, Bjørbæk C, Ahima RS, Flier JS, Saper CB. Distributions of leptin receptor mRNA isoforms in the rat brain. J Comp Neurol. 1998;

92. Scott MM, Lachey JL, Sternson SM, Lee CE, Elias CF, Friedman JM, et al. Leptin targets in the mouse brain. J Comp Neurol. 2009;

93. Patterson CM, Leshan RL, Jones JC, Myers MG. Molecular mapping of mouse brain regions innervated by leptin receptor-expressing cells. Brain Res. 2011;

94. Kobelt P, Wisser AS, Stengel A, Goebel M, Inhoff T, Noetzel S, et al. Peripheral injection of ghrelin induces Fos expression in the dorsomedial hypothalamic nucleus in rats. Brain Res. 2008 Apr 14;1204:77–86.

95. Hyland L, Park S Bin, Abdelaziz Y, Abizaid A. Ghrelin infused into the dorsomedial hypothalamus of male mice increases food intake and adiposity. Physiol Behav [Internet]. 2020;220(October 2019):112882. Available from: https://doi.org/10.1016/j.physbeh.2020.112882

96. Merkestein M, van Gestel M a, van der Zwaal EM, Brans M a, Luijendijk MC, van Rozen a J, et al. GHS-R1a signaling in the DMH and VMH contributes to food anticipatory activity. Int J Obes (Lond). 2014;38(4):610–8.

97. Dodd GT, Worth AA, Nunn N, Korpal AK, Bechtold DA, Allison MB, et al. The thermogenic effect of leptin is dependent on a distinct population of prolactin-

releasing peptide neurons in the dorsomedial hypothalamus. Cell Metab [Internet]. 2014 Oct 7 [cited 2020 May 1];20(4):639–49. Available from: http://dx.doi.org/10.1016/j.cmet.2014.07.022

98. Satoh A, Brace CS, Ben-Josef G, West T, Wozniak DF, Holtzman DM, et al. SIRT1 promotes the central adaptive response to diet restriction through activation of the dorsomedial and lateral nuclei of the hypothalamus. J Neurosci. 2010 Jul 28;30(30):10220–32.

99. Bi S, Robinson BM, Moran TH. Acute food deprivation and chronic food restriction differentially affect hypothalamic NPY mRNA expression. Am J Physiol - Regul Integr Comp Physiol. 2003;

100. Bi S, Kim YJ, Zheng F. Dorsomedial hypothalamic NPY and energy balance control. Neuropeptides. 2012.

101. Yang L, Scott KA, Hyun J, Tamashiro KL, Tray N, Moran TH, et al. Role of dorsomedial hypothalamic NPY in modulating food intake and energy balance. J Neurosci. 2009;29(1):179–90.

102. Berthoud HR. Vagal and hormonal gut-brain communication: From satiation to satisfaction. Neurogastroenterology and Motility. 2008.

103. Maniscalco JW, Kreisler AD, Rinaman L. Satiation and stress-induced hypophagia: Examining the role of hindbrain neurons expressing prolactin-releasing peptide or glucagon-like peptide 1. Frontiers in Neuroscience. 2012.

104. Sam AH, Troke RC, Tan TM, Bewick GA. The role of the gut/brain axis in modulating food intake. Neuropharmacology. 2012.

105. Peters JH, Karpiel AB, Ritter RC, Simasko SM. Cooperative activation of cultured vagal afferent neurons by leptin and cholecystokinin. Endocrinology. 2004;

106. Young AA. Brainstem sensing of meal-related signals in energy homeostasis. Neuropharmacology. 2012.

107. Wislocki GB, Putnam TJ. Note on the anatomy of the areae postremae. Anat Rec. 1920;

108. Wislocki GB, Putnam TJ. Further observations on the anatomy and physiology of the areae postremae. Anat Rec. 1924;

109. Manuscript A. the Circumventricular Organs of the Mouse Brain. 2014;521(15):3389–405.

110. Grill HJ, Hayes MR. Hindbrain neurons as an essential hub in the neuroanatomically distributed control of energy balance. Cell Metabolism. 2012.

111. Wang Y, Kim JM, Schmit MB, Cho TS, Fang C, Cai H. A bed nucleus of stria terminalis microcircuit regulating inflammation-associated modulation of feeding. Nat Commun. 2019 Dec 1;10(1).

112. Dong HW, Swanson LW. Projections from bed nuclei of the stria terminalis, anteromedial area: Cerebral hemisphere integration of neuroendocrine, autonomic, and behavioral aspects of energy balance. J Comp Neurol. 2006 Jan 1;494(1):142–78.

113. Van Den Heuvel JK, Furman K, Gumbs MCR, Eggels L, Opland DM, Land BB, et al. Neuropeptide Y activity in the nucleus accumbens modulates feeding behavior and neuronal activity. Biol Psychiatry. 2015 Apr 1;77(7):633–41.

114. Sweeney P, Yang Y. An inhibitory septum to lateral hypothalamus circuit that

suppresses feeding. J Neurosci. 2016 Nov 2;36(44):11185–95.

115. Morton GJ, Meek TH, Schwartz MW. Neurobiology of food intake in health and disease. Vol. 15, Nature Reviews Neuroscience. 2014. p. 367–78.

116. Dhopeshwarkar GA, Mead JF. Fatty acid uptake by the brain. III. Incorporation of [I-14C]oleic acid into the adult ratbrain. Biochim Biophys Acta (BBA)/Lipids Lipid Metab. 1970;

117. Dhopeshwarkar GA, Subramanian C, Mead JF. Fatty acid uptake by the brain V. incorporation of [1-14c]linolenic acid into adult rat brain. Biochim Biophys Acta (BBA)/Lipids Lipid Metab. 1971;

118. Panov A, Orynbayeva Z, Vavilin V, Lyakhovich V. Fatty acids in energy metabolism of the central nervous system. Biomed Res Int [Internet]. 2014;2014:472459. Available from: http://www.ncbi.nlm.nih.gov/pubmed/24883315%5Cnhttp://downloads.hindawi.com/journals/bmri/2014/472459.pdf

119. Banks WA, Farr SA, Salameh TS, Niehoff ML, Rhea EM, Morley JE, et al. Triglycerides cross the blood-brain barrier and induce central leptin and insulin receptor resistance. Int J Obes [Internet]. 2018;42(3):391–7. Available from: http://dx.doi.org/10.1038/ijo.2017.231

120. Steffens AB, Scheurink AJW, Luiten PGM, Bohus B. Hypothalamic food intake regulating areas are involved in the homeostasis of blood glucose and plasma FFA levels. Physiol Behav. 1988;44(4–5):581–9.

121. Hofmann K, Lamberz C, Piotrowitz K, Offermann N, But D, Scheller A, et al. Tanycytes and a differential fatty acid metabolism in the hypothalamus. Glia. 2016;65(2):231–49.

122. Milanski M, Degasperi G, Coope A, Morari J, Denis R, Cintra DE, et al. Saturated fatty acids produce an inflammatory response predominantly through the activation of TLR4 signaling in hypothalamus: Implications for the pathogenesis of obesity. J Neurosci. 2009;

123. Buckman LB, Hasty AH, Flaherty DK, Buckman CT, Thompson MM, Matlock BK, et al. Obesity induced by a high-fat diet is associated with increased immune cell entry into the central nervous system. Brain Behav Immun. 2014;

124. Lee CH, Kim HJ, Lee YS, Kang GM, Lim HS, Lee S hwan, et al. Hypothalamic Macrophage Inducible Nitric Oxide Synthase Mediates Obesity-Associated Hypothalamic Inflammation. Cell Rep [Internet]. 2018;25(4):934-946.e5. Available from: https://doi.org/10.1016/j.celrep.2018.09.070

125. Thaler JP, Yi CX, Schur EA, Guyenet SJ, Hwang BH, Dietrich MO, et al. Obesity is associated with hypothalamic injury in rodents and humans. J Clin Invest. 2012;122(1):153–62.

126. Carlin JL, Grissom N, Ying Z, Gomez-Pinilla F, Reyes TM. Voluntary exercise blocks Western diet-induced gene expression of the chemokines CXCL10 and CCL2 in the prefrontal cortex. Brain Behav Immun. 2016;

127. Wang S, Huang XF, Zhang P, Wang H, Zhang Q, Yu S, et al. Chronic rhein treatment improves recognition memory in high-fat diet-induced obese male mice. J Nutr Biochem. 2016;

128. Pistell PJ, Morrison CD, Gupta S, Knight AG, Keller JN, Ingram DK, et al. Cognitive impairment following high fat diet consumption is associated with brain inflammation. J Neuroimmunol. 2010;219(1–2):25–32.

129. Jayaraman A, Lent-Schochet D, Pike CJ. Diet-induced obesity and low testosterone increase neuroinflammation and impair neural function. J Neuroinflammation. 2014;

130. Guillemot-Legris O, Masquelier J, Everard A, Cani PD, Alhouayek M, Muccioli GG. High-fat diet feeding differentially affects the development of inflammation in the central nervous system. J Neuroinflammation. 2016;

131. Guillemot-Legris O, Muccioli GG. Obesity-Induced Neuroinflammation: Beyond the Hypothalamus. Trends Neurosci. 2017;40(4):237–53.

132. Zhang X, Zhang G, Zhang H, Karin M, Bai H, Cai D. Hypothalamic IKKb/NF-kB and ER stress Link Overnutrition. October. 2009;135(1):61–73.

133. Reis WL, Yi CX, Gao Y, Tschöp MH, Stern JE. Brain innate immunity regulates hypothalamic arcuate neuronal activity and feeding behavior. Endocrinology. 2015;156(4):1303–15.

134. Rodriguez-Navas C, Morselli E, Clegg DJ. Sexually dimorphic brain fatty acid composition in low and high fat diet-fed mice. Mol Metab [Internet]. 2016;5(8):680–9. Available from: http://dx.doi.org/10.1016/j.molmet.2016.06.014

135. Morselli E, Frank AP, Palmer BF, Rodriguez-Navas C, Criollo A, Clegg DJ. A sexually dimorphic hypothalamic response to chronic high-fat diet consumption. Int J Obes [Internet]. 2016;40(2):206–9. Available from: http://www.nature.com/doifinder/10.1038/ijo.2015.114

136. Muldoon LL, Alvarez JI, Begley DJ, Boado RJ, Del Zoppo GJ, Doolittle ND, et al. Immunologic privilege in the central nervous system and the blood-brain barrier. J Cereb Blood Flow Metab [Internet]. 2013;33(1):13–21. Available from: http://dx.doi.org/10.1038/jcbfm.2012.153

137. Sierra A, Encinas JM, Deudero JJP, Chancey JH, Enikolopov G, Overstreet-Wadiche LS, et al. Microglia shape adult hippocampal neurogenesis through apoptosis-coupled phagocytosis. Cell Stem Cell. 2010 Oct 8;7(4):483–95.

138. Ransohoff RM, Cardona AE. The myeloid cells of the central nervous system parenchyma. Vol. 468, Nature. 2010. p. 253–62.

139. Nimmerjahn A, Kirchhoff F, Helmchen F. Neuroscience: Resting microglial cells are highly dynamic surveillants of brain parenchyma in vivo. Science (80-). 2005 May 27;308(5726):1314–8.

140. Askew K, Li K, Olmos-Alonso A, Garcia-Moreno F, Liang Y, Richardson P, et al. Coupled Proliferation and Apoptosis Maintain the Rapid Turnover of Microglia in the Adult Brain. Cell Rep. 2017 Jan 10;18(2):391–405.

141. Bernard S, Druid H, Frise J, Khosravi A, Bernard S, Mold JE, et al. The Lifespan and Turnover of Microglia in the Human Brain: Cell Reports. 2017;779–84. Available from: http://www.cell.com/cell-reports/fulltext/S2211-1247(17)30943-9

142. Shigemoto-Mogami Y, Hoshikawa K, Goldman JE, Sekino Y, Sato K. Microglia enhance neurogenesis and oligodendrogenesis in the early postnatal subventricular zone. J Neurosci. 2014 Feb 5;34(6):2231–43.

143. Perea G, Navarrete M, Araque A. Tripartite synapses: astrocytes process and control synaptic information. Vol. 32, Trends in Neurosciences. 2009. p. 421–31.

144. Simpson IA, Carruthers A, Vannucci SJ. Supply and demand in cerebral energy metabolism: the role of nutrient transpoters. J Cereb Blood Flow Metab. 2007;27(11):1766–91.

145. Pellerin L, Bouzier-Sore AK, Aubert A, Serres S, Merle M, Costalat R, et al.

Activity-dependent regulation of energy metabolism by astrocytes: An update. Vol. 55, GLIA. 2007. p. 1251–62.

146. Mason S. Lactate shuttles in neuroenergetics-homeostasis, allostasis and beyond. Front Neurosci. 2017;11(FEB):1–15.

147. Mishra A. Binaural blood flow control by astrocytes: listening to synapses and the vasculature. J Physiol [Internet]. 2017;595(6):1885–902. Available from: http://doi.wiley.com/10.1113/JP270979

148. Nedergaard M, Ransom B, Goldman SA. New roles for astrocytes: Redefining the functional architecture of the brain. Trends Neurosci. 2003;26(10):523–30.

149. Kang K, Lee S-W, Han JE, Choi JW, Song M-R. The complex morphology of reactive astrocytes controlled by fibroblast growth factor signaling. Glia [Internet]. 2014 Aug 1 [cited 2020 Jul 22];62(8):1328–44. Available from: http://doi.wiley.com/10.1002/glia.22684

150. Wilhelmsson U, Bushong EA, Price DL, Smarr BL, Phung V, Terada M, et al. Redefining the concept of reactive astrocytes as cells that remain within their unique domains upon reaction to injury. Proc Natl Acad Sci U S A. 2006;103(46):17513–8.

151. Cano V, Valladolid-Acebes I, Hernández-Nuño F, Merino B, del Olmo N, Chowen JA, et al. Morphological changes in glial fibrillary acidic protein immunopositive astrocytes in the hippocampus of dietary-induced obese mice. Neuroreport [Internet]. 2014 Aug [cited 2020 Apr 17];25(11):819–22. Available from: http://content.wkhealth.com/linkback/openurl?sid=WKPTLP:landingpage&an=00001756-201408060-00003

152. Rodríguez EM, Blázquez JL, Pastor FE, Peláez B, Peña P, Peruzzo B, et al. Hypothalamic tanycytes: A key component of brain-endocrine interaction. Int Rev Cytol. 2005;247(05):89–164.

153. Langlet F, Mullier A, Bouret SG, Prevot V, Dehouck B. Tanycyte-like cells form a blood-cerebrospinal fluid barrier in the circumventricular organs of the mouse brain. J Comp Neurol. 2013 Oct 15;521(15):3389–405.

154. Langlet F, Levin BE, Luquet S, Mazzone M, Messina A, Dunn-Meynell AA, et al. Tanycytic VEGF-A boosts blood-hypothalamus barrier plasticity and access of metabolic signals to the arcuate nucleus in response to fasting. Cell Metab. 2013;

155. Frayling C, Britton R, Dale N. ATP-mediated glucosensing by hypothalamic tanycytes. J Physiol. 2011;589(9):2275–86.

156. Lee DA, Bedont JL, Pak T, Wang H, Song J, Miranda-Angulo A, et al. Tanycytes of the hypothalamic median eminence form a diet-responsive neurogenic niche. Nat Neurosci [Internet]. 2012;15(5):700–2. Available from: http://www.nature.com/doifinder/10.1038/nn.3079

157. Balland E, Dam J, Langlet F, Caron E, Steculorum S, Messina A, et al. Hypothalamic tanycytes are an ERK-gated conduit for leptin into the brain. Cell Metab. 2014;19(2):293–301.

158. Elizondo-Vega R, Cortes-Campos C, Barahona MJ, Oyarce KA, Carril CA, García-Robles MA. The role of tanycytes in hypothalamic glucosensing. J Cell Mol Med. 2015;19(7):1471–82.

159. Djogo T, Robins SC, Schneider S, Kryzskaya D, Liu X, Mingay A, et al. Adult NG2-Glia Are Required for Median Eminence-Mediated Leptin Sensing and

Body Weight Control. Cell Metab [Internet]. 2016;23(5):797–810. Available from: http://dx.doi.org/10.1016/j.cmet.2016.04.013

160. Lazutkaite G, Soldà A, Lossow K, Meyerhof W, Dale N. Amino acid sensing in hypothalamic tanycytes via umami taste receptors. Mol Metab [Internet]. 2017; Available from: http://linkinghub.elsevier.com/retrieve/pii/S2212877817305379

161. Benford H, Bolborea M, Pollatzek E, Lossow K, Hermans-Borgmeyer I, Liu B, et al. A sweet taste receptor-dependent mechanism of glucosensing in hypothalamic tanycytes. Glia. 2017;65(5):773–89.

162. Elizondo-Vega RJ, Recabal A, Oyarce K. Nutrient sensing by hypothalamic tanycytes. Vol. 10, Frontiers in Endocrinology. 2019.

163. Geller S, Arribat Y, Netzahualcoyotzi C, Lagarrigue S, Carneiro L, Zhang L, et al. Tanycytes Regulate Lipid Homeostasis by Sensing Free Fatty Acids and Signaling to Key Hypothalamic Neuronal Populations via FGF21 Secretion. Cell Metab [Internet]. 2019;30(4):833-844.e7. Available from: https://doi.org/10.1016/j.cmet.2019.08.004

164. Dietrich MO, Horvath TL. Fat incites tanycytes to neurogenesis. Nat Neurosci [Internet]. 2012;15(5):651–3. Available from: http://dx.doi.org/10.1038/nn.3091

165. Haan N, Goodman T, Najdi-Samiei A, Stratford CM, Rice R, El Agha E, et al. Fgf10-expressing tanycytes add new neurons to the appetite/energy-balance regulating centers of the postnatal and adult hypothalamus. J Neurosci. 2013;33(14):6170–80.

166. De Vries EM, Nagel S, Haenold R, Sundaram SM, Pfrieger FW, Fliers E, et al. The role of hypothalamic NF-κB signaling in the response of the HPT-axis to acute inflammation in female mice. Endocrinology. 2016;157(7):2947–56.

167. Böttcher M, Müller-Fielitz H, Sundaram SM, Gallet S, Neve V, Shionoya K, et al. NF-κB signaling in tanycytes mediates inflammation-induced anorexia. Mol Metab. 2020;

168. Verkhratsky A, Zorec R, Parpura V. Stratification of astrocytes in healthy and diseased brain. Brain Pathol. 2017;27(5):629–44.

169. Boche D, Perry VH, Nicoll JAR. Review: Activation patterns of microglia and their identification in the human brain [Internet]. Vol. 39, Neuropathology and Applied Neurobiology. John Wiley & Sons, Ltd; 2013 [cited 2020 Jul 7]. p. 3–18. Available from: https://onlinelibrary.wiley.com/doi/full/10.1111/nan.12011

170. Amici SA, Dong J, Guerau-de-Arellano M. Molecular mechanisms modulating the phenotype of macrophages and microglia. Front Immunol. 2017;8(NOV):1–18.

171. Noh H, Jeon J, Seo H. Systemic injection of LPS induces region-specific neuroinflammation and mitochondrial dysfunction in normal mouse brain. Neurochem Int [Internet]. 2014;69(1):35–40. Available from: http://dx.doi.org/10.1016/j.neuint.2014.02.008

172. Kuhlmann AC, Guilarte TR. Cellular and subcellular localization of peripheral benzodiazepine receptors after trimethyltin neurotoxicity. JNeurochem. 2000;74(4):1694–704.

173. Liddelow SA, Guttenplan KA, Clarke LE, Bennett FC, Bohlen CJ, Schirmer L, et al. Neurotoxic reactive astrocytes are induced by activated microglia. Nature [Internet]. 2017;541(7638):481–7. Available from: http://www.nature.com/doifinder/10.1038/nature21029

174. Valdearcos M, Douglass JD, Robblee MM, Dorfman MD, Stifler DR, Bennett ML, et al. Microglial Inflammatory Signaling Orchestrates the Hypothalamic Immune Response to Dietary Excess and Mediates Obesity Susceptibility. Cell Metab [Internet]. 2017;26(1):185-197.e3. Available from: http://dx.doi.org/10.1016/j.cmet.2017.05.015

175. Valdearcos M, Robblee MM, Benjamin DI, Nomura DK, Xu AW, Koliwad SK. Microglia Dictate the Impact of Saturated Fat Consumption on Hypothalamic Inflammation and Neuronal Function. Cell Rep [Internet]. 2014;9(6):2124–39. Available from: http://dx.doi.org/10.1016/j.celrep.2014.11.018

176. Baufeld C, Osterloh A, Prokop S, Miller KR, Heppner FL. High-fat diet-induced brain region-specific phenotypic spectrum of CNS resident microglia. Acta Neuropathol. 2016 Sep 8;132(3):361–75.

177. Kim JD, Yoon NA, Jin S, Diano S. Microglial UCP2 Mediates Inflammation and Obesity Induced by High-Fat Feeding. Cell Metab. 2019;30(5):952-962.e5.

178. Cope EC, Lamarca EA, Monari PK, Olson LB, Martinez S, Zych AD, et al. Microglia play an active role in obesity-associated cognitive decline. J Neurosci. 2018;38(41):8889–904.

179. Gao Y, Ottaway N, Schriever SC, Legutko B, García-Cáceres C, de la Fuente E, et al. Hormones and diet, but not body weight, control hypothalamic microglial activity. Glia. 2014;62(1):17–25.

180. Buckman LB, Thompson MM, Moreno HN, Ellacott KLJ. Regional astrogliosis in the mouse hypothalamus in response to obesity. J Comp Neurol. 2013;521(6):1322–33.

181. Graham LC, Harder JM, Soto I, De Vries WN, John SWM, Howell GR. Chronic consumption of a western diet induces robust glial activation in aging mice and in a mouse model of Alzheimer's disease. Sci Rep [Internet]. 2016;6(September 2015):1–13. Available from: http://dx.doi.org/10.1038/srep21568

182. Harrison L, Pfuhlmann K, Schriever SC, Pfluger PT. Profound weight loss induces reactive astrogliosis in the arcuate nucleus of obese mice. Mol Metab [Internet]. 2019 Jun;24:149–55. Available from: https://linkinghub.elsevier.com/retrieve/pii/S221287781930225X

183. Daly CM, Saxena J, Singh J, Bullard MR, Bondy O, Saxena A, et al. Sex differences in response to a high fat , high sucrose diet in both the gut microbiome and hypothalamic astrocytes and microglia. Nutr Neurosci [Internet]. 2020;0(0):1–15. Available from: https://doi.org/10.1080/1028415X.2020.1752996

184. Gzielo K, Kielbinski M, Ploszaj J, Janeczko K, Gazdzinski SP, Setkowicz Z. Long-Term Consumption of High-Fat Diet in Rats: Effects on Microglial and Astrocytic Morphology and Neuronal Nitric Oxide Synthase Expression. Cell Mol Neurobiol. 2016;1–7.

185. Burda JE, Sofroniew M V. Reactive gliosis and the multicellular response to CNS damage and disease. Vol. 81, Neuron. 2014. p. 229–48.

186. Tracy LM, Bergqvist F, Ivanova E V., Jacobsen KT, Iverfeldt K. Exposure to the saturated free fatty acid palmitate alters BV-2 microglia inflammatory response. J Mol Neurosci. 2013 Nov 25;51(3):805–12.

187. Gupta S, Knight AG, Gupta S, Keller JN, Keller AJB-. Saturated Long Chain Fatty acids Activate Inflammatory Signaling in Astrocytes. 2013;120(6):1060–71.

188. Butovsky O, Jedrychowski MP, Moore CS, Cialic R, Lanser AJ, Gabriely G, et al. Identification of a unique TGF-β-dependent molecular and functional signature in

microglia. Nat Neurosci. 2014 Jan 8;17(1):131–43.

189. Yi C-X, Tschop MH, Woods SC, Hofmann SM. High-fat-diet exposure induces IgG accumulation in hypothalamic microglia. Dis Model Mech [Internet]. 2012;5(5):686–90. Available from: http://dmm.biologists.org/cgi/doi/10.1242/dmm.009464

190. Burfeind KG, Zhu X, Norgard MA, Levasseur PR, Huisman C, Michaelis KA, et al. Microglia in the hypothalamus respond to tumor-derived factors and are protective against cachexia during pancreatic cancer. Glia. 2020;(January):1–16.

191. Yoo S, Cha D, Kim S, Jiang L, Cooke P, Adebesin M, et al. Tanycyte ablation in the arcuate nucleus and median eminence increases obesity susceptibility by increasing body fat content in male mice. Glia. 2020;(August 2019):1–14.

192. Mauerer R, Walczak Y, Langmann T. Comprehensive mRNA profiling of lipid-related genes in microglia and macrophages using taqman arrays. Methods Mol Biol. 2009;580:187–201.

193. Zhang Y, Chen K, Sloan SA, Bennett ML, Scholze AR, O'Keeffe S, et al. An RNA-sequencing transcriptome and splicing database of glia, neurons, and vascular cells of the cerebral cortex. J Neurosci. 2014;

194. Nagy AM, Fekete R, Horvath G, Koncsos G, Kriston C, Sebestyen A, et al. Versatility of microglial bioenergetic machinery under starving conditions. Biochim Biophys Acta - Bioenerg. 2018;

195. Kalsbeek MJT, Mulder L, Yi CX. Microglia energy metabolism in metabolic disorder. Mol Cell Endocrinol. 2016;

196. Payne J, Maher F, Simpson I, Mattice L, Davies P. Glucose transporter Glut 5 expression in microglial cells. Glia. 1997;

197. Fernandez AM, Hernandez-Garzón E, Perez-Domper P, Perez-Alvarez A, Mederos S, Matsui T, et al. Insulin Regulates Astrocytic Glucose Handling Through Cooperation With IGF-I. Diabetes. 2017;66(1):64–74.

198. García-Cáceres C, Quarta C, Varela L, Gao Y, Gruber T, Legutko B, et al. Astrocytic Insulin Signaling Couples Brain Glucose Uptake with Nutrient Availability. Cell. 2016;166(4):867–80.

199. Allard C, Carneiro L, Grall S, Cline BH, Fioramonti X, Chrétien C, et al. Hypothalamic astroglial connexins are required for brain glucose sensing-induced insulin secretion. J Cereb Blood Flow Metab. 2014;34(2):339–46.

200. van Deijk ALF, Camargo N, Timmerman J, Heistek T, Brouwers JF, Mogavero F, et al. Astrocyte lipid metabolism is critical for synapse development and function in vivo. Glia. 2017;65(4):670–82.

201. Ioannou MS, Jackson J, Sheu SH, Chang CL, Weigel A V, Liu H, et al. Neuron-Astrocyte Metabolic Coupling Protects against Activity-Induced Fatty Acid Toxicity. Cell [Internet]. 2019;177(6):1522-1535.e14. Available from: https://doi.org/10.1016/j.cell.2019.04.001

202. Fuente-Martín E, Garciá-Cáceres C, Granado M, De Ceballos ML, Sánchez-Garrido MÁ, Sarman B, et al. Leptin regulates glutamate and glucose transporters in hypothalamic astrocytes. J Clin Invest. 2012;122(11):3900–13.

203. Fuente-Martín E, García-Cáceres C, Argente-Arizón P, Díaz F, Granado M, Freire-Regatillo A, et al. Ghrelin Regulates Glucose and Glutamate Transporters in Hypothalamic Astrocytes. Sci Rep. 2016;6(November 2015):23673.

204. Reiner DJ, Mietlicki-Baase EG, McGrath LE, Zimmer DJ, Bence KK, Sousa GL,

et al. Astrocytes Regulate GLP-1 Receptor-Mediated Effects on Energy Balance. J Neurosci [Internet]. 2016;36(12):3531–40. Available from: http://www.jneurosci.org/cgi/doi/10.1523/JNEUROSCI.3579-15.2016

205. Katsurada K, Maejima Y, Nakata M, Kodaira M, Suyama S, Iwasaki Y, et al. Endogenous GLP-1 acts on paraventricular nucleus to suppress feeding: Projection from nucleus tractus solitarius and activation of corticotropin-releasing hormone, nesfatin-1 and oxytocin neurons. Biochem Biophys Res Commun [Internet]. 2014;451(2):276–81. Available from: http://dx.doi.org/10.1016/j.bbrc.2014.07.116

206. De Silva A, Salem V, Long CJ, Makwana A, Newbould RD, Rabiner EA, et al. The gut hormones PYY 3-36 and GLP-1 7-36 amide reduce food intake and modulate brain activity in appetite centers in humans. Cell Metab [Internet]. 2011;14(5):700–6. Available from: http://dx.doi.org/10.1016/j.cmet.2011.09.010

207. MacDonald AJ, Holmes FE, Beall C, Pickering AE, Ellacott KLJ. Regulation of food intake by astrocytes in the brainstem dorsal vagal complex. Glia. 2019;68(6):1241–54.

208. Eyo UB, Wu LJ. Bidirectional microglia-neuron communication in the healthy brain. Neural Plast. 2013;2013.

209. Cai W, Xue C, Sakaguchi M, Konishi M, Shirazian A, Ferris HA, et al. Insulin regulates astrocyte gliotransmission and modulates behavior. J Clin Invest. 2018;128(7):2914–26.

210. Bouyakdan K, Taïb B, Budry L, Zhao S, Rodaros D, Neess D, et al. A novel role for central ACBP/DBI as a regulator of long-chain fatty acid metabolism in astrocytes. J Neurochem. 2015;133(2):253–65.

211. Bouyakdan K, Martin H, Liénard F, Budry L, Taib B, Rodaros D, et al. The gliotransmitter ACBP controls feeding and energy homeostasis via the melanocortin system. J Clin Invest. 2019;129(6):2417–30.

212. Kronschlager MTT, Drdla-Schutting R, Gassner M, Honsek SD, Teuchmann HL, Sandkuhler J. Gliogenic LTP spreads widely in nociceptive pathways. Science (80-). 2016;354(6316):1144–8.

213. Ma Z, Stork T, Bergles DE, Freeman MR. Neuromodulators signal through astrocytes to alter neural circuit activity and behaviour. Nature [Internet]. 2016;539(7629):428–32. Available from: http://www.nature.com/doifinder/10.1038/nature20145

214. Martineau M, Baux G, Mothet JP. Gliotransmission at central glutamatergic synapses: D-serine on stage. J Physiol Paris. 2006;99(2–3):103–10.

215. Barros LF, Weber B. CrossTalk proposal: an important astrocyte-to-neuron lactate shuttle couples neuronal activity to glucose utilisation in the brain. J Physiol. 2018;

216. Douglass JD, Dorfman MD, Fasnacht R, Shaffer LD, Thaler JP. Astrocyte IKK/NF-KB signaling is required for diet-induced obesity and hypothalamic inflammation. Mol Metab [Internet]. 2017;6(4):366–73. Available from: http://dx.doi.org/10.1016/j.molmet.2017.01.010

217. Fiacco TA, McCarthy KD. Multiple lines of evidence indicate that gliotransmission does not occur under physiological conditions. J Neurosci. 2018;38(1):3–13.

218. Gao Y, Layritz C, Legutko B, Eichmann TO, Laperrousaz E, Moullé VS, et al. Disruption of lipid uptake in astroglia exacerbates diet-induced obesity. Diabetes.

2017;

219. Yang L, Qi Y, Yang Y. Astrocytes Control Food Intake by Inhibiting AGRP Neuron Activity via Adenosine A<inf>1</inf> Receptors. Cell Rep [Internet]. 2015;11(5):798–807. Available from: http://dx.doi.org/10.1016/j.celrep.2015.04.002

220. Hidalgo J, Florit S, Giralt M, Ferrer B, Keller C, Pilegaard H. Transgenic mice with astrocyte-targeted production of interleukin-6 are resistant to high-fat diet-induced increases in body weight and body fat. Brain Behav Immun [Internet]. 2010;24(1):119–26. Available from: http://dx.doi.org/10.1016/j.bbi.2009.09.002

221. Choi I, Rickert E, Fernandez M, Webster NJG. SIRT1 in astrocytes regulates glucose metabolism and reproductive function. Endocrinology. 2019;160(6):1547–60.

222. Milanova I V, Kalsbeek MJT, Wang XL, Korpel NL, Stenvers DJ, Wolff SEC, et al. Diet-induced obesity disturbs microglial immunometabolism in a time-of-day manner. Front Endocrinol (Lausanne). 2019;10(JUN):1–14.

223. Marschallinger J, Iram T, Zardeneta M, Lee SE, Lehallier B, Haney MS, et al. Lipid-droplet-accumulating microglia represent a dysfunctional and proinflammatory state in the aging brain. Nat Neurosci [Internet]. 2020;23(2):194–208. Available from: http://dx.doi.org/10.1038/s41593-019-0566-1

224. Tsai S, Wu H, Chen P, Chen Y, Yu M, Wang T, et al. High-fat diet suppresses the astrocytic process arborization and downregulates the glial glutamate transporters in the hippocampus of mice. Brain Res [Internet]. 2018;1700:66–77. Available from: https://doi.org/10.1016/j.brainres.2018.07.017

225. Papa M, De Luca C, Petta F, Alberghina L, Cirillo G. Astrocyte-neuron interplay in maladaptive plasticity. Neurosci Biobehav Rev [Internet]. 2014;42:35–54. Available from: http://dx.doi.org/10.1016/j.neubiorev.2014.01.010

226. Robb JL, Hammad NA, Weightman Potter PG, Chilton JK, Beall C, Ellacott KLJ. The metabolic response to inflammation in astrocytes is regulated by nuclear factor-kappa B signaling. Glia. 2020;

227. Lavisse S, Guillermier M, Herard AS, Petit F, Delahaye M, Van Camp N, et al. Reactive Astrocytes Overexpress TSPO and Are Detected by TSPO Positron Emission Tomography Imaging. J Neurosci. 2012;32(32):10809–18.

228. Beckers L, Ory D, Geric I, Declercq L, Koole M, Kassiou M, et al. Increased Expression of Translocator Protein (TSPO) Marks Pro-inflammatory Microglia but Does Not Predict Neurodegeneration. Mol Imaging Biol. 2018;20(1):94–102.

229. Chen M-KK, Guilarte TR. Translocator protein 18 kDa (TSPO): Molecular sensor of brain injury and repair. Pharmacol Ther [Internet]. 2008;118(1):1–17. Available from: http://www.pubmedcentral.nih.gov/articlerender.fcgi?artid=2453598&tool=pmcentrez&rendertype=abstract

230. Barron AM, Garcia-segura LM, Caruso D, Jayaraman A, Lee W, Melcangi RC, et al. model of Alzheimer ' s disease. 2013;33(20):8891–7.

231. Daugherty DJ, Selvaraj V, Chechneva O V., Liu XB, Pleasure DE, Deng W. A TSPO ligand is protective in a mouse model of multiple sclerosis. EMBO Mol Med. 2013;5(6):891–903.

232. Li M, Ren H, Sheth KN, Shi F-D, Liu Q. A TSPO ligand attenuates brain injury after intracerebral hemorrhage. FASEB J [Internet]. 2017;(8):fj.201601377RR.

Available from: http://www.fasebj.org/lookup/doi/10.1096/fj.201601377RR

233. Christensen A, Pike CJ. TSPO ligand PK11195 improves Alzheimer-related outcomes in aged female 3xTg-AD mice. Neurosci Lett. 2018;683(April):7–12.

234. Arbo BD, Ribeiro MF, Garcia-Segura LM. Development of new treatments for Alzheimer's disease based on the modulation of translocator protein (TSPO) [Internet]. Vol. 54, Ageing Research Reviews. Elsevier; 2019. p. 100943. Available from: https://doi.org/10.1016/j.arr.2019.100943

235. Tonon M, Vaudry H, Chuquet J, Guillebaud F, Fan J, Masmoudi-Kouki O, et al. Endozepines and their receptors: Structure, functions and pathophysiological significance. Pharmacol Ther [Internet]. 2019; Available from: https://doi.org/10.1016/j.pharmthera.2019.06.008

236. Li H, Papadopoulos V. Peripheral-type benzodiazepine receptor function in cholesterol transport. Identification of a putative cholesterol recognition/interaction amino acid sequence and consensus pattern. Endocrinology. 1998;

237. Li H. Cholesterol binding at the cholesterol recognition/ interaction amino acid consensus (CRAC) of the peripheral-type benzodiazepine receptor and inhibition of steroidogenesis by an HIV TAT-CRAC peptide. Vol. 98, Proceedings of the National Academy of Sciences. 2001. p. 1267–72.

238. Murail S, Robert JC, Coïc YM, Neumann JM, Ostuni MA, Yao ZX, et al. Secondary and tertiary structures of the transmembrane domains of the translocator protein TSPO determined by NMR. Stabilization of the TSPO tertiary fold upon ligand binding. Biochim Biophys Acta - Biomembr [Internet]. 2008 [cited 2020 Jun 28];1778(6):1375–81. Available from: https://pubmed.ncbi.nlm.nih.gov/18420025/

239. Jaipuria G, Leonov A, Giller K, Vasa SK, Jaremko Ł, Jaremko M, et al. Cholesterol-mediated allosteric regulation of the mitochondrial translocator protein structure. Nat Commun [Internet]. 2017;8:14893. Available from: http://www.nature.com/doifinder/10.1038/ncomms14893

240. McNeela AM, Bernick C, Hines RM, Hines DJ. TSPO regulation in reactive gliotic diseases. J Neurosci Res. 2018;96(6):978–88.

241. Iatmanen-Harbi S, Senicourt L, Papadopoulos V, Lequin O, Lacapere JJ. Characterization of the high-affinity drug ligand binding site of mouse recombinant TSPO. Int J Mol Sci. 2019;20(6).

242. Delavoie F, Li H, Hardwick M, Robert JC, Giatzakis C, Péranzi G, et al. In vivo and in vitro peripheral-type benzodiazepine receptor polymerization: Functional significance in drug ligand and cholesterol binding. Biochemistry. 2003;42(15):4506–19.

243. Owen DR, Fan J, Campioli E, Venugopal S, Midzak A, Daly E, et al. *TSPO* mutations in rats and a human polymorphism impair the rate of steroid synthesis. Biochem J [Internet]. 2017;474(23):3985–99. Available from: http://biochemj.org/lookup/doi/10.1042/BCJ20170648

244. Berroterán-Infante N, Tadić M, Hacker M, Wadsak W, Mitterhauser M. Binding affinity of some endogenous and synthetic TSPO ligands regarding the rs6971 polymorphism. Int J Mol Sci. 2019;20(3).

245. Mcenery MW, Snowman AM, Trifiletti RR, Snyder SH, Trifiletti RR. Isolation of the mitochondrial benzodiazepine receptor: association with the voltage-dependent anion channel and the adenine nucleotide carrier. Proc Natl Acad Sci U S A [Internet]. 1992;89(8):3170–4. Available from:

http://www.ncbi.nlm.nih.gov/pubmed/1373486%5Cnhttp://www.pubmedcentral.nih.gov/articlerender.fcgi?artid=PMC48827

246. Hanukoglu I. Steroidogenic enzymes: Structure, function, and role in regulation of steroid hormone biosynthesis. J Steroid Biochem Mol Biol [Internet]. 1992 Dec 1 [cited 2020 Jun 29];43(8):779–804. Available from: https://linkinghub.elsevier.com/retrieve/pii/0960076092903075

247. Papadopoulos V, Amri H, Boujrad N, Cascio C, Culty M, Garnier M, et al. Peripheral benzodiazepine receptor in cholesterol transport and steroidogenesis. In: Steroids. 1997. p. 21–8.

248. Wiers CE, Martins De Carvalho L, Hodgkinson CA, Schwandt M, Kim SW, Diazgranados N, et al. TSPO polymorphism in individuals with alcohol use disorder: Association with cholesterol levels and withdrawal severity. Addict Biol. 2019;(September):1–8.

249. Verma A, Nye JS, Snyder SH. Porphyrins are endogenous ligands for the mitochondrial (peripheral-type) benzodiazepine receptor. Proc Natl Acad Sci. 1987;

250. Yeliseev AA, Kaplan S. A sensory transducer homologous to the mammalian peripheral-type benzodiazepine receptor regulates photosynthetic membrane complex formation in Rhodobacter sphaeroides 2.4.1. J Biol Chem. 1995 Sep;270(36):21167–75.

251. Taketani, S., Kohno, H., Furukawa, T. and Tokunaga R. Involvement Intracellular of Peripheral-Type Transport of Heme Benzodiazepine and Porphyrins1 Receptors in the of drugs prescribed to treat patients with anxiety , convul central-type receptors are coupled to GABA receptors , located on neurons while the. J Biochem. 1995;880:875–80.

252. Frank W, Baar KM, Qudeimat E, Woriedh M, Alawady A, Ratnadewi D, et al. A mitochondrial protein homologous to the mammalian peripheral-type benzodiazepine receptor is essential for stress adaptation in plants. Plant J. 2007;

253. Wang JKT, Morgan JI, Spector S. Differentiation of Friend erythroleukemia cells induced by benzodiazepines. Proc Natl Acad Sci U S A [Internet]. 1984 [cited 2020 Jun 29];81(12 I):3770–2. Available from: /pmc/articles/PMC345301/?report=abstract

254. Taketani S, Kohno H, Okuda M, Furukawa T, Tokunaga R. Induction of peripheral-type benzodiazepine receptors during differentiation of mouse erythroleukemia cells. A possible involvement of these receptors in heme biosynthesis. J Biol Chem. 1994;

255. Zhao AH, Tu LN, Mukai C, Sirivelu MP, Pillai V V, Morohaku K, et al. Mitochondrial translocator protein (TSPO) function is not essential for heme biosynthesis. J Biol Chem. 2016;291(4):1591–603.

256. Huang H, Atshaves BP, Frolov A, Kier AB, Schroeder F. Acyl-coenzyme A binding protein expression alters liver fatty acyl-coenzyme A metabolism. Biochemistry. 2005;

257. Lanfray D, Arthaud S, Ouellet J, Compère V, Do Rego JL, Leprince J, et al. Gliotransmission and brain glucose sensing critical role of endozepines. Diabetes. 2013;62(3):801–10.

258. do Rego J-CC, Orta M-HH, Leprince JJ, Tonon M-CC, Vaudry H, Costentin J. Pharmacological characterization of the receptor mediating the anorexigenic action of the octadecaneuropeptide: Evidence for an endozepinergic tone

regulating food intake. Neuropsychopharmacology [Internet]. 2006;32(7):1641–8. Available from: http://dx.doi.org/10.1038/sj.npp.1301280%5Cnhttp://www.nature.com/npp/journal/v32/n7/full/1301280a.html

259. Bravo-San Pedro JM, Sica V, Martins I, Anagnostopoulos G, Maiuri C, Kroemer G. Cell-autonomous, paracrine and neuroendocrine feedback regulation of autophagy by DBI/ACBP (diazepam binding inhibitor, acyl-CoA binding protein): the obesity factor [Internet]. Vol. 15, Autophagy. Taylor & Francis; 2019. p. 2036–8. Available from: https://doi.org/10.1080/15548627.2019.1662585

260. Burton M, Rose TM, Færgeman NJ, Knudsen J. Evolution of the acyl-CoA binding protein (ACBP). Biochem J. 2005;

261. Færgeman NJ, Wadum M, Feddersen S, Burton M, Kragelund BB, Knudsen J. Acyl-CoA binding proteins; structural and functional conservation over 2000 MYA. Mol Cell Biochem. 2007;

262. Compère V, Lanfray D, Castel H, Morin F, Leprince J, Dureuil B, et al. Acute food deprivation reduces expression of diazepam-binding inhibitor, the precursor of the anorexigenic octadecaneuropeptide ODN, in mouse glial cells. J Mol Endocrinol. 2010;44(5):295–9.

263. Garcia de Mateos-Verchere J, Leprince J, Tonon MC, Vaudry H, Costentin J. The octadecaneuropeptide [diazepam-binding inhibitor (33-50)] exerts potent anorexigenic effects in rodents. Eur J Pharmacol. 2001;414(2–3):225–31.

264. Slobodyansky E, Guidotti A, Wambebe C, Berkovich A, Costa E. Isolation and Characterization of a Rat Brain Triakontatetraneuropeptide, a Posttranslational Product of Diazepam Binding Inhibitor: Specific Action at the Ro 5- 4864 Recognition Site. J Neurochem. 1989;

265. Lesouhaitier O, Feuilloley M, Vaudry H. Effect of the triakontatetraneuropeptide (TTN) on corticosteroid secretion by the frog adrenal gland. J Mol Endocrinol. 1998;

266. Papadopoulos V, Berkovich A, Krueger KE, Costa E, Guidotti A. Diazepam binding inhibitor and its processing products stimulate mitochondrial steroid biosynthesis via an interaction with mitochondrial benzodiazepine receptor. Endocrinology. 1991;

267. Taupin V, Herbelin A, Descamps-Latscha B, Zavala F. Endogenous anxiogenic peptide, ODN-diazepam-binding inhibitor, and benzodiazepines enhance the production of interleukin-1 and tumor necrosis factor by human monocytes. Lymphokine Cytokine Res. 1991;

268. Taupin V, Gogusev J, Descamps-Latscha B, Zavala F. Modulation of tumor necrosis factor-α, interleukin-1β, interleukin-6, interleukin-8, and granulocyte/macrophage colony-stimulating factor expression in human monocytes by an endogenous anxiogenic benzodiazepine ligand, triakontatetraneuropeptide: Evidence. Mol Pharmacol. 1993;

269. St e ̨pień H, Agro A, Crossley J, Padol I, Richards C, Stanisz A. Immunomodulatory properties of diazepam-binding inhibitor: Effect on human interleukin-6 secretion, lymphocyte proliferation and natural killer cell activity in vitro. Neuropeptides. 1993;

270. Richards EM, Zanotti-Fregonara P, Fujita M, Newman L, Farmer C, Ballard ED, et al. PET radioligand binding to translocator protein (TSPO) is increased in unmedicated depressed subjects. EJNMMI Res. 2018;8.

271. Scaini G, Barichello T, Fries GR, Kennon EA, Andrews T, Nix BR, et al. TSPO

upregulation in bipolar disorder and concomitant downregulation of mitophagic proteins and NLRP3 inflammasome activation. Neuropsychopharmacology. 2019 Jun 1;44(7):1291–9.

272. Attwells S, Setiawan E, Wilson AA, Rusjan PM, Mizrahi R, Miler L, et al. Inflammation in the neurocircuitry of obsessive-compulsive disorder. JAMA Psychiatry. 2017;74(8):833–40.

273. Attwells S, Setiawan E, Rusjan PM, Xu C, Hutton C, Rafiei D, et al. Translocator Protein Distribution Volume Predicts Reduction of Symptoms During Open-Label Trial of Celecoxib in Major Depressive Disorder. Biol Psychiatry. 2020 Mar 29;1–8.

274. Notter T, Coughlin JM, Gschwind T, Weber-Stadlbauer U, Wang Y, Kassiou M, et al. Translational evaluation of translocator protein as a marker of neuroinflammation in schizophrenia. Mol Psychiatry [Internet]. 2018;23(2):323–34. Available from: http://dx.doi.org/10.1038/mp.2016.248

275. Schifani C, Hafizi S, Tseng H-H, Gerritsen C, Kenk M, Wilson AA, et al. Preliminary data indicating a connection between stress-induced prefrontal dopamine release and hippocampal TSPO expression in the psychosis spectrum. Schizophr Res [Internet]. 2019 Nov 1 [cited 2020 Feb 27];213:80–6. Available from: http://www.ncbi.nlm.nih.gov/pubmed/30409695

276. Plavén-Sigray P, Cervenka S. Erratum: Meta-analytic studies of the glial cell marker TSPO in psychosis - a question of apples and pears?: A commentary on “Neuroinflammation in schizophrenia: metaanalysis of in-vivo microglial imaging” by Marques et al. - ERRATUM (Psychological medici. Vol. 49, Psychological medicine. 2019. p. 1583–4.

277. Hillmer AT, Sandiego CM, Hannestad J, Angarita GA, Kumar A, McGovern EM, et al. In vivo imaging of translocator protein, a marker of activated microglia, in alcohol dependence. Mol Psychiatry [Internet]. 2017;(December 2016):1–8. Available from: http://www.nature.com/doifinder/10.1038/mp.2017.10

278. Kohno M, Link J, Dennis LE, McCready H, Huckans M, Hoffman WF, et al. Neuroinflammation in addiction: A review of neuroimaging studies and potential immunotherapies [Internet]. Vol. 179, Pharmacology Biochemistry and Behavior. Elsevier Inc; 2019. p. 34–42. Available from: https://doi.org/10.1016/j.pbb.2019.01.007

279. Shehadeh M, Palzur E, Apel L, Soustiel JF. Reduction of Traumatic Brain Damage by Tspo Ligand Etifoxine. Int J Mol Sci. 2019;20(11).

280. Giatti S, Pesaresi M, Cavaletti G, Bianchi R, Carozzi V, Lombardi R, et al. Neuroprotective effects of a ligand of translocator protein-18kDa (Ro5-4864) in experimental diabetic neuropathy. Neuroscience [Internet]. 2009;164(2):520–9. Available from: http://dx.doi.org/10.1016/j.neuroscience.2009.08.005

281. Ma L, Zhang H, Liu N, Wang P qi, Guo W zhi, Fu Q, et al. TSPO ligand PK11195 alleviates neuroinflammation and beta-amyloid generation induced by systemic LPS administration. Brain Res Bull. 2016;121:192–200.

282. Costa B, Cavallini C, Da Pozzo E, Taliani S, Da Settimo F, Martini C. The Anxiolytic Etifoxine Binds to TSPO Ro5-4864 Binding Site with Long Residence Time Showing a High Neurosteroidogenic Activity. ACS Chem Neurosci. 2017;8(7):1448–54.

283. Tu LN, Zhao AH, Stocco DM, Selvaraj V. PK11195 effect on steroidogenesis is not mediated through the translocator protein (TSPO). Endocrinology. 2015;156(3):1033–9.

284. Betlazar C, Harrison-Brown M, Middleton RJ, Banati R, Liu GJ. Cellular sources and regional variations in the expression of the neuroinflammatory marker translocator protein (TSPO) in the normal brain. Int J Mol Sci. 2018;19(9).

285. Leaver KR, Reynolds A, Bodard S, Guilloteau D, Chalon S, Kassiou M. Effects of translocator protein (18 kDa) ligands on microglial activation and neuronal death in the quinolinic-acid-injected rat striatum. ACS Chem Neurosci. 2012;3(2):114–9.

286. Bae KR, Shim HJ, Balu D, Kim SR, Yu SW. Translocator protein 18 kDa negatively regulates inflammation in microglia. J Neuroimmune Pharmacol. 2014;9(3):424–37.

287. Liu GJ, Middleton RJ, Hatty CR, Kam WWY, Chan R, Pham T, et al. The 18 kDa translocator protein, microglia and neuroinflammation. Brain Pathol. 2014;24(6):631–53.

288. Rodríguez-chinchilla T, Quiroga-varela A, Molinet-dronda F. [18 F] -DPA-714 PET as a specific in vivo marker of early microglial activation in a rat model of progressive dopaminergic degeneration. 2020;

289. Yamagishi S, Iga Y, Nakamura M, Takizawa C, Fukumoto D, Kakiuchi T, et al. Upregulation of cannabinoid receptor type 2, but not TSPO, in senescence-accelerated neuroinflammation in mice: A positron emission tomography study. J Neuroinflammation. 2019 Nov 10;16(1):1–10.

290. Da Pozzo E, Tremolanti C, Costa B, Giacomelli C, Milenkovic VM, Bader S, et al. Microglial pro-inflammatory and anti-inflammatory phenotypes are modulated by translocator protein activation. Int J Mol Sci. 2019;20(18):1–21.

291. Azrad M, Zeineh N, Weizman A, Veenman L, Gavish M. The TSPO ligands 2-CL-MGV-1, MGV-1, and PK11195 differentially suppress the inflammatory response of BV-2 microglial cell to LPS. Int J Mol Sci. 2019;20(3):1–14.

292. Ryu JK, Choi HB, McLarnon JG. Peripheral benzodiazepine receptor ligand PK11195 reduces microglial activation and neuronal death in quinolinic acid-injected rat striatum. Neurobiol Dis. 2005;20(2):550–61.

293. Nack A, Brendel M, Nedelcu J, Daerr M, Nyamoya S, Beyer C, et al. Expression of Translocator Protein and [18F]-GE180 Ligand Uptake in Multiple Sclerosis Animal Models. Cells. 2019;8(2):94.

294. Cosenza-Nashat M, Zhao M, Suh H, Morgan J, Morgello S, Lee SC, et al. NIH Public Access. 2009;35(3):306–28.

295. Vlodavsky E, Soustiel JF. Immunohistochemical expression of peripheral benzodiazepine receptors in human astrocytomas and its correlation with grade of malignancy, proliferation, apoptosis and survival. J Neurooncol. 2007;81(1):1–7.

296. Lee JW, Nam H, Yu SW. Systematic analysis of translocator protein 18 kDa (TSPO) ligands on toll-like receptors-mediated pro-inflammatory responses in microglia and astrocytes. Exp Neurobiol. 2016;25(5):262–8.

297. Baez E, Guio-Vega GP, Echeverria V, Sandoval-Rueda DA, Barreto GE. 4′-Chlorodiazepam Protects Mitochondria in T98G Astrocyte Cell Line from Glucose Deprivation. Neurotox Res [Internet]. 2017 Aug 1 [cited 2020 Apr 23];32(2):163–71. Available from: http://link.springer.com/10.1007/s12640-017-9733-x

298. Veiga S, Carrero P, Pernia O, Azcoitia I, Garcia-Segura LM. Translocator protein (18 kDa) is involved in the regulation of reactive gliosis. Glia. 2007;55(14):1426–

36.

299. Palzur E, Sharon A, Shehadeh M, Soustiel JF. Investigation of the mechanisms of neuroprotection mediated by Ro5-4864 in brain injury. Neuroscience. 2016;

300. Notter T, Coughlin JM, Sawa A, Meyer U. Reconceptualization of translocator protein as a biomarker of neuroinflammation in psychiatry. Mol Psychiatry [Internet]. 2018;23(1):36–47. Available from: http://www.nature.com/doifinder/10.1038/mp.2017.232

301. Kim S, Kim N, Park S, Jeon Y, Lee J, Yoo SJ, et al. Tanycytic TSPO inhibition induces lipophagy to regulate lipid metabolism and improve energy balance. Autophagy [Internet]. 2019;0(0):1–21. Available from: https://doi.org/10.1080/15548627.2019.1659616

302. Notter T, Schalbetter SM, Clifton NE, Mattei D, Richetto J, Thomas K, et al. Neuronal activity increases translocator protein (TSPO) levels. Mol Psychiatry [Internet]. 2020; Available from: http://dx.doi.org/10.1038/s41380-020-0745-1

303. Biswas L, Farhan F, Reilly J, Bartholomew C, Shu X. TSPO ligands promote cholesterol efflux and suppress oxidative stress and inflammation in choroidal endothelial cells. Int J Mol Sci. 2018;19(12).

304. Brendel M, Focke C, Blume T, Peters F, Deussing M, Probst F, et al. Time Courses of Cortical Glucose Metabolism and Microglial Activity Across the Life-Span of Wild-Type Mice: A PET Study. J Nucl Med [Internet]. 2017;58(0):1984–90. Available from: http://jnm.snmjournals.org/lookup/doi/10.2967/jnumed.117.195107

305. Wang HJ, Fan J, Papadopoulos V. Translocator protein (Tspo) gene promoter-driven green fluorescent protein synthesis in transgenic mice: An in vivo model to study Tspo transcription. Cell Tissue Res. 2012 Nov;350(2):261–75.

306. Selvaraj V, Stocco DM, Tu LN. Minireview: Translocator Protein (TSPO) and Steroidogenesis: A Reappraisal. Mol Endocrinol [Internet]. 2015;29(4):490–501. Available from: http://press.endocrine.org/doi/10.1210/me.2015-1033

307. Gut P, Zweckstetter M, Banati RB. Lost in translocation: The functions of the 18-kD translocator protein. Trends Endocrinol Metab [Internet]. 2015;26(7):349–56. Available from: http://dx.doi.org/10.1016/j.tem.2015.04.001

308. Hirsch JD. Pharmacological and physiological properties of benzodiazepine binding sites in rodent brown adipose tissue. Comp Biochem Physiol Part C, Comp. 1984;77(2):339–43.

309. Gonzalez Solveyra C, Romeo HE, Rosenstein RE, Estevez AG, Cardinali DP. Benzodiazepine binding sites in rat interscapular brown adipose tissue: effect of cold environment, denervation and endocrine ablations. Life Sci [Internet]. 1988 [cited 2020 Apr 3];42(4):393–402. Available from: http://www.ncbi.nlm.nih.gov/pubmed/2828790

310. Thompson MM, Manning HC, Ellacott KLJ. Translocator protein 18 kDa (TSPO) is regulated in white and brown adipose tissue by obesity. PLoS One. 2013;8(11):1–10.

311. Li J, Papadopoulos V. Translocator protein (18 kDa) as a pharmacological target in adipocytes to regulate glucose homeostasis. Biochem Pharmacol [Internet]. 2015;97(1):99–110. Available from: http://dx.doi.org/10.1016/j.bcp.2015.06.020

312. Hartimath S V, Khanapur S, Boominathan R, Jiang L, Cheng P, Yong FF, et al. Imaging adipose tissue browning using the TSPO-18kDa tracer [18F]FEPPA. Mol Metab [Internet]. 2019;25:154–8. Available from:

https://doi.org/10.1016/j.molmet.2019.05.003

313. Sileikyte J, Blachly-Dyson E, Sewell R, Carpi A, Menabo R, Di Lisa F, et al. Regulation of the Mitochondrial Permeability Transition Pore by the Outer Membrane Does Not Involve the Peripheral Benzodiazepine Receptor (Translocator Protein of 18 kDa (TSPO)). J Biol Chem. 2014;289(20):13769–81.

314. Thai PN, Daugherty DJ, Frederich BJ, Lu X, Deng W, Bers DM, et al. Cardiac-specific Conditional Knockout of the 18-kDa Mitochondrial Translocator Protein Protects from Pressure Overload Induced Heart Failure. Sci Rep [Internet]. 2018;8(1):1–17. Available from: http://dx.doi.org/10.1038/s41598-018-34451-2

315. Thackeray JT, Hupe HC, Wang Y, Bankstahl JP, Berding G, Ross TL, et al. Myocardial Inflammation Predicts Remodeling and Neuroinflammation After Myocardial Infarction. J Am Coll Cardiol. 2018;71(3):263–75.

316. Ilkan Z, Akar FG. The mitochondrial translocator protein and the emerging link between oxidative stress and arrhythmias in the diabetic heart. Vol. 9, Frontiers in Physiology. 2018. p. 1–8.

317. Gut P. Targeting mitochondrial energy metabolism with TSPO ligands. Biochem Soc Trans [Internet]. 2015;43(4):537–42. Available from: http://biochemsoctrans.org/lookup/doi/10.1042/BST20150019

318. Narayan N, Mandhair H, Smyth E, Dakin SG, Kiriakidis S, Wells L, et al. The macrophage marker translocator protein (TSPO) is down-regulated on pro-inflammatory 'M1' human macrophages. PLoS One [Internet]. 2017;12(10):1–19. Available from: http://dx.doi.org/10.1371/journal.pone.0185767

319. Zhou D, Ji L, Chen Y. TSPO Modulates IL-4-Induced Microglia/Macrophage M2 Polarization via PPAR-γ Pathway. J Mol Neurosci. 2019;

320. Wu L pan, Gong Z fan, Wang H, Zhou Z shu, Zhang M ming, Liu C, et al. TSPO ligands prevent the proliferation of vascular smooth muscle cells and attenuate neointima formation through AMPK activation. Acta Pharmacol Sin [Internet]. 2020 Jan 1 [cited 2020 Aug 2];41(1):34–46. Available from: https://pubmed.ncbi.nlm.nih.gov/31515530/

321. Caridis AM, Lightbody RJ, Tarlton JMR, Dolan S, Graham A. Genetic obesity increases pancreatic expression of mitochondrial proteins which regulate cholesterol efflux in BRIN-BD11 insulinoma cells. Biosci Rep. 2019;39(3).

322. Tu LN, Morohaku K, Manna PR, Pelton SH, Butler WR, Stocco DM, et al. Peripheral benzodiazepine receptor/translocator protein global knock-out mice are viable with no effects on steroid hormone biosynthesis. J Biol Chem. 2014;289(40):27444–54.

323. Šileikyte J, Blachly-Dyson E, Sewell R, Carpi A, Menabò R, Di Lisa F, et al. Regulation of the mitochondrial permeability transition pore by the outer membrane does not involve the peripheral benzodiazepine receptor (translocator protein of 18 kDa (TSPO)). J Biol Chem. 2014;289(20):13769–81.

324. Liu GJ, Middleton RJ, Kam WWY, Chin DY, Hatty CR, Chan RHY, et al. Functional gains in energy and cell metabolism after TSPO gene insertion. Cell Cycle [Internet]. 2017;16(5):436–47. Available from: http://dx.doi.org/10.1080/15384101.2017.1281477

325. Banati RB, Middleton RJ, Chan R, Hatty CR, Kam WW-Y, Quin C, et al. Positron emission tomography and functional characterization of a complete PBR/TSPO knockout. Nat Commun [Internet]. 2014;5:5452. Available from: http://www.pubmedcentral.nih.gov/articlerender.fcgi?artid=4263137&tool=pmcentrez&rendertype=abstract

326. Fu Y, Wang D, Wang H, Cai M, Li C, Zhang X, et al. TSPO deficiency induces mitochondrial dysfunction, leading to hypoxia, angiogenesis, and a growth-promoting metabolic shift toward glycolysis in glioblastoma. Neuro Oncol. 2020;

327. Milenkovic VM, Slim D, Bader S, Koch V, Heinl ES, Alvarez-Carbonell D, et al. CRISPR-cas9 mediated TSPO gene knockout alters respiration and cellular metabolism in human primary microglia cells. Int J Mol Sci. 2019;20(13).

328. Da Pozzo E, Giacomelli C, Costa B, Cavallini C, Taliani S, Barresi E, et al. TSPO PIGA Ligands Promote Neurosteroidogenesis and Human Astrocyte Well-Being. Int J Mol Sci. 2016;17(7).

329. Bader S, Wolf L, Milenkovic VM, Gruber M, Nothdurfter C, Rupprecht R, et al. Differential effects of TSPO ligands on mitochondrial function in mouse microglia cells. Psychoneuroendocrinology. 2019;106(November 2018):65–76.

330. Tu LN, Zhao AH, Hussein M, Stocco DM, Selvaraj V. Translocator protein (TSPO) affects mitochondrial fatty acid oxidation in steroidogenic cells. Endocrinology. 2016;157(3):1110–21.

331. Gong Z, Han Y, Wu L, Xia T, Ren H, Yang D, et al. Translocator protein 18 kDa ligand alleviates neointimal hyperplasia in the diabetic rat artery injury model via activating PKG. Life Sci [Internet]. 2019 Mar 15 [cited 2020 May 17];221(February):72–82. Available from: https://doi.org/10.1016/j.lfs.2019.02.015

332. Alamri A, Biswas L, Watson DG, Shu X. Deletion of TSPO resulted in change of metabolomic profile in retinal pigment epithelial cells. Int J Mol Sci. 2019;20(6).

333. Ran C, Albrecht DS, Bredella MA, Yang J, Yang J, Liang SH, et al. PET Imaging of Human Brown Adipose Tissue with the TSPO Tracer [11C]PBR28. Mol Imaging Biol [Internet]. 2018 Apr 1 [cited 2020 Apr 3];20(2):188–93. Available from: http://www.ncbi.nlm.nih.gov/pubmed/28983743

334. Calevro A, Cotel MC, Natesan S, Modo M, Vernon AC, Mondelli V. Effects of chronic antipsychotic drug exposure on the expression of Translocator Protein and inflammatory markers in rat adipose tissue. Psychoneuroendocrinology. 2018 Sep 1;95:28–33.

335. Campioli E, Carnevale G, Avallone R, Guerra D, Baraldi M. Morphological and Receptorial Changes in the Epididymal Adipose Tissue of Rats Subjected to a Stressful Stimulus. 2011 [cited 2020 Apr 3]; Available from: www.obesityjournal.org

336. Han HS, Kang G, Kim JS, Choi BH, Koo SH. Regulation of glucose metabolism from a liver-centric perspective [Internet]. Vol. 48, Experimental and Molecular Medicine. Nature Publishing Group; 2016 [cited 2020 Jul 6]. p. e218. Available from: /pmc/articles/PMC4892876/?report=abstract

337. Wang X, Cai B, Yang X, Tontonoz P, Schwabe RF, Tabas I, et al. Cholesterol Stabilizes TAZ in Hepatocytes to Promote Experimental Non-alcoholic Article Cholesterol Stabilizes TAZ in Hepatocytes to Promote Experimental Non-alcoholic Steatohepatitis. Cell Metab [Internet]. 2020;1–18. Available from: https://doi.org/10.1016/j.cmet.2020.03.010

338. Kraus-Friedmann N. Hormonal regulation of hepatic gluconeogenesis [Internet]. Vol. 64, Physiological Reviews. Physiol Rev; 1984 [cited 2020 Aug 2]. p. 170–259. Available from: https://pubmed.ncbi.nlm.nih.gov/6141578/

339. Bercovici JP, Mauvais-Jarvis P. [The liver and hormonal steroids. Physiological and pathological problems]. Pathol Biol (Paris) [Internet]. 1972 Mar [cited 2020 Aug 2];20(5):305–14. Available from:

http://www.ncbi.nlm.nih.gov/pubmed/4556215

340. Hue L. [Hormonal control of liver gluconeogenesis]. Rev Can Biol Exp [Internet]. 1982 Mar [cited 2020 Aug 2];41(1):73–6. Available from: http://www.ncbi.nlm.nih.gov/pubmed/6285426

341. Panickar KS, Jayakumar AR, Rama Rao K V., Norenberg MD. Downregulation of the 18-kDa translocator protein: Effects on the ammonia-induced mitochondrial permeability transition and cell swelling in cultured astrocytes. Glia [Internet]. 2007 Dec 1 [cited 2020 Apr 21];55(16):1720–7. Available from: http://doi.wiley.com/10.1002/glia.20584

342. Lin Y-MM, Sun H-YY, Chiu W-TT, Su H-CC, Chien Y-CC, Chang H-CCH-AA, et al. Etifoxine, a TSPO Ligand, Worsens Hepatitis C-Related Insulin Resistance but Relieves Lipid Accumulation. Biomed Res Int. 2019;2019.

343. Xie L, Yui J, Hatori A, Yamasaki T, Kumata K, Wakizaka H, et al. Translocator protein (18 kDa), a potential molecular imaging biomarker for non-invasively distinguishing non-alcoholic fatty liver disease. J Hepatol. 2012 Nov 1;57(5):1076–82.

344. Hatori A, Yui J, Xie L, Kumata K, Yamasaki T, Fujinaga M, et al. Utility of translocator protein (18 kDa) as a molecular imaging biomarker to monitor the progression of liver fibrosis. Sci Rep. 2015 Nov 27;5.

345. Dimitrova-Shumkovska J, Veenman L, Ristoski T, Leschiner S, Gavish M. Chronic high fat, high cholesterol supplementation decreases 18 kDa Translocator Protein binding capacity in association with increased oxidative stress in rat liver and aorta. Food Chem Toxicol. 2010 Mar 1;48(3):910–21.

346. Nothdurfter C, Baghai TC, Schüle C, Rupprecht R. Translocator protein (18 kDa) (TSPO) as a therapeutic target for anxiety and neurologic disorders. Eur Arch Psychiatry Clin Neurosci. 2012;262(2 SUPPL.).

347. Gut P, Baeza-Raja B, Andersson O, Hasenkamp L, Hsiao J, Hesselson D, et al. Whole-organism screening for gluconeogenesis identifies activators of fasting metabolism. Nat Chem Biol. 2013;9(2):97–104.

348. Taylor JMW, Allen AM, Graham A. Targeting mitochondrial 18 kDa translocator protein (TSPO) regulates macrophage cholesterol efflux and lipid phenotype. Clin Sci. 2014 Nov 1;127(10):603–13.

349. de Vinci Kanda Kupa L, Drewes CC, Barioni ED, Neves CL, Sampaio SC, Farsky SHP. Role of translocator 18 KDa ligands in the activation of leukotriene B4 activated G-protein coupled receptor and toll like receptor-4 pathways in neutrophils. Front Pharmacol. 2017;

350. Owen DR, Narayan N, Wells L, Healy L, Smyth E, Rabiner EA, et al. Pro-inflammatory activation of primary microglia and macrophages increases 18 kDa translocator protein expression in rodents but not humans. J Cereb Blood Flow Metab. 2017;37(8):2679–90.

351. Shapouri-Moghaddam A, Mohammadian S, Vazini H, Taghadosi M, Esmaeili SA, Mardani F, et al. Macrophage plasticity, polarization, and function in health and disease [Internet]. Vol. 233, Journal of Cellular Physiology. Wiley-Liss Inc.; 2018 [cited 2020 Aug 2]. p. 6425–40. Available from: https://pubmed.ncbi.nlm.nih.gov/29319160/

352. Yao R, Pan R, Shang C, Li X, Cheng J, Xu J, et al. Translocator Protein 18 kDa (TSPO) Deficiency Inhibits Microglial Activation and Impairs Mitochondrial Function. Front Pharmacol. 2020;11(June):1–10.

353. Van Der Laken CJ, Elzinga EH, Kropholler MA, Molthoff CFM, Van Der Heijden JW, Maruyama K, et al. Noninvasive imaging of macrophages in rheumatoid synovitis using 11C-(R)-PK11195 and positron emission tomography. Arthritis Rheum. 2008 Nov;58(11):3350–5.

354. Horiguchi Y, Ohta N, Yamamoto S, Koide M, Fujino Y. Midazolam suppresses the lipopolysaccharide-stimulated immune responses of human macrophages via translocator protein signaling. Int Immunopharmacol [Internet]. 2019;66(March 2018):373–82. Available from: https://doi.org/10.1016/j.intimp.2018.11.050

355. Ghosh S. Macrophage cholesterol homeostasis and metabolic diseases: Critical role of cholesteryl ester mobilization. Vol. 9, Expert Review of Cardiovascular Therapy. NIH Public Access; 2011. p. 329–40.

356. Adamson S, Leitinger N. Phenotypic modulation of macrophages in response to plaque lipids. Vol. 22, Current Opinion in Lipidology. 2011. p. 335–42.

357. Graham A. Mitochondrial regulation of macrophage cholesterol homeostasis [Internet]. Vol. 89, Free Radical Biology and Medicine. Elsevier; 2015. p. 982–92. Available from: http://dx.doi.org/10.1016/j.freeradbiomed.2015.08.010

358. Lecanu L, Yao ZX, McCourty A, Sidahmed EK, Orellana ME, Burnier MN, et al. Control of hypercholesterolemia and atherosclerosis using the cholesterol recognition/interaction amino acid sequence of the translocator protein TSPO. Steroids [Internet]. 2013 Feb [cited 2020 Apr 3];78(2):137–46. Available from: http://www.ncbi.nlm.nih.gov/pubmed/23182766

359. Fan J, Wang K, Zirkin B, Papadopoulos V. CRISPR/Cas9–Mediated tspo gene mutations lead to reduced mitochondrial membrane potential and steroid formation in MA-10 mouse tumor leydig cells. Endocrinology. 2018;159(2):1130–46.

360. Morohaku K, Pelton SH, Daugherty DJ, Butler WR, Deng W, Selvaraj V. Translocator protein/peripheral benzodiazepine receptor is not required for steroid hormone biosynthesis. Endocrinology. 2014;155(1):89–97.

361. Barron AM, Ji B, Kito S, Suhara T, Higuchi M. Steroidogenic abnormalities in translocator protein knockout mice and significance in the aging male. Biochem J [Internet]. 2017;BCJ20170645. Available from: http://www.ncbi.nlm.nih.gov/pubmed/29127254%0Ahttp://biochemj.org/lookup/doi/10.1042/BCJ20170645

362. Fan J, Campioli E, Midzak A, Culty M, Papadopoulos V. Conditional steroidogenic cell-targeted deletion of TSPO unveils a crucial role in viability and hormone-dependent steroid formation. Proc Natl Acad Sci U S A. 2015;112(23):7261–6.

363. Fan J, Campioli E, Papadopoulos V. Nr5a1-Cre-mediated Tspo conditional knockout mice with low growth rate and prediabetes symptoms – A mouse model of stress diabetes. Biochim Biophys Acta - Mol Basis Dis [Internet]. 2019;1865(1):56–62. Available from: https://doi.org/10.1016/j.bbadis.2018.10.022

364. Falchi AM, Battetta B, Sanna F, Piludu M, Sogos V, Serra M, et al. Intracellular cholesterol changes induced by translocator protein (18 kDa) TSPO/PBR ligands. Neuropharmacology. 2007;53(2):318–29.

365. Giatti S, Diviccaro S, Garcia-Segura LM, Melcangi RC. Sex differences in the brain expression of steroidogenic molecules under basal conditions and after gonadectomy. J Neuroendocrinol. 2019;31(6):1–9.

366. Lane MD, Wolfgang M, Cha S-H, Dai Y. Regulation of food intake and energy expenditure by hypothalamic malonyl-CoA. Int J Obes (Lond) [Internet]. 2008;32:S49–54. Available from: http://www.nature.com/doifinder/10.1038/ijo.2008.123

367. De Souza CT, Araujo EP, Bordin S, Ashimine R, Zollner RL, Boschero AC, et al. Consumption of a fat-rich diet activates a proinflammatory response and induces insulin resistance in the hypothalamus. Endocrinology. 2005;146(10):4192–9.

368. Burda JE, Sofroniew M V. Reactive gliosis and the multicellular response to CNS damage and disease. Neuron [Internet]. 2014;81(2):229–48. Available from: http://dx.doi.org/10.1016/j.neuron.2013.12.034

369. Barron AM, Tokunaga M, Zhang MR, Ji B, Suhara T, Higuchi M. Assessment of neuroinflammation in a mouse model of obesity and β-amyloidosis using PET. J Neuroinflammation [Internet]. 2016;13(1):1–14. Available from: http://dx.doi.org/10.1186/s12974-016-0700-x

370. Gui Y, Marks JD, Das S, Hyman BT, Serrano- Pozo A. Characterization of the 18 kDa translocator protein (TSPO) expression in post- mortem normal and Alzheimer's disease brains. Brain Pathol. 2019;0–3.

371. Toye AA, Lippiat JD, Proks P, Shimomura K, Bentley L, Hugill A, et al. A genetic and physiological study of impaired glucose homeostasis control in C57BL/6J mice. Diabetologia. 2005 Apr;48(4):675–86.

372. Freeman HC, Hugill A, Dear NT, Ashcroft FM, Cox RD. Deletion of nicotinamide nucleotide transhydrogenase: A new quantitive trait locus accounting for glucose intolerance in C57BL/6J mice. Diabetes. 2006;

373. Huang TT, Naeemuddin M, Elchuri S, Yamaguchi M, Kozy HM, Carlson EJ, et al. Genetic modifiers of the phenotype of mice deficient in mitochondrial superoxide dismutase. Hum Mol Genet. 2006;

374. Nilsson C, Raun K, Yan FF, Larsen MO, Tang-Christensen M. Laboratory animals as surrogate models of human obesity [Internet]. Vol. 33, Acta Pharmacologica Sinica. Nature Publishing Group; 2012. p. 173–81. Available from: http://dx.doi.org/10.1038/aps.2011.203

375. Gong S, Zheng C, Doughty ML, Losos K, Didkovsky N, Schambra UB, et al. A gene expression atlas of the central nervous system based on bacterial artificial chromosomes. Nature. 2003;

376. Taniguchi H, He M, Wu P, Kim S, Paik R, Sugino K, et al. A Resource of Cre Driver Lines for Genetic Targeting of GABAergic Neurons in Cerebral Cortex. Neuron. 2011;

377. López-Bendito G, Sturgess K, Erdélyi F, Szabó G, Molnár Z, Paulsen O. Preferential origin and layer destination of GAD65-GFP cortical interneurons. Cereb Cortex. 2004;

378. Tspo Mouse Gene Details | translocator protein | International Mouse Phenotyping Consortium [Internet]. [cited 2021 Apr 5]. Available from: https://www.mousephenotype.org/data/genes/MGI:88222

379. Fan J, Campioli E, Sottas C, Zirkin B, Papadopoulos V. Amhr2-Cre-mediated global Tspo knockout. J Endocr Soc. 2020;4(February):1–29.

380. Van Den Pol AN, Yao Y, Fu LY, Foo K, Huang H, Coppari R, et al. Neuromedin B and Gastrin-releasing peptide excite arcuate nucleus neuropeptide y neurons in a novel transgenic mouse expressing strong renilla green fluorescent protein in NPY neurons. J Neurosci. 2009 Apr 8;29(14):4622–39.

381. Paxinos G, Franklin KBJ. The Mouse Brain in Stereotaxic Coordinates, 2nd edition. Academic Press. 2001.

382. Bradford MM. A rapid and sensitive method for the quantitation of microgram quantities of protein utilizing the principle of protein-dye binding. Anal Biochem. 1976;

383. Longair MH, Baker DA, Armstrong JD. Simple neurite tracer: Open source software for reconstruction, visualization and analysis of neuronal processes. Bioinformatics. 2011;

384. Sholl DA. The organization of the visual cortex in the cat. J Anat. 1955;

385. Banati RB, Newcombe J, Gunn RN, Cagnin A, Turkheimer F, Heppner F, et al. The peripheral benzodiazepine binding site in the brain in multiple sclerosis. Quantitative in vivo imaging of microglia as a measure of disease activity. Brain. 2000;123(11):2321–37.

386. Macotela Y, Boucher J, Tran TT, Kahn CR. Sex and depot differences in adipocyte insulin sensitivity and glucose. Diabetes. 2009 Apr;58(4):803–12.

387. Mauvais-Jarvis F, Clegg DJ, Hevener AL. The role of estrogens in control of energy balance and glucose homeostasis. Endocr Rev. 2013 Jun;34(3):309–38.

388. Palmer BF, Clegg DJ. The sexual dimorphism of obesity. Vol. 402, Molecular and Cellular Endocrinology. Elsevier Ireland Ltd; 2015. p. 113–9.

389. Lainez NM, Jonak CR, Nair MG, Ethell IM, Wilson EH, Carson MJ, et al. Diet-induced obesity elicits macrophage infiltration and reduction in spine density in the hypothalami of male but not female mice. Front Immunol. 2018;9(SEP):1–16.

390. Freire-Regatillo A, Fernández-Gómez MJ, Díaz F, Barrios V, Sánchez-Jabonero I, Frago LM, et al. Sex differences in the peripubertal response to a short-term, high-fat diet intake. J Neuroendocrinol. 2019;0–2.

391. Choi DC, Furay AR, Evanson NK, Ostrander MM, Ulrich-Lai YM, Herman JP. Bed nucleus of the stria terminalis subregions differentially regulate hypothalamic-pituitary-adrenal axis activity: Implications for the integration of limbic inputs. J Neurosci. 2007;27(8):2025–34.

392. Meek TH, Nelson JT, Matsen ME, Dorfman MD, Guyenet SJ, Damian V, et al. Functional identification of a neurocircuit regulating blood glucose. Proc Natl Acad Sci U S A. 2016;113(14):E2073–82.

393. Matsuda T, Hiyama TY, Niimura F, Matsusaka T, Fukamizu A, Kobayashi K, et al. Distinct neural mechanisms for the control of thirst and salt appetite in the subfornical organ. Nat Neurosci. 2017;20(2):230–41.

394. Péterfi Z, Farkas E, Nagyunyomi-Sényi K, Kádár A, Ottó S, Horváth A, et al. Role of TRH/UCN3 neurons of the perifornical area/bed nucleus of stria terminalis region in the regulation of the anorexigenic POMC neurons of the arcuate nucleus in male mice and rats. Brain Struct Funct. 2018 Apr 1;223(3):1329–41.

395. Hawken ER, Normandeau CP, Gardner Gregory J, Cécyre B, Bouchard JF, Mackie K, et al. A novel GPR55-mediated satiety signal in the oval Bed Nucleus of the Stria Terminalis. Neuropsychopharmacology. 2019 Jun 1;44(7):1274–83.

396. Sofroniew M V. Molecular dissection of reactive astrogliosis and glial scar formation. Vol. 32, Trends in Neurosciences. 2009. p. 638–47.

397. Sweeney P, Qi Y, Xu Z, Yang Y. Activation of hypothalamic astrocytes suppresses feeding without altering emotional states. Glia. 2016;64(12):2263–

73.

398. Graeber MB, Streit WJ. Microglia: Biology and pathology. Acta Neuropathologica. 2010.

399. Madry C, Kyrargyri V, Arancibia-Cárcamo IL, Jolivet R, Kohsaka S, Bryan RM, et al. Microglial Ramification, Surveillance, and Interleukin-1β Release Are Regulated by the Two-Pore Domain K+ Channel THIK-1. Neuron. 2018;97(2):299-312.e6.

400. Rodríguez E, Guerra M, Peruzzo B, Blázquez JL. Tanycytes: A rich morphological history to underpin future molecular and physiological investigations. Vol. 31, Journal of Neuroendocrinology. Blackwell Publishing Ltd; 2019.

401. Eliasson C, Sahlgren C, Berthold CH, Stakeberg J, Celis JE, Betsholtz C, et al. Intermediate filament protein partnership in astrocytes. J Biol Chem. 1999 Aug 20;274(34):23996–4006.

402. Battaglia RA, Delic S, Herrmann H, Snider NT. Vimentin on the move: New developments in cell migration [version 1; referees: 2 approved]. Vol. 7, F1000Research. F1000 Research Ltd; 2018.

403. Schnitzer J, Franke WW, Schachner M. Immunocytochemical demonstration of vimentin in astrocytes and ependymal cells of developing and adult mouse nervous system. J Cell Biol. 1981;90(2):435–47.

404. Waniek A, Hartlage-Rübsamen M, Höfling C, Kehlen A, Schilling S, Demuth HU, et al. Identification of thyrotropin-releasing hormone as hippocampal glutaminyl cyclase substrate in neurons and reactive astrocytes. Biochim Biophys Acta - Mol Basis Dis. 2015 Jan 1;1852(1):146–55.

405. Wamsteeker Cusulin JI, Füzesi T, Watts AG, Bains JS. Characterization of Corticotropin-Releasing Hormone neurons in the Paraventricular Nucleus of the Hypothalamus of Crh-IRES-Cre Mutant Mice. PLoS One. 2013;8(5):1–10.

406. Chen Y, Molet J, Gunn BG, Ressler K, Baram TZ. Diversity of reporter expression patterns in transgenic mouse lines targeting corticotropin- releasing hormone-expressing neurons. Endocrinology. 2015 Dec 1;156(12):4769–80.

407. Nguyen AQ, Dela Cruz JAD, Sun Y, Holmes TC, Xu X. Genetic cell targeting uncovers specific neuronal types and distinct subregions in the bed nucleus of the stria terminalis. J Comp Neurol. 2016;524(12):2379–99.

408. Calogero AE, Kamilaris TC, Bernardini R, Johnson EO, Chrousos GP, Gold PW. Effects of peripheral benzodiazepine receptor ligands on hypothalamic-pituitary-adrenal axis function in the rat. J Pharmacol Exp Ther. 1990;253(2):729–37.

409. Kim J, Richter W, Aanstoot HJ, Shi Y, Fu Q, Rajotte R, et al. Differential expression of GAD65 and GAD67 in human, rat, and mouse pancreatic islets. Diabetes. 1993;42(12):1799–808.

410. Erlander MG, Tillakaratne NJK, Feldblum S, Patel N, Tobin AJ. Two genes encode distinct glutamate decarboxylases. Neuron. 1991;7(1):91–100.

411. Guidotti A, Forchetti CM, Corda MG, Konkel D, Bennett CD, Costa E. Isolation, characterization, and purification to homogeneity of an endogenous polypeptide with agonistic action on benzodiazepine receptors. Proc Natl Acad Sci U S A. 1983;80(11 I):3531–5.

412. Bonsack F, Sukumari-Ramesh S. TSPO: An evolutionarily conserved protein with elusive functions. Vol. 19, International Journal of Molecular Sciences.

2018.

413. Schildge S, Bohrer C, Beck K, Schachtrup C. Isolation and Culture of Mouse Cortical Astrocytes. J Vis Exp [Internet]. 2013 Jan 19 [cited 2021 Aug 24];(71). Available from: https://pubmed.ncbi.nlm.nih.gov/23380713/

414. Vlachaki Walker JM, Robb JL, Cruz AM, Malhi A, Weightman Potter PG, Ashford MLJ, et al. AMP-activated protein kinase (AMPK) activator A-769662 increases intracellular calcium and ATP release from astrocytes in an AMPK-independent manner. Diabetes, Obes Metab [Internet]. 2017 Jul 1 [cited 2021 Aug 24];19(7):997–1005. Available from: https://pubmed.ncbi.nlm.nih.gov/28211632/

415. Robb JL. Characterisation of immunometabolic responses in astrocytes [Internet]. University of Exeter; 2020 [cited 2021 Aug 24]. Available from: https://ore.exeter.ac.uk/repository/handle/10871/121246

416. Chowen JA, Argente-Arizón P, Freire-Regatillo A, Frago LM, Horvath TL, Argente J. The role of astrocytes in the hypothalamic response and adaptation to metabolic signals. Prog Neurobiol [Internet]. 2016;144:68–87. Available from: http://dx.doi.org/10.1016/j.pneurobio.2016.03.001

417. Rose CR, Kirchhoff F. Glial heterogeneity: the increasing complexity of the brain. e-Neuroforum. 2015 Sep;6(3):59–62.

418. Brioschi S, Peng V, Colonna M. Fifty Shades of Microglia [Internet]. Vol. 42, Trends in Neurosciences. Elsevier Ltd; 2019. p. 440–3. Available from: https://doi.org/10.1016/j.tins.2019.03.010

419. Stein LM, Lhamo R, Cao A, Workinger J, Tinsley I, Doyle RP, et al. Dorsal vagal complex and hypothalamic glia differentially respond to leptin and energy balance dysregulation. Transl Psychiatry [Internet]. 2020;10(1). Available from: http://dx.doi.org/10.1038/s41398-020-0767-0

420. Wang H, Zhai K, Xue Y, Yang J, Yang Q, Fu Y, et al. Global deletion of TSPO does not affect the viability and gene expression profile. PLoS One. 2016;11(12):8–10.

421. Bindocci E, Savtchouk I, Liaudet N, Becker D, Carriero G, Volterra A. Three-dimensional Ca 2+ imaging advances understanding of astrocyte biology. Science (80-). 2017 May 19;356(6339):eaai8185.

422. Senicourt L, Iatmanen-Harbi S, Hattab C, Ostuni MA, Giraud MF, Lacapere JJ. Recombinant overexpression of mammalian TSPO Isoforms 1 and 2. In: Methods in Molecular Biology [Internet]. Humana Press Inc.; 2017 [cited 2020 Aug 18]. p. 1–25. Available from: https://pubmed.ncbi.nlm.nih.gov/28755361/

423. Miller WL. Role of mitochondria in steroidogenesis. Pediatr Adrenal Dis [Internet]. 2010;20(6):1–19. Available from: http://dx.doi.org/10.1016/j.beem.2012.05.002

424. Yim NH, Cha MH, Kim MS. Hypermethylation of the TSPOAP1-AS1 Promoter May Be Associated with Obesity in Overweight/Obese Korean Subjects. Int J Mol Sci. 2020;21(9):1–10.

425. Freeman LR, Zhang L, Nair A, Dasuri K, Francis J, Fernandez-Kim SO, et al. Obesity increases cerebrocortical reactive oxygen species and impairs brainfunction. Free Radic Biol Med. 2013;

426. Cavaliere G, Trinchese G, Penna E, Cimmino F, Pirozzi C, Lama A, et al. High-Fat Diet Induces Neuroinflammation and Mitochondrial Impairment in Mice Cerebral Cortex and Synaptic Fraction. Front Cell Neurosci. 2019;13(November):1–13.

427. Posey K a, Clegg DJ, Printz RL, Byun J, Morton GJ, Vivekanandan-giri A, et al. Hypothalamic proinflammatory lipid accumulation , inflammation , and insulin resistance in rats fed a high-fat diet. Am J Physiol Endocrinol Metab 296 [Internet]. 2009;296:1003–12. Available from: http://www.ajpendo.org

428. Miller AA, Spencer SJ. Obesity and neuroinflammation: A pathway to cognitive impairment. Brain Behav Immun [Internet]. 2014;42:10–21. Available from: http://dx.doi.org/10.1016/j.bbi.2014.04.001

429. Martin-Jiménez CA, Gaitán-Vaca DM, Echeverria V, González J, Barreto GE. Relationship Between Obesity, Alzheimer's Disease, and Parkinson's Disease: an Astrocentric View. Mol Neurobiol [Internet]. 2017 Nov 28;54(9):7096–115. Available from: http://dx.doi.org/10.1007/s12035-016-0193-8

430. Alam A, Hana Z, Jin Z, Suen KC, Ma D. Surgery, neuroinflammation and cognitive impairment. Vol. 37, EBioMedicine. Elsevier B.V.; 2018. p. 547–56.

431. Bowman GL, Dayon L, Kirkland R, Wojcik J, Peyratout G, Severin IC, et al. Blood-brain barrier breakdown, neuroinflammation, and cognitive decline in older adults. Alzheimer's Dement. 2018 Dec 1;14(12):1640–50.

432. Bradburn S, Murgatroyd C, Ray N. Neuroinflammation in mild cognitive impairment and Alzheimer's disease: A meta-analysis. Vol. 50, Ageing Research Reviews. Elsevier Ireland Ltd; 2019. p. 1–8.

433. Jensen MD, Haymond MW, Rizza RA, Cryer PE, Miles JM. Influence of body fat distribution on free fatty acid metabolism in obesity. J Clin Invest. 1989;

434. Longo M, Zatterale F, Naderi J, Parrillo L, Formisano P, Raciti GA, et al. Adipose tissue dysfunction as determinant of obesity-associated metabolic complications. Int J Mol Sci. 2019;20(9).

435. Duffy CM, Xu H, Nixon JP, Bernlohr DA, Butterick TA. Identification of a fatty acid binding protein4-UCP2 axis regulating microglial mediated neuroinflammation. Mol Cell Neurosci [Internet]. 2017 Apr 1 [cited 2020 Apr 24];80:52–7. Available from: http://dx.doi.org/10.1016/j.mcn.2017.02.004

436. Böttcher M, Müller-fielitz H, Sundaram SM, Gallet S, Neve V. NF- k B signaling in tanycytes mediates in fl ammation-induced anorexia. 2020;(June):1–14.

437. Arlicot N, Tronel C, Bodard S, Garreau L, De La Crompe B, Vandevelde I, et al. Translocator protein (18 kDa) mapping with [125I]-CLINDE in the quinolinic acid rat model of excitotoxicity: A longitudinal comparison with microglial activation, astrogliosis, and neuronal death. Mol Imaging. 2014;13(2):1–11.

438. Pannell M, Economopoulos V, Wilson TC, Kersemans V, Isenegger PG, Larkin JR, et al. Imaging of translocator protein upregulation is selective for pro-inflammatory polarized astrocytes and microglia. Glia. 2019;(August):1–18.

439. Giannaccini G, Betti L, Palego L, Pirone A, Schmid L, Lanza M, et al. Serotonin transporter (SERT) and translocator protein (TSPO) expression in the obese ob/ob mouse. BMC Neurosci [Internet]. 2011;12(1):18. Available from: http://www.pubmedcentral.nih.gov/articlerender.fcgi?artid=3044656&tool=pmcentrez&rendertype=abstract

440. Wilhelmsson U, Bushong EA, Price DL, Smarr BL, Phung V, Terada M, et al. Redefining the concept of reactive astrocytes as cells that remain within their unique domains upon reaction to injury. Proc Natl Acad Sci U S A [Internet]. 2006 Nov 14 [cited 2020 Jul 22];103(46):17513–8. Available from: www.pnas.orgcgidoi10.1073pnas.0602841103

441. Lassance L, Haghiac M, Minium J, Catalano P, Mouzon SH De. Obesity-induced

down-regulation of the mitochondrial translocator protein (TSPO) impairs placental steroid production. J Clin Endocrinol Metab. 2015;100(1):E11–8.

442. Korkhov VM, Sachse C, Short JM, Tate CG. Three-Dimensional Structure of TspO by Electron Cryomicroscopy of Helical Crystals. Structure. 2010;

443. O'Neill LAJJ, Kishton RJ, Rathmell J. A guide to immunometabolism for immunologists. Nat Rev Immunol [Internet]. 2016;16(9):553–65. Available from: http://www.nature.com/doifinder/10.1038/nri.2016.70

444. Robb JL, Morrissey NA, Potter PGW, Smithers HE, Beall C, Ellacott KLJ. Immunometabolic Changes in Glia – A Potential Role in the Pathophysiology of Obesity and Diabetes. Neuroscience [Internet]. 2019;(November). Available from: https://doi.org/10.1016/j.neuroscience.2019.10.021

445. Garcia-Segura LM, Perez-Marquez J. A new mathematical function to evaluate neuronal morphology using the Sholl analysis. J Neurosci Methods. 2014;

446. Briggs DI, Lockie SH, Benzler J, Wu Q, Stark R, Reichenbach A, et al. Evidence that diet-induced hyperleptinemia, but not hypothalamic gliosis, causes ghrelin resistance in NPY/AgRP neurons of male mice. Endocrinology. 2014;155(7):2411–22.

447. Santos CL, Roppa PHA, Truccolo P, Fontella FU, Souza DO, Bobermin LD, et al. Age-Dependent Neurochemical Remodeling of Hypothalamic Astrocytes. Mol Neurobiol. 2017;1–15.

448. Bellaver B, Souza DG, Souza DO, Quincozes-Santos A. Hippocampal Astrocyte Cultures from Adult and Aged Rats Reproduce Changes in Glial Functionality Observed in the Aging Brain. Mol Neurobiol. 2017;

449. Higa TS, Spinola A V, Fonseca-Alaniz MH, Anna Evangelista FS. Comparison between cafeteria and high-fat diets in the induction of metabolic dysfunction in mice. Int J Physiol Pathophysiol Pharmacol. 2014;6(1):47–54.

450. Monsanto SP, Hintze KJ, Ward RE, Larson DP, Lefevre M, Benninghoff AD. The new total Western diet for rodents does not induce an overweight phenotype or alter parameters of metabolic syndrome in mice. Nutr Res [Internet]. 2016;36(9):1031–44. Available from: http://dx.doi.org/10.1016/j.nutres.2016.06.002

451. Hu S, Wang L, Yang D, Li L, Togo J, Wu Y, et al. Dietary Fat, but Not Protein or Carbohydrate, Regulates Energy Intake and Causes Adiposity in Mice. Cell Metab. 2018;28(3):415-431.e4.

452. Speakman JR. Use of high-fat diets to study rodent obesity as a model of human obesity [Internet]. Vol. 43, International Journal of Obesity. Springer US; 2019. p. 1491–2. Available from: http://dx.doi.org/10.1038/s41366-019-0363-7

453. Lejri I, Grimm A, Hallé F, Abarghaz M, Klein C, Maitre M, et al. TSPO Ligands Boost Mitochondrial Function and Pregnenolone Synthesis. J Alzheimer's Dis. 2019;1–14.

454. Wang C, Liao JK. A mouse model of DIO and insulin resistance. Science (80-) [Internet]. 2012;821(5):421–33. Available from: http://www.springerlink.com/index/10.1007/978-1-61779-430-8

455. Alquier T, Poitout V. Considerations and guidelines for mouse metabolic phenotyping in diabetes research. Diabetologia. 2017;1–13.

456. Sacca L, Vigorito C, Cicala M. Role of gluconeogenesis in epinephrine-stimulated hepatic glucose production in humans. Am J Physiol - Endocrinol

Metab. 1983;8(3).

457. Ziegler MG, Elayan H, Milic M, Sun P, Gharaibeh M. Epinephrine and the metabolic syndrome. Curr Hypertens Rep. 2012 Feb;14(1):1–7.

458. Wu Y, Kazumura K, Maruyama W, Osawa T, Naoi M. Rasagiline and selegiline suppress calcium efflux from mitochondria by PK11195-induced opening of mitochondrial permeability transition pore: a novel anti-apoptotic function for neuroprotection. J Neural Transm [Internet]. 2015;122(10):1399–407. Available from: http://dx.doi.org/10.1007/s00702-015-1398-0

459. Zhang XY, Wei W, Zhang YZ, Fu Q, Mi WD, Zhang LM, et al. The 18 kDa translocator protein (TSPO) overexpression in hippocampal dentate gyrus elicits anxiolytic-like effects in a mouse model of post-traumatic stress disorder. Front Pharmacol. 2018 Nov 23;9(NOV):1–11.

460. Qiu ZK, He JL, Liu X, Zhang GH, Zeng J, Nie H, et al. The antidepressant-like activity of AC-5216, a ligand for 18KDa translocator protein (TSPO), in an animal model of diabetes mellitus. Sci Rep [Internet]. 2016;6(May):1–13. Available from: http://dx.doi.org/10.1038/srep37345

461. Li L, Wang W, Zhang LM, Jiang XY, Sun S, Sun LJ, et al. Overexpression of the 18 kDa translocator protein (TSPO) in the hippocampal dentate gyrus produced anxiolytic and antidepressant-like behavioural effects. Neuropharmacology. 2017 Oct 1;125:117–28.

462. Krestinina O V, Grachev DE, Odinokova I V, Reiser G, Evtodienko Y V, Azarashvili TS. Effect of peripheral benzodiazepine receptor (PBR/TSPO) ligands on opening of Ca2+-induced pore and phosphorylation of 3.5-kDa polypeptide in rat brain mitochondria. Biochemistry-Moscow. 2009;74(4):421–9.

463. Fritsche L, Hoene M, Lehmann R, Ellingsgaard H, Hennige AM, Pohl AK, et al. IL-6 deficiency in mice neither impairs induction of metabolic genes in the liver nor affects blood glucose levels during fasting and moderately intense exercise. Diabetologia [Internet]. 2010 Aug 22 [cited 2020 Jul 15];53(8):1732–42. Available from: http://link.springer.com/10.1007/s00125-010-1754-4

464. Potthoff MJ, Boney-Montoya J, Choi M, He T, Sunny NE, Satapati S, et al. FGF15/19 regulates hepatic glucose metabolism by inhibiting the CREB-PGC-1α pathway. Cell Metab [Internet]. 2011 Jun 8 [cited 2020 Jul 15];13(6):729–38. Available from: /pmc/articles/PMC3131185/?report=abstract

465. El-Brolosy MA, Stainier DYR. Genetic compensation: A phenomenon in search of mechanisms. PLoS Genet. 2017 Jul 1;13(7):1–17.

466. Barabási AL, Oltvai ZN. Network biology: Understanding the cell's functional organization. Vol. 5, Nature Reviews Genetics. Nat Rev Genet; 2004. p. 101–13.

467. Davidson E, Levine M. Gene regulatory networks. Vol. 102, Proceedings of the National Academy of Sciences of the United States of America. Proc Natl Acad Sci U S A; 2005. p. 4935.

468. Wang RH, Li C, Deng CX. Liver steatosis and increased ChREBP expression in mice carrying a liver specific SIRT1 null mutation under a normal feeding condition. Int J Biol Sci. 2010;6(7):682–90.

469. Resch JM, Maunze B, Gerhardt AK, Magnuson SK, Phillips KA, Choi S, et al. Intrahypothalamic pituitary adenylate cyclase-activating polypeptide regulates energy balance via site-specific actions on feeding and metabolism. Am J Physiol Endocrinol Metab [Internet]. 2013;305(12):E1452-63. Available from: http://www.ncbi.nlm.nih.gov/pubmed/24148346%5Cnhttp://www.pubmedcentral.nih.gov/articlerender.fcgi?artid=PMC3882380

470. Vowinckel E, Reutens D, Becher B, Verge G, Evans A, Owens T, et al. PK11195 binding to the peripheral benzodiazepine receptor as a marker of microgila activation in multiple sclerosis and experimental autoimmune encephalomyelitis. J Neurosci Res. 1997 Oct 15;50(2):345–53.

471. Venneti S, Lopresti BJ, Wiley CA. The peripheral benzodiazepine receptor (Translocator protein 18 kDa) in microglia: From pathology to imaging. Vol. 80, Progress in Neurobiology. 2006. p. 308–22.

472. Koska P, Dojcsák Kiss-Tóth É, Juhász Szalai A, Kovács G, Barkai L, Rácz O, et al. Brain glucose sensing and counterregulatory response to hypoglycaemia. Acta Physiol Hung [Internet]. 2013 Jun 1 [cited 2020 Jul 16];100(2):133–9. Available from: https://pubmed.ncbi.nlm.nih.gov/23708945/

473. Verberne AJM, Korim WS, Sabetghadam A, Llewellyn-Smith IJ. Adrenaline: Insights into its metabolic roles in hypoglycaemia and diabetes. Br J Pharmacol. 2016 May 1;173(9):1425–37.

474. Kroon J, Pereira AM, Meijer OC. Glucocorticoid Sexual Dimorphism in Metabolism: Dissecting the Role of Sex Hormones. Trends Endocrinol Metab [Internet]. 2020;1–11. Available from: https://doi.org/10.1016/j.tem.2020.01.010

475. Chen C, Kuo J, Wong A, Micevych P. Estradiol modulates translocator protein (tspo) and steroid acute regulatory protein (StAR) via Protein Kinase A (PKA) signaling in hypothalamic astrocytes. Endocrinology. 2014;155(8):2976–85.

476. Votano J, Parham M, Hall L. Interaction between cytokines, nutrition and infection. Nutr Res [Internet]. 1995;15(12):1815–44. Available from: http://onlinelibrary.wiley.com/doi/10.1002/cbdv.200490137/abstract

477. Stephen T-L, Gupta-Agarwal S, Kittler JT. Mitochondrial dynamics in astrocytes. Biochem Soc Trans [Internet]. 2014;42(5):1302–10. Available from: http://biochemsoctrans.org/lookup/doi/10.1042/BST20140195

478. Loftus RM, Finlay DK. Immunometabolism: Cellular metabolism turns immune regulator. J Biol Chem. 2016;291(1):1–10.

479. Fiebig C, Keiner S, Ebert B, Schäffner I, Jagasia R, Lie DC, et al. Mitochondrial dysfunction in astrocytes impairs the generation of reactive astrocytes and enhances neuronal cell death in the cortex upon photothrombotic lesion. Front Mol Neurosci. 2019;12(February):1–13.

480. Tiku V, Tan MW, Dikic I. Mitochondrial Functions in Infection and Immunity. Trends Cell Biol [Internet]. 2020;xx(xx):1–13. Available from: https://doi.org/10.1016/j.tcb.2020.01.006

481. Soto-Heredero G, Gómez de las Heras MM, Gabandé-Rodríguez E, Oller J, Mittelbrunn M. Glycolysis: a key player in the inflammatory response. FEBS Journal. 2020. 0–2 p.

482. Zhang X, Zhang G, Zhang H, Karin M, Bai H, Cai D. Hypothalamic IKKβ/NF-κB and ER Stress Link Overnutrition to Energy Imbalance and Obesity. Cell. 2008 Oct 3;135(1):61–73.

483. Torres SR, Fröde TS, Nardi GM, Vita N, Reeb R, Ferrara P, et al. Anti-inflammatory effects of peripheral benzodiazepine receptor ligands in two mouse models of inflammation. Eur J Pharmacol. 2000;408(2):199–211.

484. Brendel M, Focke C, Blume T, Peters F, Deussing M, Probst F, et al. Time Courses of Cortical Glucose Metabolism and Microglial Activity Across the Life-Span of Wild-Type Mice: A PET Study. J Nucl Med [Internet]. 2017;49(0):jnumed.117.195107. Available from:

http://jnm.snmjournals.org/lookup/doi/10.2967/jnumed.117.195107

485. Frankle WG, Narendran R, Wood AT, Suto F, Himes ML, Kobayashi M, et al. Brain translocator protein occupancy by ONO-2952 in healthy adults: A Phase 1 PET study using [11C]PBR28. Synapse. 2017;

486. Fujinaga M, Luo R, Kumata K, Zhang Y, Hatori A, Yamasaki T, et al. Development of a 18F-labeled radiotracer with improved brain kinetics for positron emission tomography imaging of translocator protein (18 kDa) in ischemic brain and glioma. J Med Chem [Internet]. 2017;acs.jmedchem.7b00374. Available from: http://pubs.acs.org/doi/abs/10.1021/acs.jmedchem.7b00374

487. Ghadery C, Best LA, Pavese N, Tai YF, Strafella AP. PET Evaluation of Microglial Activation in Non-neurodegenerative Brain Diseases. Vol. 19, Current Neurology and Neuroscience Reports. Current Neurology and Neuroscience Reports; 2019.

488. Hieu Tran V, Park H, Park J, Kwon Y Do, Kang S, Ho Jung J, et al. Synthesis and evaluation of novel potent TSPO PET ligands with 2-phenylpyrazolo[1,5-a]pyrimidin-3-yl acetamide. Bioorganic Med Chem [Internet]. 2019;27(18):4069–80. Available from: https://doi.org/10.1016/j.bmc.2019.07.036

489. MacAskill MG, Walton T, Williams L, Morgan TEF, Alcaide-Corral CJ, Dweck MR, et al. Kinetic modelling and quantification bias in small animal PET studies with [18F]AB5186, a novel 18 kDa translocator protein radiotracer. PLoS One. 2019;14(5):1–14.

490. Sridharan. Sridharan et al, 2019 - Confirmation of Specific Binding of the 18-kDaTranslocator Protein (TSPO) Radioligand[18F]GE-180; a Blocking Study Using XBD173in Multiple Sclerosis Normal Appearing Whiteand Grey Matter.pdf.

491. Takano A, Gulyás B, Varrone A, Karlsson P, Sjoholm N, Larsson S, et al. Biodistribution and radiation dosimetry of the 18 kDa translocator protein (TSPO) radioligand [18F]FEDAA1106: A human whole-body PET study. Eur J Nucl Med Mol Imaging. 2011;38(11):2058–65.

492. Tuisku J, Plavén-Sigray P, Gaiser EC, Airas L, Al-Abdulrasul H, Brück A, et al. Effects of age, BMI and sex on the glial cell marker TSPO — a multicentre [11C]PBR28 HRRT PET study. Eur J Nucl Med Mol Imaging. 2019;46(11):2329–38.

493. Tong J, Williams B, Rusjan PM, Mizrahi R, Lacapère JJ, McCluskey T, et al. Concentration, distribution, and influence of aging on the 18 kDa translocator protein in human brain: Implications for brain imaging studies. J Cereb Blood Flow Metab. 2019;

494. Tyler RE, Kim SW, Guo M, Jang YJ, Damadzic R, Stodden T, et al. Detecting neuroinflammation in the brain following chronic alcohol exposure in rats: A comparison between in vivo and in vitro TSPO radioligand binding. Eur J Neurosci. 2019;50(1):1831–42.

495. Werry EL, Bright FM, Piguet O, Ittner LM, Halliday GM, Hodges JR, et al. Recent developments in TSPO PET imaging as a biomarker of neuroinflammation in neurodegenerative disorders. Vol. 20, International Journal of Molecular Sciences. 2019. p. 1–21.

496. Zhao L, Zabel MK, Wang X, Ma W, Shah P, Fariss RN, et al. Microglial phagocytosis of living photoreceptors contributes to inherited retinal degeneration. EMBO Mol Med [Internet]. 2015 Sep [cited 2020 Aug 17];7(9):1179–97. Available from: https://pubmed.ncbi.nlm.nih.gov/26139610/

497. Loth MK, Choi J, McGlothan JL, Pletnikov M V., Pomper MG, Guilarte TR. TSPO in a murine model of Sandhoff disease: Presymptomatic marker of neurodegeneration and disease pathophysiology. Neurobiol Dis [Internet]. 2016 Jan 1 [cited 2020 Aug 17];85:174–86. Available from: https://pubmed.ncbi.nlm.nih.gov/26545928/

498. James ML, Belichenko NP, Shuhendler AJ, Hoehne A, Andrews LE, Condon C, et al. [18F]GE-180 PET detects reduced microglia activation after LM11A-31 therapy in a mouse model of Alzheimer's disease. Theranostics [Internet]. 2017 [cited 2020 Aug 17];7(6):1422–36. Available from: https://pubmed.ncbi.nlm.nih.gov/28529627/

499. Li HD, Li M, Shi E, Jin WN, Wood K, Gonzales R, et al. A translocator protein 18 kDa agonist protects against cerebral ischemia/reperfusion injury. J Neuroinflammation [Internet]. 2017 Jul 28 [cited 2020 Aug 17];14(1). Available from: https://pubmed.ncbi.nlm.nih.gov/28754131/

500. Fukudome D, Hayes LN, Faust TE, Foss CA, Kondo MA, Lee BJ, et al. Translocator protein (TSPO) and stress cascades in mouse models of psychosis with inflammatory disturbances. Schizophr Res [Internet]. 2018 Jul 1 [cited 2020 Aug 17];197:492–7. Available from: https://pubmed.ncbi.nlm.nih.gov/29398205/

501. Chaney A, Bauer M, Bochicchio D, Smigova A, Kassiou M, Davies KE, et al. Longitudinal investigation of neuroinflammation and metabolite profiles in the APP swe ×PS1 Δe9 transgenic mouse model of Alzheimer's disease. J Neurochem [Internet]. 2018 Feb 1 [cited 2020 Aug 17];144(3):318–35. Available from: https://pubmed.ncbi.nlm.nih.gov/29124761/

502. Hosomi S, Watabe T, Mori Y, Koyama Y, Adachi S, Hoshi N, et al. Inflammatory projections after focal brain injury trigger neuronal network disruption: An 18F-DPA714 PET study in mice. NeuroImage Clin [Internet]. 2018 Jan 1 [cited 2020 Aug 17];20:946–54. Available from: https://pubmed.ncbi.nlm.nih.gov/30312938/

503. Tournier BB, Tsartsalis S, Rigaud D, Fossey C, Cailly T, Fabis F, et al. TSPO and amyloid deposits in sub-regions of the hippocampus in the 3xTgAD mouse model of Alzheimer's disease. Neurobiol Dis. 2019 Jan 1;121:95–105.

504. Thau-Zuchman O, Gomes RN, Dyall SC, Davies M, Priestley J V., Groenendijk M, et al. Brain Phospholipid Precursors Administered Post-Injury Reduce Tissue Damage and Improve Neurological Outcome in Experimental Traumatic Brain Injury. J Neurotrauma [Internet]. 2019 Jan 1 [cited 2020 Aug 17];36(1):25–42. Available from: https://pubmed.ncbi.nlm.nih.gov/29768974/

505. Crabbé M, Van Der Perren A, Bollaerts I, Kounelis S, Baekelandt V, Bormans G, et al. Increased P2X7 receptor binding is associated with neuroinflammation in acute but not chronic rodent models for Parkinson's disease. Front Neurosci [Internet]. 2019 [cited 2020 Aug 17];13(JUL). Available from: https://pubmed.ncbi.nlm.nih.gov/31417352/

506. Carlezon WA, Kim W, Missig G, Finger BC, Landino SM, Alexander AJ, et al. Maternal and early postnatal immune activation produce sex-specific effects on autism-like behaviors and neuroimmune function in mice. Sci Rep [Internet]. 2019 Dec 1 [cited 2020 Aug 17];9(1). Available from: https://pubmed.ncbi.nlm.nih.gov/31729416/

507. Cropper HC, Johnson EM, Haight ES, Cordonnier SA, Chaney AM, Forman TE, et al. Longitudinal translocator protein-18 kDa-positron emission tomography imaging of peripheral and central myeloid cells in a mouse model of complex regional pain syndrome. Pain [Internet]. 2019 Sep 1 [cited 2020 Aug 17];160(9):2136–48. Available from: https://pubmed.ncbi.nlm.nih.gov/31095093/

508. Aires ID, Madeira MH, Boia R, Rodrigues-Neves AC, Martins JM, Ambrósio AF, et al. Intravitreal injection of adenosine A2A receptor antagonist reduces neuroinflammation, vascular leakage and cell death in the retina of diabetic mice. Sci Rep [Internet]. 2019 Dec 1 [cited 2020 Aug 17];9(1). Available from: https://pubmed.ncbi.nlm.nih.gov/31748653/

509. Gong J, Szego ÉM, Leonov A, Benito E, Becker S, Fischer A, et al. Translocator protein ligand protects against neurodegeneration in the MPTP mouse model of parkinsonism. J Neurosci. 2019;39(19):3752–69.

510. Wang M, Wang X, Zhao L, Ma W, Rodriguez IR, Fariss RN, et al. Macroglia-Microglia Interactions via TSPO Signaling Regulates Microglial Activation in the Mouse Retina. J Neurosci [Internet]. 2014;34(10):3793–806. Available from: http://www.jneurosci.org/cgi/doi/10.1523/JNEUROSCI.3153-13.2014

511. Karlstetter M, Nothdurfter C, Aslanidis A, Moeller K, Horn F, Scholz R, et al. Translocator protein (18 kDa) (TSPO) is expressed in reactive retinal microglia and modulates microglial inflammation and phagocytosis. J Neuroinflammation [Internet]. 2014 Jan 8 [cited 2020 Aug 17];11. Available from: https://pubmed.ncbi.nlm.nih.gov/24397957/

512. Chai H, Diaz-Castro B, Shigetomi E, Monte E, Octeau JC, Yu X, et al. Neural Circuit-Specialized Astrocytes: Transcriptomic, Proteomic, Morphological, and Functional Evidence. Neuron [Internet]. 2017;1–19. Available from: http://linkinghub.elsevier.com/retrieve/pii/S0896627317305536

513. John Lin C-C, Yu K, Hatcher A, Huang T-W, Lee HK, Carlson J, et al. Identification of diverse astrocyte populations and their malignant analogs. Nat Neurosci [Internet]. 2017;20(3). Available from: http://www.nature.com/doifinder/10.1038/nn.4493

514. Zhang Z, Ma Z, Zou W, Guo H, Liu M, Ma Y, et al. The Appropriate Marker for Astrocytes: Comparing the Distribution and Expression of Three Astrocytic Markers in Different Mouse Cerebral Regions. Biomed Res Int. 2019;2019.

515. Filippi BM, Abraham MA, Silva PN, Rasti M, LaPierre MP, Bauer P V, et al. Dynamin-Related Protein 1-Dependent Mitochondrial Fission Changes in the Dorsal Vagal Complex Regulate Insulin Action. Cell Rep [Internet]. 2017;18(10):2301–9. Available from: http://dx.doi.org/10.1016/j.celrep.2017.02.035

516. Fecher C, Trovò L, Müller SA, Snaidero N, Wettmarshausen J, Heink S, et al. Cell-type-specific profiling of brain mitochondria reveals functional and molecular diversity. Nat Neurosci [Internet]. 2019;22(10):1731–42. Available from: http://dx.doi.org/10.1038/s41593-019-0479-z

517. Costa B, Da Pozzo E, Martini C. 18-kDa translocator protein association complexes in the brain: From structure to function. Biochem Pharmacol [Internet]. 2020;177(May):114015. Available from: https://doi.org/10.1016/j.bcp.2020.114015

518. Shoshan-Barmatz V, Pittala S, Mizrachi D. VDAC1 and the TSPO: Expression, interactions, and associated functions in health and disease states. Int J Mol Sci. 2019;20(13).

519. Xia Y, Ledwitch K, Kuenze G, Duran A, Li J, Sanders CR, et al. A unified structural model of the mammalian translocator protein (TSPO). J Biomol NMR [Internet]. 2019;73(6–7):347–64. Available from: https://doi.org/10.1007/s10858-019-00257-1

520. Sierra A, Lavaque E, Perez-Martin M, Azcoitia I, Hales DB, Garcia-Segura LM.

Steroidogenic acute regulatory protein in the rat brain: Cellular distribution, developmental regulation and overexpression after injury. Eur J Neurosci. 2003;18(6):1458–67.

521. Manna PR, Dyson MT, Stocco DM. Regulation of the steroidogenic acute regulatory protein gene expression: Present and future perspectives. Vol. 15, Molecular Human Reproduction. 2009. p. 321–33.